Forschungszentrum Karlsruhe
in der Helmholtz-Gemeinschaft

Wissenschaftliche Berichte
FZKA 6999

Investigations on the Complexation Behaviour of Humic Acids and Their Influence on the Migration of Radioactive and Non-radioactive Substances Under Conditions Close to Nature

C. M. Marquardt (Editor)

Institut für Nukleare Entsorgung

in collaboration with:

**Forschungszentrum Rossendorf e.V.,
Institut für Radiochemie**

Institut für Kernchemie, Universität Mainz

Institut für Anorganische und Analytische Chemie und Radiochemie, Universität des Saarlandes

Institut für Interdisziplinäre Isotopenforschung e.V., Leipzig

September 2004

Forschungszentrum Karlsruhe

in der Helmholtz-Gemeinschaft

Wissenschaftliche Berichte

FZKA 6999

Investigations on the complexation behaviour of humic acids and their influence on the migration of radioactive and non-radioactive substances under conditions close to nature

C.M. Marquardt (Editor)

Institut für Nukleare Entsorgung

in collaboration with:

Forschungszentrum Rossendorf e.V., Institut für Radiochemie

Institut für Kernchemie, Universität Mainz

Institut für Anorganische und Analytische Chemie und Radiochemie, Universität des Saarlandes

Institut für Interdisziplinäre Isotopenforschung e.V., Leipzig

Forschungszentrum Karlsruhe GmbH, Karlsruhe

2004

Impressum der Print-Ausgabe:

Als Manuskript gedruckt

Forschungszentrum Karlsruhe GmbH
Postfach 3640, 76021 Karlsruhe

Mitglied der Hermann von Helmholtz-Gemeinschaft
Deutscher Forschungszentren (HGF)

ISSN 0947-8620

urn:nbn:de:0005-069999

The work described in this report has been financially supported by the German Federal Ministry of Economics and Labour (BMWA) under the Contract Numbers 02 E 9299, 02 E 9309 5, and 02 E 9329. The authors are responsible for the content of their contribution.

BMWA Project No.: 02 E 9299

Partner No. 1: Forschungszentrum Rossendorf e.V.
Institut für Radiochemie
S. Sachs, K. Schmeide, V. Brendler, A. Křepelová,
J. Mibus, G. Geipel, T. Reich, K.H. Heise, G. Bernhard

Duration of the project: 01.00 – 06.03

BMWA Project No.: 02 E 9309 5

Partner No. 2: Institut für Kernchemie, Universität Mainz
B.Kuczewski, A. Seibert, J. V. Kratz, N. Trautmann,
N. L.. Banik, S. Bürger, G. Getahun, C. Lüttinger, J. Maul

Partner No. 3: Institut für Anorganische und Analytische Chemie und Radiochemie, Universität des Saarlandes
H.P. Beck, H. Wagner, T. Gottfreund, M. Zeitz

Duration of the project: 01.00 – 06.03

BMWA Project No.02 E 9329

Partner No. 4 Institut für Interdisziplinäre Isotopenforschung e.V., Leipzig
H. Lippold, D. Rößler, H. Kupsch

Duration of the project: 01.00 – 02.03

External Partner without support

Partner No. 5 Forschungszentrum Karlsruhe GmbH,
Institut für Nukleare Entsorgung
R. Artinger, C. M. Marquardt, T. Schäfer, A. Seibert,
H. Geckeis, Th. Fanghänel, J. I. Kim

Foreword

The present report summarises the progress and the final results obtained within the BMWA[1]-Project "*Investigations on the complexation behaviour of humic acids and their influence on the migration of radioactive and non-radioactive substances under conditions close to nature*". This project, which lasted for 3.5 years, was conducted in the frame of a BMWA supporting program directed towards the assessment of final repositories / underground disposal facilities in deep geological formations. The work presented in this report is a continuation of the work within a former BMBF[2] project performed in the years 1995 to 1999. These results are published in a Scientific Report of the Forschungszentrum Karlsruhe [1]

Five partners have been concerned in this project; four of them have received funding and one partner (FZK) have attended the project with its long experiences in the field of metal ion interaction with humic substances, but without financial support. All the partners are listed on page i.

The report contains an executive summary of the final reports prepared by the four financially supported partners. These final reports are enclosed as Appendices A – D. The executive summary gives an overview of the covered topics and the obtained results without going into details. Especially, the relationships among the different studies are pointed out.

By this approach, results rapidly become available in compact form prior to their publication in various scientific journals and conference proceedings. Furthermore, some of the preliminary results may not appear in scientific journals or conference proceedings.

The elaborated results are important contributions which can be introduced into safety assessment of nuclear and toxic waste disposal in deep geologic formations.

The following abbreviations are used in the text for each partner:

- Forschungszentrum Rossendorf e.V., Institut für Radiochemie FZR
- Universität Mainz, Institut für Kernchemie UMz
- Universität des Saarlandes, Institut für Anorganische Chemie und Radiochemie USa
- Institut für Interdisziplinäre Isotopenforschung e.V., Leipzig IIF
- Forschungszentrum Karlsruhe GmbH, Institut für Nukleare Entsorgung FZK

[1] German Federal Ministry of Economics and Labour (Bundesministerium für Wirtschaft und Arbeit)

[2] German Federal Ministry of Education and Research (Bundesministerium für Bildung und Forschung)

Content

Executive Summary

1 Introduction

For the long-term safety assessment of waste repositories, detailed information about the geochemical behaviour of radioactive and toxic metal ions under environmental conditions (geologic matrix and aquifer systems) is necessary. It includes the knowledge of the mechanism of relevant geochemical reactions, as well as thermodynamic and kinetic data. Several previous studies have shown that humic acid can play an important role in the immobilisation or mobilisation of metal ions due to complexation and colloid formation. Furthermore, humic substances are involved in redox processes of redox sensitive metal ions and they interfere into sorption processes of metal ions onto mineral surfaces. The project presented in the following was supported by the German Federal Ministry of Economics and Labour (BMWA) in the frame of a program concerning the assessment of final repositories / underground disposal facilities in deep geological formations. The project started at January 2000 and lasted three and a half years. It is a continuation of a previous project supported by the German Federal Ministry of Education and Research (BMBF) and performed in the years from 1995 to 1999. These results are published in a Scientific Report of the Forschungszentrum Karlsruhe [1].

The basic approach of the present is to provide fundamental process understanding. It differs from previous activities by introducing new reference humic substances and new techniques, and to extend its scope by focusing on ternary systems. Along these lines it encompassed the synthesis and characterisation of humic acids with distinct redox functionalities, complexation studies of metal ions (Cu(II), Zn(II), Cd(II), Pb(II), La(III), Th(IV), U(IV,VI), Np(IV,V), Pu(III-VI)), the role of phenolic OH groups in the complexation reaction, EXAFS studies on different metal humates (Th(IV), Np(IV), Np(V), Pu(III)), sorption studies of metal ions onto quartz sand and other mineral surfaces in the presence and absence of humic acid, and migration experiments with metal ions. As new techniques capillary electrophoresis (**CE**) coupled to ICP-MS and the Wageningen-Donnan-Membrane-Technique (**WDMT**) have been introduced, optimised and applied for different studies.

Humic acid is a large organic molecule with reductive properties whose origin is not exactly known. It is assumed that hydroquinone-like groups and phenolic OH groups can deliver electrons for electron transfer reactions. To prove these assumptions and to elucidate redox processes between humic substances and metal ions, synthetic humic substances with pronounced redox functionalities have been developed.

The mechanism of humate complexation of metal ions is not well understood, especially with respect to the role of phenolic OH groups. Additionally, the influence of metal ion and humic acid concentrations on the humate complexation, the role of metal ions on aggregation of

humic molecules, and the kinetics of the involved reactions are unsolved problems so far. The experiments performed within this project should tackle these difficult problems.

Concerning radioactive waste disposal, one of the most important and interesting metal ions, the plutonium ion, has been quite neglected in earlier studies, due to its complex chemistry. Plutonium can co-exist in four oxidation states under relevant conditions, and it can change its redox state very easily depending on the redox environment. Besides its complex redox behaviour, plutonium shows tremendous tendencies to hydrolysis and colloid formation in the tetravalent oxidation state. Both types of reactions interfere the humate complexation, limit the methods used for the speciation of plutonium and complicate the interpretations of experimental results. Therefore, it is very urgent to continue investigations on the behaviour of plutonium, because a lot of experience is needed to perform such experiments and to interpret the results.

In the next chapters the scope of the project is summarised without being exhaustive. More details are given in the final reports of the partners presented in the Appendices A – D.

2 Experimental

2.1 Methods

2.1.1 New adopted and improved methods

*Capillary electrophoresis (**CE**) coupled to ICP-MS*
The insufficient reliability of speciation methods for the studies of different oxidation states of plutonium of low metal ion concentrations induced the project group to look for an alternative method. After a lot of preliminary experiments with different methods like HPLC, capillary electrophoresis (CE), ion chromatography, ion exchange chromatography, CE was selected and coupled to ICP-MS for plutonium oxidation state speciation. With the **CE-ICP-MS** and an acetate buffer system, the trivalent, tetravalent, pentavalent and hexavalent plutonium ions can be simultaneously separated and determined within 10 min in various aquatic solutions (Appendix. B).

*Wageningen-Donnan-Membrane-Technique (**WDMT**)*
The Donnan Membrane technique developed at the University of Wageningen (Netherlands) was improved and adapted for studies on the humic acid complexation of heavy metal ions. The experiments during the project showed reproducible results obtained with WDM-Technique. WDMT was applied to Cu, Cd, and Zn humate complexation (Appendix C).

2.1.2 Other methods

The following methods were used during the whole project:

Speciation methods for free and complexed metal ions:

Direct methods:

- X-ray absorption spectroscopy (**XANES** and **EXAFS**) for oxidation states, bond lengths and coordination studies at the European Synchroton Radiation Facility (**ESRF**) in Grenoble (France) (Appendix A)
- **UV-VIS-NIR** spectroscopy for neptunium and plutonium speciation, quantification of $K_3[Fe^{(III)}(CN)_6]$ and detection of Fe(II) as 1,10-phenanthroline complex in redox studies (Appendix A, B)
- Laser-induced photoacoustic spectroscopy (**LIPAS**) for oxidation states and complexation of uranium (Appendix A)

Indirect methods to distinguish between free and complexed metal ions :

- Ion focusing (**IF**) with capillary electrophoresis (**CE**) coupled to ICP-MS (Appendix C)
- Anodic stripping voltammetry (**ASV**) for detection of Zn, Cd, Pb and Cu ions (Appendix C)
- Ultrafiltration (**UF**) for separation of free metal from metal humate complex (Appendix B, C)
- Anionic exchange with Sephadex DEAE A-25 to separate free metal from metal humate complex. (Appendix D)

Detection methods for metals:

- Radiometric methods like liquid scintillation counting, α- and γ-spectrometry
- Resonance ionisation mass spectrometry (**RIMS**) for measurements of very low amounts of plutonium (Appendix B)
- **ICP-MS, ICP-OES**

Characterisation of humic material:

- FTIR spectroscopy for the characterisation of humic substances (Appendix A)
- Elemental composition of humic material (Appendix A)
- Potentiometric titration, calcium acetate exchange for exchangeable protons, radiometric determination of phenolic/acidic OH groups (Appendix A)
- Sequential gel permeation chromatography for humic acid characterisation (Appendix D)

Miscellaneous methods:

- Liquid-liquid extraction with **TTA, DPMB** as extractants for uranium and plutonium oxidation state speciation (Appendix A, B)
- Glove boxes for oxygen free atmosphere (~1-10 ppm) and defined CO_2 partial pressure (1 %) (Appendix A, B)
- Neutron irradiation at the TRIGA Mainz reactor to produce different radioactive tracers (^{140}Ba, ^{160}Tb, ^{239}Np) (Appendix B)
- Electrolysis at constant potential for the preparation of oxidation states of metal ions (Appendix B)
- **DOC** (Dissolved organic carbon) measurements for determining humic acid contents

2.2 Humic material

As in the previous project [1], commercially available natural humic acid from Aldrich (AHA) has been used by all project partners as reference material. To make some intercomparison between different humic acids, several other humic acids have been applied in the studies. A list of the humic acids is given below.

a) Natural humic acids
   1) Aldrich humic acid (**AHA**)
      i. Purified **AHA**
      ii. Aldrich humic acid with blocked phenolic OH groups prepared by methylating with diazomethane (**AHA-PB**) (Appendix A)
      iii. **^{131}I**-radiolabelled **AHA** (Appendix D)
      iv. **^{111}In**-radiolabelled **AHA** (Appendix D)
   2) Aquatic and soil humic substances from the raised bog “Kleiner Kranichsee” near Carlsfeld, Saxony, Germany (**Bog soil HA, bog water HA/FA**) (Appendix D)

b) Synthetic humic acids (Appendix A)
   1) HA with different carboxylate/phenolic OH groups content (**M1, M42**)
      i. unmodified **M1** and **M42**
      ii. HA with blocked phenolic OH groups prepared by methylating with diazomethane (**M42-PB**)
      iii. ^{14}C-labelled humic acids (**^{14}C-M42**)
   2) humic acid-like oxidation products with distinct redox functionalities (**Type Hyd, Hyd-Gly, Hyd-Glu, Cat-Gly, Van-Gly**)

i. unmodified **Type Hyd, Hyd-Gly, Hyd-Glu, Cat-Gly, Van-Gly**

ii. HA from i. with blocked phenolic OH groups prepared by methylating with diazomethane (**Type Hyd-Gly-PB, Hyd-Glu-PB, Cat-Gly-PB**)

The humic acids with blocked phenolic OH-groups were used for humate complexation and redox studies of metal ions to compare these results with results obtained by unblocked humic acids. Differences in their behaviour are ascribed to properties of the phenolic OH-groups.

The redox variability of the synthetic humic acids are achieved by taking different phenolic compounds like hydroquinone, catechol or vanillic acid and amino acids for the synthesis followed by an oxidation step with potassium peroxodisulfate. By this method humic acid-like substances have been obtained with a redox capacity for Fe(III) to Fe(II) between 5 and 15 meq/g at pH 3 and about 35 meq/g at pH 9. This redox capacity is considerably higher than that for the natural Aldrich humic acid as well as the synthetic humic acid M42. Studies with these designed humic acids whose phenolic OH groups were blocked by methylation revealed that the OH groups might be involved in the redox processes. Generally, the redox effect is more pronounced than what would be expected from simple oxidation of OH-groups.

For those studies, where the interaction of humic acid with sediments is investigated, radio-labelled humic material is used. In this way small amounts of humic acids can be measured very sensitively by radiometric methods. The humic acids were radio-labelled with three radioactive isotopes: ^{14}C, ^{111}In, and ^{131}I. For the ^{14}C-labelling, a synthetic humic acid must be synthesised with ^{14}C-compounds and hence, the ^{14}C is irreversible fixed into the molecules backbone and keeps very stable during the experiments. For the ^{111}In- and ^{131}I-labelling at carboxylic groups and double bonds of benzoic rings, respectively, natural humic acids can be used. Unfortunately, because both bonds are not very stable during experiments, some loss of radio-labelled material must be taken into account. This is expressed in widely deviant results obtained with both labelled materials.

2.3 Groundwater

Original Gorleben groundwater was taken for investigations of the behaviour of Pu in batch and column experiments. The groundwater was sampled nearby the exploration salt mine in the area of Gorleben (Borehole 532, Lower Saxony, Germany) and stored under near oxygen-free conditions. Its main feature consists in a high content of humic substances (~60 – 70 mg/L) and an Eh-value of about –200 mV when kept under oxygen-free atmosphere.

2.4 Metal ions

The interaction of humic substances, mineral phases, or both with the following metal ions in their characteristic oxidation states in solution were studied:

Divalent metal ions: Cu^{2+}, Zn^{2+}, Cd^{2+}, Pb^{2+}

Trivalent metal ions: Al^{3+}, Ga^{3+}, In^{3+}, Sc^{3+}, Y^{3+}, La^{3+}, Tb^{3+}, Pu^{3+}

Tetravalent metal ions: U^{4+}, Np^{4+}, Pu^{4+}

Pentavalent metal ions: NpO_2^{+}

Hexavalent metal ions: UO_2^{2+}, PuO_2^{2+}

2.5 Solid material for sorption and column experiments

The partners used quartz sand (Sea sand) from Merck for adsorption studies and column experiments to ensure a better intercomparison of the obtained results.
Besides that

- fine-grained quartz (100% SiO_2, 63-200 µm, Merck),
- marine quartz sand (100-300 µm, Heerlen, Netherlands),
- pleistocene aeolian quartz sand sampled from the near surface at the Gorleben site,
- granite from Eibenstock (Germany), and its components orthoclase, biotite, albite, and muscovite,
- granite, phyllite and diabase from “Mansfelder Land” (Saxony-Anhalt, Germany)

have been applied for sorption studies or column experiments.

3 Complexation of metal ions with humic acid

One goal of the project was to study the complexation of metal ions by humic acid and to evaluate the complexation constants. These complexation constants are required for geochemical modelling of metal-ion behaviour in the environment and are to be installed into a thermodynamic database. Among the different complexation models to describe the metal ion complexation by humic substances the metal-ion charge neutralisation (MICN) model was favoured within this project. The MICN model is relatively simple and requires only a few parameters which can be determined experimentally. The parameters are the proton exchange capacity (PEC) and the loading capacity (LC) of the humic acid (s. Appendix A, Chapter 8). Both parameters are necessary to estimate the actual free humic acid concentration.

To guarantee reliable results, a large variety of different analytical methods are used to determine the complexation reaction by differentiating between free metal ions and metal ions which are bound to humic substances.

Nevertheless, the mechanism of the complexation reaction is not known yet and therefore, it is necessary to progress in detailed studies on the complexation reactions on a molecular level. For that, EXAFS measurements have been performed for selected metal-ion complexation reactions to learn something about the coordination of the metal ions bound to different humic acids.

To investigate the role of phenolic OH groups in the complexation reactions, experiments with modified humic substances were performed. The phenolic OH groups of the humic acids were blocked by methylation to prevent any contribution to the complexation reaction.

The metal ions under consideration were heavy metal ions like copper, lead, zinc, and cadmium and the actinide elements uranium, neptunium, and plutonium.

3.1 Heavy metal ions

Tab. 1 summarises the experimental conditions and the complexation constants log β_{LC} for the heavy metal ions Cu, Zn, Cd, and Pb. Log β_{LC} is deduced according to the metal-ion charge neutralisation model by introducing the loading capacity (LC). The corresponding loading capacities are found in Fig. 1 and Appendix C. The complexation constants for Pb, Zn, and Cd presented here are similar to the constants given in previous studies within a previous project [1].

Tab. 1: Complexation constants for complexes between the heavy metal ions copper, zinc, cadmium, lead and Aldrich humic acid. For better comparison some experimental conditions are also given.

Metal	[Me] (mol/L)	HA	[HA] mg/L	I	log β_{LC}	Methods
Divalent:						
Pb^{2+}	10^{-6} – 10^{-4}	AHA	25	0.01	5.1 – 5.6	ASV, IF-CE, WDMT
		M42	25	0.01	5.1	ASV
Zn^{2+}	10^{-6} – 10^{-4}	AHA	25	0.01	4.0 – 4.1	ASV
	10^{-6} – 10^{-4}	M42	25	0.01	4.0 – 4.1	ASV
Cd^{2+}	10^{-6} – 10^{-4}	AHA	25	0.01	4.0 – 4.1	ASV
	10^{-6} – 10^{-4}	AHA	25	0.01	4.2 – 4.4	ASV
Cu^{2+}	10^{-6} – 10^{-4}	AHA	25	0.01	5.3	WDMT

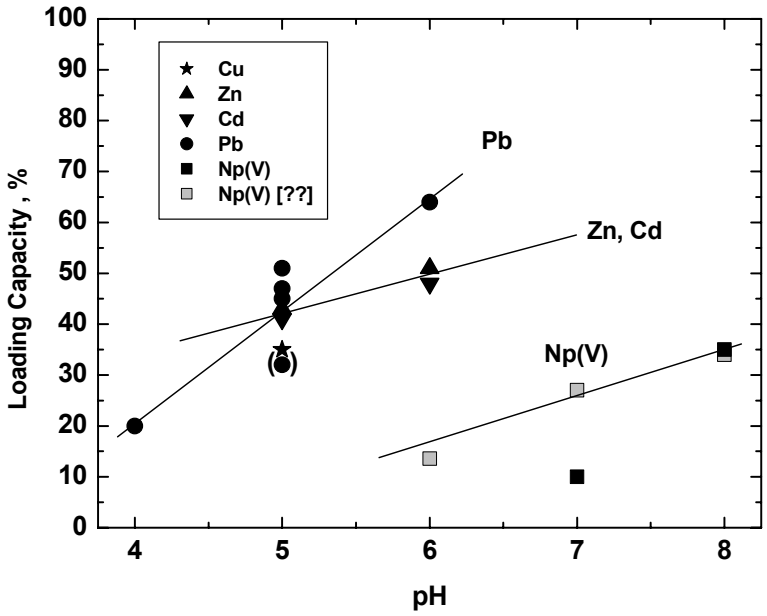

Fig. 1: Variation of the loading capacity for Aldrich humic acid with pH value for divalent heavy metal ions copper, zinc, cadmium, lead and for comparison the pentavalent actinide neptunium (Values for Np(V) partly from [2]).

3.2 Actinides

With pentavalent neptunium, the influence of the metal ion concentration, the humic acid concentration, humic acid molecules with blocked phenolic OH groups, and synthetic humic acids has been studied using different methods. These effects on neptunium humate complexation are illustrated in Fig. 2 and Fig. 3. With a decrease of the total neptunium concentration at constant humic acid concentration, the complexation constants $\log\beta_{LC}$ increase by 0.4–0.9 units for AHA, M42, and M1. The fact, that this phenomenon also occurs for synthetic humic acids excludes any inorganic impurities in natural HA as origin for stronger complexation. A reason for that apparently stronger complexation of NpO_2^+ is not found yet but it is supposed that, at low metal concentration, the complexation and dissociation kinetics vary considerably, i.e., the system might not be in equilibrium within the time period of the experiments.

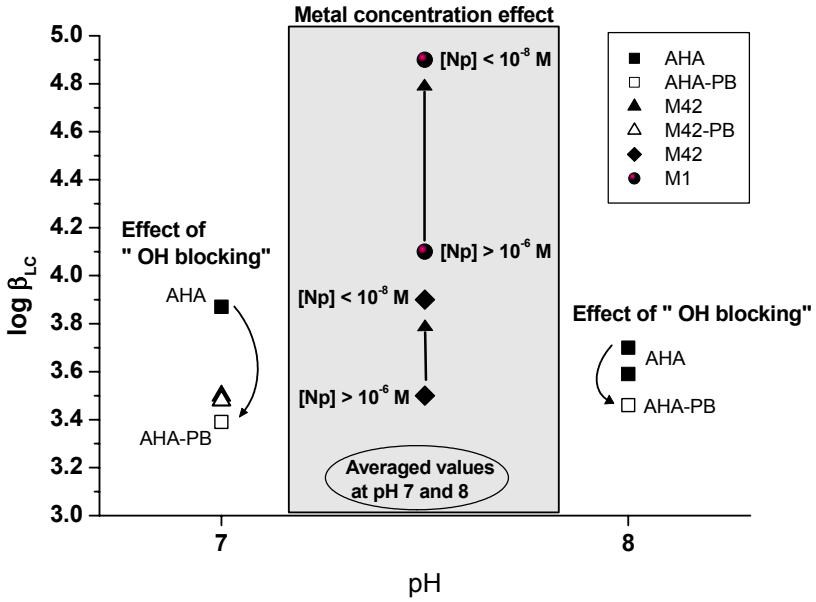

Fig. 2: Impact of metal concentration effect and blocking of phenolic OH groups on the complexation constants $\log\beta_{LC}$ for Np(V) humate complexation. Blocking of phenolic OH-groups minimise the $\log\beta_{LC}$. Decreasing metal ion concentration enlarges the complexation constant (grey box). Because $\log\beta_{LC}$ does not vary significantly with pH in a small metal concentration range, averaged values are plotted in the grey box.

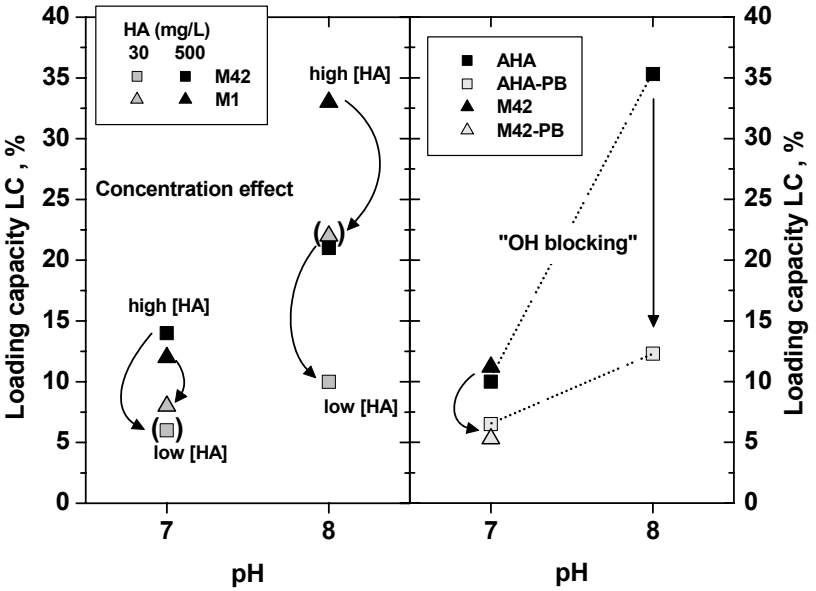

Fig. 3: Impact of humic acid concentration and blocking of phenolic OH groups on the loading capacity (LC). *Right:* LC is reduced by blocking the phenolic OH groups of humic acid. *Left:* LC is also reduced with decreasing humic acid concentration. The values in the brackets show, however, very large uncertainties in the fit used to determine LC. Explanations for humic acid abbreviations are found in section 2.2.

A smaller effect on the complexation constant is observed between AHA and the “OH-blocked” AHA-PB: here the $\log\beta_{LC}$ decreases by about 0.3–0.5 units, which is close to the uncertainty of the complexation constant. For the synthetic humic acid M42, no such effect was observed at pH 7. The effect of blocking the OH groups is more pronounced by looking at the loading capacity: not only with decreasing pH value but also with “blocking” the loading capacity decreases significantly. This could be a hint that phenolic groups are also involved in the complexation process.

Studies of the humate complexation of neptunyl ions in a wide concentration range of humic acid (30 – 500 mg/L) have shown a decrease of the loading capacity with decreasing humic acid concentration, (Fig. 3). A conclusive explanation for this behaviour cannot be given so far, but may be explained by kinetic effects.

Preliminary experiments on the humate complexation of tetravalent Pu have been performed. They revealed the complex nature of plutonium and that its chemistry is dominated by kinetically controlled reactions like hydrolysis, colloid formation, and redox reactions. Further experiments will be part of a new project.

3.3 EXAFS studies

A better understanding of the metal-HA interaction may be possible if some information is available concerning its structure and stereochemistry as well as the nature and the number of complexing functional groups of the humic acid molecules. The nearest-neighbour coordination of Pu(III), Th(IV), Np(IV) and Np(V) humate complexes were investigated by EXAFS. Several different humic acids have been taken including the humic acids with blocked phenolic OH groups. For comparison, the cation exchanger Bio-Rex 70 acts as a well defined polyelectrolyte with only carboxylic groups as complexing groups.

Coordination number and distances of the different humic acids and the Bio-Rex 70 (Appendix A) are very similar. These results may be interpreted such that monodentate coordination of all metal ions with the carboxylic group dominates. Furthermore, the coordination environment is not changed when the physico-chemical conditions vary.

Tab. 2: List of some coordination parameters obtained by EXAFS measurements:

Metal-Humate	Coordination number N	Distance R (Å)	References
Pu(III)-HA	6.1–7.3	2.45	
Pu^{3+} aquo ion	*7.6*	*2.48*	*[3]*
Th(IV)-HA	10.6	2.44	
Th(IV)-HA	9.4–10.1	2.43–2.44	[4]
Th^{4+} aquo ion	*10.8*	*2.45*	*[5]*
Np(IV)-HA	10.1–11.3	2.36	
Np^{4+} aquo ion	*9.0 – 11.2*	*2.37–2.40*	*[6,7]*
Np(V) – O-eq.	2.3–2.8	2.48–2.49	
Np(V) – O-eq.	5.2	2.47	[8]
NpO_2^+ aquo ion (-O-eq.)	*5*	*2.50*	*[7]*

The differences in the coordination number of the equatorial O-atoms for the pentavalent neptunyl ion cannot be explained (2.3–2.8 ←→ 5.2). A final conclusion of the coordination of humic complexed metal ions requires more studies (Appendix A).

4 Redox Chemistry

Reduction of U(VI) to U(IV) by HA

To elucidate the redox stability of redox sensitive actinide ions, studies were done with U(VI) and AHA, Hyd-Glu, and Cat-Gly. The two latter humic acids are synthetic ones with much higher redox capacities than AHA. By laser-induced photoacoustic spectroscopy (LPAS) it was shown that both synthetic humic acids reduce U(VI) to U(IV), whereas no reduction occurred with AHA. These results confirm not only the high redox capacity but also the high reducing strength of the synthetic HA in contrast to AHA. The formation of a tetravalent uranium is proven by the absorption bands at 640 and 646 nm for a complexed U(IV) species (Appendix A).

Reduction of Pu(VI) by HA

To reduce U(VI) to the tetravalent state, a humic acid with high reducing strength is necessary. Contrary to that, Pu(VI) can be reduced much easier. Already with AHA about 60 % of Pu(VI) is converted to Pu(V) after 50 hours. By taking a natural Gorleben groundwater, that was kept under anaerobic conditions and had an Eh value near –200 mV, Pu(VI) was reduced quantitatively within a few minutes. At pH 1.7 Pu(III), Pu(IV), and Pu(V) were found by monitoring the reduction reaction over 20 hours with liquid-liquid extraction and CE. At higher pH values the reduction proceeds much faster. When the same experiment was repeated

with the same groundwater after having removed the humic substances by ultrafiltration, it becomes evident that the humic substances are responsible for the reduction. The mechanisms of the reduction reactions are rather complex and require further studies (Appendix B)

Clarification of redox mechanism

In order to get insight in the redox processes of humic acids, reduction of Fe(III) by designed humic acids with variable redox functionalities has been studied. Although these experiments point out that phenolic OH groups may be involved in the redox reaction, the redox mechanisms are not clear because the amount of phenolic OH groups is still in contradiction to the redox capacity, which is much higher than what can be expected from a single oxidation of an OH group. This high capacity points to secondary reactions of phenoxy radicals, phenolic OH groups, aldehydes, conjugated double bond systems and others that could be involved in the redox process. (Appendix A)

5 Sorption Experiments

Sorption of metal ions onto mineral surfaces in the presence of humic acid is one important process that has to be understood to assess migration behaviour of metal ions in environment. Within the project several experiments on the sorption of metal ions onto mineral phases have been performed in the presence and absence of humic acids – mainly with quartz sand, but also with granite and other minerals. These experiments are summarised in Tab. 3.

Tab. 3: Experimental conditions of sorption experiments performed within this project.

Metal ion	Solid phase	HA	[Me] mol/L	[HA] mg/L	m(Solid) g/L	pH
Cu^{2+}	Quartz sand	AHA	10^{-9} – 10^{-3}	0 and 25	250	3-9
Zn^{2+}	Quartz sand	AHA	10^{-9} – 10^{-3}	0 and 25	250	3-9
Cd^{2+}	Quartz sand	AHA	10^{-9} – 10^{-3}	0 and 25	250	3-9
Pb^{2+}	Quartz sand	AHA	10^{-9} – 10^{-3}	0 and 25	250	3-9
La^{3+}	Quartz sand	AHA	10^{-11}–10^{-6}	0 and 5	70	4 and 6
*Tb^{3+}	Quartz sand	AHA	1×10^{-7}	0 and 5	70	3 – 6.5
*Tb^{3+}	Granite	AHA	1×10^{-7}	0 and 5	70	3 – 6.5
*Tb^{3+}	Phyllite	AHA	1×10^{-7}	0 and 5	7	3 – 6.5
*Tb^{3+}	Diabase	AHA	1×10^{-7}	0 and 5	7	3 – 6.5
*Th(IV)	Quartz	^{14}C-M42	1.2×10^{-8}	0 and 20	5 and 50	3 – 7
*Th(IV)	Quartz sand	^{14}C-M42	1.2×10^{-8}	0 and 20	5 and 50	3 – 7
*NpO_2^+	Quartz	^{14}C-M42	1.3×10^{-6}	0 and 27	5	4 – 11
*NpO_2^+	Granite	^{14}C-M42	1.3×10^{-6}	0 and 27	5	4 – 11
*NpO_2^+	Muscovite	^{14}C-M42	1.3×10^{-6}	0 and 27	5	4 – 11
*NpO_2^+	Orthoclase	^{14}C-M42	1.3×10^{-6}	0 and 27	5	4 – 11
*NpO_2^+	Albite	^{14}C-M42	1.3×10^{-6}	0 and 27	5	4 – 11
*NpO_2^+	Biotite	^{14}C-M42	1.3×10^{-6}	0 and 27	5	4 – 11

*: Parallel to the ternary system, sorption of the metal ion (without HA) and the HA (without metal ion) on the solid have been studied.

Also the sorption of humic acid onto the same solid phases has been studied in the absence of interfering metal ions in solution. The competitive character of calcium and magnesium ions – components of the natural bulk solution – on the metal sorption has also been probed. Generally the following results were obtained:

- Humic acid absorption onto the used mineral surfaces decreases with increasing pH value (pH 3 to 11), due to increasing deprotonation of the surface. However, biotite is an exception, that shows the same behaviour from pH 3 to 9, but has a minimum at pH 9 with subsequently increasing HA sorption from pH 9 to 11.

- Th(IV), Np(V), La, Tb, Cu, Zn, Cd, and Pb show an increasing sorption with increasing pH (starting at pH 3, no HA present), reaching a plateau at a certain pH depending on the metal ion. However, sometimes the sorption becomes weaker at higher pH values like for Tb sorption onto phyllite.

- The presence of HA in solution makes the sorption of metal ions onto solid phases much more complex, because the interaction between the metal ion and HA, HA and the mineral surface, are in competition with the metal ion sorption itself.

    - The sorption of Th(IV) is slightly affected by HA. Strength and kind of the influence depend on the mineral phase and pH value. The sorption behaviour is described for quartz and quartz sand in Appendix A.

    - For Np(V) the sorption keeps constant or is reduced at pH values between 4 and 11. However, muscovite and orthoclase slightly enhance the sorption between pH 6 and 8.5 (s. Appendix A).

    - For trivalent metal ions like La and Tb, the sorption is enhanced at pH values lower than about 5 and is reduced at higher pH values. This can be explained by the sorption pattern of HA – sorption at low pH and decreasing sorption with increasing pH. Trivalent metal ions are strongly complexed with HA in solution for high pH values and complexed with HA sorbed on the mineral surface at lower pH values. This typical behaviour is not found for phyllite, where the sorption of Tb is reduced over the total pH range (3–7). (s. Appendix D).

    - HA has only a small effect on the sorption of Cd and Zn, whereas the sorption of Cu and Pb is reduced at pH lower than 5 as known from the trivalent metal ions (s. Appendix C).

6 Column Experiments

The column experiments performed in this project are summarised very briefly in Table 4. In most experiments, the surface of the stationary phase was not in equilibrium with the humic acid from the mobile phase. These type of experiment should demonstrate a sudden break-in of a strange solution containing toxic metal ions and humic substances into a geologic matrix. Fundamental process elucidation is very difficult because the kinetics of all possible reactions – adsorption of humic acid, metal ion, and metal humate to the mineral surface, as well as dissociation of metal humate complexes – govern the observations. Usually, in deep geological systems, the geologic matrix is in equilibrium with aquifer solutions that becomes disturbed by the toxic metal ions only. To simulate this, 3 column experiments were conducted with stationary phases that were equilibrated with the mobile phase for weeks up to months prior to spiking the metal ion.

All experiments reveal that the migration of metal ions is enhanced by humate complexation. The amount of metal humate that can migrate unretardedly depends basically on the complexation constant of the humate, the pH value, equilibration time between metal ion and humic acid, migration time in the column, and type of the mineral phase. More data are found in certain chapters of the Appendices.

7 Miscellaneous Studies and Work

Within the project, a lot of additional work has been done, that is described very briefly in the following. Again, more details are found in the Appendices.

Competition of potassium, calcium, aluminium and magnesium ions on humate complexation of metal ions

The competition effects of K, Ca, and Mg ions on the humate complexation were examined. At a 1000 fold excess of K^+, Mg^{2+}, and Ca^{2+} the complexation of Zn^{2+} is suppressed by ~20, ~30, and ~ 70 %. For Pb^{2+}, that is stronger bound to humic acid, with 1000 fold excess of K^+, Mg^{2+}, Ca^{2+}, and Al^{3+}, no significant effect for K^+ and Mg^{2+} has been observed, whereas for Ca^{2+} 60 % and Al^{3+} 95 % of lead ions were displaced. The competition effect between La^{3+} and Al^{3+} depends on different kinetic modes. The lowest La complexation occurs when Al^{3+} is pre-equilibrated with HA prior spiking the La^{3+} to the solution. In the reverse experiment when La^{3+} is pre-equilibrated with the humic acid, the displacement of lanthanum by Al^{3+} is much lower.

Tab. 4: Experimental conditions of column experiments performed within this project.

Metal ion	Stationary phase	HA in the Mobile phase	Equilibration time Me ←→ HA	Migration time	pH	Column length x diameter (cm)	Recovery %	Appendix
U(VI), $1x10^{-5}$ M	Quartz sand[i]	^{14}C-M42 (50 mg/L)	98 h	~ 21 h	7.5	25 x 5	80 ± 1	A
U(VI), $1x10^{-5}$ M	Quartz sand[i]	–	–	~ 21 h	7.5	25 x 5	43 ± 2	A
U(IV)/(VI), $1x10^{-6}$ M	Quartz sand[i]	^{14}C-M42 (50 mg/L)	2 h	~ 21 h	7.5	25 x 5	66 ± 5 (U(IV))	A
–	Quartz sand[i]	^{14}C-M42 (50 mg/L)	–	~ 21 h	7.5	25 x 5	91 ± 1 (HA)	A
Pu(IV), $9.5x10^{-6}$ M	Gorleben sand[i]	Groundwater GoHy 532 (60-70 mg/L HA)	18 – 23.5h	5.7 h	6.8	25 x 5	≤ 4	B
Cu(II)[ii], Zn(II)[ii], Cd(II), Pb(II)[ii], $1x10^{-5}$ M	Quartz sand	AHA (25 mg/L)	24 h	~ 7 min	6.4, 7.4	25 x 1	80 –90 (Cd(II))	C
Cu(II)[ii], Zn(II)[ii], Cd(II), Pb(II)[ii], $1x10^{-5}$ M	Quartz sand	–	24 h	~ 7 min	6.4, 7.4	25 x 1	80 –90 (Cd(II))	C
without metal ions	Quartz sand, Granite, Phyllite, Diabase	AHA[iii], Bog Soil HA[iii], Bog water HA and FA[iii], M42[iii]	–	~2.5 h	6.0	40 x 1.6	60 – 90 (HA)	D

i: Equilibrated more than 3 weeks with mobile phase before spiked with metal ions.

ii: Cu(II), Pb(II) show very high sorption on sand. Measurement of Zn(II) was impossible due to a high underground signal.

iii: HA and FA were radio-labelled with ^{111}In or ^{131}I

In the same way the competition effects of the divalent and trivalent metal ions Ca^{2+}, Mg^{2+}, and Al^{3+} on the sorption of heavy metal ions on mineral phases were studied. The results are found in the Appendices C and D.

Studies on hydrophilicity of humic acids

Octanol-water partitioning of humic acids under certain conditions was used to monitor changes in the hydrophilicity of the humic molecules. By changing pH, ionic strength, HA concentration and labelling of the humic acid, different distributions of HA between octanol and water occur, pointing to changes in the hydrophilicity.

Integration of the Metal Ion Charge Neutralisation Model (MICN) into the geochemical speciation code EQ3/6

There are many models in the literature that describe interactions between humic substances and metal ions. They differ in their approaches to describe the binding sites at the humic acid molecules – a short overview is given in Appendix A. For the description of the interaction between metal ion and humic acid, the metal ion charge neutralisation model (MICN) was chosen. The decision is caused by the relative simplicity of MICN, and experience with a lot of experimental data records from several earlier studies.

The MICN was embedded into the geochemical speciation code EQ3/6. The metal-humate complexation is usually not considered in such codes, but cannot be neglected in many natural systems. In Appendix A the procedure, the progress and the problems are described.

Establishment of a "Database for Humics complexation – DHC"

One essential part in modelling the behaviour of metal ions in the environment is a consistent thermodynamic database. Unfortunately, the present situation in humate complexation data cannot comply with the requirement of such a consistent data base. The data quality of metal humate complexation is very heterogeneous and data from different research groups are difficult to compare. One reason is the physico-chemical description of the complexation reaction, which is not uniform. For a humate complexation database, only one model has to be used to evaluate the complexation constant. Therefore, the metal charge neutralisation model (MICN), which is based on experimental parameters, was chosen to make humate complexation data comparable. Re-assessing of all data with respect to MICN and integrating the data in a well designed data base would be a possible way to achieve the goal.

Within the project period, a database was established covering all the complexation constants published so far. Its name is "Database for Humics Complexation – DHC". It provides an overview concerning types of humic substances, ligands, and parameter ranges like concentration, ionic strength, pH, Eh,… The most critical gaps in the database can be identified and the data quality can be assessed more easily. So far the DHC contains 12 different types of HA, 20 data records of PEC and 81 complexation constants together with the LC (s. Appendix A).

8 References

[1] Marquardt, C. M. (Ed.): Influence of Humic Acids on the Migration Behaviour of Radio active and Non-radioactive Substances under Conditions Close to Nature, *Wissenschaftliche Berichte*, FZKA 6557, Forschungszentrum Karlsruhe, Germany, 2000.

[2] Seibert, A., Mansel, A., Marquardt, C.M., Keller, C., Kratz, J.V., Trautmann, N.: Complexation Behaviour of Neptunium With Humic Acid, Radiochim. Acta, **89**, 505 (2001).

[3] Reich, T., Geipel, G., Funke, H., Hennig, C., Roßberg, A., Bernhard, G.: First XANES and EXAFS Measurements of Plutonium Solutions at ROBL, *Annual Report,* FZR-285, Forschungszentrum Rossendorf, Germany, 2000.

[4] Denecke, M.A., Bublitz, D., Kim, J.I., Moll, H., Farkes, I.: EXAFS Investigation of the Interaction of Hafnium and Thorium With Humic Acid and Bio-Rex 70, J. Synchroton Rad., **6**, 394 (1999).

[5] Moll, H., Denecke, M.A., Jalilehvand, F., Sandström, M., Grenthe, I.: Structure of the Aqua Ions and Fluoride Complexes of Uranium(IV) and Thorium(IV) in Aqueous Solution an EXAFS Study, Inorg. Chem., **38**, 1795 (1999).

[6] Antonio, M.R., Soderholm, L., Williams, C.W., Blaudeau, J.-P., Bursten, B.E.: Neptunium Redox Speciation, Radiochim. Acta, **89**, 17 (2001).

[7] Allen, P.G., Bucher, J.J., Shuh, D.K., Edelstein, N.M., Reich, T.: Investigation of Aquo and Chloro Complexes of $UO2^{2+}$, NpO_2^{+}, Np^{4+}. and Pu^{3+} by X-Ray Absorption Fine Structure Spectroscopy, Inorg. Chem., **36**, 4676 (1997).

[8] Denecke, M.A., Dardenne, K., Marquardt, C.M.: Np(IV) / Np(V) Valence Determinations from Np L3 edge XANES/EXAFS, to be published, 2004.

Appendix A Institut für Radiochemie, Forschungszentrum Rossendorf

INVESTIGATION OF THE COMPLEXATION AND THE MIGRATION OF ACTINIDES AND NON-RADIOACTIVE SUBSTANCES WITH HUMIC ACIDS UNDER GEOGENIC CONDITIONS

COMPLEXATION OF HUMIC ACIDS WITH ACTINIDES IN THE OXIDATION STATE IV Th, U, Np

S. Sachs, K. Schmeide, V. Brendler, A. Křepelová, J. Mibus,

G. Geipel, T. Reich[1], K.H. Heise, G. Bernhard

Final Report

Support Contract Number
02 E 9299

Forschungszentrum Rossendorf e.V.
P.O. Box 510119
D-01314 Dresden, Germany
Internet: www.fz-rossendorf.de

[1] present adress:
Institut für Kernchemie
Johannes-Gutenberg Universität Mainz
Fritz-Straßmann-Weg 2
55099 Mainz
Internet: www.kernchemie.uni-mainz.de

Content

Abstract

Objective of this project was the study of basic interaction and migration processes of actinides in the environment in presence of humic acids (HA). To obtain more basic knowledge on these interaction processes synthetic HA with specific functional properties as well as ^{14}C-labeled HA were synthesized and applied in comparison to the natural HA Aldrich. One focus of the work was on the synthesis of HA with distinct redox functionalities. The obtained synthetic products that are characterized by significantly higher Fe(III) redox capacities than Aldrich HA were applied to study the redox properties of HA and the redox stability of U(VI) humate complexes. It was confirmed that phenolic OH groups play an important role for the redox properties of HA. However, the results indicate that there are also other processes than the single oxidation of phenolic OH groups and/or other functional groups contributing to the redox behaviour of HA. A first direct-spectroscopic proof for the reduction of U(VI) by synthetic HA with distinct redox functionality was obtained.

The complexation behaviour of synthetic and natural HA with actinides (Th, Np, Pu) was studied. Structural parameters of Pu(III), Th(IV), Np(IV) and Np(V) humates were determined by X-ray absorption spectroscopy (XAS). The results show that carboxylate groups dominate the interaction between HA and actinide ions. These are predominant monodentately bound. The influence of phenolic OH groups on the Np(V) complexation by HA was studied with modified HA (blocked phenolic OH groups). The blocking of phenolic OH groups induces a decrease of the number of maximal available complexing sites of HA, whereas complex stability constant and Np(V) near-neighbour surrounding are not affected.

The effects of HA on the sorption and migration behaviour of actinides was studied in batch and column experiments. Th(IV) sorption onto quartz and Np(V) sorption onto granite and its mineral constituents are affected by the pH value and the presence of HA. HA exhibits a significant influence on the transport of U(IV) and U(VI) in a laboratory quartz sand system.

In order to provide the basis for a more reliable modelling of the actinide transport, the metal ion complexation with HA has to be integrated into existing geochemical speciation codes. Within this project the metal ion charge neutralization model was embedded into the geochemical modelling code EQ3/6. In addition to that, a digital data base was developed which covers HA complexation data basing on the charge neutralization model.

1 Introduction

Studies on the migration behaviour of radioactive and non-radioactive toxic substances are of high importance for the reliable long-term risk assessment of potential underground nuclear waste repositories, of facilities of the former uranium mining and milling sites in Saxony and Thuringia (Germany), and of subsurface dumps and sites with radioactive and/or heavy metal containing inventory. Depending on the prevailing geochemical conditions different materials and processes can influence the behaviour of such pollutants in natural aquifer systems. Therefore, knowledge on these processes and materials is indispensable for the trustworthy modelling of the migration of radioactive and toxic metal ions, e.g., actinide ions, in the nature.

Besides inorganic ligands such as sulfate, phosphate, arsenate and silicate, humic acids (HA), organic macromolecules ubiquitous found in natural environments, play an important role in the interaction processes of actinide ions. HA are soluble in the pH range of natural waters and possess the ability for complex and colloid formation. In addition to that, HA are characterized by redox properties, which can influence the oxidation state of metal ions. For instance, HA can reduce Np(VI) to Np(V), Pu(VI) to Pu(IV) [1] and U(VI) to U(IV) [2]. Due to these properties HA can affect the speciation of metal ions, e.g., actinide ions, and therefore, their migration in the environment. The colloidal behaviour of HA together with their high complexing ability for metal ions may cause an effective transport mechanism for actinides.

The chemistry of penta- and hexavalent actinides under aerobic conditions was already subject of a number of investigations also in the presence of HA. However, under reducing conditions, as prevalent in deep underground environments, e.g., in deep groundwaters [3], actinides can occur in the tetravalent oxidation state, which then dominates their speciation and migration. The data base for the interaction behaviour of actinides in the tetravalent oxidation state is small and the basic scientific understanding of these processes is low. The existing data on the interaction between HA and tetravalent actinides (e.g., [4-9]) is not sufficient for the geochemical modelling of the migration behaviour of actinides.

The main focus of this research project was on the study of basic interaction and migration processes of actinides (U, Np, Pu, Th) in different oxidation states, especially in the tetravalent, in the presence of HA. In order to gain a more basic knowledge on these processes, synthetic HA with different functional properties and ^{14}C-labeled HA were applied in comparison to natural HA from Aldrich. Partially, these substances were already developed and successfully used in our previous project funded by BMBF (contract number 02 E 88150), where the interaction between HA and uranium under aerobic conditions was the main subject of interest [10]. Within the present project new batches of HA were prepared and synthesis methods were optimised. In addition to that, synthetic HA with distinct redox functionalities were developed for detailed studies on the redox properties of HA and on the redox stability of actinide humate complexes. In order to improve the knowledge on the complexation between HA and actinides in lower oxidation states and for the enhancement of existing complexation models for the HA complexation, thermodynamic and structural studies on actinide (Pu(III), Np(IV), Np(V), Th(IV)) humate complexes were performed. The influence of HA on the sorption and migration behaviour of actinides (U(IV), U(VI), Th(IV), Np(V)) was studied in

batch and column experiments, respectively. The reliable geochemical modelling of the actinide transport requires the integration of the actinide HA complexation as well as of current experimental data into existing modelling programs. It was the aim of this project to integrate the HA metal ion complexation in a suitable modelling code. In addition to that, it was focused on the development of a digital data base on the HA metal ion complexation because no accepted and consistent data base is available for that up to now.

The research project was performed in close collaboration with the R&D projects of the Universities of Mainz and Saarbrücken and of the Institute for Interdisciplinary Isotope Research Leipzig (IIF) that were funded by the Bundesministerium für Wirtschaft und Arbeit (BMWA) under contract number 02 E 9309 and 02 E 9329, respectively, and with the Institute for Nuclear Waste Management (INE) of the Forschungszentrum Karlsruhe.

Within the framework of this project the main emphasis of the studies of the Institute of Radiochemistry (Forschungszentrum Rossendorf) was on the following topics:

1. Synthesis and characterization of HA model substances with different functionalities including their modification and ^{14}C-labeling. Synthetic HA were to be provided to the project partners. Development of synthetic HA with distinct redox functionalities.

2. Studies on the redox properties of HA and on the redox stability of actinide humate complexes.

3. Structural and thermodynamical studies on the actinide complexation by HA applying synthetic HA model substances and natural HA. The main focus was on structural studies on the interaction of HA with actinides in lower oxidation states (Th, Np, Pu) and on the influence of phenolic OH groups on the Np(V) complexation by HA.

4. Studies on the influence of HA on the sorption of Np(V), Th(IV) onto relevant rock materials and minerals and on the migration of U(IV)/U(VI) in a laboratory system.

5. Software and model development: Integration of the metal ion charge neutralization model [11] for the description of the HA complexation into the speciation code EQ3/6 [12].

6. Development of a digital data base for the HA complexation based on the metal ion charge neutralization model.

The scientific results of this project are described in detail in the following sections.

2 Natural humic acid reference material

As in the previous project [10], commercially available natural HA from Aldrich (AHA; Aldrich, Steinheim, Germany) was used as reference material. Before use, the sodium salt of AHA

(Batch H1, 675-2) was purified according to the purification method described by Kim and Buckau [13] in order to remove inorganic contaminants of this substance.

For preparation of batch A2/98, the sodium salt of AHA was dissolved in 0.1 M NaOH (Merck, Darmstadt, Germany) containing 0.01 M NaF. The solution was stirred over night under nitrogen atmosphere. After that, the solution was centrifuged to separate the alkali-insoluble components of the sodium humate. To precipitate the HA, the supernatant was acidified with HCl (Merck) to pH 1. The HA precipitate was isolated by centrifugation and washed with 0.1 M HCl and water. The whole purification procedure was repeated three times. Subsequently, purified HA AHA (batch A2/98) was dried by lyophilisation.

3 Synthesis and characterization of humic acids with specific functional properties

In order to improve the knowledge on the interaction processes between HA and metal ions, e.g., actinide ions, various HA model substances with different functional properties were already developed at the Institute of Radiochemistry. These include synthetic HA with different functional group contents and various structural elements [10,14], chemically modified HA with blocked phenolic OH groups [10,15,16] as well as ^{14}C-labeled HA [10,17]. Within this project, synthetic HA with distinct redox functionalities were developed.

The following paragraphs show the synthesis, modification, ^{14}C-labeling and characterization of different synthetic HA model substances with various functional properties that were performed within the scope of this project.

3.1 Synthesis and ^{14}C-labeling of humic acid type M42

3.1.1 Synthesis of humic acid type M42

Within this project a new batch of synthetic HA type M42 (batch M145) was synthesized. It was made available to all project partners for comparative studies.
The basic synthesis of HA type M42 was already described in detail in [10]. It starts from a mixture of 22 g glutamic acid monohydrate (Merck), 33 g xylose (Merck) and 60 mL water which is heated for 92 hours at 80 ± 2 °C under reflux and inert gas. After expiration of the reaction time and cooling of the reaction mixture the formed solid melanoidin fraction is separated from the liquid fraction by centrifugation. Then, the solid product is washed and ground with ethanol (Merck) and ether (Merck). Similar to the isolation of natural HA [18], the HA-like melanoidin fractions are extracted by stirring the solid product with 2 M NaOH (Merck) for 8 hours under inert gas. The synthetic HA is precipitated from the alkaline solution with 2 M HCl (Merck). The resulting HA precipitate is washed, dialyzed using dialysis tubes (Spectra/Por®, exclusion limit MWCO <1000, Roth, Karlsruhe, Germany) against purified water, and lyophilised.

52 g synthetic HA type M42 (batch M145) were synthesized. For that, seven synthesis sequences, each with six parallel batches, were performed.

3.1.2 Synthesis of ^{14}C-labeled humic acid type M42 ([^{14}C]M42)

Carbon-14 labelled synthetic HA are synthesized according to the unlabeled HA type M42, however, applying ^{14}C-labeled amino acids, e.g., [u-^{14}C]glutamic acid, as starting materials [10,17]. In the present project two batches of ^{14}C-labeled synthetic HA type M42 ([^{14}C]M42) were synthesized as described above, batch M170 and M180. Batch M170 was synthesized starting from 27.75 g xylose, 18.33 g glutamic acid monohydrate and 50 mL water. 2 mg [u-^{14}C]glutamic acid (111 MBq) were added to the precursor substances. Batch M180 was prepared from 8.95 g xylose, 5.91 g glutamic acid monohydrate, 5.4 mg [u-^{14}C]glutamic acid (296 MBq) and 16 mL water. These syntheses resulted in 932 mg (batch M170) and 368 mg (batch M180) synthetic HA type [^{14}C]M42 with specific activities of 2.38 MBq/g and 17.0 MBq/g, respectively. In both syntheses, only 2 % of the starting ^{14}C-activity were incorporated into the HA-like synthetic product. Evaluating this radiochemical yield is has to be taken into account that the HA-like fraction of the reaction product is small compared to the other fractions that are formed during the synthesis, e.g., preliminary products, human and fulvic acid-like fractions. The differences in the specific activities of the reaction product are due to the different specific activities of the reaction mixtures used for the syntheses.
100 mg of synthetic HA type [^{14}C]M42 (batch M180) were provided to the Institute of Interdisciplinary Isotope Research Leipzig for sorption experiments.

3.1.3 Characterization of synthetic humic acid type M42 and [^{14}C]M42

Table 3.1 summarizes the elemental compositions and the functional group contents of the newly synthesized batches of HA type M42 and [^{14}C]M42 in comparison to the data of the purified, commercially available, natural HA from Aldrich (AHA) and natural HA from literature [19,20].
Synthetic HA type M42 shows an elemental composition that is similar to those of AHA and other natural HA. It contains no sulfur due to the use of sulfur-free precursor substances. Comparing the ash content of synthetic HA type M42 with that of AHA it becomes obvious that the synthetic product is characterized by a very low content on inorganic constituents.

The carboxyl group content and the proton exchange capacity (PEC) of HA type M42 are comparable to those of AHA and other naturally occurring HA. In addition to that, HA type M42 shows an amount of phenolic/acidic OH groups that is similar to natural HA. Comparing the functional group contents of the unlabeled and ^{14}C-labeled synthetic HA type M42 it becomes obvious that these agree well in the range of their standard deviations. This fact points to a good reproducibility of the synthesis with regard to the HA functional group content.

Tab. 3.1: Characterization of HA type M42 (batch M145) and [^{14}C]M42 (batch M170 and M180) in comparison to natural HA.

HA	Elemental composition						
	C (%)	H [a] (%)	N (%)	S (%)	O [b] (%)	Ash (%)	Mois-ture (%)
Type M42 (batch M145)	56.1 ± 0.3	4.1 ± 0.1	4.4 ± 0.1	-	26.8 ± 0.3	0.11	8.4
AHA (batch A2/98)	58.6 ± 0.1	3.0 ± 0.1	0.8 ± 0.1	3.8 ± 0.1	23.5 ± 0.1	2.39	7.9
Natural [19]	50 - 60	4 – 6	2 - 6	0 - 2	30 – 35		

	Functional groups		
	COOH [c] (meq/g)	PEC [d] (meq/g)	Phenolic/acidic OH [e] (meq/g)
Type M42 (batch M145)	3.76 ± 0.09	3.51 ± 0.07	2.0 ± 0.2
Type [^{14}C]M42 (batch M170)	3.63 ± 0.03	3.55 ± 0.05	Not measured
Type [^{14}C]M42 (batch M180)	3.59 ± 0.01	3.36 ± 0.53	Not measured
AHA (batch A2/98)	4.49 ± 0.14	4.60 ± 0.08	3.1 ± 0.1
Natural [20]	1.5 – 5.7		2.1 – 5.7

[a] Corrected for the water content of the HA. [b] The oxygen content was calculated from the difference to 100 % in consideration of the ash and moisture content of the HA. [c] Determined by calcium acetate exchange [21]. [d] PEC: Proton Exchange Capacity. Determined by potentiometric titration. [e] Radiometrically determined [10,22].

In Fig. 3.1 the FTIR spectra (FTIR spectrometer Spectrum 2000, Perkin Elmer; KBr method) of HA type M42 and [^{14}C]M42 are depicted in comparison to that of natural HA from Aldrich. In general, synthetic HA type M42 shows IR absorption bands which are similar to those observed for natural HA [10,19]. The comparison of the FTIR spectra of HA type M42 and [^{14}C]M42 in terms of the position of the IR absorption bands and the band intensities shows that all three spectra are nearly identical. Thus, it can be concluded that the unlabeled and ^{14}C-labeled synthetic HA type M42 show comparable structures, which points to a good reproducibility of the synthesis concerning the HA structure.

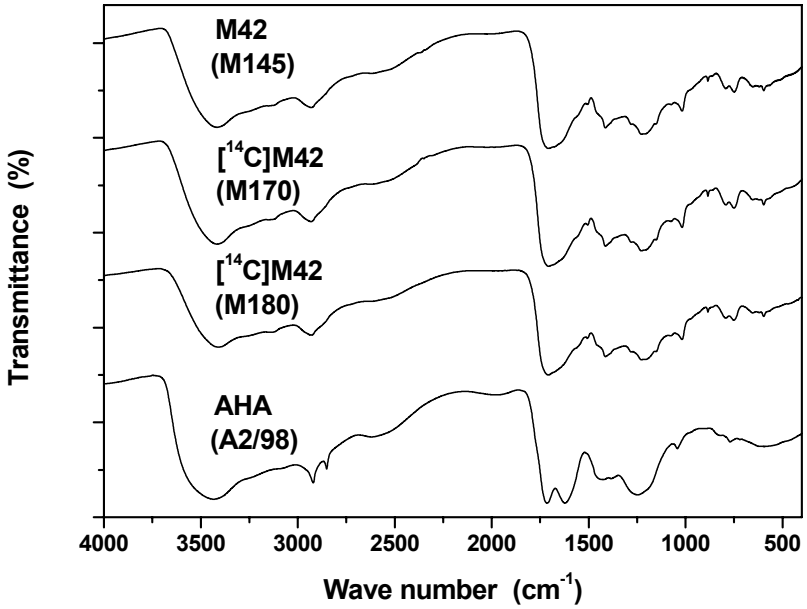

Fig. 3.1: FTIR spectra of unlabeled and ^{14}C-labeled synthetic HA type M42 in comparison to natural HA AHA.

3.2 Synthesis and characterization of chemically modified humic acids with blocked phenolic OH groups

In order to study the influence of phenolic OH groups on the interaction behaviour of HA we developed and verified a method for the synthesis of chemically modified HA with blocked phenolic OH groups by methylation with diazomethane [10,15,16]. Such modified HA were already successfully used to study the influence of phenolic OH groups on the U(VI) complexation by natural and synthetic HA [15,23].

Figure 3.2 shows the reaction scheme for the chemical modification process applied. In the first modification step the original HA is methylated with diazomethane for three hours at –5 to 5 °C in methanolic solution. This methylation results in the formation of methyl esters of carboxyl groups and methyl ethers of phenolic/acidic OH groups. The methylation is repeated several times and stopped when the incorporation of diazomethane into the HA molecule is completed. The solvent, that is distilled from the reaction mixture, shows then the yellow colour of the non-reacted excess of diazomethane. In the second modification step the methylated HA is treated with alkaline solution (2 M NaOH) at room temperature under inert gas to hydrolyse the methyl esters of carboxyl groups that were formed by methylation with diazomethane. However, methyl ether groups of phenolic OH groups remain blocked because these cannot be decomposed by alkaline hydrolysis. After hydrolysis, the modified HA with blocked phenolic OH groups is precipitated with 2 M HCl, separated by centrifugation, dialyzed (MWCO < 1000), and lyophilised. It should be noted that in addition to phenolic OH groups also other acidic OH groups of the HA, i.e., enolic OH groups or acidic OH groups substituted to five-membered heterocycles can be methylated with diazomethane, resulting in non-hydrolisable ether groups. Applying this method we obtained partially modifications of

HA phenolic/acidic OH groups. We modified for instance, 68 % and 74 % of the originally occurring phenolic/acidic OH groups of HA AHA and M42, respectively [10].

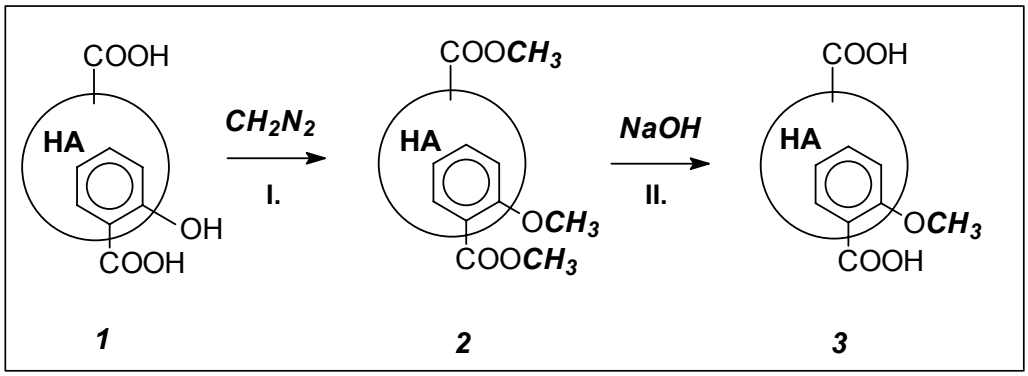

Fig. 3.2: Scheme for the synthesis of chemically modified HA with blocked phenolic OH groups. 1: original HA, 2: methylated HA (type HA-B), 3: HA with blocked phenolic OH groups (type HA-PB).

In the present project the modification procedure that was applied up to now was optimised. In order to achieve a complete blocking of all phenolic/acidic OH groups of HA type M42 and AHA the whole modification procedure (step 1: methylation with diazomethane, step 2: alkaline hydrolysis of the methylated HA) was repeated three times. That means, the methylated HA with blocked phenolic/acidic OH groups that was obtained within the first modification cycle was subjected to a second and third methylation cycle.

Table 3.2 shows the functional group contents of modified HA type M42 (M42-PB) and AHA (AHA-PB) that were obtained with the optimised methylation procedure in comparison to those of the unmodified HA. After three methylation cycles 75 % and 84 % of the initially occurring phenolic/acidic OH groups of HA type M42 and AHA, respectively, were modified. These results show that even after a threefold replication of the methylation procedure a complete blocking of all phenolic/acidic OH groups is not possible.

Tab. 3.2: Functional group contents of modified and unmodified HA type M42 and AHA.

HA	COOH [a] (meq/g)	PEC [b] (meq/g)	Phenolic/acidic OH [c] (meq/g)	Phenolic/acidic OH : COOH
Type M42 (batch M145)	3.76 ± 0.09	3.51 ± 0.07	2.0 ± 0.2	0.53
M42-PB (batch M171)	3.12 ± 0.07	3.23 ± 0.15	0.5	0.16
AHA (batch A2/98)	4.49 ± 0.14	4.60 ± 0.08	3.1 ± 0.1	0.69
AHA-PB (batch M173)	2.67 ± 0.01	3.13 ± 0.15	0.5	0.19

[a] Determined by calcium acetate exchange [21]. [b] PEC: Proton Exchange Capacity. Determined by potentiometric titration. [c] Radiometrically determined [10,22].

Up to now, it could not be confirmed whether those functional groups that are determined after the modification are unmodified original phenolic/acidic OH groups of the HA or acidic OH groups that were released during the derivatisation process by uncovering formerly sterically hindered functional groups. Comparing the carboxyl group content and the PEC of the corresponding unmodified and modified HA it becomes obvious that the modified HA, especially HA AHA, have less carboxyl groups and lower PEC than the original unmodified HA. An incomplete hydrolysis of methyl ester groups that were formed during the methylation could be one possible reason for that observation. ^{13}C-CP/MAS-NMR spectroscopic results support this conclusion [16]. Nevertheless, for both HA the molar ratio of phenolic/acidic OH to carboxyl groups becomes smaller due to the modification. This enables us to use these chemically modified HA to study the impact of phenolic/acidic OH groups on the interaction between HA and metal ions.

3.3 Humic acids with distinct redox functionalities

The migration behaviour of toxic and radiotoxic metal ions, e.g., actinides, strongly depends on their oxidation state that can be influenced by HA [1]. Therefore, the detailed description of the influence of HA on the mobility of actinides in the environment requires the understanding of the effects of HA on the oxidation states of actinides besides the knowledge on the actinide ion complexation by HA. In order to study the redox properties of HA and the redox stability of actinide humate complexes in more detail, we developed synthetic HA model substances with pronounced redox functionalities.

3.3.1 Synthesis of humic acid-like oxidation products from phenolic compounds

The redox activity of humic substances can be ascribed to the redox system hydroquinone-quinone and the oxidation of phenolic OH groups to phenoxy radicals [24] with their typical subsequent reactions, such as coupling reactions and tautomerisations. Both systems are schematically shown in Fig. 3.3 [25]. Based on this knowledge, we decided to synthesize HA with high amounts of phenolic OH groups in order to obtain HA with distinct redox functionalities.

The performed syntheses are based on the oxidation of different phenolic compounds in alkaline solution in the absence or presence of amino acids. Potassium peroxodisulfate was used as oxidizing agent [26,27]. Within the project different types of HA-like oxidation products of phenolic compounds were synthesized starting from hydroquinone, catechol or vanillic acid in the absence or presence of glycine or glutamic acid. Table 3.3 summarizes the starting materials for the synthesized HA model substances.

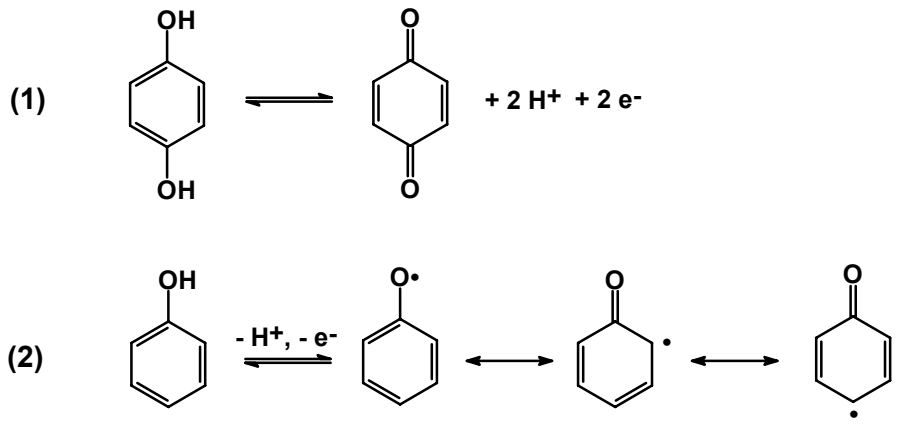

Fig. 3.3: Scheme for the redox system hydroquinone-quinone (1) and the oxidation of phenols to phenoxy radicals (2).

Tab. 3.3: Starting materials for the synthesis of HA based on the oxidation of phenolic compounds (basic batch sizes).

HA	Phenolic compound		Amino acid	
Type Hyd	11.35 mmol	Hydroquinone	-	-
Type Hyd-Gly	11.35 mmol	Hydroquinone	11.35 mmol	Glycine
Type Hyd-Glu	11.35 mmol	Hydroquinone	5.69 mmol	Glutamic acid
Type Cat-Gly	11.35 mmol	Catechol	11.35 mmol	Glycine
Type Van-Gly	11.30 mmol	Vanillic acid	11.35 mmol	Glycine

For syntheses, the starting materials were dissolved in 0.1 M NaOH (425 mL for HA type Hyd and 450 mL for the other HA per basic batch size) at room temperature. Within one hour potassium peroxodisulfate (6.25 g per basic batch size) was charged to the reaction mixture at room temperature (HA type Hyd) or at 60 °C (HA type Hyd-Gly, Hyd-Glu, Cat-Gly, Van-Gly). After that, the reaction mixtures were cooled down and the HA-like fractions of the oxidation products were precipitated by addition of HCl. The HA precipitates were separated by centrifugation, purified by dialysis against purified water (MWCO <1000), and lyophilised.

3.3.2 Characterization of humic acid-like oxidation products from hydroquinone, catechol and vanillic acid

The HA-like oxidation products from phenolic compounds were characterized in terms of their elemental composition, functional group content and structure. In order to characterize

the redox properties of these synthetic products we determined their Fe(III) redox capacities in comparison to HA type M42 and AHA. The Fe(III) redox capacity represents the charge equivalents per mass unit HA that can be transferred to Fe(III).

Elemental composition

The elemental compositions of the different oxidation products from phenolic compounds are summarized in Tab. 3.4 in comparison to those of HA type M42, AHA and natural HA from literature [19].

All synthetic products exhibit elemental compositions that are close to those of natural HA. Those oxidation products that were synthesized in the presence of glycine or glutamic acid are characterized by higher nitrogen contents compared to that of AHA due to the use of the nitrogen-containing starting materials. In comparison to synthetic HA type M42 (synthesis product of xylose and glutamic acid, cf. 3.1), the oxidation products from hydroquinone and catechol show lower hydrogen contents. This result points to a higher aromaticity of these substances due to their aromatic precursor substances.

Tab. 3.4: Elemental composition of HA-like oxidation products of phenolic compounds in comparison to HA type M42 and natural HA.

HA	C (%)	H [a] (%)	N (%)	S (%)	O [b] (%)	Ash (%)	Moisture (%)
Type Hyd (batch R9/01)	59.8 ± 0.4	3.2 ± 0.1[c]	0.3 ± 0.1	0.3 ± 0.1	36.4 ± 0.4	n.m.[d]	n.m.
Type Hyd-Gly (batch R12/02)	54.2 ± 0.2	2.3 ± 0.2	5.3 ± 0.1	0.4 ± 0.1	26.7 ± 0.2	1.3	9.9
Type Hyd-Glu (batch R13/02)	53.7 ± 0.1	2.3 ± 0.1	2.0 ± 0.1	0.2 ± 0.1	28.2 ± 0.1	1.6	11.9
Type Cat-Gly (batch R18/02)	48.8 ± 0.1	2.8 ± 0.2	5.1 ± 0.1	0.9 ± 0.1	31.1 ± 0.2	1.7	9.5
Type Van-Gly (batch R5/02)	52.5 ± 0.5	4.0 ± 0.1[c]	4.5 ± 0.1	1.0 ± 0.3	38.0 ± 0.2	n.m.	n.m.
Type M42 (batch M145)	56.1 ± 0.3	4.1 ± 0.1	4.4 ± 0.1	-	26.8 ± 0.3	0.1	8.4
AHA (batch A2/98)	58.6 ± 0.1	3.0 ± 0.1	0.8 ± 0.1	3.8 ± 0.1	23.5 ± 0.1	2.4	7.9
Natural [19]	50 – 60	4 – 6	2 – 6	0 – 2	30 – 35		

[a] Corrected for the water content of the HA. [b] The oxygen content was calculated from the difference to 100 % in consideration of the ash and moisture content of the HA. [c] Not corrected for the water content of the HA. [d] n.m.: not measured.

Functional groups

Table 3.5 summarizes the functional group contents of the oxidation products from hydroquinone, catechol and vanillic acid in comparison to those of HA type M42 and natural HA. From this table it can be concluded that all HA-like oxidation products from di-phenolic compounds (hydroquinone and catechol) show significantly higher phenolic/acidic OH group contents than HA type M42 and AHA. As expected, HA type Hyd shows the lowest carboxyl group content, but the highest amount on phenolic/acidic OH groups. In contrast to that, HA

type Hyd-Gly, Hyd-Glu, Cat-Gly and Van-Gly, that were synthesized in the presence of amino acids show higher carboxyl group contents and PEC values. These are similar to those of HA type M42, AHA and other natural HA. Comparing the functional group contents of the oxidation products that were synthesized from different phenolic precursor substances (Hyd-Gly, Cat-Gly, Van-Gly) in the presence of glycine it becomes obvious that the synthetic product of vanillic acid and glycine (Van-Gly) shows the highest carboxyl group content but the lowest phenolic/acidic OH group as expected. Its amount on phenolic/acidic OH groups is comparable to that of AHA.

Tab. 3.5: Functional group contents of the HA-like oxidation products of phenolic compounds in comparison to HA type M42 and natural HA.

HA	COOH [a] (meq/g)	PEC [b] (meq/g)	Phenolic/acidic OH [c] (meq/g)
Hyd (batch R9/01)	1.92 ± 0.05	2.68 ± 0.01	7.2 ± 0.1
Hyd-Gly (batch R12/02)	4.30 ± 0.14	4.29 ± 0.13	5.3 ± 0.7
Hyd-Glu (batch R13/02)	3.84 ± 0.27	3.65 ± 0.14	5.8 ± 0.2
Cat-Gly (batch R18/02)	4.16 ± 0.04	3.59 ± 0.01	6.6 ± 0.7
Van-Gly (batch R5/02)	5.74 ± 0.08	5.17 ± 0.33	3.3 ± 1.3
M42 (batch M145)	3.76 ± 0.09	3.51 ± 0.07	2.0 ± 0.2
AHA (batch A2/98)	4.49 ± 0.14	4.60 ± 0.08	3.1 ± 0.1
Natural [20]	1.5 – 5.7		2.1 – 5.7

[a] Determined by calcium acetate exchange [21]. [b] PEC: Proton Exchange Capacity. Determined by potentiometric titration. [c] Radiometrically determined [10,22].

From these results it can be concluded that it is possible to vary the functionality of HA-like oxidation products from phenolic compounds by varying their precursor substances. A comparable conclusion was already drawn for the synthesis of HA model substances based on the melanoidin concept by condensation of reducing sugars and α-amino acids [14].

Structure

All synthetic HA were characterized by FTIR spectroscopy. By these measurements it was found that the oxidation products of phenolic compounds show FTIR absorption bands that are also characteristic for natural HA [10,19]. As expected, the synthetic products show variations in their structural elements due to the use of different precursor substances.
As example, Fig. 3.4 shows the FTIR spectra of the oxidation products from hydroquinone that were synthesized in the absence or presence of glycine and glutamic acid, respectively. The spectra are compared to that of HA AHA.

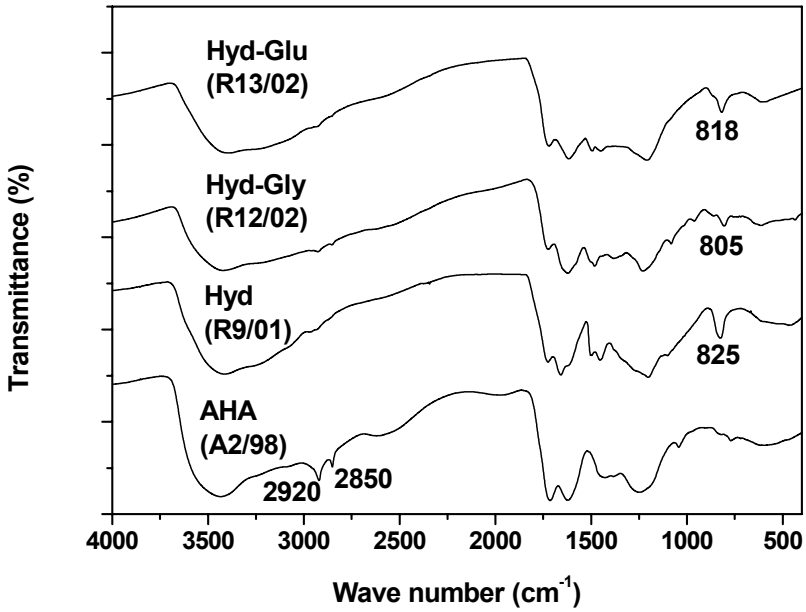

Fig. 3.4: FTIR spectra of HA-like oxidation products from hydroquinone in comparison to natural HA AHA.

In comparison to AHA all hydroquinone-based synthetic products show an intense absorption signal between 805 and 825 cm^{-1}. These bands are characteristic for para–substituted aromatic structural elements due to the use of hydroquinone as starting material. In addition to that, there are no significant FTIR bands indicating high amounts on aliphatic structural elements, as found for AHA at 2850 and 2920 cm^{-1}. From that it can be concluded that these synthetic products show a higher aromaticity than AHA. In all spectra FTIR absorption bands are found that confirm the occurrence of carboxyl groups in the HA structure (~1720 cm^{-1}).

Determination of Fe(III) redox capacities

According to Mack et al. [28,29] we determined for the synthetic HA the Fe(III) redox capacities in comparison to HA type M42 and AHA at pH 3. For that, suspensions of $FeCl_3$ and HA were shaken under nitrogen atmosphere and exclusion of light ([$FeCl_3$]: 8.2-8.5 mmol/L, [HA]: 0.12 g/L, pH 3, I: 0.1 M KCl). The Fe(II) ions formed by the reduction process depending on time were quantified in aliquots of the suspensions. Fe(II) was measured in form of the 1,10-phenanthroline complex by UV-VIS spectroscopy (mod. 8452, Hewlett Packard) [30]. Prior to the quantification of Fe(II), the HA were separated by precipitation with H_2SO_4 and Fe(III) was masked by NH_4F. Besides the separation of HA from the sample aliquots, the addition of H_2SO_4 causes also the release of Fe(II) ions complexed with and/or sorbed onto HA molecules.

Furthermore, we determined for selected HA the Fe(III) redox capacities at pH 9.2 as described by Matthiessen [31]. For this we investigated solutions of $K_3[Fe(CN)_6]$ and HA under nitrogen atmosphere and exclusion of light ([$K_3[Fe(CN)_6]$]: 0.5 mmol/L, [HA]: 5 mg/L, I: 0.1 M KCl, borate buffer: pH 9.2). The time-dependent consumption of $K_3[Fe(CN)_6]$ due to the reduction of Fe(III) was followed by UV-VIS spectroscopy.

The Fe(III) redox capacities of the HA depending on time were calculated from the measured Fe(II) concentrations in the HA suspensions with $FeCl_3$ and from the decrease of the $K_3[Fe(CN)_6]$ concentration in the solutions with HA.

Fe(III) redox capacities at pH 3

In Fig. 3.5 the Fe(III) redox capacities of the hydroquinone-based oxidation products are displayed in dependence on the reaction time. They are compared to those of HA type M42 and AHA.

In the initial phase of the reaction between HA and $FeCl_3$ the redox capacities increase fast with increasing reaction time. Then, a slower increase of the redox capacities was observed. This pH- and time-dependent Fe(III) reduction by HA was kinetically studied by Mack [29]. It was described by a fast and a subsequent slow kinetically controlled process.

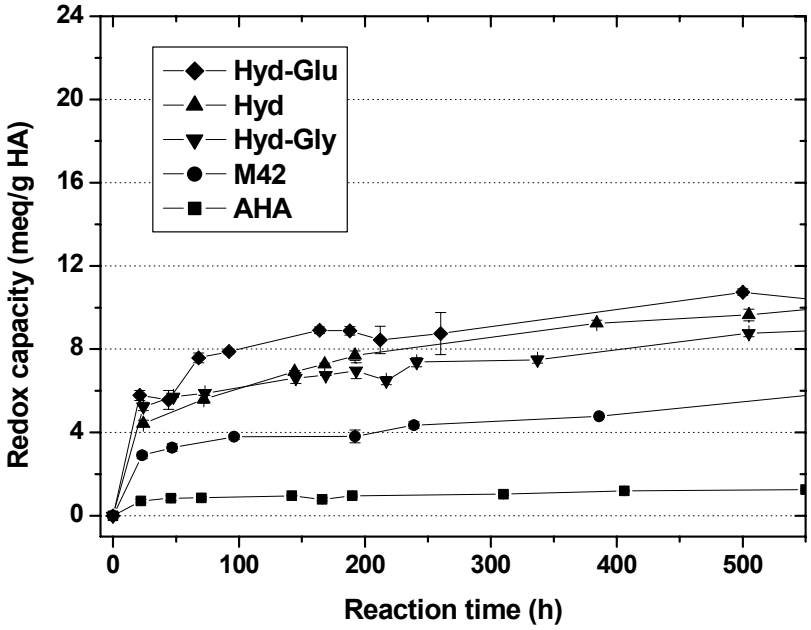

Fig. 3.5: Fe(III) redox capacities of hydroquinone-based HA-like oxidation products in comparison to HA AHA and M42.

From Fig. 3.5 it can be concluded that all synthetic HA based on hydroquinone show significantly higher Fe(III) redox capacities than HA type M42 and AHA. These higher redox capacities can be ascribed to the higher phenolic/acidic OH group contents of the oxidation products from hydroquinone. Similar results were found comparing the data of the oxidation products from different phenolic compounds and glycine which are depicted in Fig. 3.6.

Although synthetic HA type Van-Gly has a phenolic/acidic OH group content that is comparable to AHA (Tab. 3.5), all synthetic products exhibit higher redox capacities than AHA. The differences in the redox capacities of HA AHA and type Van-Gly points to structural differences of both HA influencing their redox behaviour. Compared to the synthetic products of di-phenols and glycine (Hyd-Gly, Cat-Gly), HA type Van-Gly has the lowest redox capacity

which can be attributed to its lower phenolic/acidic OH group content. Among these, HA type Cat-Gly shows the highest Fe(III) redox capacity at pH 3 and also the highest phenolic/acidic OH group content. These results point to a correlation between the phenolic/acidic OH group content of the HA-like oxidation products from different phenolic precursor substances and glycine and their Fe(III) redox capacities.

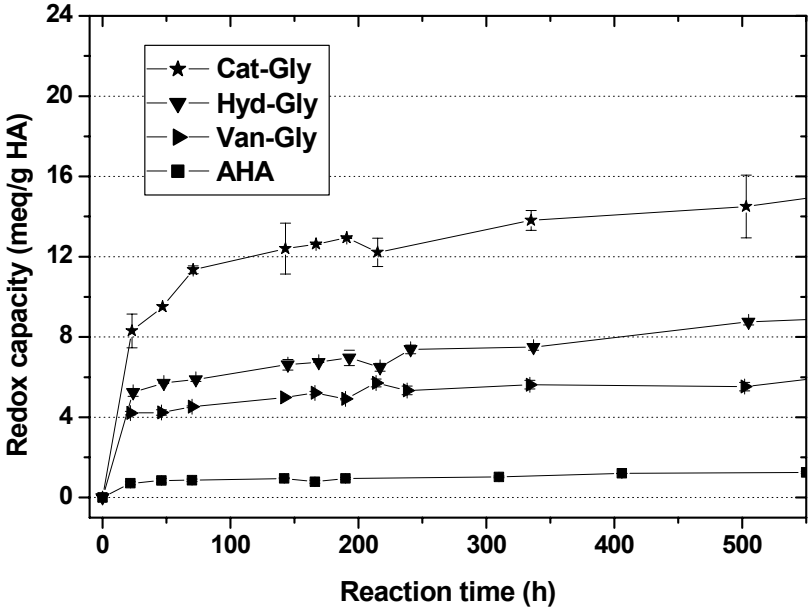

Fig. 3.6: Fe(III) redox capacities of synthetic HA based on the oxidation of different phenolic compounds in the presence of glycine.

Table 3.6 summarizes the Fe(III) redox capacities at pH 3 after about 3 weeks for all HA under investigation. From that it becomes obvious that synthetic HA type Cat-Gly shows the highest Fe(III) redox capacity under the considered experimental conditions. It is about twelve times higher than that of AHA.

Tab. 3.6: Fe(III) redox capacities for different synthetic HA in comparison to AHA at pH 3 after about 3 weeks reaction time.

HA	Redox capacity [a] (meq/g HA)
Hyd (batch R9/01)	9.6 ± 0.3
Hyd-Gly (batch R12/02)	8.8 ± 0.2
Hyd-Glu (batch R13/02)	10.7 ± 0.2
Cat-Gly (batch R18/02)	14.5 ± 1.6
Van-Gly (batch R5/02)	5.5 ± 0.2
M42 (batch M145)	6.1 ± 0.1
AHA (batch A2/98)	1.2 ± 0.1

[a] Mean values of duplicate measurements.

Referring the redox capacities of the HA to their phenolic/acidic OH group content, it becomes possible to draw conclusions concerning the kind of the redox active, i.e. electron-transferring, functional groups. In Fig. 3.7 the redox capacities of all studied HA after about 3

weeks are compared to their phenolic/acidic OH group contents. In contrast to HA AHA, all synthetic HA show redox capacities at pH 3 that are higher than their phenolic/acidic OH group contents. This result indicates that there are additional HA functional groups or other redox processes than the single oxidation of phenolic OH groups contributing to the reduction of Fe(III) within 3 weeks reaction time. For AHA the redox capacity is lower than its amount on phenolic/acidic OH groups which points to the fact that not all of these functional groups are contributing to the redox process.

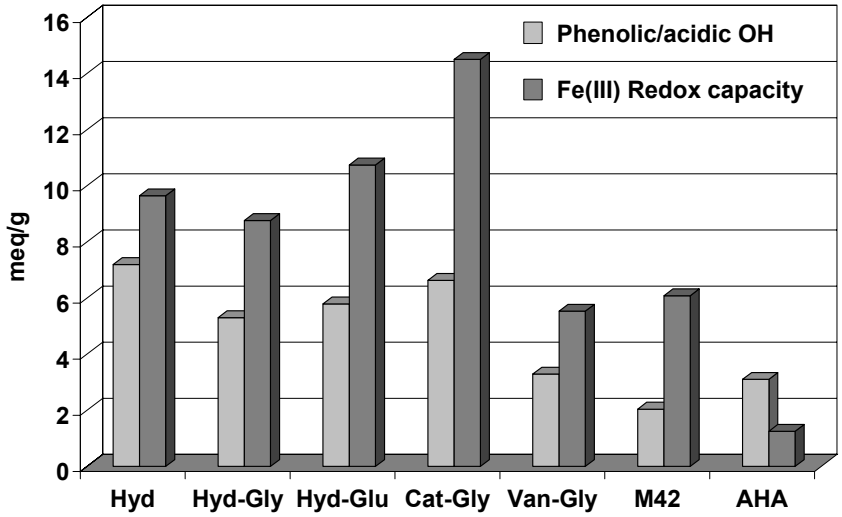

Fig. 3.7: Fe(III) redox capacities of the studied HA at pH 3 after 3 weeks reaction time in comparison to their phenolic/acidic OH group contents.

Based on the results of the Fe(III) redox capacity measurements at pH 3 HA type Hyd-Gly, Hyd-Glu and Cat-Gly were chosen as reference materials for HA model substances with pronounced redox functionalities. Therefore, they were additionally characterized with regard to their redox properties in the alkaline pH range.

Fe(III) redox capacities at pH 9.2

Figure 3.8 shows the ferricyanide redox capacities of HA type Hyd-Gly, Hyd-Glu and Cat-Gly as a function of time. They are compared to those of HA type M42 and AHA. The measured redox capacities at pH 9.2 after about 3 weeks are listed in Tab. 3.7.

Tab. 3.7: Fe(III) redox capacities for different synthetic HA in comparison to AHA at pH 9.2 after about 3 weeks reaction time.

HA	Redox capacity [a] (meq/g HA)
Hyd-Gly (batch R12/02)	27.5 ± 2.7
Hyd-Glu (batch R13/02)	33.6 ± 4.0
Cat-Gly (batch R18/02)	36.9 ± 0.2
M42 (batch M145)	18.1 ± 0.6
AHA (batch A2/98)	7.2 ± 1.9

[a] Mean values of duplicate measurements.

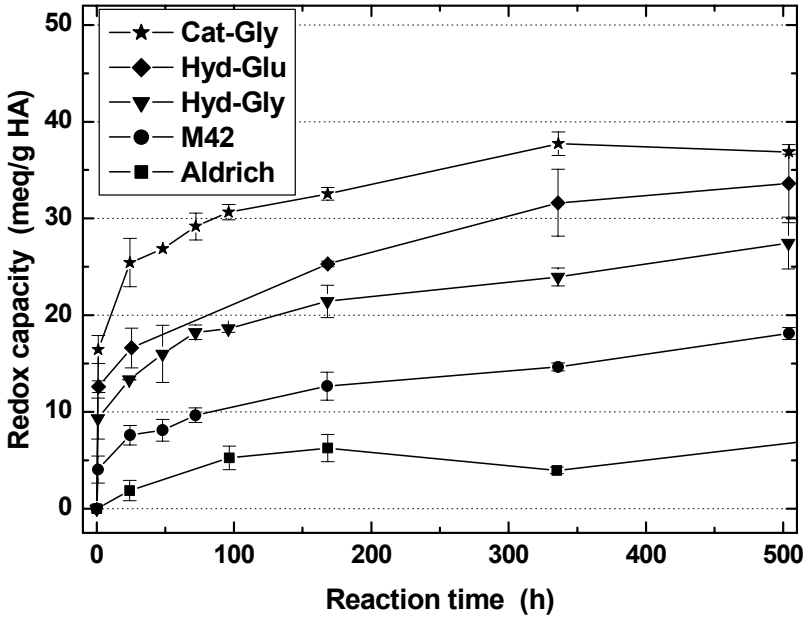

Fig. 3.8: Fe(III) redox capacities of synthetic HA based on the oxidation of hydroquinone and catechol at pH 9.2 in comparison to HA type M42 and AHA.

From Fig. 3.8 and Tab. 3.7 it becomes obvious that all studied HA show higher Fe(III) redox capacities at pH 9.2 than at pH 3. Even at pH 9.2, all HA-like oxidation products from hydroquinone and catechol are characterized by higher redox capacities than AHA and M42 which can be ascribed to their higher phenolic/acidic OH group contents. The highest redox capacity at pH 9.2 exhibits HA type Cat-Gly. This result is comparable to that at pH 3. Figure 3.9 displays the Fe(III) redox capacities of the HA at pH 9.2 after about 3 weeks in comparison to their phenolic/acidic OH group contents.

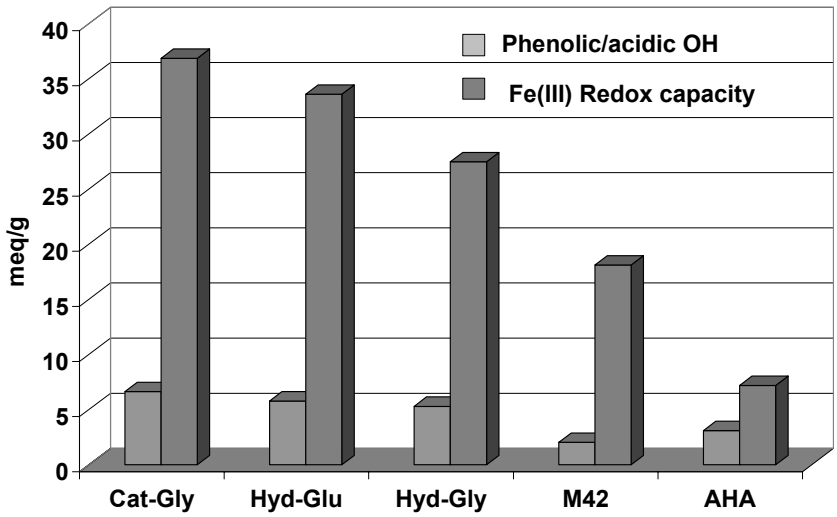

Fig. 3.9: Fe(III) redox capacities of the studied HA at pH 9.2 after 3 weeks reaction time in comparison to their phenolic/acidic OH group contents.

Also at pH 9.2, all HA show significantly higher redox capacities than those which would be expected assuming that only phenolic OH groups contribute to the reduction of Fe(III). From that it can be concluded again, that there are further processes than the single oxidation of phenolic OH groups or further HA functional groups that are also contributing to the reduction of Fe(III).

From all characterization results the conclusion can be drawn that it is possible to synthesize HA-like substances with pronounced redox functionalities by oxidation of phenolic compounds in the presence or absence of amino acids. By variation of the starting materials synthetic HA with varying elemental, functional and structural properties can be obtained.
Applying these HA model substances further studies on the redox properties of humic substances and on the redox stability of actinide humate complexes were performed. These are described in chapter 4 and 5, respectively.

4 Studies on the influence of phenolic OH groups on the redox behaviour of natural and synthetic humic acids

The redox behaviour of HA is ascribed to the system hydroquinone-quinone and the oxidation of phenolic OH groups (Fig. 3.3). However, the Fe(III) redox capacities at pH 3 and pH 9.2 that were measured for the HA-like oxidation products of phenolic compounds (see chapter 3.3.2) and also for HA type M42 and AHA (pH 9.2) are higher than those which would be expected assuming that only phenolic OH groups contribute to the reduction of Fe(III). In order to characterize the role of phenolic/acidic OH groups on the redox behaviour of HA type Hyd-Gly, Hyd-Glu, Cat-Gly, M42 and AHA, we synthesized the corresponding HA with blocked phenolic/acidic OH groups by methylation with diazomethane (cf. 3.2). Applying these modified HA we determined the Fe(III) redox capacities at pH 3 (comparable to [29]) and at pH 9.2. We compared the results with those of the corresponding unmodified, original HA.

Table 4.1 summarizes the functional group contents of the studied unmodified and modified HA with blocked phenolic OH groups (HA-PB). Due to the modification with diazomethane all HA show significantly lower phenolic/acidic OH group contents. The amounts on these functional groups were decreased by 72 to 84 %. For all HA a lowering of the carboxyl group content due to the modification was observed. This could be due to an incomplete hydrolysis of the carbonic methyl esters as already discussed in chapter 3.2. However, the molar ratio of phenolic/acidic OH to carboxyl groups is decreased for all HA. Therefore, we were able to apply these modified HA for the study of the influence of phenolic OH groups on the redox behaviour of HA.
Figure 4.1 shows exemplary for the unmodified and modified HA type Hyd-Glu the Fe(III) redox capacities at pH 3 and pH 9.2. In Tab. 4.2 the results for all studied HA are listed.

Tab. 4.1: Functional group contents of HA before and after modification with diazomethane.

HA	Modification	COOH (meq/g)	Phenolic/acidic OH (meq/g)	Phenolic/acidic OH : COOH
Hyd-Gly (batch R12/02)	Original	4.30 ± 0.14	5.3 ± 0.7	1.23
	Blocked phenolic/acidic OH	2.99 ± 0.10	1.5 ± 0.1	0.50
Hyd-Glu (batch R13/02)	Original	3.63 ± 0.20	5.8 ± 0.2	1.60
	Blocked phenolic/acidic OH	2.67 ± 0.03	1.4 ± 0.1	0.52
Cat-Gly (batch R18/02)	Original	4.16 ± 0.04	6.6 ± 0.7	1.59
	Blocked phenolic/acidic OH	2.88	1.3 ± 0.1	0.45
M42 (batch M145)	Original	3.76 ± 0.09	2.0 ± 0.2	0.53
	Blocked phenolic/acidic OH	3.12 ± 0.07	0.5	0.16
AHA (batch A2/98)	Original	4.49 ± 0.14	3.1 ± 0.1	0.69
	Blocked phenolic/acidic OH	2.67 ± 0.01	0.5	0.19

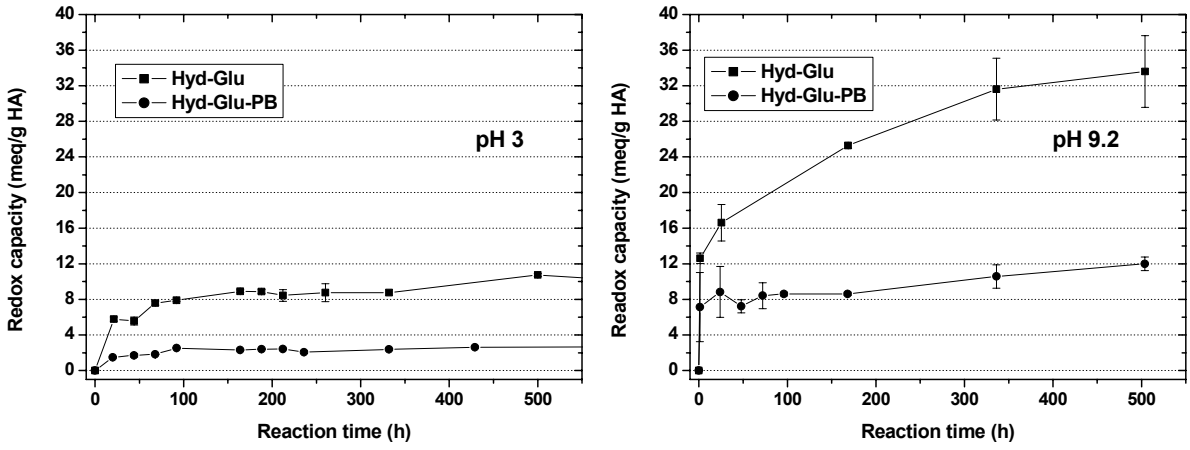

Fig. 4.1: Redox capacities of the unmodified and modified HA type Hyd-Glu with blocked phenolic/acidic OH groups.

Tab. 4.2: Redox capacities of the unmodified and modified HA after a reaction time of about 3 weeks.

HA	Modification	Fe(III) redox capacity at pH 3 [a] (meq/g HA)	Fe(III) redox capacity at pH 9.2 [a] (meq/g HA)
Hyd-Gly (batch R12/02)	Original	8.8 ± 0.2	27.5 ± 2.7
	Blocked phenolic/acidic OH	3.0 ± 0.2	10.1 ± 1.8
Hyd-Glu (batch R13/02)	Original	10.7 ± 0.2	33.6 ± 4.0
	Blocked phenolic/acidic OH	2.6 ± 0.1	12.0 ± 0.8
Cat-Gly (batch R18/02)	Original	14.5 ± 1.6	36.9 ± 0.2
	Blocked phenolic/acidic OH	2.7 ± 0.2	13.4 ± 0.1
M42 (batch M145)	Original	6.1 ± 0.1	18.1 ± 0.6
	Blocked phenolic/acidic OH	1.8 ± 0.1	7.6 ± 1.2
AHA (batch A2/98)	Original	1.2 ± 0.1	7.2 ± 1.9
	Blocked phenolic/acidic OH	0.5 ± 0.1	3.4 ± 1.4

[a] Mean values of duplicate measurements.

From Fig. 4.1 and Tab. 4.2 it becomes obvious that all modified HA with blocked phenolic/acidic OH groups show significant lower redox capacities at pH 3 and pH 9.2 than the corresponding unmodified, original HA. The observed decrease of the redox capacities at pH 3 is in agreement with first data described by Mack [29].

Due to the modification, the phenolic/acidic OH group content decreases, for instance, for HA type Hyd-Glu by 76 %. As a consequence of that the Fe(III) redox capacity at pH 3 and pH 9.2 is reduced by 76 % and 64 %, respectively. These results indicate that phenolic/acidic OH groups play a major role in the redox behaviour of the studied HA-like oxidation product from hydroquinone. However, also for the modified HA Fe(III) redox capacities were determined that are higher than their remaining phenolic/acidic OH group contents, which is depicted in Fig. 4.2.

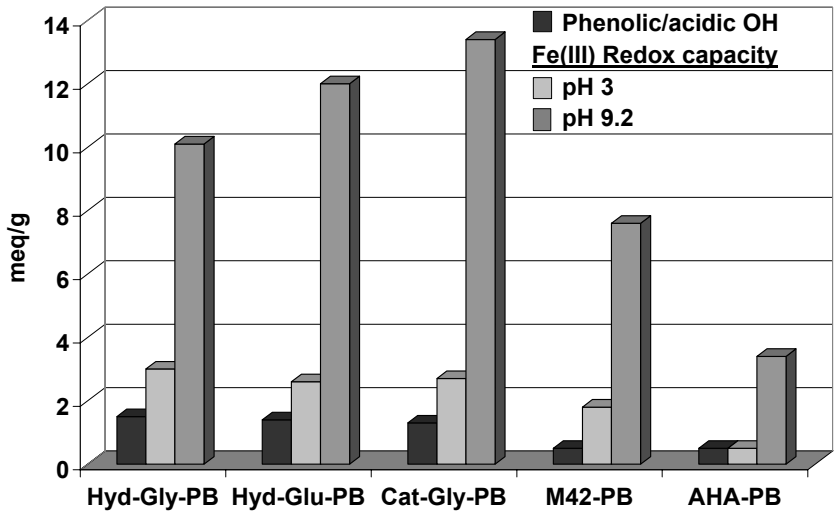

Fig. 4.2: Redox capacities of the modified HA in comparison to their phenolic/acidic OH group contents.

At pH 3, all modified synthetic HA show redox capacities that are slightly increased compared to those which would be expected assuming that only phenolic OH groups contribute to the redox process. In contrast to that, HA AHA-PB exhibits a redox capacity that is comparable to its amount on phenolic/acidic OH groups. However, at pH 9.2 all studied modified HA show significantly higher redox capacities than expected. These results support the assumption that there are other processes than the single oxidation of phenolic OH groups and/or other functional groups that are also contributing to the reduction of Fe(III), especially in the alkaline pH range.

The oxidation of phenols by $[Fe(CN)_6]^{3-}$ proceeds via intermediate phenoxy radicals that can undergo coupling reactions to various, often complex products. Tautomerisation of the coupled products can result in a regeneration of phenolic hydroxyl groups, which may undergo further oxidation reactions. The oxidation rate is higher in alkaline solution [e.g., 32-34]. In addition to that, it is possible that aldehydes, ketones and nitroalkanes can be oxidized by $[Fe(CN)_6]^{3-}$ in alkaline solution [32]. Due to the complicated nature of HA, such secondary reactions could occur during the reduction of $[Fe(CN)_6]^{3-}$ by HA. Thus, this could result in the observed redox capacities that are higher than the phenolic/acidic OH group content of the investigated HA.

From these studies we conclude that phenolic/acidic OH groups play a significant role for the redox behaviour of the studied synthetic (HA-like oxidation products of di-phenolic compounds and a HA-like melanoidin) and natural HA. However, there exist other processes than the single phenol oxidation or other HA functional groups that are also contributing to the redox properties of the studied substances.

5 Studies on the redox stability of uranium(VI) complexes with synthetic and natural humic acids

In order to further improve the knowledge on the redox stability of actinide humate complexes as well in continuation of the characterization of the HA-like oxidation products from phenolic compounds described in chapter 3.3.2, we performed studies on the redox stability of U(VI) humate complexes. For this investigation we applied synthetic HA type Hyd-Glu and Cat-Gly (see chapter 3.3.2). Both model substances show significantly higher Fe(III) redox capacities than natural HA AHA. The studies were performed according to that published by Abraham [2], where the redox stability of U(VI) in the presence of lignin, wood degradation products and natural HA (e.g., unpurified natural HA from Aldrich) was investigated. For the first time, it was found in this investigation, that these organic materials are able to reduce U(VI) starting at pH values higher than pH 4.5. The direct spectroscopic proof for the occurrence of U(IV) in uranium solutions with lignin and wood degradation products at pH 9 and pH 8, respectively, was successful.

5.1 Experimental

The redox stability of U(VI) humate complexes of HA type Hyd-Glu, Cat-Gly and AHA was studied at pH 9 in 0.1 M $NaClO_4$ solutions. For that, U(VI) humate solutions with initial U(VI) and HA concentrations of $1 \cdot 10^{-4}$ M and 0.4 g/L, respectively, were prepared under nitrogen atmosphere applying CO_2-free solutions. The pH value of the samples was set to pH 9.0 using NaOH and $HClO_4$ solutions. In order to keep the pH value of the solutions constant during the experiment it was periodically checked and readjusted. The samples were stored under exclusion of light.
Laser-induced photoacoustic spectroscopy (LIPAS) was applied for the direct spectroscopic detection of U(IV) in the sample solutions. A tuneable laser system was used. It is described in detail in [35]. The wavelength range between 600 and 675 nm was studied. For sample preparation 1 mL 6 M H_2SO_4 was added to 5 mL of the sample solutions. The addition of H_2SO_4 effects the precipitation of HA, the decomposition of possibly formed U(IV) humate complexes as well as the stabilization of U(IV) in the solutions in form of the U(IV) sulfate complex. After acidification, the HA precipitates were separated by centrifugation and the supernatants were studied by LIPAS.

5.2 Results and discussion

In Fig. 5.1 the photoacoustic spectra of the studied solutions after different reaction times are shown together with the peak deconvolution of the spectra. Comparing the spectra it becomes obvious that the spectra of the synthetic products are characterized by a high background absorption. This is due to an incomplete HA exclusion from the solutions which results in a HA contribution to the obtained absorption signal. However, from these spectra it becomes clear that HA AHA exhibits no absorption signals in the studied wavelength range, whereas for both synthetic products two absorption bands were detected. Thus, we conclude

that after 92 days reaction time no detectable U(IV) concentration (detection limit: 10^{-5}-10^{-6} mol/L [2]) was formed by the possibly occurring U(VI) reduction by HA AHA. In absence of HA, the solvated U^{4+} ion shows characteristic absorption maxima at 629.5 nm, 649.1 nm and 671.7 nm [36]. These absorption wavelengths are close to that detected in the solutions with synthetic HA type Hyd-Glu and Cat-Gly after different reaction times. This result points to the occurrence of detectable quantities of U(IV) in the solutions with the HA-like oxidation products from hydroquinone and catechol. Therefore, it can be concluded that U(VI) was reduced by both HA model substances. The shift of the absorption bands could be due to the formation of U(IV) sulfate complexes in the studied solutions. Similar peak shifts were observed by Geipel et al. [36] for U(IV) complexes with arsenate. The spectra which were obtained for the synthetic products are similar to that of an uranium solution with wood degradation products published in [2], where the reduction of U(VI) by these substances was found.

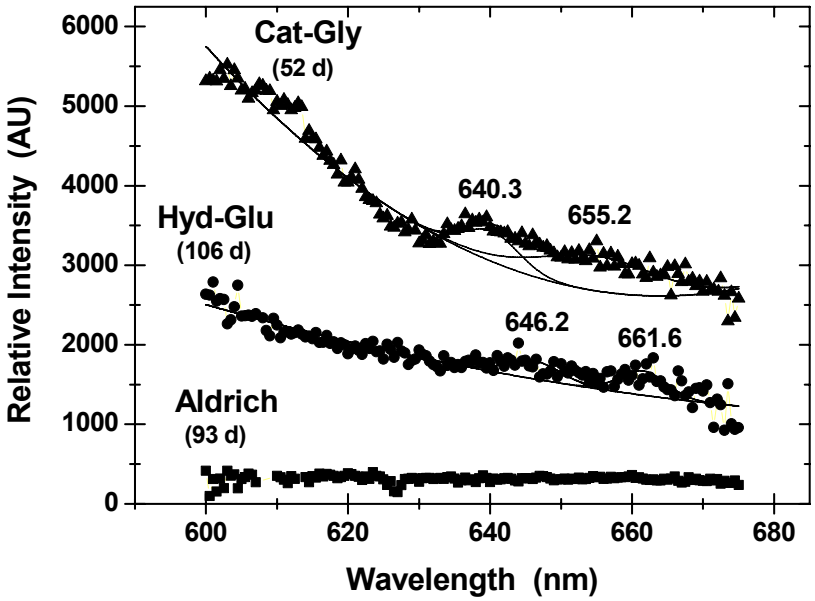

Fig. 5.1: Photoacoustic spectra of the studied HA solutions (starting conditions: $[UO_2^{2+}]$: $1 \cdot 10^{-4}$ mol/L, [HA]: 0.4 g/L, 0.1 M $NaClO_4$, pH 9.0). The numbers in brackets indicate the equilibration time of the samples.

From our spectroscopic results we conclude that the synthetic HA with pronounced redox functionalities show both higher Fe(III) and U(VI) redox capacities than HA AHA. The obtained results represent a first qualitative and direct spectroscopic proof for the reduction of uranium(VI) by HA. Further studies are performed in order to quantify the U(VI) redox capacities of the HA alike oxidation products from hydroquinone (Hyd-Glu) and catechol (Cat-Gly).

6 Investigations on the actinide complexation by humic substances

6.1 Structural studies on plutonium(III), thorium(IV), neptunium(IV) and neptunium(V) humate complexes by means of XAFS spectroscopy

Humic substances (humic acids and fulvic acids) are known for their strong complexing ability towards radionuclides thereby influencing their migration behaviour. Therefore, to understand and predict the mobility of actinides in natural aquifer systems, amongst others, information on the coordination chemistry of the actinides in humate and fulvate complexes is necessary. We studied the coordination environment of Pu(III), Th(IV), Np(IV) and Np(V) in complexes with HA and fulvic acid (FA) by means of X-ray absorption fine structure (XAFS) spectroscopy. This includes the X-ray absorption near-edge structure (XANES) spectroscopy and the extended X-ray absorption fine structure (EXAFS) spectroscopy. The XANES spectroscopy provides information on the electronic structure and the molecular symmetry of the absorbing atom and the EXAFS spectroscopy contains information on coordination numbers and bond lengths to neighbour atoms [37].
Bio-Rex70 was used as reference substance to study the nature of metal complexation sites in humic substances further. Bio-Rex70 is a cation exchange resin that, in contrast to humic substances, has no phenolic OH groups but exclusively carboxyl groups as functional groups capable of binding metal ions. Thus, Th(IV), Np(IV) and Np(V) sorbates onto Bio-Rex70 were studied to determine structural parameters for the interaction of the respective actinide ion with carboxyl groups.
In case of Np(V), the influence of HA phenolic/acidic OH groups on the interaction between Np(V) and HA was studied at pH 7 applying modified HA with blocked phenolic/acidic OH groups in addition to the respective unmodified HA.
The structural parameters determined for the actinide humate complexes are further compared with structural parameters of the respective aqueous actinide ions and of solid actinide carboxylate complexes given in the literature.

6.1.1 Experimental

Sorbents

Both natural and synthetic humic substances were applied for the study. The natural humic substances were Kranichsee FA (KFA) that was isolated from surface water of the mountain bog ‘Kleiner Kranichsee’ (Johanngeorgenstadt, Saxony, Germany) [38] as well as the commercially available, purified Aldrich HA (AHA). The synthetic HA model substances were the HA type M1 [10,39] and type M42 (see chapter 3.1). Furthermore, from AHA, M1 and M42 also modified HA with blocked phenolic/acidic OH groups (AHA-PB, M1-PB, M42-PB) (see chapter 3.2 and [15]) were applied. Bio-Rex70 (Bio-Rad, München, Germany) was used as reference substance.

Th(IV) samples

^{232}Th(IV) samples were prepared from AHA and from Bio-Rex70 at pH 1 (0.1 M $HClO_4$). The Th loading of the resulting wet pastes was 40.8 mg Th/g AHA and 1.9 mg Th/g Bio-Rex70 which corresponds to a Th loading of 14.7 % and 0.3 % of the proton exchange capacity (PEC) of the sorbents.

Np(IV) samples

A ^{237}Np(IV) stock solution was prepared by electrochemical reduction of a Np(V) solution to Np(III) followed by air oxidation to Np(IV). The tetravalent oxidation state of Np was verified by near infrared (NIR) absorption spectroscopy. Np(IV) samples were prepared from AHA, KFA, M42 and from Bio-Rex70 at pH 1 (0.1 M $HClO_4$) under inert gas conditions. The Np loading of the resulting wet pastes was between 4 and 41 mg Np/g sorbent (0.7 % to 15 % of the PEC of the sorbents).

Np(V) samples

^{237}Np(V) complexes were prepared from the unmodified HA AHA, M1 and M42 and from modified HA AHA-PB, M1-PB and M42-PB with blocked phenolic/acidic OH groups as well as from Bio-Rex70. The Np(V) humate solutions were prepared at pH 7 under inert gas conditions with Np and HA concentrations of 0.88-1.04 mmol/L and of 8.1-27.5 g/L, respectively (ionic strength: 0.1 M $NaClO_4$). The Np loading was between 2.3 and 2.8 % of the PEC of the sorbents. The Np(V)-Bio-Rex70 sorbate was prepared at pH 7 in 0.1 M $NaClO_4$. The Np loading of the resulting wet paste was 121.3 mg Np/g Bio-Rex70 (5.1 % PEC).

Pu(III) samples

^{242}Pu was purified in the tetravalent oxidation state by anion exchange chromatography using TEVA resin^{TM}. Purified Pu(IV) was electrochemically reduced to Pu(III). The trivalent oxidation state of Pu was verified by NIR absorption spectroscopy. Pu(III) samples were prepared from KFA and from M42 at pH 1 (0.1 M $HClO_4$) under inert gas conditions. The Pu loading of the resulting wet pastes of KFA and M42 was 11.6 and 3.9 mg Pu per g sorbent, respectively.

The experimental conditions are described in more detail in Schmeide et al. [40,41] and Sachs et al. [42].

XAFS measurements and data analysis

The XAFS measurements were carried out at the Rossendorf Beamline (ROBL) [43] at the European Synchrotron Radiation Facility (ESRF) in Grenoble, France. The actinide L_{III}-edge X-ray absorption spectra were collected in fluorescence mode (Th(IV) samples, Pu(III) samples, Np(V) humates) and transmission mode (Np(IV) samples, Np(V)-Bio-Rex70), respectively, at room temperature. A Si(111) double-crystal monochromator was used in fixed-exit mode. Several EXAFS scans were collected from each sample and averaged.

Data analysis was performed according to standard procedures [37] using the EXAFSPAK software [44]. The program FEFF6 [45] was used to calculate theoretical scattering amplitudes and phase-shift functions.

The EXAFS oscillations were fitted to the EXAFS equation using one coordination shell with oxygen as backscatterer in case of Th(IV), Np(IV) and Pu(III). In case of Np(V), a two-shell fit with axial and equatorial oxygen atoms (O_{ax}, O_{eq}) as backscatterers was used. The multiple scattering along the neptunyl unit (O_{ax}-Np-O_{ax}) was also included in the fit.

6.1.2 Results and discussion

Th(IV) humate and Bio-Rex70 complexes

The raw Th L_{III}-edge k^3-weighted EXAFS spectra and the corresponding Fourier transforms (FT) of the Th(IV) complexes with AHA and Bio-Rex70 are shown in Fig. 6.1. Both the EXAFS spectra and the FT of the samples are comparable. The FT are dominated by a peak at about 1.8 Å representing oxygen atoms coordinated to Th(IV).

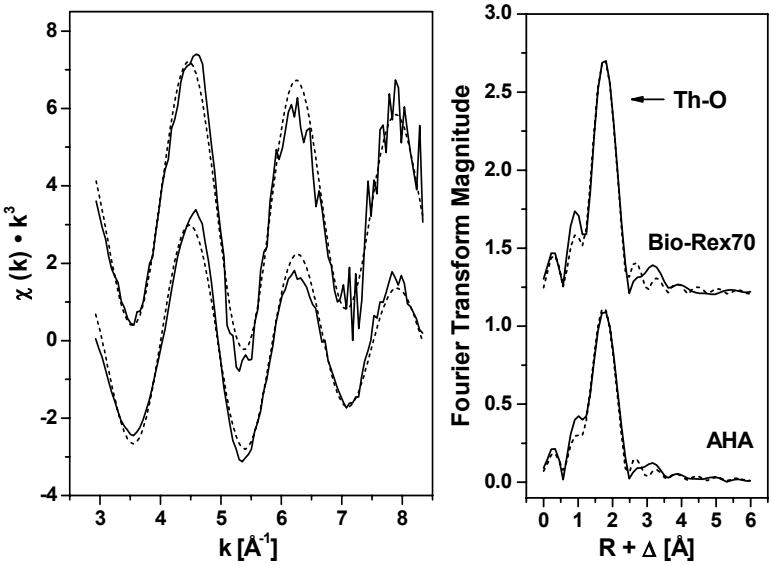

Fig. 6.1: Th L_{III}-edge k^3-weighted EXAFS spectra and corresponding FT of Th(IV) samples. Solid lines: experiment, dashed lines: fit.

In Tab. 6.1 the structural parameters determined for the Th(IV) complexes are summarized such as coordination number (N), bond length (R) and Debye-Waller factor (σ^2) obtained from fits to the EXAFS equation. The coordination numbers and Th-O bond lengths of Th(IV)-AHA and Th(IV)-Bio-Rex70 are comparable. In both samples, Th(IV) is surrounded by 11 oxygen atoms at a distance of 2.44 Å. Since Bio-Rex70 has no phenolic OH groups but exclusively carboxyl groups as functional groups capable of binding metal ions, it can be concluded that the interaction between AHA and Th(IV) is dominated by HA carboxyl groups under the experimental conditions applied. This result was expected since at pH 1 the phenolic OH groups of the humic substances are fully protonated. The larger EXAFS Debye-Waller factor determined for the oxygen coordination shell of Th(IV)-AHA in comparison to those of Th(IV)-Bio-Rex70 and the aqueous Th(IV) ion points to a broader distribution of Th-O bond lengths in the Th(IV) humate complex.

Tab. 6.1: EXAFS structural parameters of Th(IV) complexes in comparison to literature data of Th(IV) samples.

Sample	Th-O			ΔE_0 (eV)	Ref.
	N	R (Å)	σ^2 (Å^2)		
Th(IV)-AHA	10.6 ± 1.5	2.44 ± 0.01	0.013	-17.3	
Th(IV)-Bio-Rex70	11.0 ± 2.1	2.45 ± 0.02	0.009	-17.3	
Th(IV)-AHA	10.1	2.43	0.013	1.0	[46]
Th(IV)-Bio-Rex70	9.4	2.44	0.012	1.0	[46]
$Th(H_2O)_x^{4+}$	10.8 ± 0.5	2.45 ± 0.01	0.007	4.0	[47]

The 95 % confidence limits are given for N and R as estimated by EXAFSPAK.

Within the experimental error, the structural parameters determined for the Th(IV) humate and Bio-Rex70 complexes agree with those determined by Denecke et al. [46]. Furthermore, the data of Th(IV)-AHA are comparable to those of the aqueous Th(IV) ion [47]. This shows that the interaction between Th(IV) and HA carboxyl groups induces no shortening of the Th-O bond length. Furthermore, since no carbon atoms of the binding HA carboxylate groups can be detected, it is not possible to determine separate coordination numbers for carboxylate groups and water molecules coordinated to Th(IV) by EXAFS analysis.
To identify the binding mode (monodentate, bidentate or bridging) of HA carboxylate groups to Th(IV), the Th-O bond length of Th(IV) humate is compared with those of Th(IV) model compounds which contain carboxyl groups. The average Th-O bond length observed for monodentate coordinated carboxylate groups in various Th(IV) malonates [48] as well as in Th(IV) oxalate [49] is 2.42 ± 0.04 Å. This bond length is comparable to the bond length obtained for Th(IV)-AHA (2.44 ± 0.01 Å). This points to a predominant monodentate coordination of HA carboxylate groups to Th(IV).

Np(IV) humate and Bio-Rex70 complexes

The tetravalent oxidation state of Np and its stability in the humate and Bio-Rex70 complexes within the time of our experiment was verified by means of NIR absorption spectroscopy [40] and XANES spectroscopy. In Fig. 6.2, the XANES spectrum of Np(IV)-AHA is shown in comparison to that of the corresponding Np(V) sample. The spectrum of Np(IV) humate shows the characteristic near-edge features of Np(IV) compounds: A more intense ‘white line’ peak, but no additional shoulder on the high energy side of the ‘white line’ as generally observed for Np(V) samples. Identical spectral features were obtained for the Np(IV) complexes of KFA, M42 and Bio-Rex70.

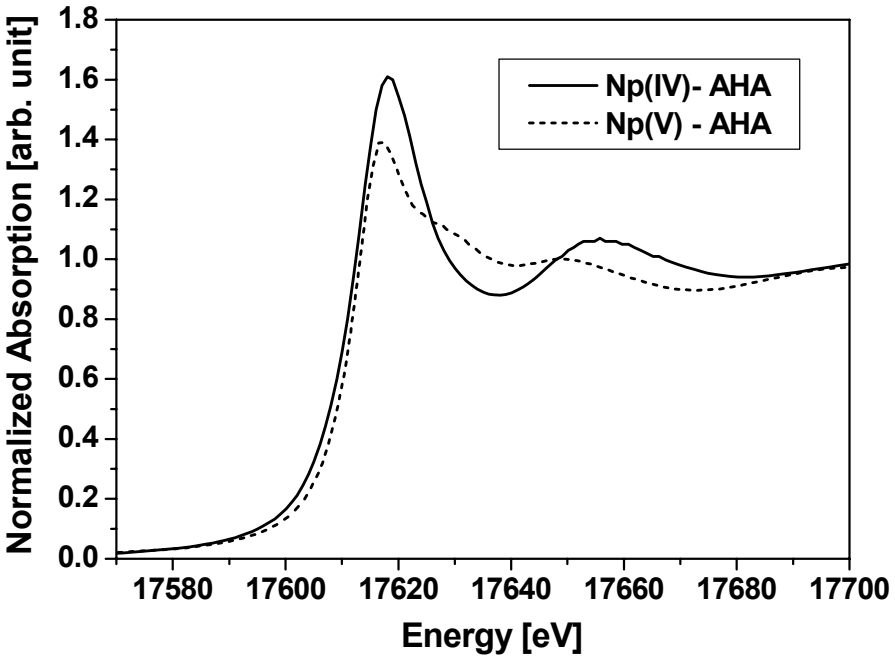

Fig. 6.2: Normalized Np L_{III}-edge XANES spectra.

The raw Np L_{III}-edge k^3-weighted EXAFS spectra and the corresponding FT of the Np(IV) samples are shown in Fig. 6.3. Both the EXAFS oscillations and the FT of all Np(IV) complexes are similar. The FT are dominated by one peak at about 1.7 Å representing one coordination shell with oxygen as backscatterer. No Np-Np contributions were observed in the spectra, i.e., polynuclear Np species did not form.

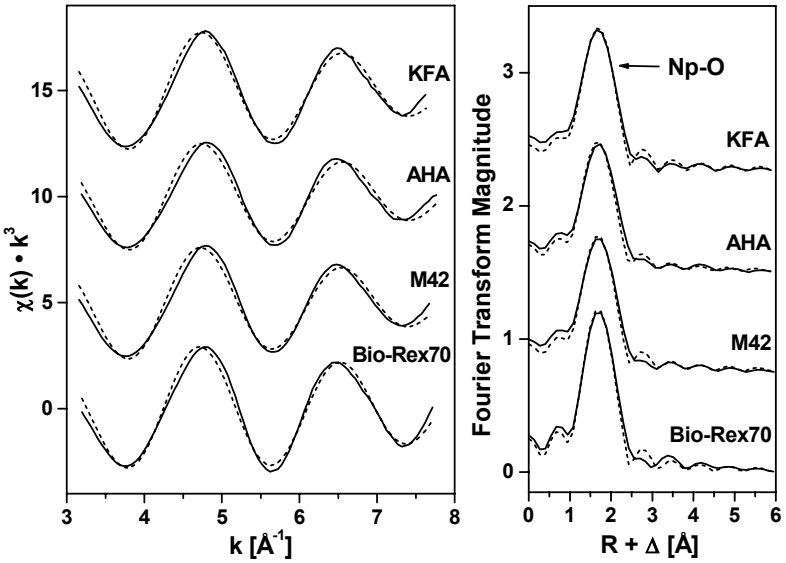

Fig. 6.3: Np L_{III}-edge k^3-weighted EXAFS spectra and corresponding FT of Np(IV) samples. Solid lines: experiment, dashed lines: fit.

The EXAFS structural parameters determined for the Np(IV) complexes are compiled in Tab. 6.2 and compared to literature data of Np(IV) samples.

In the Np(IV) humate complexes, the Np(IV) ion is surrounded by about 11 oxygen atoms at a distance of 2.36 Å. Comparable parameters are determined for the Np(IV) complex with Bio-Rex70. This again verifies the dominance of carboxyl groups for the complexation of actinide ions by humic substances at pH 1 (cf. Th(IV) humates).

Tab. 6.2: EXAFS structural parameters of Np(IV) complexes in comparison to literature data of Np(IV) samples.

Sample	Shell	N	R (Å)	σ^2 (Å^2)	ΔE_0 (eV)	Ref.
Np(IV)-KFA	Np-O	11.3 ± 1.7	2.36 ± 0.01	0.0162	-11.1	
Np(IV)-AHA	Np-O	10.1 ± 1.7	2.36 ± 0.01	0.0159	-11.1	
Np(IV)-M42	Np-O	11.0 ± 1.7	2.36 ± 0.01	0.0166	-11.1	
Np(IV)-Bio-Rex70	Np-O	10.2 ± 1.3	2.37 ± 0.01	0.0127	-11.1	
$Np(H_2O)_x^{4+}$ in 1 M $HClO_4$	Np-O	9 ± 1	2.37 ± 0.02	0.007		[50]
$Np(H_2O)_x^{4+}$ in 1 M HCl	Np-O	11.2 ± 1.1	2.40 ± 0.012	0.0075		[51]
$Np(H_2O)_x^{4+}$ in 2 M H_2SO_4	Np-O Np-S	11 ± 1 2.2 ± 0.9	2.39 ± 0.01 3.07 ± 0.02	0.0118 0.0070		[43]

The 95 % confidence limits are given for N and R as estimated by EXAFSPAK.

Compared to the aqueous Np(IV) ion in hydrochloric or sulfuric medium [43,51], the coordination number of the humates is similar, only the Np-O bond length is shortened by about 0.04 Å due to humate complexation. A similar shortening of the bond length has been previously observed for U(VI) humate complexes ($R_{U\text{-}Oeq}$ = 2.37-2.39 Å) [23,52,53] compared to $UO_2(H_2O)_5^{2+}$ ($R_{U\text{-}Oeq}$ = 2.41 Å) [51] and can be interpreted as further evidence of actinide humate complex formation. However, as found for Th(IV), a differentiation between HA carboxylate groups and water molecules coordinated to the Np(IV) ion is not possible by means of EXAFS spectroscopy.

The comparison of the bond length determined for the Np(IV) humates with those of Np(IV) model compounds containing carboxyl groups shows that the bond length of the Np(IV) humates is smaller than found for bridging and chelate forming carboxylate groups in Np(IV) oxalate (R = 2.39 Å and 2.51 Å with an average of 2.45 Å) [54] or for bidentate binding carboxylate groups in Np(IV) formate (R = 2.50 Å) [55]. From this we conclude that the HA carboxylate groups are predominantly monodentate bound to Np(IV) ions.
The comparison of the structural parameters of Np(IV) humate and Bio-Rex70 complexes with those of the corresponding Th(IV) complexes shows that both tetravalent actinides are surrounded by 11 oxygen atoms. However, the Np-O bond length (2.36 ± 0.02 Å) is about 0.08 Å shorter than the Th-O bond length (2.44 ± 0.02 Å). This difference approximates the difference of the effective ionic radii of Np^{4+} (1.02 ± 0.02 Å [56]) and Th^{4+} (1.08 ± 0.02 Å, [56]) in aqueous solution which is 0.06 ± 0.02 Å.

Np(V) humate and Bio-Rex70 complexes

For all Np(V) humates the complexation of NpO_2^+ by HA was verified by means of NIR absorption spectroscopy [42].

The raw Np L_{III}-edge k^2-weighted EXAFS spectra and the corresponding FT of the Np(V) complexes are shown in Fig. 6.4. The FT show two Np-O coordination shells (Np-O_{ax}, Np-O_{eq}). No Np-Np interactions are indicated in the FT. The structural parameters determined for the Np(V) complexes are summarized in Tab. 6.3 and compared to literature data of the aqueous Np(V) ion.

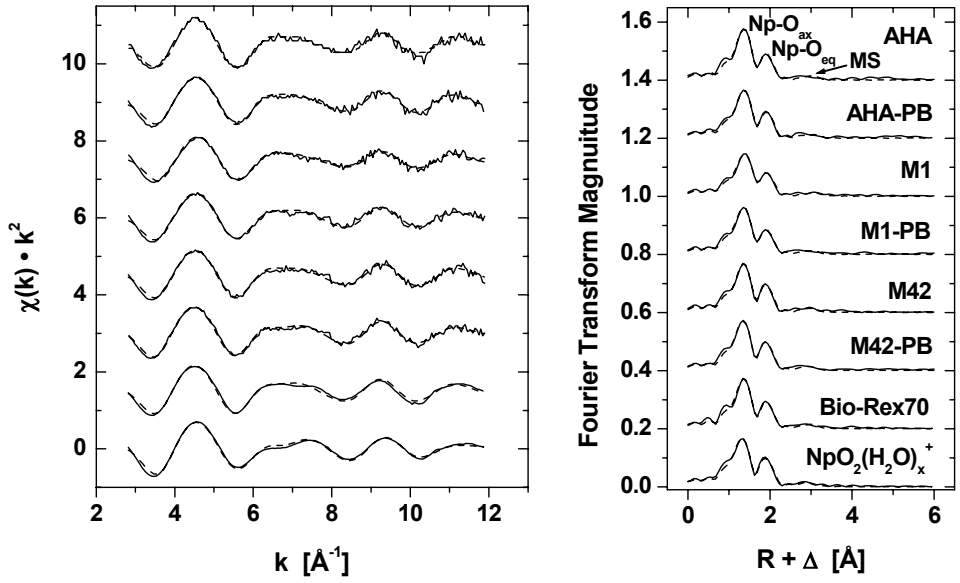

Fig. 6.4: Np L_{III}-edge k^2-weighted EXAFS spectra and corresponding FT of Np(V) samples. Solid lines: experiment, dashed lines: fit, MS: multiple scattering along the neptunyl unit.

Within the experimental error, identical structural parameters were determined for Np(V) humates prepared from original HA and from modified HA with blocked phenolic/acidic OH groups. From this it can be concluded that the blocking of the phenolic/acidic OH groups of the HA has no influence on the local structure around the Np(V) ion in the Np(V) humates. Furthermore, the structural data of the Np(V) humates are also comparable to those of Np(V)-Bio-Rex70. This indicates that carboxylate groups dominate the interaction between Np(V) and HA at pH 7. However, a contribution of HA phenolic/acidic OH groups to the complexation of Np(V) ions cannot completely be excluded by EXAFS analysis, since the EXAFS results represent average values over all interactions between Np(V) and HA functional groups. There is the possibility that phenolic OH groups interacting with Np(V) show equatorial bond lengths that are similar to those of carboxylate groups.

Tab. 6.3: EXAFS structural parameters of Np(V) complexes in comparison to literature data of the aqueous Np(V) ion.

Sample	$Np\text{-}O_{ax}$			$Np\text{-}O_{eq}$			ΔE_0
	N	R (Å)	σ^2 (Å^2)	N	R (Å)	σ^2 (Å^2)	(eV)
Np(V)-AHA	2.0 ± 0.3	1.85 ± 0.01	0.0017	2.8 ± 0.7	2.49 ± 0.02	0.0050	-8.1
Np(V)-AHA-PB	2.0 ± 0.3	1.85 ± 0.01	0.0021	2.3 ± 0.6	2.49 ± 0.01	0.0028	-7.7
Np(V)-M1	1.8 ± 0.3	1.86 ± 0.01	0.0026	2.6 ± 0.6	2.49 ± 0.02	0.0053	-6.4
Np(V)-M1-PB	2.0 ± 0.2	1.85 ± 0.01	0.0026	2.5 ± 0.6	2.49 ± 0.02	0.0043	-8.4
Np(V)-M42	1.9 ± 0.2	1.84 ± 0.01	0.0014	2.8 ± 0.6	2.48 ± 0.01	0.0041	-9.3
Np(V)-M42-PB	2.0 ± 0.2	1.84 ± 0.01	0.0020	2.8 ± 0.5	2.49 ± 0.01	0.0037	-10.0
Np(V)-Bio-Rex70	2.0 ± 0.2	1.85 ± 0.01	0.0017	2.7 ± 0.5	2.50 ± 0.01	0.0043	-8.8
$NpO_2(H_2O)_x^+$ [43]	2.0 ± 0.2	1.82 ± 0.01	0.0026	2.9 ± 0.4	2.49 ± 0.01	0.0038	-9.2
$NpO_2(H_2O)_x^+$ [51]	2	1.85	0.0018	5.0	2.50	0.007	

The 95 % confidence limits are given for N and R as estimated by EXAFSPAK.

The coordination number determined for the equatorial shell of Np(V) humate and Np(V)-Bio-Rex70 complexes as well as for the equatorial shell of the aqueous ion of Np(V) [43] is smaller than the theoretically expected value of 5. Up to now, this cannot be explained.
The equatorial Np-O bond lengths of the humates are comparable to the mean equatorial Np-O bond lengths of monodentate and/or bridging coordinated carboxylate groups in crystalline Np(V) carboxylate complexes reported in the literature (2.46 ± 0.04 Å) that are summarized in [42]. Moreover, the equatorial Np-O bond lengths of the humates are also comparable to the equatorial Np-O bond length of the aqueous Np(V) ion. Thus, a differentiation between monodentate/bridging carboxylate groups and water molecules is not possible. However, a predominant bidentate coordination of HA carboxylate groups to Np(V) can be excluded, since bidentate coordinated carboxylate groups in different crystalline Np(V) carboxylates show a mean equatorial Np-O bond length of 2.59 ± 0.08 Å (summarized in [42]) which is significantly longer.

Pu(III) humate complexes

The trivalent oxidation state of Pu and its stability in the complexes with humic substances within the time of the experiment was verified by means of XANES spectroscopy. In Fig. 6.5, the XANES spectra of Pu(III)-KFA and Pu(III)-M42 are shown in comparison to that of the aqueous ion of Pu(III) [59]. The energy scale of the spectra was calibrated with a Zr metal foil (Zr K edge at 17998 eV). The edge energy, determined as the inflection point of the edge, of the three spectra is identical (aqueous Pu(III) ion: 18059.0 eV, Pu(III) humates: 18059.2 eV). This confirms that the humate complexes contain exclusively Pu(III).

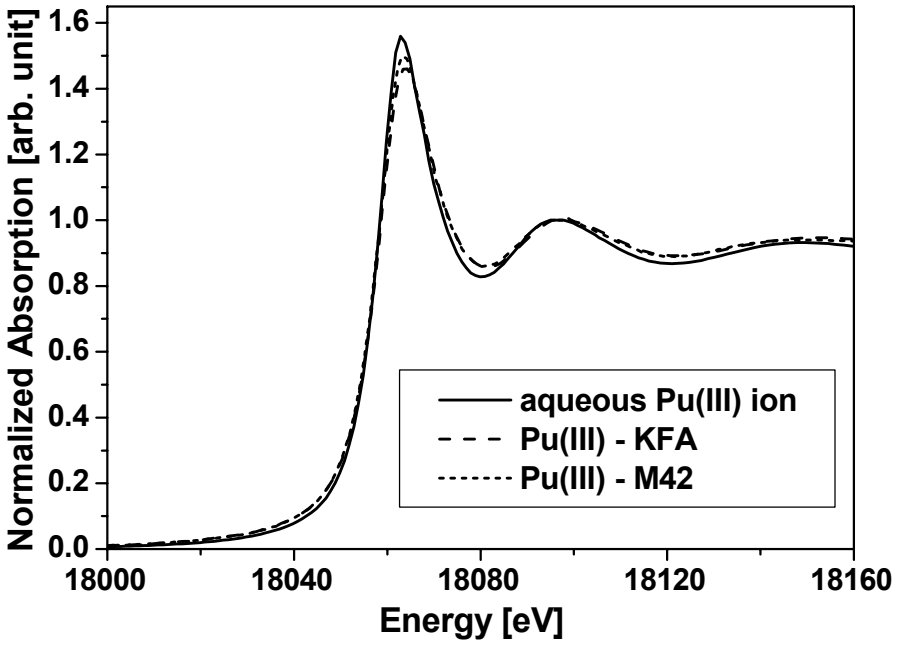

Fig. 6.5: Normalized Pu L_{III}-edge XANES spectra.

The raw Pu L_{III}-edge k^3-weighted EXAFS spectra and the corresponding FT of the Pu(III) humates are shown in Fig. 6.6. The FT indicate a single coordination shell (Pu-O) arising from the ligands.

The structural parameters determined for the Pu(III) complexes are summarized in Tab. 6.4 and compared to literature data of aqueous ions of Pu(III) and Pu(IV). In the Pu(III) humate complexes the Pu(III) ion is surrounded by about 7 oxygen atoms at a distance of 2.45 Å. The Pu-O bond length in the Pu(III) humate complexes is significantly longer than that of the aqueous Pu(IV) ion. Furthermore, no evidence for the formation of polynuclear Pu(IV) species was found in the EXAFS spectra. That means, the EXAFS structural parameters confirm the conclusion drawn from the XANES spectra namely that the humate complexes contain exclusively Pu(III).

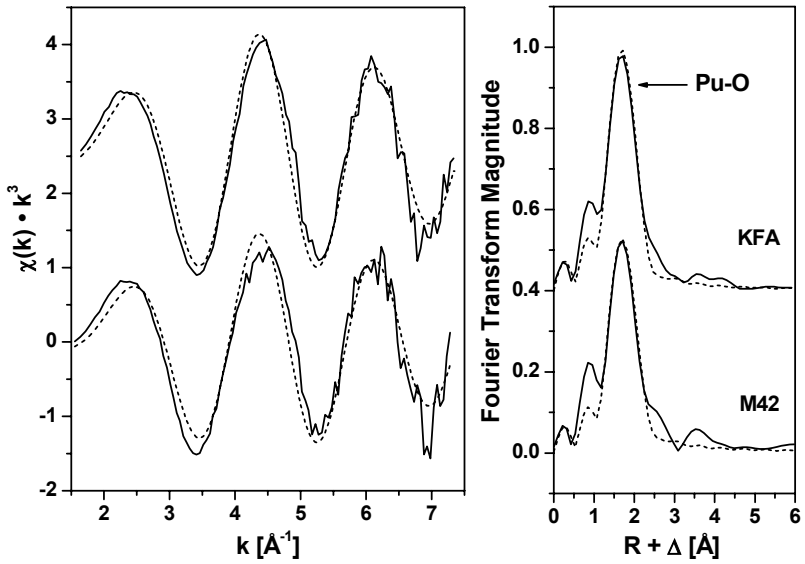

Fig. 6.6: Pu L_{III}-edge k^3-weighted EXAFS spectra and corresponding FT of Pu(III) samples. Solid lines: experiment, dashed lines: fit.

Tab. 6.4: EXAFS structural parameters of Pu(III) complexes in comparison to literature data of aqueous ions of Pu(III) and Pu(IV).

Sample	Shell	N	R (Å)	σ^2 (Å^2)	E_0 (eV)	Ref.
Pu(III)-KFA	Pu-O	7.3 ± 1.2	2.45 ± 0.02	0.0150	-17.3	
Pu(III)-M42	Pu-O	6.1 ± 1.4	2.45 ± 0.02	0.0137	-17.0	
$Pu(H_2O)_x^{3+}$	Pu-O	7.6 ± 0.6	2.48 ± 0.01	0.0102	-16.8	[59]
$Pu(H_2O)_x^{4+}$	Pu-O	8	2.39	0.0118		[60]

The 95 % confidence limits are given for N and R as estimated by EXAFSPAK.

Within the experimental error, the coordination numbers determined for the Pu-O shell of the humate complexes agree well with the value reported for the aqueous Pu(III) ion in 1 M $HClO_4$ [59]. The bond length determined for the Pu(III) humate complexes is 0.03 Å shorter than that determined for the aqueous Pu(III) ion. This shortening of the bond length is similar to that observed for U(VI) and Np(IV) humates upon complexation of these actinides with the functional groups of the humic substances.

6.2 Studies on the influence of phenolic OH groups on the neptunium(V) complexation by humic acids

In order to further improve the knowledge on the influence of phenolic OH groups on the metal ion complexation by HA in neutral and alkaline solutions we continued our studies on the Np(V)-HA-complexation using modified HA with blocked phenolic OH groups. In continuation of our EXAFS investigations (chapter 6.1), which resulted in structural information on the near-neighbour surrounding of Np(V) in humate complexes, we determined and com-

pared loading capacities and complexation constants of Np(V) complexes with unmodified and chemically modified (phenolic OH groups blocked) HA type M42 and Aldrich. These studies were performed by near-infrared (NIR) spectroscopy.

6.2.1 Experimental

Np(V) humate solutions were prepared under nitrogen atmosphere from natural HA Aldrich (AHA, batch A2/98), synthetic HA type M42 (batch M145), as well as modified HA AHA and M42 with blocked phenolic OH groups (AHA-PB, M42-PB). For synthesis and characterization of these HA see chapter 3.2.
In our experiments the HA concentration ([HA(I)] [11]) was held constant at $1 \cdot 10^{-3}$ mol/L and the Np(V) concentration was varied between $5.3 \cdot 10^{-5}$ and $1.3 \cdot 10^{-3}$ mol/L. The studies were performed at room temperature in 0.1 M $NaClO_4$ solutions at pH 7 for all HA and at pH 8 for AHA and AHA-PB. The samples were prepared from stock solutions of HA and NpO_2^+ (^{237}Np, $4.6 \cdot 10^{-3}$ M, 0.01 M HNO_3). The ionic strength was adjusted applying 1 M $NaClO_4$ solution. The total neptunium concentration in solution was determined by liquid scintillation counting (LSC, Beckman Instruments). NIR absorption spectra of all Np(V) humate solutions were recorded in the wavelength range between 950 and 1010 nm with the UV-VIS-NIR spectrophotometer CARY-5G (Varian).
The Np(V) species distribution in the absence of HA at pH 7 and pH 8 ([NpO_2^+]: $1 \cdot 10^{-5}$ M and $1 \cdot 10^{-3}$ M, 0.1 M $NaClO_4$, 0 % CO_2) was calculated with the program EQ3/6 [12] based on complex formation constants compiled in [61]. Under the considered conditions the NpO_2^+ ion dominates the Np(V) speciation. It occurs with a relative concentration of 100.00 % and 99.96 % at pH 7 and pH 8, respectively. Therefore, it can be concluded that NpO_2^+ is the Np(V) species which reacts with HA under the studied experimental conditions.

6.2.2 Results and discussion

The measured NIR absorption spectra represent the sum of the absorption signals of the uncomplexed NpO_2^+ ion (980 nm) and the Np(V) humate complex ($NpO_2HA(I)$, 985-989 nm depending on HA). The spectra were deconvoluted into single peaks for both species in order to determine their concentration in solution. Figure 6.7 shows a measured NIR absorption spectrum of a Np(V) solution with HA AHA and its deconvolution.

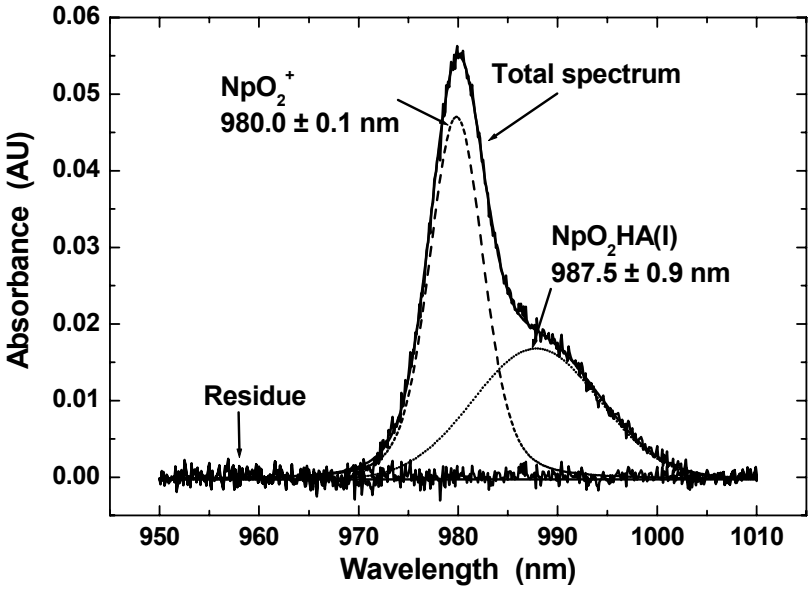

Fig. 6.7: NIR absorption spectrum of Np(V) in HA solution and its deconvoluted absorption bands (AHA, [HA(I)]: $1 \cdot 10^{-3}$ mol/L, [NpO_2^+]: $1.7 \cdot 10^{-4}$ mol/L, pH 7, 0.1 M $NaClO_4$).

The experimental data were evaluated with the metal ion charge neutralization model [11]. According to this model, NpO_2^+ occupies one proton exchanging site of the HA molecule [Eq. (6.1)]:

$$NpO_2^+ + HA(I) \; \Phi \; NpO_2HA(I) \qquad (6.1)$$

where HA(I) represents the HA ligand and $NpO_2HA(I)$ stands for the neptunyl humate complex. The stability constant β is given by

$$\beta = \frac{[NpO_2HA(I)]}{[NpO_2^+]_{free} \cdot [HA(I)]_{free}} \qquad (6.2)$$

where $[NpO_2HA(I)]$ is the neptunyl humate complex concentration, $[NpO_2^+]_{free}$ the free NpO_2^+ concentration and $[HA(I)]_{free}$ the free HA ligand concentration [11]. This model introduces the loading capacity (LC, [Eq. (6.3)]) which represents the mole fraction of maximal available complexing sites of HA under the applied experimental conditions.

$$LC = \frac{[NpO_2HA(I)]_{max}}{[HA(I)]_{tot}} \qquad (6.3)$$

$[NpO_2HA(I)]_{max}$ is the maximum concentration of NpO_2^+ that can be complexed by functional sites of HA and $[HA(I)]_{tot}$ stands for the total molar HA concentration [11]. Taking the LC into account the free HA concentration in solution can be determined according to [11] and the stability constant (β) can be described by Eq. (6.4).

$$\beta = \frac{[NpO_2HA(I)]}{[NpO_2^+]_{free} \cdot ([HA(I)]_{tot} \cdot LC - [NpO_2HA(I)])} \qquad (6.4)$$

The LC is graphically determined by linear regression after rearranging Eq. (6.4) for the free NpO_2^+ ion concentration [11]. Considering the graphically determined LC, we computed a complexation constant for each experimental point.

Applying this model, the complexation behaviour of HA can be described independently of the experimental conditions and the HA origin. From this it follows, that comparable complexation constants are determined for the complexation of a metal ion, e.g., Np(V), with different HA. Differences in the complexation behaviour of various HA under the same experimental conditions are reflected in different LC values. A significant lower LC for HA with blocked phenolic/acidic OH groups should result, if the blocking of these HA functional groups has an influence on the complexation behaviour of HA with Np(V) in the neutral and alkaline pH range.

Table 6.5 summarizes the spectroscopically determined complexation data (LC, log β) for the investigated HA at pH 7 and pH 8. Figure 6.8 shows, exemplary for modified and unmodified HA type M42, the mole ratios $[NpO_2HA(I)]/[HA(I)]_{tot}$ versus $[NpO_2^+]_{tot}/[HA(I)]_{tot}$ which illustrate the LC values.

Tab. 6.5: Complexation data for the complexation of Np(V) with unmodified and modified HA type M42 and AHA in comparison to literature data.

HA	pH	LC (%) [a]	log β [a]
AHA (batch A2/98)	7.0	10.0 ± 1.5	3.87 ± 0.19
	8.0	35.3 ± 3.7	3.59 ± 0.17
AHA-PB (batch M173)	7.0	6.5 ± 2.4	3.39 ± 0.15
	8.0	12.3 ± 2.6	3.46 ± 0.22
M42 (batch M145)	7.0	11.2 ± 1.1	3.50 ± 0.15
M42-PB (batch M171)	7.0	5.3 ± 1.0	3.48 ± 0.11
GoHy-573 [62]	7	9.9 ± 0.2	3.65 ± 0.03
	8	14.9 ± 0.3	3.68 ± 0.08
GoHy-573 [63]	7	13.0 ± 1.0	3.53 ± 0.05
	8	22.0 ± 1.5	3.61 ± 0.07
Aldrich [64]	8	32.4	3.7

[a] ± 3 σ.

Within the experimental errors, the studied HA show similar Np(V) complexation constants that are close to literature data for HA GoHy-573 [62,63] and Aldrich [64]. However, there are

differences in the LC of HA AHA, M42 and GoHy-573 especially at pH 8. These could be explained by the different origin of the HA resulting in various complexation properties. The obtained LC for AHA at pH 8 agrees with that data reported by Seibert et al. [64].

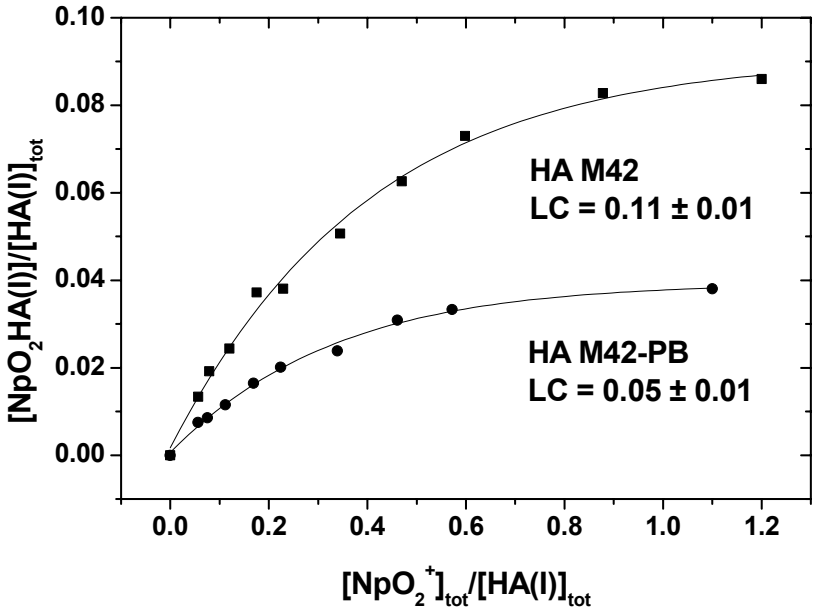

Fig. 6.8: Illustration of the Np(V) loading capacity (LC) of modified (M42-PB) and unmodified (M42) synthetic HA type M42 at pH 7.

Comparing the LC values of the corresponding modified and unmodified HA at pH 7 and pH 8 it becomes obvious that modified HA AHA-PB and M42-PB have significantly lower LC than the original, unmodified HA AHA and M42, respectively. Due to the modification of phenolic/acidic OH groups (75 % M42 and 84 % AHA, see Tab. 3.2) the LC of HA M42 and AHA at pH 7 decreases for 53 % and 35 %, respectively. The LC of AHA at pH 8 is reduced for 65 %. These results point to a decrease of the mole fraction of HA binding sites for the Np(V) complexation due to the blocking of phenolic/acidic OH groups. Thus, it can be concluded that phenolic/acidic OH groups are involved into the interaction between HA and Np(V) in the neutral and alkaline pH range. Comparable results were already found for the uranium(VI) complexation at pH 4 with various HA at pH 4 [15]. Although the blocking of phenolic/acidic OH groups decreases the number of HA complexing sites, the structural parameters of Np(V) humates are not changed due to the HA modification, which was found by the EXAFS measurements described in chapter 6.1.

Varying the pH of the studied system from pH 7 to pH 8, the LC of HA AHA as well as of AHA-PB increases as expected. However, the reduction of the LC due to the HA modification ($LC_{AHA} \rightarrow LC_{AHA\text{-}PB}$) is higher at pH 8 (65 %) than at pH 7 (35 %). That points to the fact that the influence of phenolic OH and other acidic OH groups on the Np(V) complexation by HA increases with increasing pH. This result can be attributed to a higher degree of deprotonated phenolic/acidic OH groups at pH 8 than at pH 7.

7 Studies on the influence of humic acids on the migration behaviour of actinides

7.1 Effect of humic acid on the Th(IV) sorption onto quartz and quartz sand

The migration of tetravalent actinides in natural environments is influenced by several observable factors. Among these the sorption is one of the most important, which can be strongly affected by HA. The influence of HA on the sorption behaviour of tetravalent actinides was exemplary studied for the Th(IV) sorption onto quartz and quartz sand.
The complexation of Th(IV) with humic substances [4,46,65-67] and the influence of humic or fulvic acids on Th(IV) sorption onto various minerals (especially amorphous silica or hematite) [68-72] has been described in the literature. In the present work the influence of HA on the Th(IV) sorption onto quartz and quartz sand was investigated by batch experiments in the pH range between pH 3 and pH 7.5.

7.1.1 Experimental

Materials

For the sorption experiments commercially available fine-grained quartz (100 % SiO_2, 63-200 μm) was applied (Merck). It was used without any pre-treatment. In addition to that we studied the Th(IV) sorption onto quartz sand (100–300 μm) of marine origin (Heerlen, Netherlands). Prior to its use the sand was washed with Milli-Q-water to remove soluble cations such as Na and K. Then it was annealed by 700 °C for 4 hours. After purification, the chemical composition of the sand was 0.3 % of Al, 0.02 % Ti, 0.02 % Fe, possibly illite, TiO_2, iron oxides, respectively, and 99.66 % SiO_2. In order to determine the fate of HA, ^{14}C-labeled synthetic HA type M42, charge M170 (cf. chapter 3.1) was used. For the preparation of the stock solutions (40 and 120 mg/L) HA was weighed, diluted with 0.1 M NaOH and filled to the required volume with 0.1 M $NaClO_4$ (pH 7). A Th(IV) stock solution of $5 \cdot 10^{-6}$ M ^{232}Th in 0.1M $HClO_4$ was prepared.

Sorption experiments

The sorption experiments were performed under inert gas conditions (N_2). 50 mg of mineral were weighed into 15 mL polypropylene (PP) centrifuge tubes (Nalgene). Then, 5mL 0.1 M $NaClO_4$ (pH 2.8) were added to the Merck-quartz. The samples were stirred for 30 minutes to remove adsorbed CO_2 from the mineral surface. Then, the pH values of the samples were adjusted between pH 3 and pH 7 by addition of $HClO_4$ or NaOH. For pre-equilibration the samples were continuously shaken and the pH values were controlled and readjusted over a period of 4 weeks. After pre-equilibration 5 mL 0.1 M $NaClO_4$ solution (pH 7) and 20 μL Th(IV) stock solution were added to the quartz suspension for the investigation of Th(IV) sorption onto Merck-quartz. The final concentration of Th(IV) in the solution was $1.2 \cdot 10^{-8}$ M. To determine the HA sorption onto quartz, 5 mL HA stock solution and 20 μL 0.1 M $NaClO_4$ solution (pH 7) were added to the quartz suspension. The final concentration of HA in the solution was 20 or 60 mg/L. For the investigation of the Th(IV) sorption onto Merck-quartz in

the presence of HA, 5.02 mL pre-equilibrated Th(IV)-HA solution (equilibration time: 24 hours) of three different pH values (3.5, 5.0, 6.5) were added. The final concentrations of Th(IV) and HA in the solution were $1.2 \cdot 10^{-8}$ M and 20 mg/L, respectively. After addition of Th(IV), HA or Th(IV)/HA solutions, the pH values were readjusted immediately and after 1 day of contact time, if necessary. The samples were shaken for 4 days to reach the equilibration. After shaking and short sedimentation of mineral particles, the supernatants of single samples were filtered using Minisart N membranes (Sartorius) with a pore size of 450 nm. Prior to filtering, the filters were rinsed with 1 mL of sample solution. The filtrates were analysed for the final Th(IV) and HA concentration. The Th(IV) concentration in solution was determined by ICP-MS (Inductive Coupled Plasma-Mass Spectrometry, Mod. ELAN 500, Perkin Elmer) and the HA concentration in solution was measured by liquid scintillation counting (LSC, Beckman Instruments). Prior to the determination of the Th(IV) concentrations in the samples containing HA, HA was removed by digestion in a microwave in order to avoid any disturbing effects during ICP-MS measurements. The end pH values of the samples were determined in the remaining unfiltered solutions. Finally, the Th(IV) sorption onto vial walls was investigated. The vials were washed with water and dried. Then, 7 mL 1 M HNO_3 were added and the vials were shaken for 2 days. The Th(IV) concentration in the solutions was determined by ICP-MS. The amount of Th adsorbed on the mineral surface was calculated as the difference between the initial Th(IV) concentration ($1.2 \cdot 10^{-8}$ M) and the sum of the amounts of Th(IV) remaining in solution and Th adsorbed onto the vial walls. The same experiments were performed applying quartz sand as mineral phase.

In the experiments studying the Th(IV) sorption in the presence of HA, the solution of Th(IV) and HA was pre-equilibrated. After adding Th(IV) to HA solution, the pH was adjusted to 3.5, 5.0, and 6.5, respectively, and the solutions were equilibrated for 24 hours. To be sure, that there is no loss of Th(IV) due to colloid formation, the Th(IV) concentration in the solution of Th(IV) and HA was followed during the reaction time. It was found that the Th(IV) concentration in the solutions did not change.

In order to estimate the degree of Th(IV) sorption on filter materials, one series of direct measurements of Th(IV) in non-filtered supernatants was performed The results were compared with those from experiments with filtration. It could be shown that there was no significant difference between the concentration determined from the supernatant and the 450 nm filtrate in the pH range between pH 4.5 and pH 7.5.

7.1.2 Results and discussion

Th(IV) Sorption onto vial walls

Figure 7.1 shows the sorption of Th(IV) onto the walls of the PP vials in the absence and presence of HA. Depending on the pH, significant sorption of Th(IV) on PP tubes was observed for all experiments. The amount of Th(IV) sorbed onto the vial walls in the absence of HA increases with increasing pH to a maximum of 75 % at pH 7. From that it can be concluded that the Th(IV) sorption on the PP tubes competes with sorption on Merck-quartz. The presence of HA influences Th(IV) sorption on the walls. In comparison to the experiments without HA the percentage of Th(IV) sorbed onto the vial walls decreases to 15 %. The sorption of Th(IV) onto the walls is also influenced by the solid/solution ratio. An increase of the

amount of Merck-quartz to 500 mg causes a decrease of the Th(IV) vial wall sorption of about 20 % in the acidic and about 10 % in the alkaline pH range, respectively. In the case of quartz sand comparable results were observed.

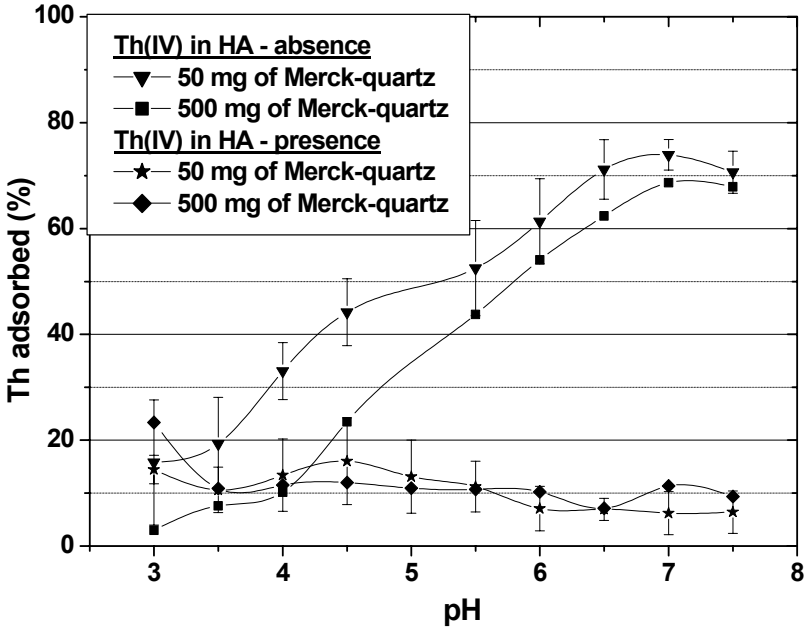

Fig. 7.1: Th(IV) sorption onto vial walls in the absence and presence of 20 mg/L HA.

HA sorption on Merck-quartz and quartz sand

Quartz sand has similar sorption properties as Merck-quartz. The observed sorption behaviour of HA was almost the same for both of these materials (Fig.7.2). The sorption of HA on these minerals depends on pH. The HA sorption decreases with increasing pH value. The results show that about 80 % of HA are sorbed onto quartz at pH 3. However, there is a possibility that a part of HA is precipitated at pH 3. There could be an overlapping of both processes, HA sorption and precipitation. At pH values ≥ pH 6 no HA adsorption was detected. These results correspond to the properties of quartz and HA in solution. Quartz has a low point of zero charge (PZC: 2.0 [73]), which results in predominantly negatively charged surface species (>SiO^-) in the pH range studied. At pH values > pH 6 carboxyl groups of HA are deprotonated, resulting in a negative charge of the HA. Due to electrostatic repulsion no HA is sorbed onto the negatively charged surface of quartz, which explains the observed sorption behaviour. These results were confirmed in the experiments with higher concentration of HA (60 mg/L). The course of the sorption curve is identical. The sorption of HA decreases faster because of its higher concentration.

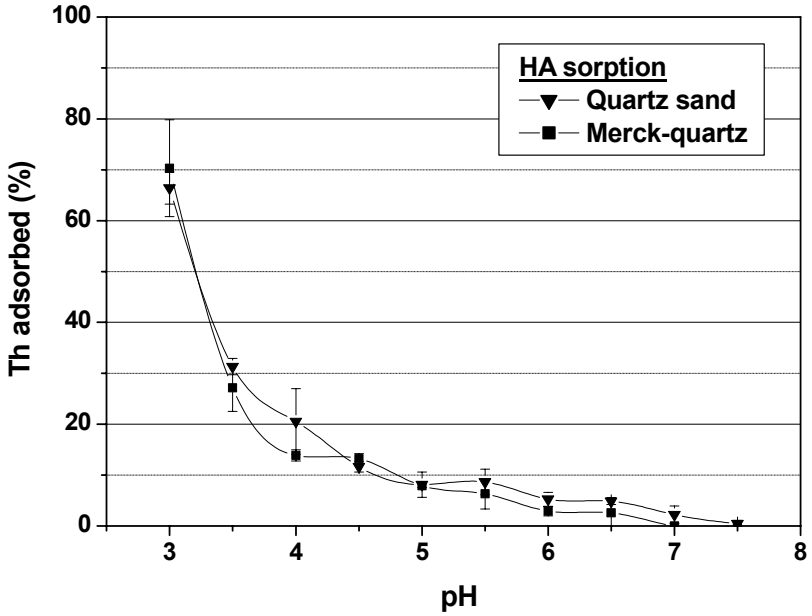

Fig. 7.2: HA uptake by Merck-quartz and quartz sand ([HA] = 20 mg/L).

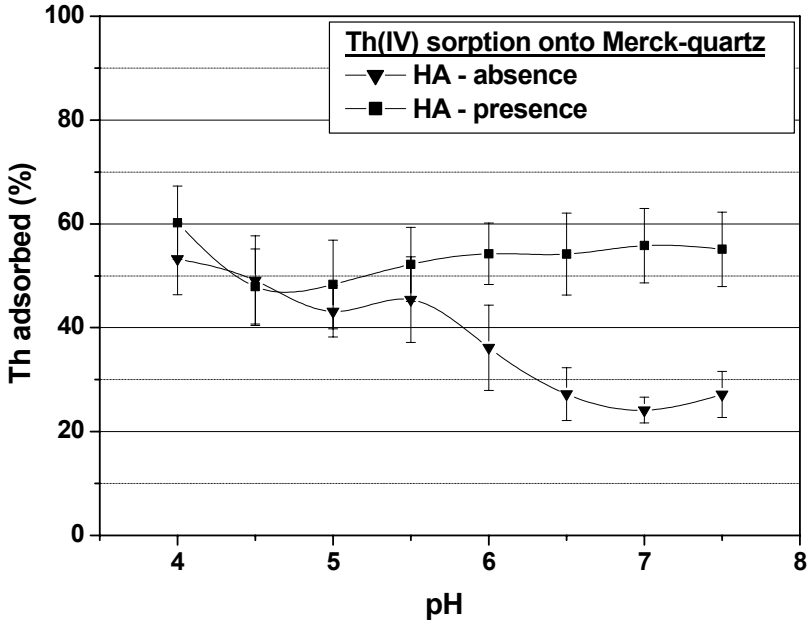

Fig. 7.3: Th(IV) uptake by Merck-quartz in the absence and presence of HA ($[Th^{4+}] = 1.2 \cdot 10^{-8}$ M, [HA] = 20 mg/L).

Th sorption on Merck-quartz and quartz sand

The Th(IV) sorption onto Merck-quartz and natural quartz sand in the presence of HA was compared with the experiments performed under identical conditions, but in the absence of HA. In Fig. 7.3 the observed pH dependent Th(IV) uptake onto Merck-quartz in the absence and presence of synthetic HA type [^{14}C]M42 is shown. Figure 7.4 shows the sorption of

Th(IV) onto quartz sand. The Th(IV) sorption onto Merck-quartz and also onto quartz sand is affected by the presence of HA. In the case of Merck-quartz the sorption curve can be divided into two parts. Between pH 4 and pH 4.5 the Th(IV) sorption in the presence of HA is slightly higher than in the HA free system. This small enhancement could be a result of the overcompensation of the number of mineral binding sites blocked by sorbed HA. Additional binding sites for Th(IV) ions thus stem from HA itself. The Th(IV) uptake onto quartz in the presence of HA decreases with increasing pH value. This could be caused by the progressive desorption of HA from the quartz surface, leading to the complexation of Th(IV) in solution. Between pH 4.5 and pH 7.5 the Th(IV) sorption in the system without HA is low due to the high Th(IV) sorption onto the vial walls mentioned above which competes with the Th(IV) sorption on the quartz surface. Contrary to expectations, the Th(IV) sorption in the binary system is lower than in the system with HA. This can also be explained by the high wall sorption of Th(IV) in the absence of HA. Therefore, conclusions concerning the influence of HA on the Th(IV) sorption onto quartz at pH values > pH 4.5 are not possible.

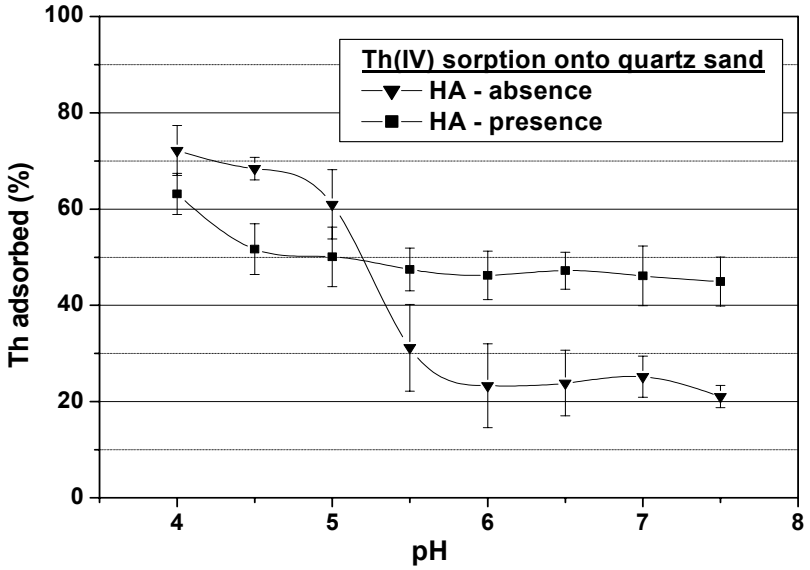

Fig. 7.4: Th(IV) uptake by quartz sand in the absence and presence of HA ([Th(IV)] = $1.2 \cdot 10^{-8}$ M, [HA] = 20 mg/L).

The sorption behaviour of Th(IV) onto quartz sand in the presence of HA is comparable to that on Merck-quartz. However, in absence of HA, between pH 4 and 5.5, the sorption of Th(IV) onto quartz sand is significantly different compared to that on Merck-quartz in the same pH range (cf. Fig. 7.3). In this range a higher Th(IV) sorption onto quartz sand in the absence of HA was observed. There is one difference between these two investigated solids. Both materials differ in trace amounts of Fe, Al, Ti in form of oxides. So it seems probable, that these minor components occurring in quartz sand contribute to an enhanced Th(IV) uptake by forming additional binding sites. In contrast to that, the presence of HA slightly reduces the Th(IV) sorption onto quartz sand. The amount of Th(IV) sorbed onto quartz sand in the presence of HA decreases with increasing pH value (pH 4 $\rightarrow$ pH 5). These observations can be due to the higher amount of dissolved HA in solution and the formation of Th(IV)-humate complexes. In the alkaline pH range the sorption of Th(IV) in the absence of HA is

weak due to the high wall adsorption of Th(IV). Thus, it is not comparable with the sorption in the presence of HA.

Th(IV) and HA type [^{14}C]M42 show a pH-dependent sorption behaviour onto Merck-quartz and natural quartz sand. The sorption of Th(IV) is slightly affected by HA. The influence of HA on the Th(IV) sorption depends on the pH and the mineral phase.

7.2 Neptunium(V) sorption onto granite in the absence and presence of humic acid

In Germany, besides salt formations also granitic subsurface environments are taken into account as potential host formations for the geological disposal of radioactive waste [74]. For this study, granite from Eibenstock was chosen which determines as geologic formation a large area of the former uranium mining areas in the Western Erzgebirge in Saxony, Germany. It was already applied for uranium(VI) sorption studies [75]. Granite is mainly composed of the minerals quartz, orthoclase, biotite, albite, and muscovite.

In this work, the sorption of Np(V) onto granite and its main mineral constituents is studied under anaerobic conditions at an ionic strength of 0.1 M as a function of pH in a series of batch equilibrium experiments. Furthermore, the effect of HA on the Np sorption is studied in order to determine whether humic material is likely to significantly influence Np sorption on granite.

7.2.1 Experimental

Materials

The rock material granite, collected in the region Eibenstock (Germany), is composed of 45 vol.% quartz (SiO_2), 35 vol.% orthoclase ($KAlSi_3O_8$), 7.5 vol.% biotite ($K(Mg,Fe^{2+},Mn)_3[(OH,F)_2/(Al,Fe^{3+})Si_3O_{10}]$), 7.5 vol.% albite ($NaAlSi_3O_8$), 4 vol.% muscovite ($KAl_2[(OH,F)_2/AlSi_3O_{10}$), and 1 vol.% opaque minerals. The 63 to 200 µm grain size fractions of the solids were applied for sorption experiments. The Np(V) stock solutions were obtained by dissolving solid $^{237}NpO_2NO_3$ in 0.1 M HNO_3. As HA the ^{14}C-labeled synthetic HA type M42 (batch M170, chapter 3.1) was used for the experiments.

Sorption experiments

For sample preparation, all solutions were prepared with CO_2-free water in a nitrogen atmosphere glove box. 5 mL of a 0.1 M $NaClO_4$ solution (pH 2.8) were added to 50 mg of the geomaterial in 15 mL vials (PP, Nalgene). The samples were stirred for 30 min to remove adsorbed CO_2 from the mineral surface. After that, the desired pH value (pH 4 to pH 11) was adjusted by addition of diluted $HClO_4$ or carbonate-free NaOH. During pre-equilibration of the samples (about 4 weeks), the samples were shaken continuously and the pH values were readjusted until they were stable. The sorption experiments in the absence and presence of HA were started by adding 5 mL 0.1 M $NaClO_4$ solution (pH about 7) and 5 mL HA stock solution (^{14}C-M42, 0.1 M $NaClO_4$), respectively, and about 80 µL of the Np(V) stock solution

simultaneously to the preconditioned minerals. The Np(V) stock solutions were prepared prior to each sorption step by separating ^{233}Pa from ^{237}Np using Dowex-50. The oxidation state of the Np in the stock solutions was spectroscopically confirmed to be pentavalent. The final Np and HA concentration in the sample solutions was 1.3×10^{-6} M and 27 mg/L, respectively. The solid solution ratio was 50 mg/10 mL. The pH was readjusted immediately after addition of the stock solutions. Then, the samples were shaken at room temperature for about 160 hours during which the Np and HA sorption onto the solids reached equilibrium. After centrifugation of the samples (3500 rpm, 15 min), the equilibrium pH values were recorded. Subsequently, the supernatant was filtered (450 nm, Minisart RC 15, Sartorius). Prior to filtering, the filters were rinsed with 1 mL of the sample solutions.
In the filtrates the final Np and HA concentration was determined by liquid scintillation counting (Beckman Instruments) using α/β-discrimination. For this, 1 mL of the filtrate was mixed with 5 mL of a Ultima Gold scintillation cocktail. The amount of Np and HA adsorbed to the mineral surface was calculated as the difference between the initial Np and HA concentrations and the final Np and HA concentrations in the 450 nm filtrates.

7.2.2 Results and discussion

The Np sorption in the absence of HA and the Np and HA sorption in experiments performed in the presence of HA is shown for granite and its mineral constituents muscovite, orthoclase, albite, quartz, and biotite in Fig. 7.5.
The sorption experiments, carried out in the absence of HA, show that the Np sorption starts between pH 7 and pH 8 and increases with increasing pH value.
For the sorption experiments performed in the presence of HA the following results were obtained. As expected, the HA sorption decreases with increasing pH value. The reason for the sudden increase of the HA sorption onto biotite between pH 9.2 and pH 11 is not known. Compared to the Np sorption in the absence of HA, the Np sorption onto granite is decreased by HA between pH 7 and pH 11. The Np sorption onto muscovite and orthoclase is somewhat increased by HA between pH 6 and pH 9 and at higher pH values relatively strongly decreased. The Np sorption onto albite and quartz is not changed by HA up to pH 10 and pH 9, respectively. At higher pH values it is again relatively strongly decreased. In case of biotite, the Np sorption is decreased by HA between pH 7 and pH 11, as was found also for granite.

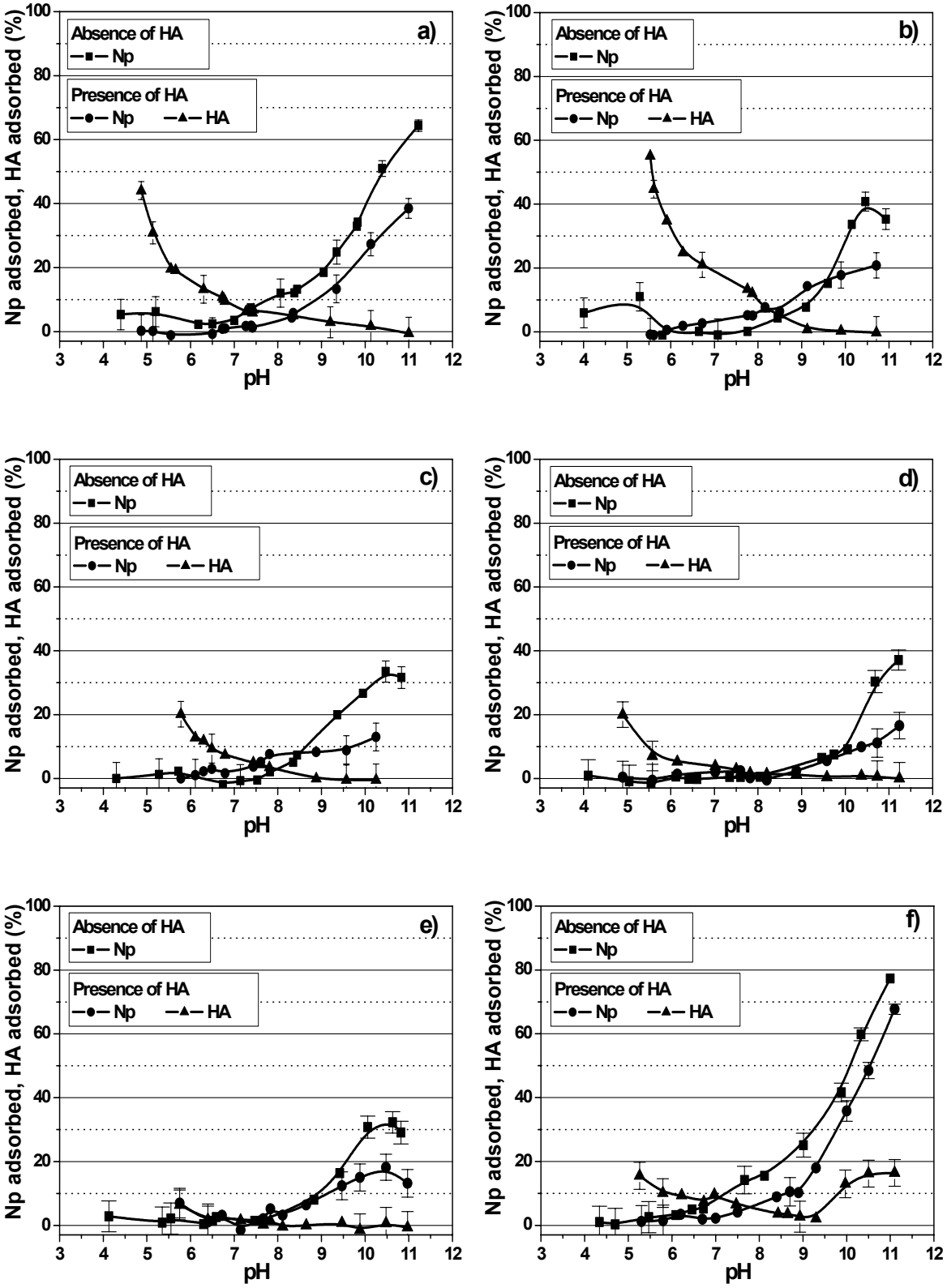

Fig. 7.5: Np and HA uptake by (a) granite, (b) muscovite, (c) orthoclase, (d) albite, (e) quartz, and (f) biotite ($[NpO_2^+] = 1.3\times10^{-6}$ M; [HA] = 27 mg/L; I = 0.1 M $NaClO_4$; CO_2-free).

The Np speciation for the experimental conditions applied in this study is shown in Fig. 7.6. It was calculated with the geochemical computer code EQ3/6 [12] applying the Np(V) hydrolysis constants compiled in the NEA data base [61], the neptunyl humate complexation constant log β = 3.6 and the pH function of the loading capacity (LC) with LC = -0.589 + 0.101 • pH (cf. Fig. 8.1 in chapter 8). The results show that the free neptunyl ion predominates the Np speciation in aqueous solution. The Np(V) hydrolysis species in solution ($NpO_2OH_{(aq)}$) is increasingly formed between pH 9.5 and pH 11. In the presence of HA, $NpO_2HA(I)$ is formed between pH 6 and pH 11 with a maximum of 13.6 % at about pH 10.5. For the pH region higher than 9, the formation of the mixed complex $[NpO_2(OH)HA]_{coll.}$ is suggested by Marquardt et al. [63]. Presently, this complex cannot be quantified thermodynamically, however, this complex would explain the strong reduction of the Np sorption by HA at pH values higher than 9 and 10, respectively.

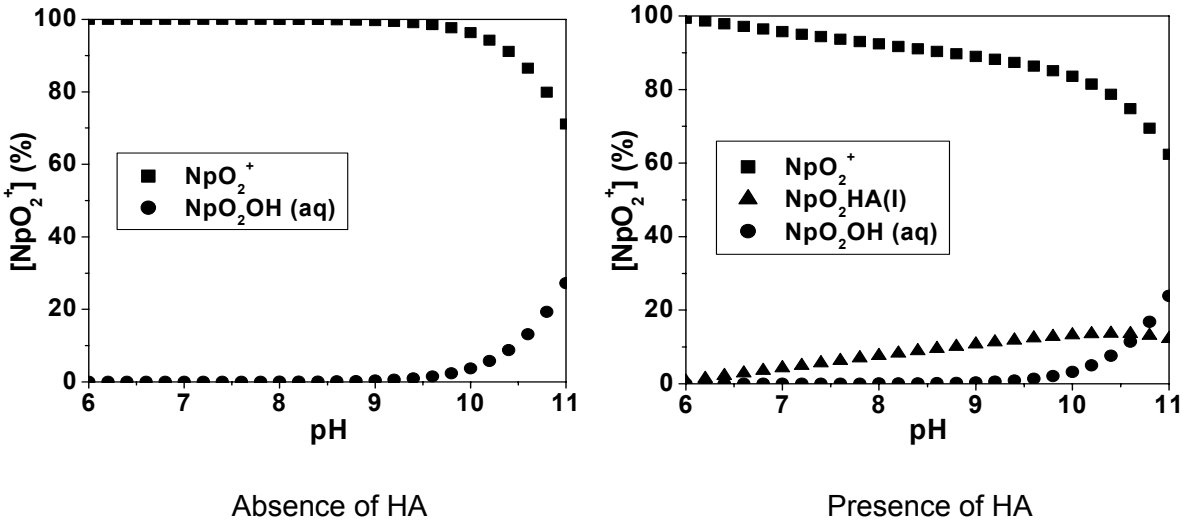

Fig. 7.6: Np speciation in solution ($[NpO_2^+] = 1.3\times10^{-6}$ M; [HA] = 27 mg/L; I = 0.1 M $NaClO_4$; CO_2-free).

The results in Fig. 7.5 have shown, that both granite and biotite show a strong Np sorption in the alkaline pH region. Furthermore, compared to the Np sorption experiments in the absence of HA, the reduction of the Np sorption by HA between pH 7 and pH 11 is similar for both materials. From this, it is concluded that biotite is the dominating mineral phase in the rock material granite for the Np sorption.

Mössbauer spectroscopic measurements have shown that in un-weathered biotite 84.5 % of Fe_{total} occur as Fe(II) [76]. This Fe(II) occurring in biotite and thus, also in granite could possibly lead to a reduction of Np(V) to Np(IV). For magnetite it was found by Nakata et al. [77] that Np(V) is reduced to Np(IV) by Fe(II) on the surface of magnetite but not by Fe(II) ions released from magnetite into solution. Such a reduction of Np(V) to Np(IV) on the mineral surface would lead to an increase of the Np sorption. However, for Np sorption experiments in the presence of HA it was found by Zeh et al. [78] that especially the combination of Fe(II) and HA could lead to a reduction of Np(V) to Np(IV). Compared to Np(V), Np(IV) is generally stronger complexed by HA due to its higher charge [79]. Thus, the Np sorption onto granite

and biotite would be reduced compared to experiments without HA. The oxidation state of Np in the supernatant solutions of the sorption samples without and with HA was checked by liquid-liquid extraction using TTA. So far, no Np(IV) could be detected in solution.

7.3 Study of the influence of humic acids on the migration of uranium(IV)/(VI) in quartz sand

The influence of HA on the migration of actinides in the environment can be studied in laboratory column experiments. Column experiments with natural sand and groundwater systems rich in humic substances demonstrated that a certain fraction of the load actinides (e.g., U(VI) [80], Am(III) [81] and Np(IV)/(V) [82]) migrate humic colloid-borne as fast as the groundwater flow. This colloid-borne migration is controlled by kinetic processes.
The present study focuses on the influence of HA on the migration of U(VI) and U(IV) in a quartz sand system at a laboratory scale. The migration of U(VI) was studied in the presence and absence of HA. In addition to that, the HA migration under the applied experimental conditions was described. In order to characterize the migration behaviour of U under reducing conditions we studied the migration of the redox couple U(IV)/(VI) in the presence of HA.

7.3.1 Experimental

Experimental set-up

Migration experiments were performed in a glove box under nitrogen atmosphere. The experimental set-up is shown in Fig. 7.7.
Columns 250 mm in length and 50 mm in diameter, tightly packed with quartz sand were used. A marine fine sand, Gaussian distributed in particle size, with a mean grain diameter of 153 µm from Heerlen, Netherlands, was chosen for its chemical purity (see chapter 7.1.1). Prior to use the quartz sand was washed with Milli-Q water and annealed for 6 hours at 700 °C. After packing, the sand columns were equilibrated with degassed $NaClO_4$ solution (0.1 M, pH 7.5) over a period of 3 weeks.

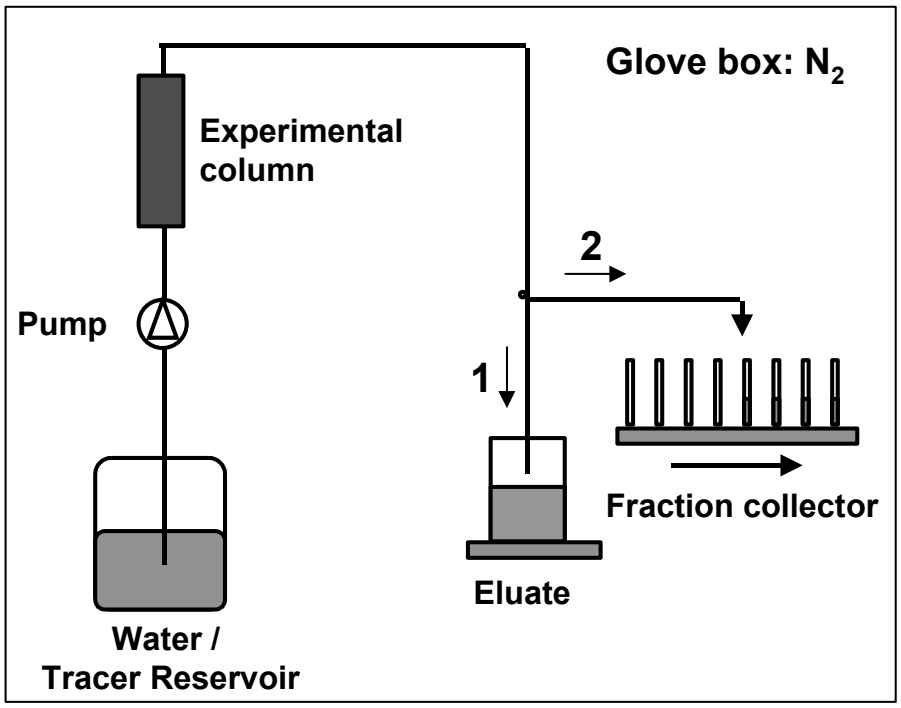

Fig. 7.7: Set-up of the column experiments.

All experiments were carried out at room temperature under absence of light, applying degassed solutions. Continuous pulse injection was applied. The tracer impulse was followed by a multiple elution of the column with 0.1 M $NaClO_4$ (pH 7.5). For the determination of the hydraulic and transport parameters of the columns, tritiated water (HTO) was used as conservative tracer. Each experimental problem was studied in a separate column in order to avoid mutual interferences. The transport parameters and the experimental conditions for all experiments are listed in Tab. 7.1. It shows a good reproducibility of the column packing.

Tab. 7.1: Experimental conditions and transport parameters of the column experiments.

Exp.	Impulse (mL)	HA (mg/L)	U (mol/L)	Darcy velocity (m/s)	Effective pore volume (mL)	Dispersion coefficient (m^2/s)
1	660	49.9	-	$3.3 \cdot 10^{-6}$	181	$5.5 \cdot 10^{-5}$
2	716	50.3	-	$4.4 \cdot 10^{-6}$	181	$5.5 \cdot 10^{-5}$
3	690	-	$1.1 \cdot 10^{-5}$	$3.4 \cdot 10^{-6}$	181	$6.0 \cdot 10^{-5}$
4	457	49.9	$1.0 \cdot 10^{-5}$	$3.3 \cdot 10^{-6}$	178	$6.1 \cdot 10^{-5}$
5	462	50.0	$1.0 \cdot 10^{-6}$	$3.6 \cdot 10^{-6}$	173	$5.0 \cdot 10^{-5}$

Humic acid migration

The HA migration in the quartz sand system in the presence and absence of U was studied applying synthetic HA type M42 (cf. chapter 3.1). It shows functional and structural properties that are comparable to natural HA. In addition to that, synthetic HA type M42 exhibits a U(VI) complexation behaviour that is comparable to natural HA [83]. In order to perform a very precise HA detection in environmentally relevant concentrations we spiked the HA solutions with ^{14}C-labeled synthetic HA type M42 (batch M170, 2.38 MBq/g, cf. chapter 3.1).

For the study of the HA migration in the absence of U (experiments 1 and 2), HA solutions with a concentration of 50 mg/L (specific activity: 70 kBq/L) were prepared by dissolving unlabeled and ^{14}C-labeled synthetic HA type M42 in 0.1 M $NaClO_4$ solution. The pH values of these solution were adjusted to pH 7.5 using dilute $HClO_4$ and NaOH solution.

Uranium(VI) migration in absence and presence of humic acid

The U(VI) migration in the absence of HA (experiment 3) was studied applying a $1.1 \cdot 10^{-5}$ M $UO_2(ClO_4)_2$ (0.1 M $NaClO_4$, pH 7.5) solution.

An acidic $UO_2(ClO_4)_2$ solution was added to a ^{14}C-labeled HA solution in order to determine the U(VI) migration in the presence of HA (experiment 4). The final uranyl humate solution with a HA concentration of 50 mg/L (^{14}C: 70 kBq/L) and an U concentration of $1.0 \cdot 10^{-5}$ M (0.1 M $NaClO_4$) was spiked with 40 kBq/L ^{234}U containing traces of ^{232}U. Before the injection into the column this solution was equilibrated for 98 hours.

Uranium(IV) migration in presence of HA

For the study of the U(IV) migration in the presence of HA (experiment 5), the U(IV) was prepared by electrochemical reduction of an acidic uranyl (^{234}U) nitrate solution. The absence of U(VI) in the U(IV) stock solution was confirmed by time-resolved laser-induced fluorescence spectroscopy. For experiment 5, the acidic ^{234}U(IV) solution was added to a ^{14}C-labeled HA solution. The final concentrations of the uranium humate solution (0.1 M $NaClO_4$, pH 7.5) amounted to 50 mg/L HA (^{14}C: 70 kBq/L) and $1.0 \cdot 10^{-6}$ M ^{234}U (60 kBq/L). This solution was equilibrated for 2 hours prior to start of the experiment.

In order to differentiate between U(IV) and U(VI) redox speciation was determined by liquid-liquid extraction using TTA (thenoyltrifluoroacetone; Fluka,) [84]. The extraction yield was found to be 90 %. The standard deviation amounts to 5 %.

Measurement of breakthrough curves

Breakthrough curves of HTO, HA and U were measured by fraction analysis using liquid scintillation counting (LSC, Beckman Instruments) for HTO, ^{14}C and ^{234}U, and ICP-MS for ^{238}U. The LSC spectra were deconvoluted to determine the activity contribution of ^{232}U daughter nuclides.

Analysis of the solids

After the end of column experiments 4 and 5 samples of the filling materials were taken at distances of about 10 mm, 125 mm, and 240 mm from the inlet. 3 g of the sample material

were shaken with 1 M NaOH and 1 HNO_3, respectively, for three days in order to elute the adsorbed amount of ^{14}C and ^{234}U. The supernatant solutions were analysed using LSC as described above.

Data processing and evaluation

For depicting the breakthrough curves all effluent concentrations were normalized to the input concentration c_0 of the tracer solution. The time axis (abscissa) is represented as the ratio of effluent pore volume and effective pore volume, determined from HTO breakthrough. The measured breakthrough curves were evaluated by means of the one-dimensional transport equation [85]. Assuming steady-state flow in a homogeneous matrix, linear sorption, and a first-order decay it may be written as

$$R_f \frac{\partial c}{\partial t} = D \frac{\partial^2 c}{\partial x^2} - v \frac{\partial c}{\partial x} - \mu c \qquad (7.1)$$

where c is the concentration, v is the average pore-water velocity, D is the hydrodynamic dispersion coefficient, μ is a first order decay coefficient, R_f is the retardation factor, x is distance, and t is time. The retardation factor may be determined from the ratio of effluent pore volume at tracer breakthrough (V) and the effective pore volume (V_P)

$$R_f = \frac{V}{V_P} \qquad (7.2)$$

and is related to the empirical distribution coefficient K_D by

$$R_f = 1 + \frac{\rho K_D}{\varepsilon} \qquad (7.3)$$

where ρ is the bulk density of the porous medium and ε is the effective porosity. Retardation factors exceeding unity indicate a retarded transport compared to a conservative tracer, whereas values less than unity refer to an accelerated transport. The last term of the right hand side of Eq. (7.1) is a sink term that describes the deposition flux of colloidal particles, also referred to as filtration [86]. The parameter μ may be interpreted as deposition rate coefficient.

The CXTFIT code [85] was utilized to estimate the parameters v, D, and μ from the break through curves using a non-linear least-square optimisation. The standard errors of the simultaneously fitted parameters were derived from the sum of squared residuals between the observed and the fitted concentrations.

The tracer recovery in the eluate R_{eluate} was approximated by numerical integration of the breakthrough curve applying the trapezoidal rule and normalization to the input quantity.

7.3.2 Results and discussion

Speciation of uranium

The interpretation of the experimental data requires detailed knowledge on the species distribution. In a 10^{-5} M carbonate free U(VI) solution at pH 7.5 the dominating U(VI) species is $UO_2(OH)_2$(aq). In presence of HA about 90 % of U(VI) are complexed in form of a ternary U(VI) humate complex (UO_2(OH)HA(I)). At a redox potential of 50 mV the U speciation in carbonate free 10^{-6} M U solution is dominated by 84 % of $UO_2(OH)_2$(aq) as shown in Fig. 7.8.

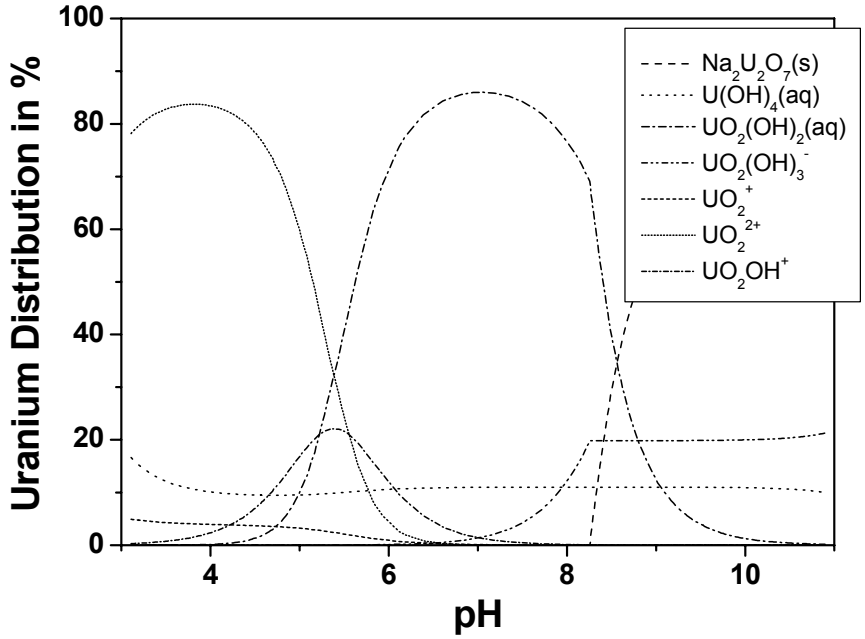

Fig. 7.8: Speciation of uranium at a redox potential of 50 mV (Thermodynamic data taken from [87]).

In addition, amounts of 11 % $U(OH)_4(aq)$ and 4 % $UO_2(OH)_3^-$ occur. No species calculations in presence of HA are possible due to the lack of thermodynamic data for the U(IV) HA complexation.
In the studied system HA type M42 controls the redox potential. A redox potential of about 50 mV can be derived for the studied system.

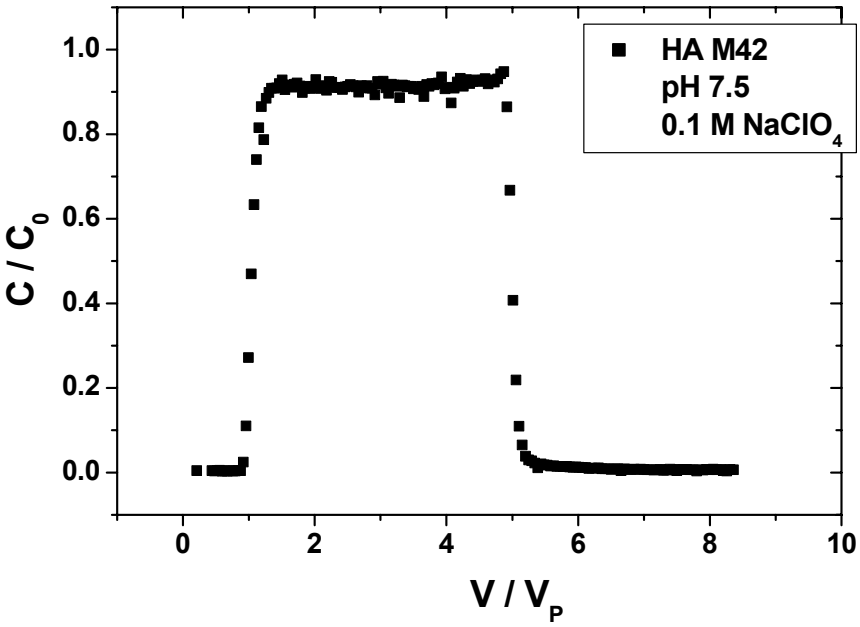

Fig. 7.9: Breakthrough curve of HA M42 in experiment 2. C: measured and C_0: initial concentration; V: effluent volume; V_P: effective pore volume.

Humic acid migration in absence of uranium (Experiments 1 and 2)

Evaluating the HA breakthrough curves as shown in Fig. 7.9, the retardation factor R_f as well as the eluate recovery on HA were determined (Tab. 7.2). The R_f values indicate an only slightly retarded transport of the HA compared to HTO (R_f: 1). Thus, there are no significant interactions between HA and the quartz sand surface, due to the negative charge of both species at pH 7.5. Batch experiments confirm this result. The detected R_f implies that there are no grain size exclusion effects which would be reflected in R_f values smaller than 1. The HA recovery of about 0.9 points to irreversible immobilization processes, e.g., filtration effects. The according filtration coefficient μ in Eq. (7.1) amounts to $(4.0 \pm 0.2) \cdot 10^{-6}$ s^{-1}.

Tab. 7.2: Retardation factors, R_f, and eluate recoveries, R_{eluate}, of the injected species.

Exp.	Species	R_f	R_{eluate}
1	HA	1.02 ± 0.02	0.91 ± 0.01
2	HA	1.02 ± 0.02	0.92 ± 0.01
3	U(VI)	2.09 ± 0.10	0.43 ± 0.02
4	HA	1.05 ± 0.02	0.85 ± 0.01
4	U(VI)+HA	1.19 ± 0.02	0.80 ± 0.01
5	HA	1.04 ± 0.02	0.90 ± 0.01
5	U(VI)+HA	1.11 ± 0.02	0.90 ± 0.06
5	U(IV)+HA	1.07 ± 0.02	0.66 ± 0.05

Uranium(VI) migration in absence of HA (Experiment 3)

The U(VI) migration in absence of HA is characterized by a strong retardation which is reflected in the R_f value greater than 1 (cf. Tab. 7.2 and Fig. 7.10). The shape of the breakthrough curve indicates kinetically controlled processes [85]. Especially the observed tailing directs to a slow release of U(VI) from the quartz surface even after five eluted pore volumes. The low U(VI) recovery can be caused by precipitation or sorption processes. At a 10^{-5} M U(VI) concentration the solid phase schoepite ($UO_3 \cdot 2H_2O$) is saturated. However, it is not expected that this solid is formed during the residence time of U in the system.

U(VI) migration in presence of HA (Experiment 4)

HA bound U(VI) exhibits a completely different breakthrough behaviour which is depicted in Figure 7.10. In presence of HA the U(VI) transport is accelerated and the U(VI) recovery is increased. This behaviour is attributed to the formation of soluble U(VI) humate complexes. However, for both components, HA and U(VI), slightly different R_f values and recoveries were detected (cf. Tab. 7.2). These effects are caused by association/dissociation processes in the system HA-U(VI)-quartz. A certain part of U(VI) dissociates from the soluble humate complex and adsorbs onto the quartz surface. Comparing differences in the recoveries of U(VI) and HA one can conclude that about 5 % of U(VI) is irreversibly bound on the quartz

surface. Considering the results reported by Artinger et al. [80], it can be assumed that these processes are kinetically controlled.

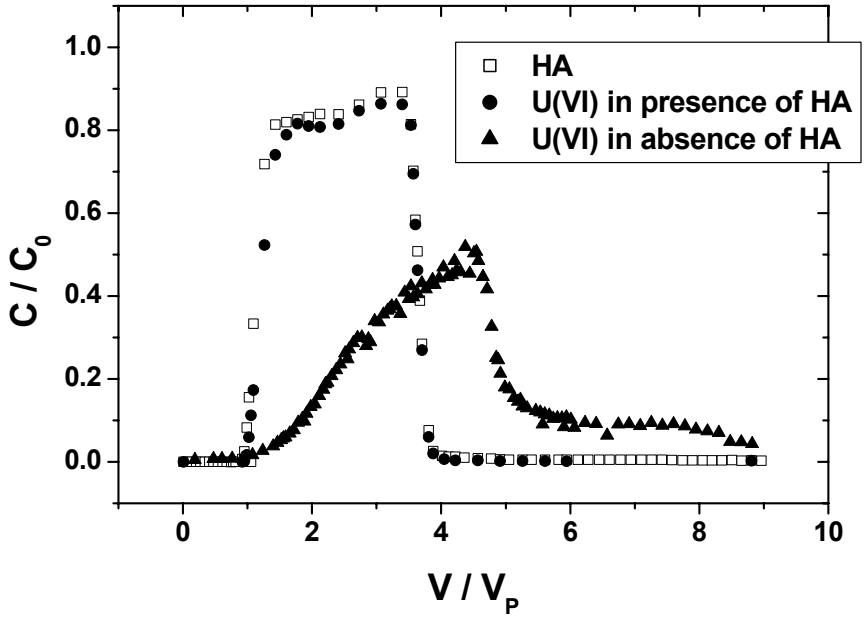

Fig. 7.10: Breakthrough curves of HA and U(VI) in experiments 3 and 4. C: measured and C_0: initial concentration; V: effluent volume; V_P: effective pore volume.

Migration of the U(IV)/U(VI) couple in presence of HA (Experiment 5)

The distribution of U(IV) and U(VI) in the starting solution amounts to 8 % and 92 %, respectively. This is comparable to the calculated redox species distribution at 50 mV mentioned above. This redox speciation was stable over the duration of the experiment. Moreover, this initial ratio of U(IV) and U(VI) was also found in the effluent solutions. This indicates that no oxidation processes occur in the column.

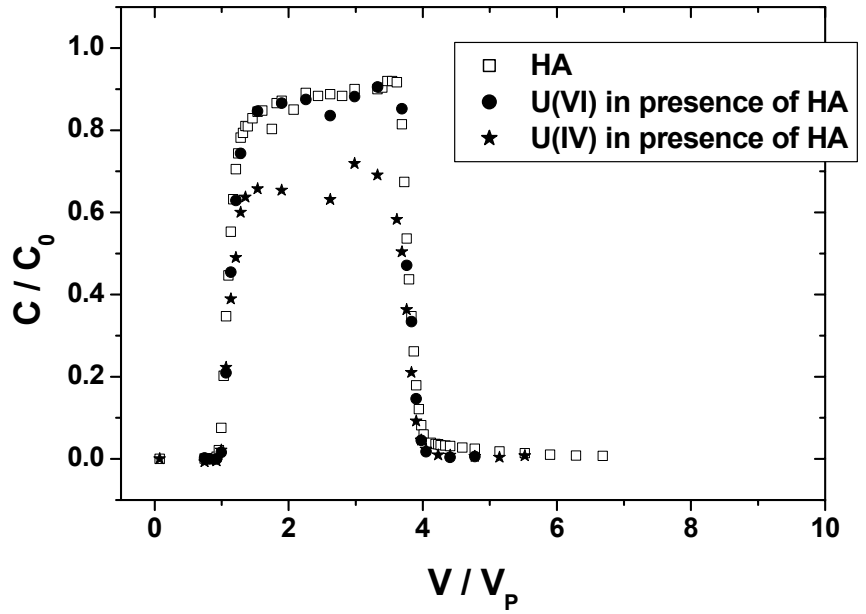

Fig. 7.11: Breakthrough curves of HA, U(IV), and U(VI) in experiment 5. C: measured and C_0: initial concentration; V: effluent volume; V_P: effective pore volume.

Figure 7.11 shows the breakthrough curves for HA, U(IV) and U(VI). Based on them R_f values and eluate recoveries listed in Tab. 7.2 are derived. As with the case of U(IV), the association/dissociation processes mentioned above control the transport behaviour in presence of HA (R_f > 1). Although U(IV) and U(VI) are characterized by different thermodynamic properties [88] no significant differences in their R_f values were observed under the applied experimental conditions.

A comparison of the U balances in experiments 4 and 5 shows that a decreased total U concentration results in a slightly higher recovery. In experiment 5 the total recoveries of both, U(VI) and HA, agree very well. This fact refers to a HA bound U(VI) transport.
In spite of the increased uncertainty of the extraction data, the U(IV) recovery is lower than that of U(VI). This points to a stronger interaction of U(IV) with the quartz sand surface and thus a more distinct immobilization. Nevertheless, there are strong indications that HA has a mobilizing effect on the U(IV) transport in the investigated system due to its complexing ability.

Balances of the reactive tracers

In addition to the eluate recoveries the adsorbed amounts of the tracers are investigated. Figure 7.12 shows the spatial distribution of ^{14}C and ^{234}U within column 4 and 5.

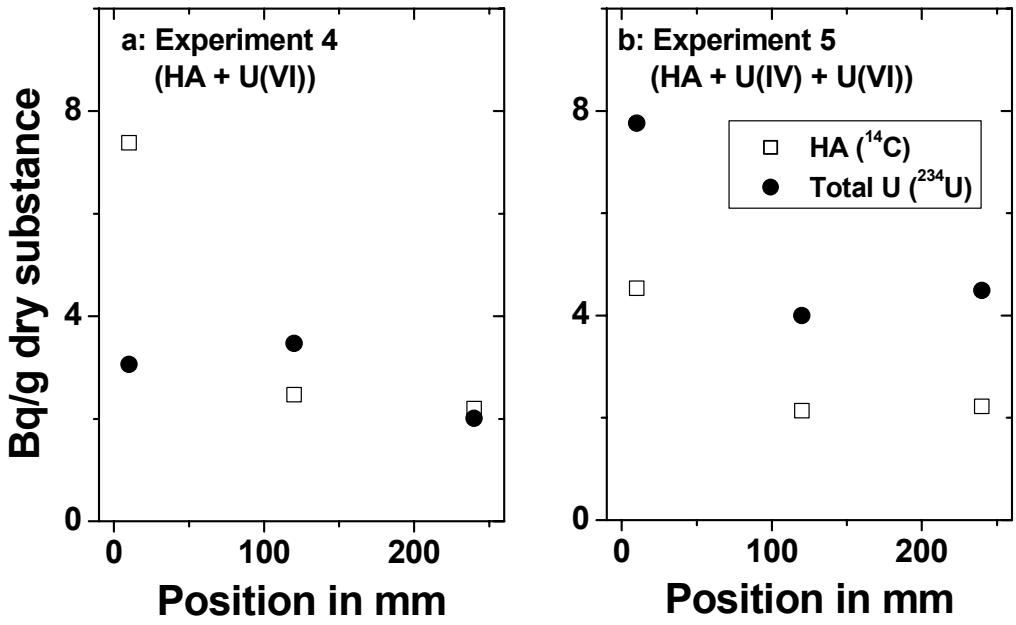

Fig. 7.12: Spatial distribution of ^{14}C and ^{234}U within column 4 and 5.

The amount of ^{234}U represents the total activity of U. U(IV) and U(VI) are not to be distinguished after contact with air and HNO_3 extraction. The curves suggest a close relation between both tracers with exception of the U concentration near the column inlet of experiment 4. Possibly this single measurement is not representative.

Tab. 7.3: Balances of reactive tracers in experiment 4 and 5.

Recovery	Experiment 4		Experiment 5	
	Humic acid (^{14}C)	Uranium (^{234}U)	Humic acid (^{14}C)	Uranium (^{234}U)
R_{eluate}	0.85 ± 0.01	0.80 ± 0.01	0.90 ± 0.01	0.82 ± 0.01
R_{solid}	0.11 ± 0.003	0.06 ± 0.002	0.07 ± 0.002	0.15 ± 0.004
R_{total}	0.96 ± 0.01	0.86 ± 0.01	0.97 ± 0.01	0.97 ± 0.01

The total balance of the reactive tracers in experiment 4 and 5 are summarized in Tab. 7.3. With exception of ^{234}U in experiment 4 the total recoveries are close to unity. Thus container walls do not adsorb significant amounts of tracer. The balances support the conclusions drawn from recoveries, in particular the close relation between the migration of HA and U.

From these experiments it can be concluded that HA affects the migration behaviour of both U(IV) and U(VI). In presence of HA U(VI) is significantly mobilized. A similar effect is supposed for U(IV). Both U redox species exhibit a different migration behaviour, in particular reflected in their effluent balances.
The system under investigation represents a strong simplification of natural aquifers in view of geology and solution composition. More complex compositions are typical in natural aquifer systems. Strong reducing conditions can occur in deep groundwaters. There, the tetravalent actinides become more important. However, the performed experiments are suitable in order to identify sensitive relationships between actinides, HA and rock matrix and to establish more sophisticated concepts for understanding and modelling of complex migration processes.

8 Integration of the Metal Ion Charge Neutralization Model into the geochemical speciation code EQ3/6

There are many different models used to describe interactions between humics and actinides. The most prominent ones can be categorized into two major groups. They differ in their approaches to describe the binding places at the humics molecule:

A) Discrete binding places
- Metal Ion Charge Neutralization [11]
- Model VI [89]
- Polyelectrolyte Model [90]

B) Continuous distribution function(s)

- NICA-Donnan model [91]
- CONICA model [92]

During this project, the metal ion charge neutralization (MICN) model was favoured due to its relative simplicity and the few parameters required. Moreover, there is ample experience and experimental data records available for this model in the project team.

One essential parameters required by the model is the proton exchange capacity (PEC). A normalization to multiple charged metal ions then gives a metal-specific total of the available binding sites. The next parameter, the loading capacity (LC) describes that part of the binding sites actually accessible for ligands (again normalized to the charge of the ligand). LC is a phenomenological parameter and thus a function of pH, ionic strength, ligand and others.

One of the tasks of the project was the embedding of the MICN into an existing geochemical speciation code. This should allow for a fast and easy computation of complex speciation patterns in real systems. Relying on an already established software ensures that algorithms and implementation is counter-checked, thus computations are reproducible and reliable. Furthermore, such software can take advantage from comprehensive pre-compiled standard databases. The software of choice was the EQ3/6 [12] geochemical speciation package well suited for thermodynamic and kinetic modelling of complex and heterogeneous systems. It was developed by Thomas J. Wolery from the Lawrence Livermore National Laboratory. All following work was based on the code version 7.2b of August 18, 1995. EQ3/6 is able to handle all reactions in aqueous solution, including redox reactions, it considers precipitation and dissolution of pure mineral phases and solid solutions, and has also kinetic modules to compute reaction paths. EQ3/6 is programmed in FORTRAN 77 (ANSI), there are both UNIX and PC versions, and an exhaustive manual is provided. Very important is the certification by the U.S. DOE as part of the Yucca Mountain Project. Several databases are included in the package.

But so far the EQ3/6 software does not consider any humics-metal interactions, despite that such interaction can not be neglected in many natural systems. Therefore, the MICN approach has been integrated into EQ3/6. This required changes in Fortran code of the modules for the data input, the addition of the computation of LC as f(pH) and the determination of the metal complex concentration. The program was compiled both as UNIX version (f77 compiler) and MS Windows NT version (Lahey LF 90 compiler). A major goal of the development was to reach a flexible solution with minimum impact on the existing input file and database structure. So unused options in the EQ3/6 input files now trigger functions such as the mode of the humics hydrolysis (see below), or the type of the pH function of LC. The data input processing is performed in a separate shell script module, allowing for the computation of LC as a function of pH or ionic strength and of the metal-specific concentration of available binding sites at the humic matter. These scripts enable semi-automatic parameter scans substantially increasing computation speed.

Humics species were included into the EQ3/6 thermodynamic database by defining pseudo-species based on fictitious elements because the very nature of humics prevents an exact stoichiometry and formation reaction based on simpler organic molecules. The humics species set exists twice: one version is based on a formally un-

charged humics molecule Hx(aq), the other one (HhH_2) considers two deprotonation steps. An input option allows the switch between these two alternative formulations. Examples for the two alternative (and mutually exclusive) formulations are given below:

a) reactions for humic acids without protolysis (standard)
- basis species Hx(aq) (formally uncharged)
- reactants UO2Hx++, UHx++++, UO2HxOH+, NpO2Hx+, ..

b) reactions for humic acids including protolysis
- basis species HhH2(aq) (formally uncharged)
- reactants Hh-, Hh--, UO2Hh, ...

Using input option switches certain species can be blocked or the log β of their formation reaction can be modified, independent form the standard database used.

A verification of the changed EQ3/6 version was done through speciation modeling of the systems U(VI)-HA and Np(V)-HA. In a first step published LC values for the HA-actinide system were fitted to a linear function as the simplest possible approach. Figure 8.1 shows the results for Np(V).

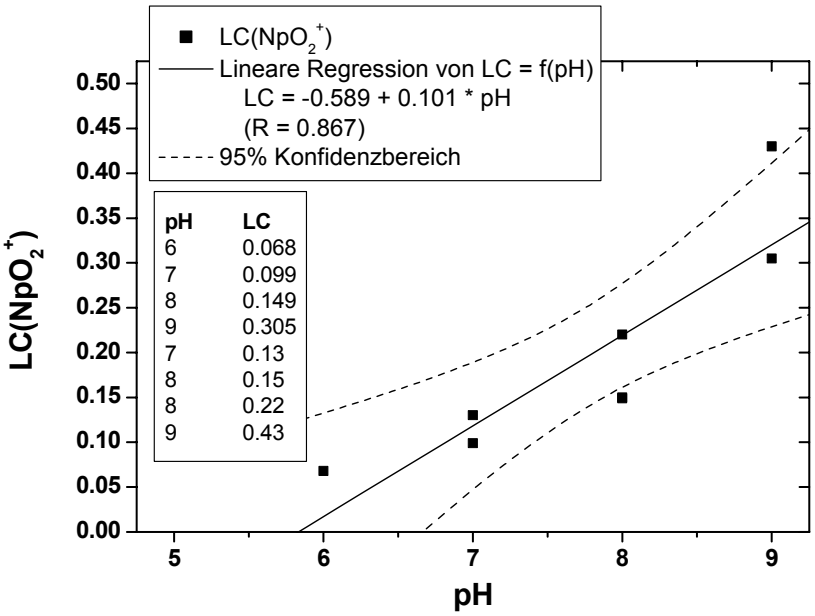

Fig. 8.1: Loading capacity $LC(NpO_2^+)$ as function of pH.

Then the obtained pH-LC relationship was used to compute the actinide speciation pattern as given in Fig. 8.2, again for Np(V). The experimental conditions are as follows: 100 mg/L HA, $2 \cdot 10^{-5}$ M NpO_2^+, 0.1 M $NaClO_4$, in air, log β = 3.6 for the formation of the complex.

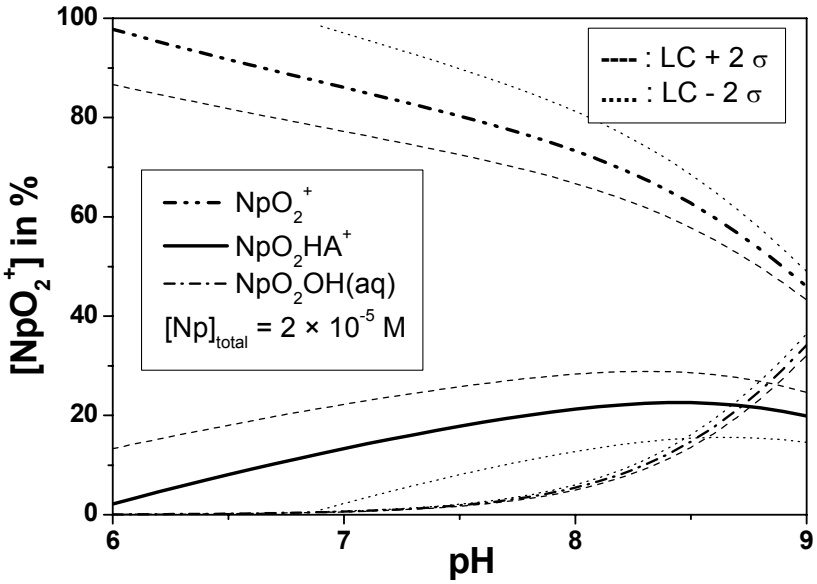

Fig. 8.2: Speciation of NpO_2^+ with HA as function of pH with uncertain LC values.

Similar results for U(VI) lead to the conclusions that a) the thermodynamic data sets for the interactions between actinides and HA are sparse and scattered, and b) LC as function of pH is not well defined, certainly caused by its very nature of being an empirical correction factor subsuming many different effects. To obtain a more comprehensive picture of the situation a development of a respective database has been initiated.

There is no easy way to do speciation scans on varying pH like it can be done by members of the PHREEQE or MINEQL code families, not to talk from scans over varying Eh or the concentration of some components. To overcome this limitation at least partially, some tools have been written to allow such scans by automatically starting a sequence of EQ3NR runs with appropriately updated input files, or by analysing and drastically shortening of the huge output from an EQ6 "titration" run. All these scripts can be found on the internet, the URL is:

http://www.fz_rossendorf.de/FWR/VB/EQ36/eq36.shtml

There is also a collection of tips and remarks for using EQ3/6 made available at:

http://www.fz_rossendorf.de/FWR/VB/EQ36/eq36_notes.shtml

Future research will focus on the separation of effects determining the LC value (namely protolysis reactions and aqueous metal ion speciation). It is also worth to investigate how to normalize properly the humic concentration with regard to the differently charged metal cations.

9 Development of a database for the application of the Metal Ion Charge Neutralization Model

Analysing the data situation with regard to the Metal Ion Charge Neutralization Model (MICN) [11] it became clear that the data quality is very heterogeneous, values from different research groups are difficult to compare. For real complex natural systems a consistent database can hardly be compiled. The best solution would be to re-assess all existing experimental raw data for metal complexation with HA and process them consistently with respect to the MICN approach. However, due to limited resources a more realistic first step was to set-up (for the first time) a database covering all so far published reaction constants for the MICN model including the reported experimental conditions and data processing details. Such a database then provides an overview concerning investigated HA types, ligands, parameter ranges (concentration of reaction partners, ionic strength, pH, Eh, ...). The most critical gaps can be identified and the data quality can be assessed more easily. At a later stage, also the automatic supply of data for speciation and reactive transport codes is possible.

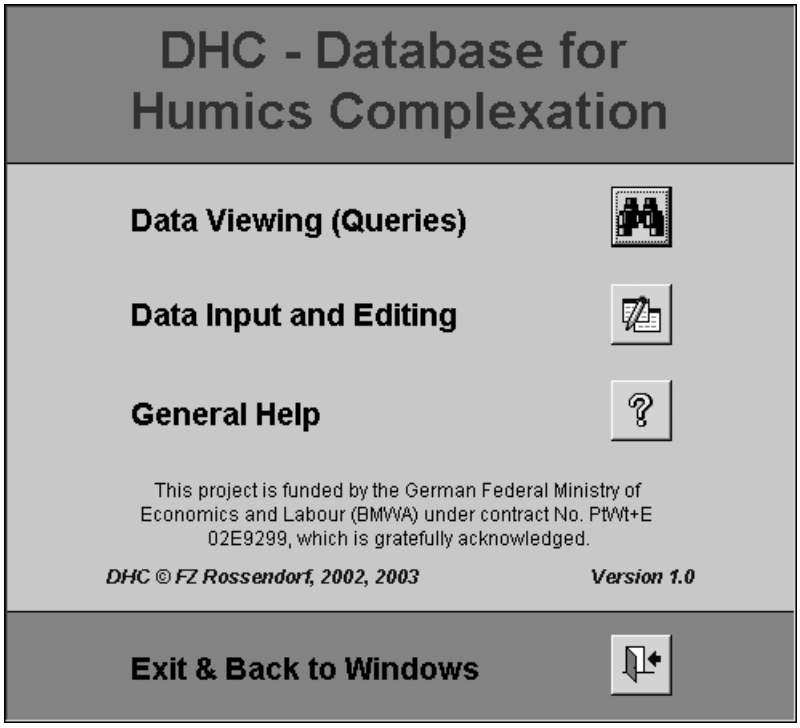

Fig. 9.1: Start menu of the humics complexation database DHC.

The “Database for Humics Complexation - DHC” is designed as a Relational Data Base System (**RDBS**), see Fig. 9.1 for the start menu. All information is structured into logical subunits, stored into separate tables which are logically connected by the RDBS. This ensures that every piece of information is only stored once. Other benefits are high efficiency with regard to storage capacity and access time, and internal consistency. In Fig. 9.2, a sketch of the major tables, their data elements, and their mutual relationships is given. The modular design also eases later extensions.

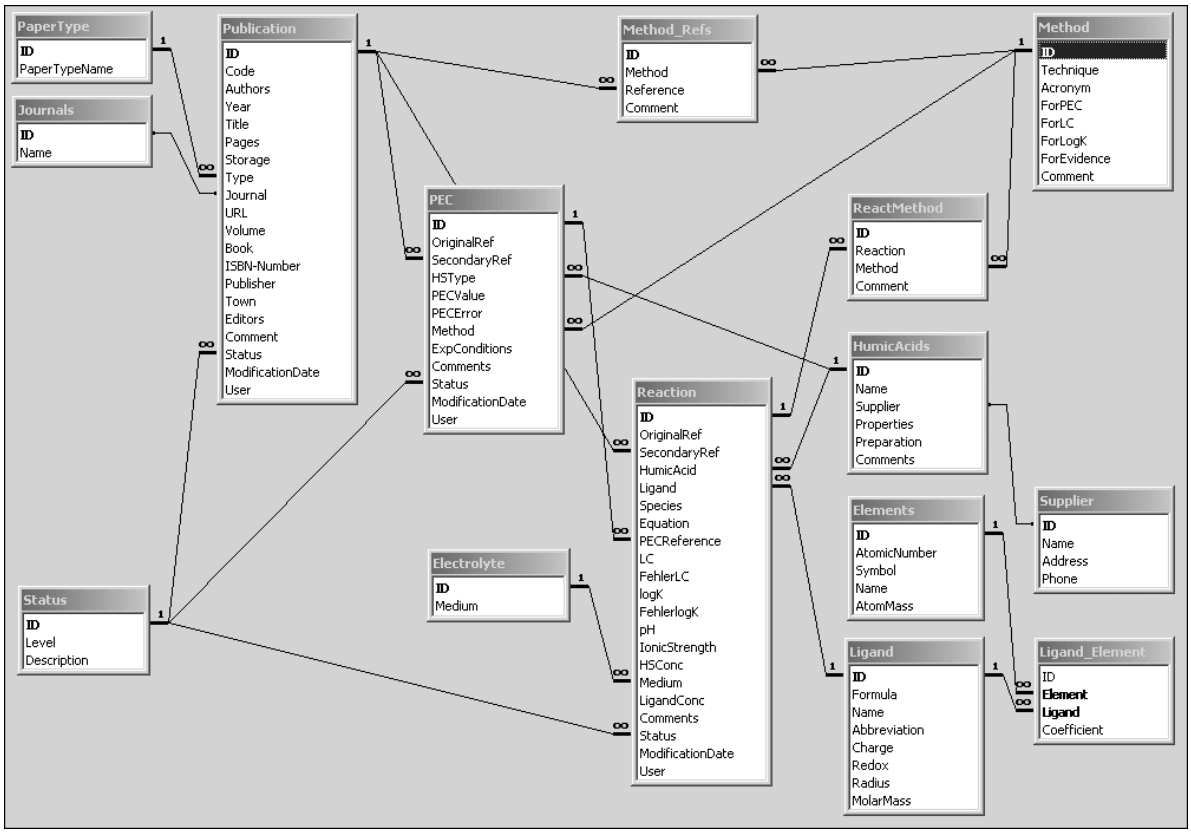

Fig. 9.2: Tables and their internal relations for the DHC RDBS.

The database is implemented in Microsoft Access on PC, providing an integrated graphical development system together with the RDBS. Data records can be displayed as tables, in forms or reports. Possible data types are: numeric, logic, text, binary object. Queries to the database can be performed with the standardized Structured Query Language (**SQL**), opening the opportunity to access external, additional databases, e.g. about spectroscopic data. Via SQL future versions of the DHC database can also be queried by web browsers. The programming of the database functionality can be enhanced by means of the Visual Basic for Application (**VBA**) programming language.

In general, all parameters recorded in the database are traced back to the original publication, including as many experimental details as possible to permit an evaluation of the data items. All internal relationships of complex data sets are stored, assuring a maximum of transparency and enabling the selection of internally consistent parameter sets. As an example, the input mask for the table containing complex formation constants is given in Fig. 9.3. Internal consistency means, that a complete data set for a HA and several aqueous complexing ligands (ions) is based upon the same values for the HA proton exchange capacity. In a strict sense, even the pertinent aqueous speciation pattern in equilibrium with the surface complexes at the experimental conditions should be recorded, which is at the moment not implemented. For any value the experimental method used to derive this value is stored, together with the respective ionic strength and background media, as well as any other information necessary to evaluate the data or to calculate other derivative values. If published, uncertainty limits for numerical data are included. This is a prerequisite for sensitivity and uncertainty analysis.

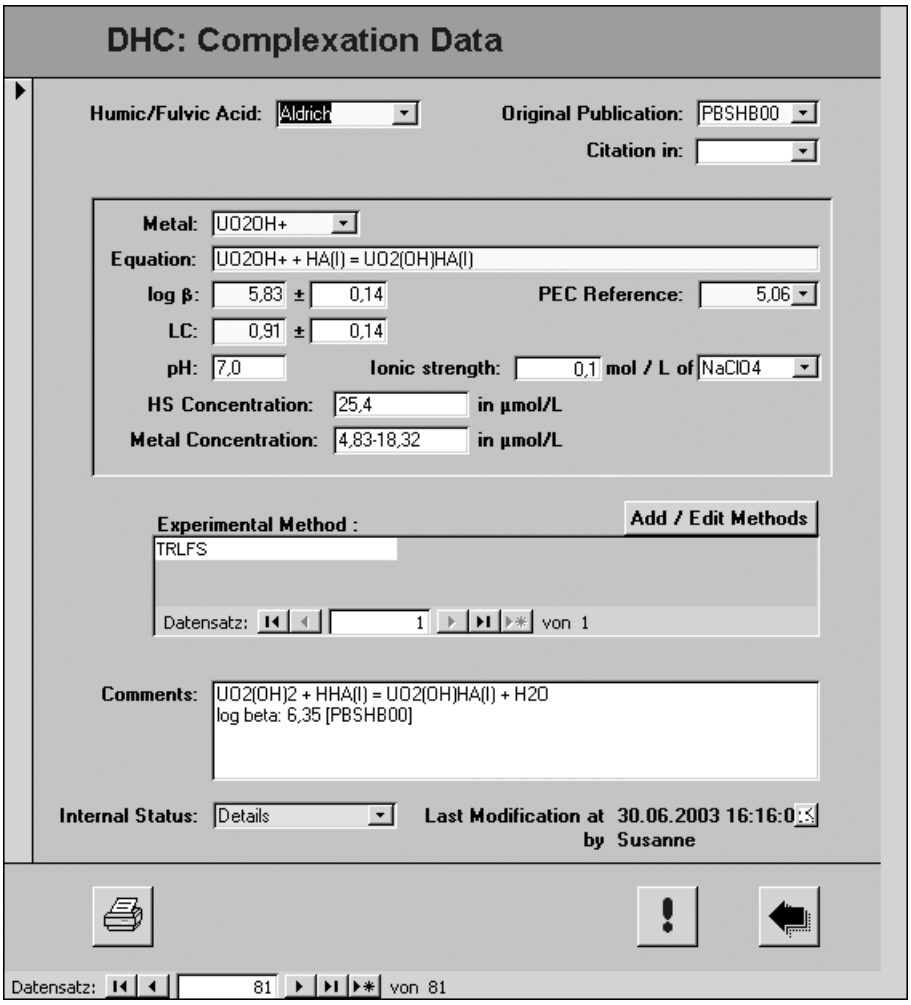

Fig. 9.3: Input mask in DHC for the loading capacity and complex formation data.

Instead of just being a (printed) collection of humics-metal complexation data, the approach presented here with a computer-based relational database opens additional opportunities of data processing by potential users via a graphical user interface.

In addition to such “hard” experimental results and parameters, an extensive bibliography is provided too. Every stored data item is linked to both original citations and secondary literature references. The references can also comprise model evaluations with respect to theoretical limitations, thermodynamic consistency and parameter sensitivity. Moreover, they cover questions of experimental design and interpretation of results from complexation experiments, or experimental methods used for such investigations with their associated error ranges and application areas.

The data records (each identified by a unique number) contain information about:

- Publication: abbreviation for citation, list of authors, year, title, pages, copy storage, type of publication, name of journal or book, volume, ISBN Number (if relevant), publisher, town, editor;
- Humic Acids: name, supplier (company or institute), properties, preparation;

- PEC: literature reference, citation, HA type, PEC value with associated error, experimental method, experimental conditions;
- Ligands: constituting elements, stoichiometry, charge, radius, redox state, molar mass;
- Method: name, abbreviation, check boxes for whether it can be applied to obtain values of PEC , LC or log β or if it is used for species identification / spectroscopic evidence;
- Reaction: literature reference, citation, HA type, ligand type, complex species, reaction equation, reference to PEC, LC with associated error, log β with associated error, pH, ionic strength, concentration of HA, background electrolyte type and concentration.

Besides, all major tables have a comment field, store the internal data record revision state, and keep the date and user name of the last editing.

The user interface allows several types of queries in addition to a mere scanning of the database content. Users can easily extract specific data sets, e.g. all records relevant for the combination of a specific HA and a specific ligand. They can also search for publications. Once a data set has been generated based on queries, it can be shown on the screen or printed out as a nicely formatted report. The results can also be exported into MS Excel spreadsheets for further processing.

As of November 2003, the DHC database covers 12 different types of HA, contains 20 data records for PEC and 81 complex formation constants with LC values. The data originate both from published papers and from research performed within the project.
The next step in the development of DHC will be the integration of an online manual. Based on a continuous extension and editing of the data content a systematic screening and data mining will help to reveal correlations and empirical internal dependencies of data. Provided enough resources can be allocated to the database, also the inclusion of the original experimental raw data is anticipated.

10 Summary and conclusions

In order to improve the knowledge on the interaction behaviour of HA with metal ions HA model substances with specific functional properties were already developed at the Institute of Radiochemistry of the Forschungszentrum Rossendorf. Within this project a new batch of synthetic HA type M42 was synthesized and characterized. It was made available to all project partners thus enabling comparative model investigations. In addition to that, ^{14}C-labeled synthetic HA type M42 was synthesized. This radio-labelled HA model substance facilitates the precise determination of the fate of HA in sorption and migration experiments under environmentally relevant conditions.
From our former studies it is known that defined chemically modified HA are of great value for the study of the influence of specific HA functionalities on the interaction behaviour of HA. In the present project a verified method for the synthesis of HA with blocked phenolic OH groups was optimised.
Within this project new HA model substances that are characterized by significantly more pronounced Fe(III) redox capacities than Aldrich HA were developed based on the oxidation

of phenolic compounds. This synthetic HA help to improve the understanding of the effects of HA on the oxidation state of actinides.
Applying original and chemically modified synthetic HA with pronounced redox functionalities in comparison to natural HA from Aldrich and synthetic HA type M42 detailed studies on the redox properties of HA were performed. It was confirmed that HA phenolic/acidic OH groups play a significant role for the redox behaviour of HA. However, the results show that there exist other processes than the single oxidation of phenolic OH groups and/or other HA functional groups that are also contributing to the redox properties of the studied substances.

The redox stability of U(VI) humate complexes of HA with distinct redox functionality was studied in comparison to Aldrich HA. Within these investigations the first direct spectroscopic proof for the reduction of U(VI) to U(IV) by the applied synthetic HA was succeeded. The qualitative results indicate that the HA-like synthetic products show higher U(VI) redox capacities than Aldrich HA.

Structural and thermodynamical studies on the actinide complexation by HA applying synthetic HA model substances and natural HA were performed. It was focused on the determination of structural parameters for the interaction of HA with actinides in lower oxidation states (Pu(III), Th(IV), Np(IV) and Np(V)). The results indicate that the interaction between the actinide ions and HA is dominated by HA carboxylate groups. These carboxylate groups act predominantly as monodentate ligands.
Furthermore, we studied the influence of HA on the Np(V) complexation by HA in the neutral pH range in order to improve the understanding on functional groups contributing to the metal ion complexation by HA. The results obtained for Np(V) complexes with unmodified and chemically modified HA with blocked phenolic/acidic OH groups show that the complex formation is not influenced by phenolic/acidic OH groups with respect to the near-neighbour surrounding of Np(V) in its humate complexes (coordination numbers and bond lengths) and stability constants. However, the maximal available number of HA complexing sites decreases for HA with blocked phenolic groups.

Batch experiments were performed in order to determine the influence of HA on the Th(IV) sorption onto quartz and the Np(V) sorption onto granite and its mineral constituents. The influence of HA on the migration of U(IV)/(VI) in quartz was studied by means of column experiments. All sorption and migration experiments were performed applying ^{14}C-labeled synthetic HA type M42. It was found that Th(IV) and Np(V) show a pH dependent sorption behaviour onto the studied materials which is affected by HA. In the case of the Np(V) sorption onto granite a slight decrease in the neptunium sorption is observed at pH values greater than pH 7 with addition of HA. Sorption studies with individual mineral components of granite show that biotite seems to be the mineral phase dominating the sorption in the studied system.
Humic acid M42 exhibits a significant influence on the transport of U(IV) and U(VI). In case of U(VI) a clear mobilizing effect was observed. There are strong indications for a similar influence of HA on the U(IV) transport. Both redox species of uranium differ slightly in their migration behaviour in presence of HA. This is mainly reflected in a disagreement of their total recoveries.

The reliable geochemical modeling of the actinide transport requires the integration of the metal ion complexation with HA into existing geochemical speciation codes. Within this project the metal ion charge neutralization model was successfully embedded into the EQ3/6 geochemical speciation package. In addition to that, a verification of the changed EQ3/6 version was performed.

Before the present project no consistent data base on the HA metal ion complexation was available. Therefore, it was initiated to develop a respective data base. During the project a digital database was developed covering so far published HA complexation data based on the metal ion charge neutralization model.

The results of these studies improve the knowledge on the interaction of HA with actinides under aerobic and anaerobic conditions. Important results were obtained on the synthesis of specific HA model substances, the redox properties of HA, their complexation towards actinides and the influence of HA on the sorption and migration of actinides in lower oxidation states. A geochemical speciation code was enhanced and a new database developed. In their combination all results contribute to a more realistic description of the migration behaviour of actinides in the environment and an improved risk assessment for instance for potential underground nuclear-waste repositories and former facilities of the uranium mining and milling.

Further studies should focus on the migration of actinides in the presence of HA in clay systems under aerobic and anaerobic conditions. In a first step kaolinite as model system for a clay environment should be investigated. In addition to that, further studies on the complexation of actinides, especially tetravalent, with HA have to be performed including kinetic processes and concurrent reactions with other metal ions. Further objectives are to continue the database for the HA metal ion complexation and to improve the metal ion charge neutralization model.

11 References

[1] Choppin, G.R.: Role of Humics in Actinide Behavior in Ecosystems. In: *Chemical Separation Technologies and Related Methods of Nuclear Waste Management* (Choppin, G.R., Khankhasayev, M. Kh., eds.). Kluwer Academic Publishers, 1999, p. 247-260.

[2] Abraham, A.: Einfluß von Huminstoffen und Holzabbauprodukten auf den Valenzzustand von Uran. PhD Thesis, TU Dresden, 2002.

[3] Kim, J.I.: Chemical Behaviour of Transuranic Elements in Natural Aquatic Systems. In: *Handbook on the Physics and Chemistry of the Actinides* (Freeman, A.J., Keller, C., eds.). Elsevier Science Publishers B.V., 1986, p. 413-455.

[4] Nash, K.L., Choppin, G.R.: Interaction of Humic and Fulvic Acids with Th(IV). J. Inorg. Chem. **42**, 1045 (1979).

[5] Li, W.C., Victor, D.M., Chakrabarti, C.L.: Effect of pH and Uranium Concentration on Interaction of Uranium(VI) and Uranium(IV) with Organic Ligands in Aqueous Solutions. Anal. Chem. **52**, 520 (1980).

[6] Choppin, G.R., Allard, B.: Complexes of Actinides with Naturally Occurring Organic Compounds. In: *Handbook on the Physics and Chemistry of the Actinides* (Freeman, A.J., Keller, C., eds.). Elsevier Science Publishers B.V., 1985, p. 407-429.

[7] Cacheris, W.P., Choppin, G.R.: Dissociation Kinetics of Thorium-Humate Complex. Radiochim. Acta **42**, 185 (1987).

[8] Moulin, V., Tits, J., Ouzounian, G.: Actinide Speciation in the Presence of Humic Acids in Natural Water Conditions. Radiochim. Acta **58/59**, 179 (1992).

[9] Rao, L.F., Choppin, G.R., Clark, S.B.: A Study of Metal-Humate Interactions using Cation Exchange. Radiochim. Acta **66/67**, 144 (1994).

[10] Pompe, S., Bubner, M., Schmeide, K., Heise, K.H., Bernhard, G., Nitsche, H.: Influence of Humic Acids on the Migration Behavior of Radioactive and Non-Radioactive Substances under Conditions Close to Nature. Synthesis, Radiometric Determination of Functional Groups, Complexation. Forschungszentrum Rossendorf, Wissenschaftlich-Technische Berichte, FZR-290, Rossendorf, Germany, 2000.

[11] Kim, J.I., Czerwinski, K.R.: Complexation of Metal Ions with Humic Acids: Metal Ion Charge Neutralization Model. Radiochim. Acta **73**, 5 (1996)

[12] Wolery, T.J.: EQ3/6, A Software Package for the Geochemical Modeling of Aqueous Systems. UCRL-MA-110662 Part 1, Lawrence Livermore National Laboratory, 1992.

[13] Kim, J.I., Buckau, G.: *Characterization of Reference and Site Specific Humic Acids.* RCM-Report 02188, TU München, 1988.

[14] Pompe, S.: Entwicklung huminsäureähnlicher Melanoidine als Funktionalitätsmodelle für Huminsäuren und ihr Vergleich mit Fluka-Huminsäure hinsichtlich ihres Komplexbildungsverhaltens gegenüber Uran(VI). PhD Thesis, TU Dresden, 1997.

[15] Pompe, S., Schmeide, K., Bubner, M., Geipel, G., Heise, K.H., Bernhard, G., Nitsche, H.: Investigation of Humic Acid Complexation Behavior with Uranyl Ions Using Modified Synthetic and Natural Humic Acids. Radiochim. Acta **88**, 553 (2000).

[16] Sachs, S., Bubner, M., Schmeide, K., Choppin, G.R., Heise, K.H., Bernhard, G.: Carbon-13 NMR Spectroscopic Studies on Chemically Modified and Unmodified Natural and Synthetic Humic Acids. Talanta **57**, 999 (2002).

[17] Bubner, M., Pompe, S., Meyer, M., Heise, K.H., Nitsche, H.: Isotopically Labelled Humic Acids for Heavy Metal Complexation. J. Labelled Cpd. Radiopharm. **XLI**, 1057 (1998).

[18] Stevenson, F.J.: *Humus Chemistry.* 2nd ed., John Wiley&Sons, New York, 1994.

[19] Stevenson, F.J.: *Humus Chemistry.* 1st ed., John Wiley&Sons, New York, 1982.

[20] Grauer, R.: Zur Koordinationschemie der Huminstoffe. Paul Scherrer Institut, Switzerland, Report No. 24, 1989, p. 7.

[21] Schnitzer, M., Khan, S.U.: *Humic Substances in the Environment* (A.D. McLaren, ed.). Marcel Dekker, Inc., New York, 1972.

[22] Bubner, M., Heise, K.H.: Characterization of Humic Acids. II. Characterization by Radioreagent-Derivatization with [^{14}C]Diazomethane. In: *FZR-43, Annual Report 1993* (Nitsche, H., Bernhard, G., eds.), Forschungszentrum Rossendorf, Institute of Radiochemistry, Rossendorf, Germany, 1994, p. 22.

[23] Schmeide, K., Sachs, S., Bubner, M., Reich, T., Heise, K.H., Bernhard, G.: Interaction of Uranium(VI) with Various Modified and Unmodified Natural and Synthetic Humic Substances Studied by EXAFS and FTIR Spectroscopy. Inorg. Chim. Acta **351**, 133 (2003).

[24] Baraniak, L., Mack, B., Abraham, A., Neubert, H.: Abschlußbericht zum Forschungsvorhaben “Untersuchung des Einflusses der in Grubenwässern gelösten organischen Verbindungen auf den Valenzzustand von Radionukliden und Schwermetallen im Hinblick auf den Flutungsprozeß der sächsischen Uranbergwerke”. Förderkennzeichen: 4-7541.83-FZR/512. Forschungszentrum Rossendorf 1997.

[25] Beyer, H., Walter, W.: Lehrbuch der organischen Chemie. S. Hirzel Verlag, Stuttgart, 22nd ed., 1991.

[26] Eller, W., Koch, K.: Synthetische Darstellung von Huminsäuren. Berichte Dt. Chem. Gesellschaft **53**, 1469 (1920).

[27] Adhikari, M., Sen, P., Krishnendu, D.: Studies on Synthesis of Humic Substances in Laboratory under Different Conditions. Proc. Indian Natn. Sci. Acad. **51A**, 876 (1985).

[28] Mack, B., Baraniak, L., Heise, K.H., Bernhard, G., Nitsche, H.: Reduction of Iron(III) by Natural and Synthetic Melanoidine-Type Humic Acids. In: *FZR-285, Annual Report 1999* (Bernhard, G., ed.), Forschungszentrum Rossendorf, Institute of Radiochemistry, Rossendorf, Germany, 2000, p. 40.

[29] Mack, B.: Redoxeigenschaften von Lignin und Huminsäuren und deren Wechselwirkung mit Eisen. PhD Thesis, TU Dresden, 2002.

[30] Standard Methods for the Examination of Water and Wastewater (Greenberg, A.E., Clesceri, L.S., Eaton, A.D., eds.). American Public Health Association, 18th ed., Washington DC, 1992.

[31] Matthiessen, A.: Determining the Redox Capacity of Humic Substances as a Function of pH. Vom Wasser **84**, 229 (1995).

[32] Stewart, R. : *Oxidation Mechanisms. Applications to Organic Chemistry.* W.A. Benjamin, Inc., New York, 1964, ch. 3.

[33] Mc Donald, P.D., Hamilton, G.A.: Mechanisms of Phenolic Oxidative Coupling Reactions. In: *Oxidation in Organic Chemistry* (Trahanovsky, W.S., ed.). Academic Press, New York, 1973, ch. 2.

[34] Helburn, R.S., MacCarthy, P.: Determination of Some Redox Properties of Humic Acid by Alkaline Ferricyanide Titration. Anal. Chim. Acta **25**, 263 (1994).

[35] Geipel, G., Bernhard, G., Brendler, V., Nitsche, H.: Complex Formation between UO_2^{2+} and CO_3^{2-}: Studied by Laser-Induced Photoacoustic Spectroscopy (LIPAS). Radiochim. Acta **82**, 59 (1998).

[36] Geipel, G., Bernhard, G., Brendler, V.: Complex Formation of Uranium(IV) with Phosphate and Arsenate. In: *Uranium in the Aquatic Environment* (Merkel, B.J., Planer-Friedrich, B., Wolkersdorfer, C., eds.). Springer Verlag, Berlin, 2002, p. 369-376.

[37] Koningsberger, D.C., Prins, R. (eds.): *X-ray Absorption: Principles, Applications, Techniques of EXAFS, SEXAFS and XANES*. Wiley, New York, USA, 1988.

[38] Schmeide, K., Zänker, H., Heise, K.H., Nitsche, H.: Isolation and Characterization of Aquatic Humic Substances from the Bog 'Kleiner Kranichsee'. In: *FZKA 6124, Wissenschaftliche Berichte* (Buckau, G., ed.), Forschungszentrum Karlsruhe, Karlsruhe, Germany, 1998, p. 161-195.

[39] Pompe, S., Bubner, M., Denecke, M.A., Reich, T., Brachmann, A., Geipel, G., Nicolai, R., Heise, K.H., Nitsche, H.: A Comparison of Natural Humic Acids with Synthetic Humic Acid Model Substances: Characterization and Interaction with Uranium(VI). Radiochim. Acta **74**, 135 (1996).

[40] Schmeide, K., Sachs, S., Reich, T., Brendler, V., Heise, K.H., Bernhard, G.: Neptunium(IV) Complexation by Humic Substances Studied by X-ray Absorption Fine Structure Spectroscopy. Radiochim. Acta, submitted.

[41] Schmeide, K., Sachs, S., Reich, T., Heise, K.H., Bernhard, G.: Plutonium(III) Complexation by Humic Substances Studied by X-ray Absorption Fine Structure Spectroscopy, in preparation.

[42] Sachs, S., Schmeide, K., Reich, T., Brendler, V., Heise, K.H., Bernhard, G.: EXAFS Study on the Neptunium(V) Complexation by Various Humic Acids under Neutral Conditions. Radiochim. Acta, submitted.

[43] Reich, T., Bernhard, G., Geipel, G., Funke, H., Hennig, C., Roßberg, A., Matz, W., Schell, N., Nitsche, H.: The Rossendorf Beam Line ROBL – A Dedicated Experimental Station for XAFS Measurements of Actinides. Radiochim. Acta **88**, 633 (2000).

[44] George, G.N., Pickering, I.J.: *EXAFSPAK: A Suite of Computer Programs for Analysis of X-Ray Absorption Spectra*. Stanford Synchrotron Radiation Laboratory, Stanford, USA, 1995.

[45] Zabinsky, S.I., Rehr, J.J., Ankudinov, A., Albers, R.C., Eller, M.J.: Multiple Scattering Calculations of X-ray Absorption Spectra. Phys. Rev. B, **52**, 2995 (1995).

[46] Denecke, M.A., Bublitz, D., Kim, J.I., Moll, H., Farkes, I.: EXAFS Investigation of the Interaction of Hafnium and Thorium with Humic Acid and Bio-Rex70. J. Synchrotron Rad. **6**, 394 (1999).

[47] Moll, H., Denecke, M.A., Jalilehvand, F., Sandström, M., Grenthe, I.: Structure of the Aqua Ions and Fluoride Complexes of Uranium(IV) and Thorium(IV) in Aqueous Solution an EXAFS Study. Inorg. Chem. **38**, 1795 (1999).

[48] Zhang, Y.-J., Collison, D., Livens, F.R., Powell, A.K., Wocadlo, S., Eccles, H.: Synthesis, Spectroscopic, and X-ray Crystallographic Characterization of Thorium(IV) and Uranium(IV) Malonato and Substituted Malonato Compounds. Polyhedron **19**, 1757 (2000).

[49] Akhtar, M.N., Smith, A.J.: The Crystal Structure of Tetrapotassium Tetraoxalatothorium(IV) Tetrahydrate, $K_4Th(C_2O_4)_4 \cdot 4H_2O$. Acta Crystallogr. **B31**, 1361 (1975).

[50] Antonio, M.R., Soderholm, L., Williams, C.W., Blaudeau, J.-P., Bursten, B.E.: Neptunium Redox Speciation. Radiochim. Acta **89**, 17 (2001).

[51] Allen, P.G., Bucher, J.J., Shuh, D.K., Edelstein, N.M., Reich, T.: Investigation of Aquo and Chloro Complexes of UO_2^{2+}, NpO_2^{+}, Np^{4+}, and Pu^{3+} by X-ray Absorption Fine Structure Spectroscopy. Inorg. Chem. **36**, 4676 (1997).

[52] Denecke, M.A., Pompe, S., Reich, T., Moll, H., Bubner, M., Heise, K.H., Nicolai, R., Nitsche, H.: Measurements of the Structural Parameters for the Interaction of Uranium(VI) with Natural and Synthetic Humic Acids using EXAFS. Radiochim. Acta **79**, 151 (1997).

[53] Denecke, M.A., Reich, T., Pompe, S., Bubner, M., Heise, K.H., Nitsche, H., Allen, P.G., Bucher, J.J., Edelstein, N.M., Shuh, D.K., Czerwinski, K.R.: EXAFS Investigations on the Interaction of Humic Acids and Model Compounds with Uranyl Cations in Solid Complexes. Radiochim. Acta **82**, 103 (1998).

[54] Grigoriev, M.S., Charushnikova, I.A., Krot, N.N., Yanovskii, A.I., Struchkov, Yu. T.: Crystal Structure of Neptunium(IV) Oxalate Hexahydrate $Np(C_2O_4)_2 \cdot 6H_2O$. Radiokhim. **39**, 419 (1997).

[55] Hauck, J.: The Crystal Structure of $Me(HCOO)_4$, Me = Th, Pa, U, Np. Inorg. Nucl. Chem. Lett. **12**, 617 (1976).

[56] Neck, V., Kim, J.I.: An Electrostatic Approach for the Prediction of Actinide Complexation Constants with Inorganic Ligands-Application to Carbonate Complexes. Radiochim. Acta **88**, 815 (2000).

[57] Grigoriev, M.S., Charushnikova, I.A., Krot, N.N., Yanovskii, A.I., Struchkov, Yu. T.: Crystal and Molecular Structure of Neptunyl Malonate Tetrahydrate $(NpO_2)_2C_3H_2O_4 \cdot 4H_2O$. Radiokhim. **4**, 24 (1993).

[58] Grigoriev, M.S., Charushnikova, I.A., Krot, N.N., Yanovskii, A.I., Struchkov, Yu. T.: Crystal Structure of the Neptunyl Formate Complex $(NH_4)NpO_2(OOCH)_2$. J. Neorgan. Chim. **39**, 1328 (1994).

[59] Reich, T., Geipel, G., Funke, H., Hennig, C., Roßberg, A., Bernhard, G.: First XANES and EXAFS Measurements of Plutonium Solutions at ROBL. In: *FZR-285, Annual Report 1999* (Bernhard, G., ed.). Forschungszentrum Rossendorf, Institute of Radiochemistry, Rossendorf, Germany, 2000, p. 72.

[60] Ankudinov, A.L., Conradson, S.D., Mustre de Leon, J., Rehr, J.J.: Relativistic XANES Calculations of Pu Hydrates. Phys. Rev. **B57**, 7518 (1998).

[61] Lemire, R.J., Fuger, J., Nitsche, H., Potter, P., Rand, M.H., Rydberg, J., Spahiu, K., Sullivan, J.C., Ullman, W.J., Vitorge, P., Wanner H.: *Chemical Thermodynamics of Neptunium and Plutonium.* Elsevier Science B.V., Amsterdam, 2001.

[62] Kim, J.I., Sekine, T.: Complexation of Neptunium(V) with Humic Acid. Radiochim. Acta **55**, 187 (1991).

[63] Marquardt, C., Kim, J.I.: Complexation of Np(V) with Humic Acid: Intercomparison of Results from Different Laboratories. **80**, 129 (1998).

[64] Seibert, A., Mansel, A., Marquardt, C.M., Keller, H., Kratz, J.V., Trautmann, N.: Complexation Behaviour of Neptunium with Humic Acid. Radiochim. Acta **89**, 505 (2001).

[65] Schild, D., Marquardt, C.M.: Analysis of Th(IV)-humate by XPS. Radiochim. Acta **88**, 587 (2000).

[66] Davis, J.R., Higgo, J.J.W., Noy, D.J., Hooker, P.J.: Complexation Studies of Uranium and Thorium with Natural Fulvic Acid. In: *FZKA 6524, Wissenschaftliche Berichte* (Buckau, G., ed.), Forschungszentrum Karlsruhe, Karlsruhe, Germany, 2000, p. 87-99.

[67] Reiller, P., Moulin, V., Dautel, Ch., Casanova, F.: Complexation of Th(IV) by Humic Substances. In: *FZKA 6524, Wissenschaftliche Berichte* (Buckau, G., ed.), Forschungszentrum Karlsruhe, Karlsruhe, Germany, 2000, p. 121-129.

[68] Östhols, E., Manceau, A., Farges, F., Charlet, L. : Adsorption of Thorium on Amorphous Silica : An EXAFS Study. J. Coll. Interf. Sci. **194**, 10 (1997).

[69] Murphy, R.J., Lenhart, J.J., Honeyman, B.D.: The Sorption of Thorium(IV) and Uranium(VI) to Hematite in the Presence of Natural Organic Matter. Colloids and Surfaces. A: Physical and Engineering Aspects **157**, 47 (1997).

[70] Reiller, P., Moulin, V., Dautel, Ch.: Sorption Behavior of Humic Substances towards Hematite : Consequences on Thorium Availability. In: *FZKA 6524, Wissenschaftliche Berichte* (Buckau, G., ed.), Forschungszentrum Karlsruhe, Karlsruhe, Germany, 2000, p. 133-147.

[71] Reiller, P., Moulin, V., Dautel, Ch.: Complexation of Eu(III), Th(IV), and U(VI) by Humic Substances. In: *FZKA 6324, Wissenschaftliche Berichte* (Buckau, G., ed.), Forschungszentrum Karlsruhe, Karlsruhe, Germany, 1999, p. 82-117.

[72] Reiller, P., Moulin, V., Casanova, F., Dautel, Ch.: On the Study of Th(IV)-Humic Acid Interactions by Competition Sorption Studies with Silica and Determination of Global Interaction Constants. Radiochim. Acta **91**, 513 (2003).

[73] Stumm, W.: *Chemistry of the Solid-Water Interface, Processes at the Mineral-Water and Particle-Water Interface in Natural Systems.* John Wiley & Sons, Inc., 1992.

[74] Papp, R.: Gegenüberstellung von Endlagerkonzepten in Salz und Hartgestein. FZKA-PTE Nr. 3, Forschungszentrum Karlsruhe GmbH, Karlsruhe 1997.

[75] Krawczyk-Bärsch, E., Arnold, T., Bernhard, G.: Das Sorptionsverhalten von U(VI) am Granit von Eibenstock (Erzgebirge) und seinen mineralogischen Komponenten. European Journal of Mineralogy **13**, 103 (2001).

[76] Arnold, T., Forschungszentrum Rossendorf, personal communication.

[77] Nakata, K., Nagasaki, S., Tanaka, S., Sakamoto, Y., Tanaka, T., Ogawa, H.: Sorption and Reduction of Neptunium(V) on the Surface of Iron Oxides. Radiochim. Acta **90**, 665 (2002).

[78] Zeh, P., Kim, J.I., Marquardt, C.M., Artinger, R.: The Reduction of Np(V) in Groundwater Rich in Humic Substances. Radiochim. Acta **87**, 23 (1999).

[79] Kim, J.I., Delakowitz, B., Zeh, P., Klotz, D., Lazik, D.: A Column Experiment for the Study of Colloidal Radionuclide Migration in Gorleben Aquifer Systems. Radiochim. Acta **66/67**, 165 (1994).

[80] Artinger, R., Rabung, T., Kim, J.I., Sachs, S., Schmeide, K., Heise, K.H., Bernhard, G., Nitsche, H.: Humic Colloid-borne Migration of Uranium in Sand Columns. J. Contam. Hydr. **58**, 1 (2002).

[81] Artinger, R., Kienzler, B., Schuessler, W., Kim, J.I.: Effects of Humic Substances on the ^{241}Am Migration in a Sandy Aquifer: Batch and Column Experiments with Gorleben Groundwater/Sediment Systems. J. Contam. Hydr. **35**, 261 (1998).

[82] Artinger, R., Seibert, A., Marquardt, C.M., Trautmann, N., Kratz, J.V., Kim, J.I.: Humic Colloid-borne Np Migration: Influence of the Oxidation State. Radiochim. Acta **88**, 609 (2000).

[83] Pompe, S., Brachmann, A., Bubner, M., Geipel, G., Heise, K.H., Bernhard, G., Nitsche, H.: Determination and Comparison of Uranyl Complexation Constants with Natural and Model Humic Acids, Radiochim. Acta **82**, 89 (1998).

[84] Bertrand, P.A., Choppin, G.R.: Separation of Actinides in Different Oxidation States by Solvent Extraction. Radiochim. Acta **31**, 135 (1982).

[85] Toride, N., Leji, F.J., van Genuchten, M.Th.: The CXTFIT Code for Estimating Transport Parameters from Laboratory or Field Tracer Experiments. Version 2.1. Research Report No. 137. U.S. Salinity Laboratory, Agricultural Research Service, U.S. Department of Agriculture, Riverside, California (1995).

[86] Grolimund, D., Elimelech, M., Borkovec, M., Barmettler, K., Kretzschmar, R., Sticher, H.: Transport of in Situ Mobilized Colloidal Particles in Packed Soil Columns. Environ. Sci. Technol. **32**, 3562 (1998).

[87] Grenthe, I., Fuger, J., Konings, R.J.M., Lemire, R.J., Muller, A.B., Nguyen-Trung, C., Wanner, H.: *Chemical Thermodynamics, Volume 1: Chemical Thermodynamics of Uranium.* North-Holland, Amsterdam, 1992.

[88] Choppin, G.R.: Solution Chemistry of the Actinides. Radiochim. Acta **32**, 43 (1983).

[89] Tipping, E.: Humic Ion-Binding Model VI: An Improved Description of the Interactions of Protons and Metal Ions with Humic Substances. Aquatic Geochem. **4**, 3 (1998).

[90] Torres, R.A., Choppin, G.R.: Europium(III) and Americium(III) Stability Constants with Humic Acid. Radiochim. Acta **35**, 143 (1984).

[91] Kinniburgh, D.G., Milne, C.J., Benedetti, M.F., Pinheiro, J.P., Filius, J., Koopal, L.K., Van Riemsdijk, W.H.: Metal Ion Binding by Humic Acid: Application of the NICA-Donnan Model. Environ. Sci. Technol. **30**, 1687 (1996).

[92] Van Riemsdijk, W.H., de Wit, J.C.M., Mous, S.L.J., Koopal, L.K., Kinniburgh, D.G.: An Analytical Isotherm Equation (CONICA) for Nonideal Mono and Bidentate Competitive Ion Adsorption to Heterogeneous Surfaces. J. Colloid Interface Sci. **183**, 35 (1996).

12 Acknowledgement

The authors would like to thank M. Meyer and R. Ruske for their valuable help in synthesizing and characterization of HA and their technical assistance. Thanks are given to H. Foerstendorf, R. Nicolai and K. Muschter for FTIR measurements and H. Görner for elemental analysis. We thank U. Schaefer for ICP-MS measurements.

EXAFS measurements were performed at BM20 at the European Synchrotron Radiation Facility in Grenoble (France). In particular, thanks are given to C. Hennig, H. Funke, A. Roßberg and H. Moll for their support during EXAFS measurements. We thank G. Grambole for her help in preparation and characterization of EXAFS samples.

Thanks are given to B. Barz and R. Jander for their help in the performance of batch experiments. We thank J. Tutschku for the electrochemical reduction of uranium(VI) and S. Brockmann for their technical assistance during the column experiments. The authors thank C. Nebelung for the evaluation of LSC spectra.

At this place we would like to thank all colleagues who contributed to the success of this work.

Appendix B Institut für Kernchemie, Universität Mainz

Investigations on the Complexation and Redox Behaviour of Neptunium and Plutonium with Humic Acids at Low Metal Ion Concentrations under Laboratory and Natural Groundwater Conditions

B. Kuczewski[1], A. Seibert[1,2], J. V. Kratz[1], N. Trautmann[1],
N. L. Banik[1], S. Bürger[1], G. Getahun[1], C. Lüttinger[1], J. Maul[3]
R. Artinger[2], C. M. Marquardt[2], T. Schäfer[2], H. Geckeis[2], Th. Fanghänel[2], J. I. Kim[2]

Final Report

Support contract number
02 E 9309 5

[1] Institut für Kernchemie, Johannes Gutenberg – Universität Mainz
[2] Institut für Nukleare Entsorgung, Forschungszentrum Karlsruhe
[3] Institut für Physik, Johannes Gutenberg – Universität Mainz

Institut für Kernchemie
Joh.-Gutenberg Universität Mainz
Fritz-Straßmann-Weg 2
55099 Mainz

www.kernchemie.uni-mainz.de

Institut für Physik
Joh.-Gutenberg Universität Mainz
Staudingerweg 7
55099 Mainz

www.physik.uni-mainz.de

Institut für Nukleare Entsorgung
Forschungszentrum Karlsruhe
Hermann-von-Helmholtz-Platz 1
76344 Eggenstein-Leopoldshafen

www.fzk.de/ine

Content

Abstract

In the framework of this project, the complexation behaviour of neptunium and plutonium with Aldrich humic acid and synthetic humic acids was investigated. For plutonium, the redox behaviour and the complexation kinetics were studied and column experiments have been carried out. Also, a separation method for the different oxidation states of plutonium and neptunium by CE-ICP-MS was developed and optimised, even for speciation in real groundwater samples. Resonance ionisation mass spectrometry (RIMS) was improved and used for ultra trace determinations of plutonium in various environmental samples.

In the case of neptunium (Np(V)), the investigations were focused on a wide range of metal-ion concentrations with the aim to investigate whether the complexation behaviour changes with the metal-ion concentration or not. This would be reflected in a change of the complex formation constants log β_{LC}. Such an effect was found not only for Aldrich humic acid but also for the synthetic ones.

For plutonium, the redox chemistry was investigated under environmental conditions. In groundwater samples from Gorleben, the reduction of Pu(VI) via Pu(V) to Pu(IV) and Pu(III) occurs in a few hours. An increasing pH value accelerates the reduction. The kinetics of the complex formation was investigated with Aldrich humic acid and Pu(IV). The adjustment of the equilibrium of Pu(IV) and humic acid took up to one week. Experiments to determine the loading capacity and the log β_{LC} value are being continued.

By use of CE-ICP-MS, it was possible to develop and to optimise a technique for the separation of the different oxidation states of plutonium and neptunium. This was done in collaboration with the “Institut für Nukleare Entsorgung (INE)“ of the „Forschungszentrum Karlsruhe“ and the „Institut für Anorganische und Analytische Chemie und Radiochemie (IAARC)“ of the „Universität des Saarlandes, Saarbrücken“. All oxidation states of plutonium and neptunium could be separated in less than 15 minutes with a detection limit of 50 ppb ($2 \cdot 10^{-7}$ M). This method was compared with UV/VIS absorption spectroscopy to demonstrate its reliability. For a sample containing Pu(V) and Pu(III) as well as for the observation of the reduction of Pu(VI) by humic acid, a good agreement of both techniques was found. CE-ICP-MS was also used successfully for the speciation of the different oxidation states of plutonium and neptunium added to natural groundwater samples from Gorleben.

In column experiments performed at the “Institut für Nukleare Entsorgung (INE)“, it could be shown that most of the plutonium is transported as the Pu(IV) humate complex in agreement with other experiments using tetravalent ions like Tc(IV) and Np(IV). The oxidation state of plutonium added to the groundwater is irrelevant for the migration behaviour as an experiment performed with Pu(VI) showed similar results as one with Pu(III). All the experiments showed that parts of the plutonium are also sorbed to the surfaces.

1 Introduction

Plutonium and the “minor actinides” represent the major contributors to the radiotoxicity of spent nuclear fuel in a radioactive waste repository after storage times of more than 100 years[1]. Their environmental behaviour, especially the migration behaviour, which depends on their complexation and the redox chemistry, are of special interest for the evaluation of the safety of a repository.

In addition to inorganic complexing ligands, the organic components of groundwater like humic substances can interact with the actinides. These humic substances can be present in concentrations up to several mg/l in natural groundwater. Humic substances are the result of the decomposition of flora and fauna and are known for their strong complexing and redox characteristics. Two types of reactive groups are mainly responsible and vary in their ratios. These are the carboxylic groups and the phenolic OH-groups. They can be determined[2] and are useful for comparisons of the properties of humic substances of different origin. In general, the humic substances are divided into three groups, depending on their solubility. Humines (HM) are not soluble, humic acids (HA) are soluble in alkaline media but insoluble in acidic media and fulvic acids (FA) are soluble in all kinds of media.

Different structures and contents of carboxylic and phenolic OH-groups are responsible for the variation of the complexation behaviour of the humic substances. Besides the structure, pH value and ionic strength play an important role. For the calculation of complexation constants, it is necessary to take this into account. Two models[3,4] are often applied for the calculation of the complex constants.

The humic acid used by all partners within this project as a reference substance was Aldrich humic acid. In addition, different types of synthetic humic acids with special functional groups and low ash residues were synthesized by the “Institut für Radiochemie” of the “Forschungszentrum Rossendorf” (FZR) and put to our disposal for studies. Furthermore, natural groundwater from the vicinity of the exploration salt mine in the area of Gorleben in Niedersachsen (Germany) with a high content of natural organic matter (NOM) - especially humic and fulvic acids - was available for the experiments.

Not only the properties of the humic acid play an important role but also the oxidation state of the metal ions are essential. Neptunium can occur in natural systems as tetra- (Np^{4+}) and pentavalent (NpO_2^+) ion, plutonium as tri- (Pu^{3+}), tetra- (Pu^{4+}), penta- (PuO_2^+), and hexavalent (PuO_2^{2+}) ion. They can partially coexist in all oxidation states. Especially plutonium is very sensitive to changes in the redox conditions of its environment. Neptunium on the other hand is less redox sensitive. The tetravalent species have a strong tendency to hydrolyse leading to mixed plutonium-hydroxo-humate complexes which makes it more difficult to determine the complex stability constants.

The complexation behaviour of Np(V) as a function of the pH value and the concentration of the metal ion was determined directly by UV/VIS absorption spectroscopy as well as by indirect speciation methods for extremely low metal-ion concentration[5,6]. For plutonium, it was necessary to investigate first the oxidation states which are formed during the contact with

humic acid and their stability under these conditions. Methods like liquid-liquid-extraction were found not to be suitable for the speciation of plutonium. Therefore, a new method for the speciation of the plutonium oxidation states was developed by coupling CE as high performance separation technique with ICP-MS [7].

The determination of the complex stability constants was performed by applying ultrafiltration separating the free ions of neptunium and plutonium from the humate complexes. The measurement of the separated ions was done by liquid scintillation counting (LSC), α- and γ-spectroscopy.

Furthermore, different environmental samples with a very low plutonium content were measured by resonance ionisation mass spectrometry (RIMS).
Column experiments with plutonium using groundwater and material from the vicinity of Gorleben under environmental conditions have been performed to improve the understanding of the migration behaviour of plutonium in the environment.

2 Experimental

2.1 Chemicals, Radionuclides, Humic Acids and Groundwater

2.1.1 Chemicals

All chemicals were purity grade „p.A." „pro analysi". The used water was filtered and purified by a Millipore system (18 MΩ).

2.1.2 Radionuclides

Plutonium-239 / Plutonium-242

The plutonium solutions were evaporated to dryness and fumed with HNO_3 conc. / H_2O_2 30 %. The residue was dissolved in 2 M HNO_3, $NaNO_2$ was added to reduce Pu to Pu(IV). The Pu was cleaned via ion exchange chromatography (BIO RAD® AG MP 1). The adsorbed Pu was washed with 2 M HNO_3 and eluted with 0.36 M HCl / 0.05 M HF. The eluate was evaporated to dryness in a PTFE beaker and fumed two times with small amounts of $HClO_4$ conc. to oxidise Pu(IV) to Pu(VI). The Pu was then dissolved in 1 M $HClO_4$ yielding the stock solution.

Neptunium-237

The neptunium solution was evaporated to dryness and dissolved in 8 M HCl. The solution was purified via anion exchange (BIO RAD® AG 1-X8). After a washing step with several millilitres of 8 M HCl, plutonium contaminations were removed with a fresh solution of 150 mg NH_4I in 5 ml 8 M HCl. Subsequently, neptunium was eluted from the ion exchanger with 4 M HCl / 0.05 M HF and evaporated to dryness in a PTFE beaker. To obtain a solution containing only Np(V), the solution was fumed three times with 1 M $HClO_4$ and the residue was dis-

solved in distilled water. This stock solution could be stored at a pH value of 3 for several days.

Neptunium-239

Neptunium-239 was produced by neutron irradiation of uranyl nitrate ($UO_2(NO_3)_2 \cdot 6\ H_2O$, ≈ 0,3 % U-235, Merck, p.A.) at the Mainz TRIGA-Reactor. The uranyl nitrate was irradiated for 4 hours at a neutron flux of $7 \cdot 10^{12}$ neutrons/cm^2·s to obtain uranium-239 which decays with a half life of 23.5 min into neptunium-239, which has a half life of $T_{½}$ = 2.35 d. Several hours after the irradiation, the sample was dissolved in 8 M HCl and separated from fission products and uranium as described for neptunium-237.

Tab. 1: Characteristics of the humic acids used for the experiments [8,9,10]

	Aldrich-HA	M1	M1b	M42
-COOH [meq/g]	4.3	1.28	2.06	3.76
-OH$_{(phenolic)}$ [meq/g]	2.9	2.31	1.06	2.04
PEC [meq/g]	4.6	1.36	1.94	3.51
C [%]	54.9	63.9	-	56.1
H [%]	3.8	4.8	-	4.1
O [%]	28.8	20.2	-	26.8
N [%]	0.8	5.3	-	4.4
ash content [%]	3.7	3.0	-	0.11

2.1.3 Humic Acids

Aldrich Humic Acid

As reference substance, a humic acid available as sodium salt provided by Aldrich was chosen. All project partners worked with the same batch (Chargennr.: 01816-054). The humic acid was purified by a procedure described in the literature[8]. After the purification, the humic acid was lyophilised and stored in the dark. Solutions of the humic acid were prepared by dissolution of a selected amount of the dry substance in a small volume of 1 M NaOH in an ultrasonic bath. The solutions were adjusted to pH 7 with 1 M $HClO_4$ and stored in the refrigerator for not longer than four weeks.

Synthetic Humic Acids

The synthetic humic acids M1 (Chargennr: FR-R36/95), M1b, and M42 were synthesized by the "Institut für Radiochemie" of the "Forschungszentrum Rossendorf"[9]and delivered to the project partners. These humic acids were already purified and characterized and the solutions were prepared in the same way as for the Aldrich humic acid. Some properties of the different humic acids used are listed in *Table 1*.

2.1.4 Groundwater

Gorleben-Groundwater

The natural groundwater used was obtained by sampling nearby the exploration salt mine in the area of Gorleben in Niedersachsen (Germany). The groundwater sample (Charge GoHy 532) has a high content of natural organic matter (NOM) of around 30 mg/l. The water was sampled and stored under oxygen free conditions. All experiments with this groundwater were performed in an inert gas glove box with an argon/CO_2 atmosphere (1 % CO_2). Further information about the groundwater can be found in the literature[8,11].

2.2 Methods

2.2.1 Preparation of the Oxidation States

The different oxidation states of plutonium and of neptunium were prepared electrolytically. For the electrolysis, special cells with three areas separated by glass frits (porosity 2) were used. The active stock solution ($c \approx 10^{-4}$ mol/l) in 1 M $HClO_4$ was filled into the middle compartment, the other compartments were filled with 1 M $HClO_4$. As working and counter electrode, a platinum coil was used and a silver/silver chloride electrode as reference electrode. The electrodes were coupled to a potentiostat as power supply. The conditions for the electrolysis were taken from the literature[12]. Starting from any oxidation state mixture, first Pu(III) and Np(III) were produced. These were subsequently oxidized to the desired oxidation state. The progress of the reduction or oxidation was observed by UV/VIS absorption spectroscopy.

An alternative procedure for the preparation of solutions containing only Pu(VI) or Np(V), is the repeated fuming with 1 M $HClO_4$. Other chemical procedures for the preparation of the oxidation states are not suitable because the oxidizing or reducing agents influence the complexation reaction and the equilibrium.

2.2.2 Determination of the Oxidation States

The standard procedure for the determination of the different oxidation states of neptunium is liquid-liquid-extraction with a fresh solution of TTA (1-(2-Thenoyl)-3,3,3-trifluoroacetone) in toluene at different pH values[5].

For the speciation of plutonium, especially at low metal-ion concentration, this procedure is not suited. Therefore, it was necessary to develop a new speciation technique. This was achieved by coupling capillary electrophoresis (CE) to inductively coupled plasma mass spectrometry (ICP-MS). The separation conditions were optimised and compared with other methods, especially UV/VIS absorption spectroscopy. The optimum separation conditions are listed in *Table 5* in *Chapter 3.1.1*.

2.2.3 Determination of the Complex Formation Constants

For neptunium, the complex formation constants could be determined at higher concentrations with UV/VIS absorption spectroscopy and ultrafiltration. The latter method can also be applied for very low metal-ion concentrations.

For the free metal ion as well as for the metal ion bound to the humate, neptunium(V) gives a suitable extinction coefficient at different wavelengths. One way cuvettes made from polystyrene were used for the measurements with absorption spectroscopy. With this technique, a concentration range from 10^{-3} to 10^{-5} mol/l can be covered.

At lower neptunium metal-ion concentrations and for plutonium, the determinations were performed by ultrafiltration separating the humic acid and the humate complexes from the free metal ions. The ultrafilters of the type MicroSep™ were obtained from PallFiltron. The pore size was 1 kDalton. With these filters, it was possible to retard all humic acids and all metal ions bound to the humate while the free metal ions passed the membrane without any hindrance. In order not to disturb the complex formation equilibrium, only 100 to 200 µl of a total sample volume of 1 ml were separated. This took between 15 and 20 minutes.

The free neptunium-239 metal ions were detected by γ-ray measurement with a NaI borehole scintillation counter. The detection of the metal ions of neptunium-237, plutonium-239, and plutonium-242 was performed by liquid scintillation counting (LSC). As scintillation cocktail Ultima Gold AB obtained from Packard was used.

To reach the complex formation equilibrium between humic acid and neptunium, a contact time of at least 24 h was necessary. In the case of plutonium, the complex formation kinetics were determined in separate experiments. It was found that contact times of up to seven days are necessary to reach equilibrium.

2.2.4 Investigations of the Redox Chemistry

The redox behaviour of plutonium was investigated in two different systems. First Pu(VI) was contacted with Aldrich humic acid in solutions of different pH values. The plutonium was in the hexavalent oxidation state in 1 M $HClO_4$ as solvent. The requested pH values were adjusted with 1 M NaOH. To some of the samples, MES (morpholinoethane sulfonic acid) was added as a buffer to stabilize the pH value. All samples in these experiments were kept at normal atmosphere. Samples measured by UV/VIS absorption spectroscopy and CE-ICP-MS were injected by a special cuvette container without decantation or special sample preparation into the CE system.

In the other system, plutonium was added to the groundwater from the vicinity of Gorleben under inert atmosphere (Ar / 1 % CO_2). Here, all the solutions and samples were prepared in the inert gas glove box. Plutonium was added from the acidic stock solutions and the pH values were adjusted by 1 M NaOH. Samples from absorption spectroscopy were taken out of the box in airtight cuvettes. The samples for CE-ICP-MS had air contact, but the time to the start of the measurement was not longer than 10 minutes.

2.2.5 Column Experiments

The mobility of plutonium was studied by column experiments on near-natural systems with a Gorleben groundwater (GoHy-532) conditioned with a pleistocene sand from the Gorleben region. Chemical and physico-chemical parameters of the system are presented in *Table 2*. More detailed information on the origin and sampling of the system compounds is given in [8, 11].

Tab. 2: Chemical and physico-chemical data for the column experiments

	original	**after conditioning**
sampling depth [m]	65-68	-
pH	8.9	6.8 – 7.0
Eh [mV]	-160	-30
conductivity [mS/cm]	0.95	-
Na^+ [mmol/l]	9.5 (3)	5.7
Ca^{2+} [mmol/l]	0.047 (0.026)	0.054
Cl^- [mmol/l]	3.7 (3.87)	3.65
HCO_3^- [mmol/l]	5.5 (3)	3.3
DOC [mg C/l]	30	27
[HA,FA] [mg/l]	-	60 - 70
sand	pleistocene quartz sand	

The experiments were carried out under Ar / 1 % CO_2-atmosphere in a glove box. From a reservoir, the groundwater is pumped over the sand-filled column (ID = 50 mm, L = 250 mm). To reach equilibrium conditions between groundwater and sediment and a stable microstructure with constant porosity, a conditioning of the system for several months prior to the experiments is necessary. Therefore, the groundwater was pumped in a circular flow over the columns. During this conditioning time, a sorption of humic colloids onto the sand was shown to be insignificant[11]. Radionuclides can be injected in a pulse as well as continuously onto the column. For the plutonium experiments with Pu(IV), a continuous introduction was chosen. The eluate is fractionated in an automated sampling device. These fractions were investigated with LSC, CE, and ultrafiltration.

2.3 Instrumentation

2.3.1 CE-ICP-MS

A capillary electrophoresis (CE) set-up was built in our institute and tests were performed with different nebulizers and spray chambers during the development of the CE and its coupling to ICP-MS. The CE-unit consists of a high voltage supply and an experimental CE set-up. The data of the HV supply and the CE are listed in *Table 3*. *Figure 1* shows the experimental set-up. It was constructed as closed box and was equipped with an interlock in order to avoid contact with HV when opening the box. The box was also used as ventilation hood to prevent the emission of radioactive aerosols in case of a malfunction of the transfer tubing to the plasma torch.
A commercial coupling of CE to ICP-MS was not available at the beginning of the project, but different techniques were described in the literature[13-15].The principle of one set-up used is shown in *Figure 2*.

Tab. 3: Technical data of the HV supply and the CE system

HV supply	
Voltage / current	0 – 30 kV 0 – 300 µA voltage and current recordable
CE system	
Electrolyte vial	injection side 20 ml fill up electrolyte 500 ml
Sample injection	hydrostatic 0 – 35 cm hydrodynamic 0 – 1000 mbar
Capillary	AD 363 µm, > 30 cm length
Temperature	room temperature by ventilation

In all configurations that were tested there was only a little gap between the inlet of the nebulizer and the capillary used for the separation. The small flux from the CE capillary (1 - 100 nl/min) was filled up with 2 % nitric acid, the so called make up electrolyte, flowing to the sample uptake of the low consumption nebulizer. The nitric acid was marked with 10 ppb Rh to control the constancy of the nebulisation. The nebuliser was used in the self aspiring mode. During the development, it could be shown that the levels of the electrolyte vial at the injection side and the make up solution vessel have to be the same. Otherwise, a back pressure can be caused or suction with a laminar flux in the separation capillary. Such a laminar flux deteriorates significantly the separation performance of the capillary electrophoresis. The electrical contact to ground was realised via the supply pipe of the make up electrolyte. The

field gradient in the supply pipe is small against the gradient inside the CE capillary because the field gradient is a function of the cross section.

Fig. 1: Photo of the experimental set-up for the coupling of CE to ICP-MS

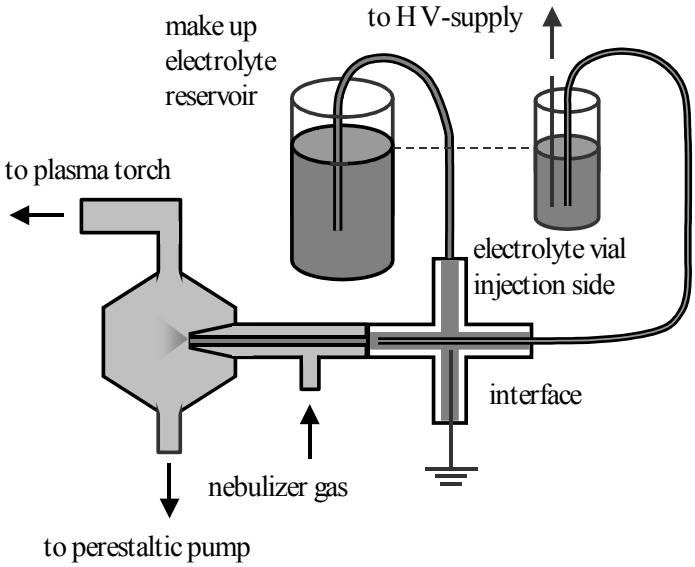

Fig. 2 : Principle of coupling CE to ICP-MS with a MicroMist nebulizer and a Cinnebar Cyclonic small volume spray chamber

During the development period, different nebulizers and spray chambers were tested. The results are summarised in *chapter 3.1.*. As ICP-MS apparatus, different systems were used. Besides the PerkinElmer ELAN 5000 (FZK, INE) with which most of the experiments were performed, also a Thermo Elemental Plasma Quad 2 (IAARC, Uni Saarbrücken), and a Per-

PerkinElmer ELAN 6000 (FZK, INE) could be used. Furthermore, an Agilent 4500 (IKC, Uni Mainz) could be bought, so that a complete CE-ICP-MS is now available at Mainz. The adaptations to the different ICP-MS systems were easy to realise. Only the Ar supply and the aerosol transport tubing had to be modified. In most cases at the INE, the aerosol was transported from the spray chamber to the plasma torch inlet via a PVC tubing of 7 m length. This was necessary because the ICP was adapted to a glove box to prevent the emission of radioactive material into the laboratory. Tests with much shorter supply tubing with inactive samples did not show an improved chromatographic resolution. The chromatographic resolution is, however, the most important factor for the quality of the separation.

2.3.2 RIMS

For the ultra trace analysis and measurements of isotope ratios of plutonium, resonance ionisation mass spectrometry (RIMS) was used.
The laser system used until very recently consisted of three dye lasers pumped by two powerful Cu-vapour lasers. Its important properties are a high repetition rate of 6.6 kHz, a broad tuning range through the use of suitable dyes and a linewidth of 1.6 - 6 GHz. However, the drawbacks of this system such as size, high maintenance efforts and costs, led to the development of a new, powerful and easy-to-handle solid-state laser system. A commercially available, Q switched and intracavity doubled Nd:YAG pump laser (Clark-MXR ORC-1000) with a repetition rate of 1 - 25 kHz, a power of up to 50 W at 532 nm and a pulse length of ~ 400 ns is applied to pump simultaneously three titanium-sapphire (Ti:Sa) lasers. Each solid state laser provides a power of up to 3 W in a tuning range from 725 nm to 895 nm with a linewidth of 2 - 5 GHz and a pulse duration of 60 - 150 ns. The three lasers are synchronised with intracavity Pockels cells used as Q-switches. An external, single-pass frequency doubling set-up using a BBO-crystal is required in order to apply a three step excitation/ionisation scheme for plutonium with an ionisation potential of ~ 6 eV. The photoions are accelerated in an electrical field and are mass separated in a reflectron time-of-flight mass spectrometer and counted with a multichannel plate detector. *Figure 3* shows the presently used set-up for RIMS.

A very efficient three step ionisation scheme for plutonium uses wavelengths λ_1 = 420.76 nm, λ_2 = 847.28 nm, and λ_3 = 767.53 nm, the latter populating a high lying Rydberg state which is ionised by an electric field. The isotope shifts in this excitation scheme have been measured for the plutonium isotopes 238, 239, 240, 241, 242, and 244 and are taken into account for exact isotope ratio measurements. With this arrangement, efficiencies of ~ $3 \cdot 10^{-5}$ could be reached for a single isotope leading to a detection limit of $1 \cdot 10^6$ atoms (0.4 fg) with a 3 σ-confidence level which is more than two orders of magnitude lower than the one for conventional α-spectroscopy of plutonium-239 ($T_{1/2} = 2.4 \cdot 10^4$ a).

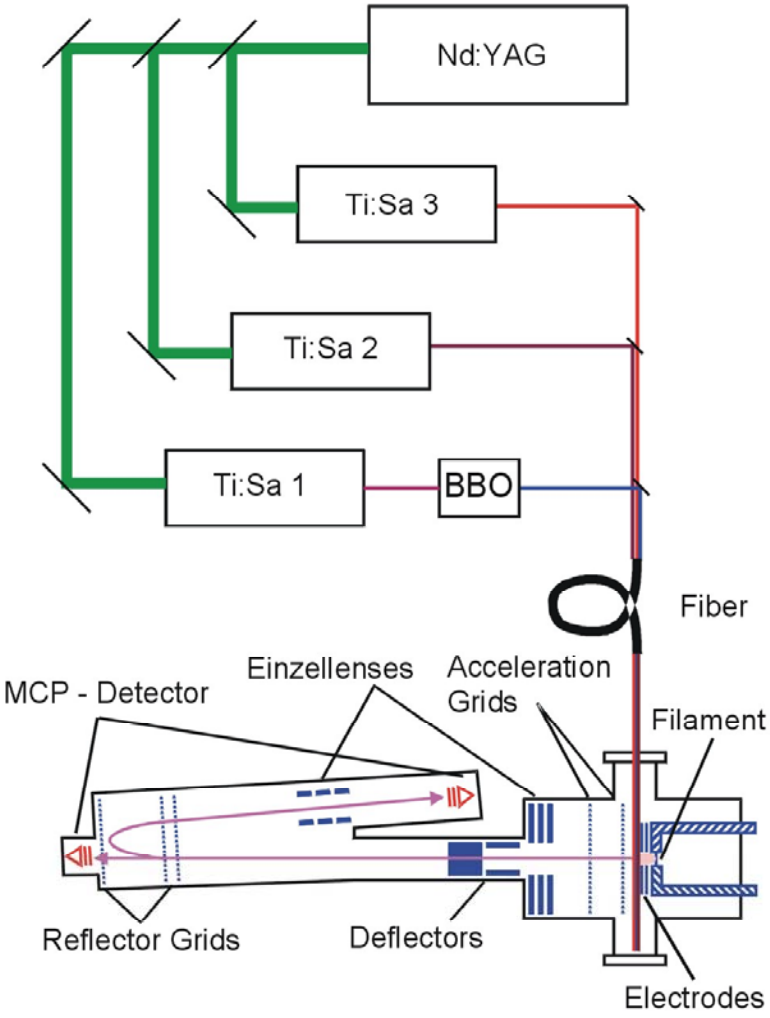

Fig. 3: Scheme of the used RIMS apparatus

3 Results and Discussion

3.1 Equipment and Method Development

3.1.1 CE-ICP-MS Development

The insufficient reliability of the classical chemical speciation methods for the different oxidation states of plutonium was the reason to search for an alternative method. Especially HPLC and CE were taken into consideration. Different tests with ion chromatography (IC) at a hyphenated HPLC-ICP-MS bared also problems with the redox equilibrium. Oxidation states of the analytes changed rapidly. A more promising approach was indicated by the successful separation of lanthanum, thorium, and uranium with the CE equipped with a conductivity detector[16]. Those ions are often used as model ions for Pu(III), Pu(IV) and Pu(VI). To realise a low limit of detection, it was necessary to couple the CE to an ICP-MS as a powerful detector. Different types of coupling interfaces were already published. Tests of different nebulizers and spray chambers were performed and *Table 4* shows the obtained qualitative results with the different nebulizers.

Tab. 4: Qualitative results of the tests with different nebulizers for the coupling of CE to ICP-MS.

Nebulizer	***CETAC MCN 100***	***Glass Expansion MM 200***	***Glass Expansion MM 50***
Stability	enough	good	very good
Limit of detection	good	average	?
Grade of nebulisation	fine	fine	very fine
Efficiency of nebulisation	good	good	very good
Cleaning	difficult	average	average
Price	expensive	average	average

The following spray chambers were tested:
- Scott type double pass spray chamber made out of glass
- Scott type double pass spray chamber made out of plastic
- Cinnebar Cyclonic small volume spray chamber made out of glass
- different home made models made out of PEEK and KEL-F

A difference between the three commercial spray chambers could not be recognised.

For most of the experiments, a MCN 100 from CETAC and a scott-type double-pass spray chamber were used. However, this combination showed a low stability and was replaced by a MicroMist 200 nebulizer with a Cinnebar Cyclonic spray chamber.

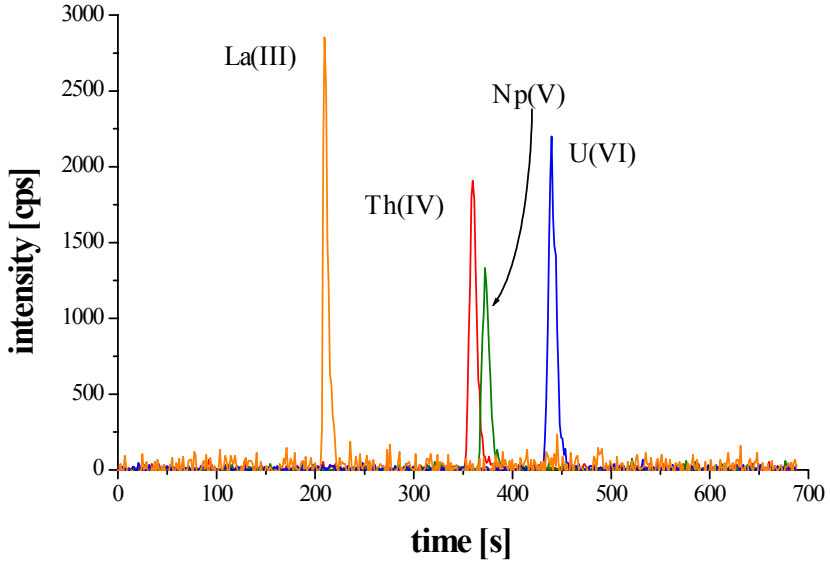

Fig 4: Electropherogram of a separation of model ions with different oxidation states by CE-ICP-MS.

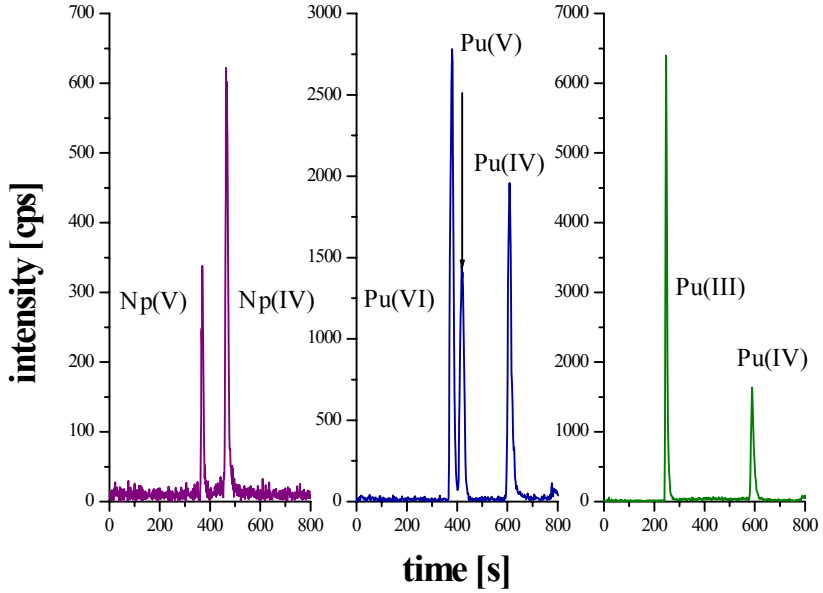

Fig 5: Electropherograms of mixtures of different oxidation states of neptunium and plutonium measured by CE-ICP-MS

First, the separation of lanthanum, thorium, and uranium was repeated in the CE-ICP-MS system. Np(V) was added as pentavalent ion. An example for an electropherogram is shown in *Figure 4*.

Next, the run times of the different oxidation states of plutonium were determined. Therefore, aliquots of the electrolytically produced stock solutions were diluted by the CE electrolyte.

The separation conditions were the same as for the model elements. This was repeated for the two oxidation states of neptunium.

With the knowledge of the different run times, mixtures of the oxidation states were prepared and analysed with the CE-ICP-MS.

Figure 5 shows three electropherograms of plutonium and neptunium present in different oxidation states. The optimised separation conditions are listed in *Table 5*.

Tab. 5: Optimised separation conditions for the oxidation states of plutonium and neptunium by CE-ICP-MS

CE conditions	
CE capillary	363 µm OD, 50 µm ID, 62.8 cm
Distance CE capillary – nebulizer inlet	1 – 3 mm
Separation conditions	
CE electrolyte	1 M AcOH, pH 2.47
Make up electrolyte	2% HNO_3 with 10 ppb Rh marker
Sample injection	100 mbar, 10 s (≈ 44 nl)
Voltage / current	30 kV, 12 - 45 µA increasing
ICP conditions	
Nebulizer flow rate	560 µl/min
Measurement conditions	peak jump, 100 ms Rh, 1000 ms Pu

Tab. 6: Reproducibility of the results pertaining to a plutonium sample containing Pu(III), Pu(IV), and Pu(V). Data in % RSD, N=5

Plutonium species	**Pu(III)**	**Pu(IV)**	**Pu(V)**
Relative amount (%)	31.3	60.3	8.4
Migration time	0.2	0.6	0.5
Peak area	4.1	4.5	4.7
Peak height	4.9	2.3	8.9

With the CE-ICP-MS method, it was possible to determine the content of the different oxidation states of plutonium and neptunium of an aqueous sample in less than 15 minutes. With the MicroMist 200 nebulizer and the Cinnebar Cyclonic spray chamber, 50 ppb for each species was found as limit of detection. With the combination of the MCN 100 and the scott-type double-pass spray chamber a detection limit of 5 ppb was achieved for uranium.

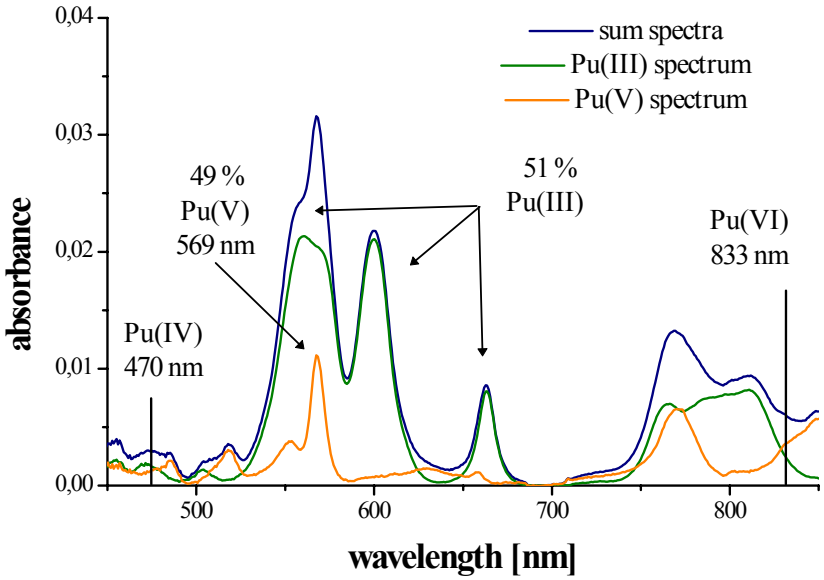

Fig. 6: Absorption spectrum of a solution containing a mixture of Pu(III) and Pu(V) superimposed by separate spectra of Pu(III) and Pu(V)

One sample was measured five times to determine the reproducibility with the coupling of the CE to ICP-MS. The obtained results were analysed with respect to the peak area, peak height, and run time for the different oxidation states. The results are given in *Table 6*. It can be seen that CE-ICP-MS has a high reproducibility for the separation of the different oxidation states.

3.1.2 Comparisons with other Methods

Besides the reproducibility, an independent verification of the results obtained with CE-ICP-MS concerning the different oxidation states was desirable. Reference samples were not available, so it was necessary to compare the results with those obtained by other methods. Therefore, a sample containing Pu(III) and Pu(V) in equal amounts was measured by absorption spectroscopy as well as with CE-ICP-MS to determine the content of the different oxidation states. The sample dissolved in 1 mM $HClO_4$ (c_{Pu} = 1.1 · 10^{-4} mol/l) was measured by a Cary 5 spectrometer in a wavelength range from 300 to 900 nm. The spectra from the sample and spectra of pure Pu(III) and Pu(V) solutions are shown in *Figure 6*. The content of the Pu(III) was determined by the 600 and 665 nm lines, the Pu(V) content by peak deconvolution.

After the spectroscopic measurement, the sample was diluted by a factor of 10 with 1 M AcOH in order not to overload the CE-capillary. This diluted sample was injected into the CE-ICP-MS and the content of the different oxidation states was determined. The electropherogram is shown in *Figure 7*. *Table 7* compares the contents of the different oxidation states of the sample as obtained by both methods. Both methods are associated with an uncertainty of 5 %. It can be seen the obtained results for both methods are in good agreement. Caused by the low extinction coefficient, it was not possible to determine a minor amount of Pu(IV) by absorption spectroscopy, whereas this was no problem for CE-ICP-MS.

Tab. 7: Oxidation state contents of a sample containing plutonium in different oxidation states measured by absorption spectroscopy and CE-ICP-MS

Plutonium species	Pu(III)	Pu(V)	Pu(IV)
Absorption spectroscopy	49.0 %	51.0 %	n.d.
CE-ICP-MS	47.5 %	51.9 %	0.6 %

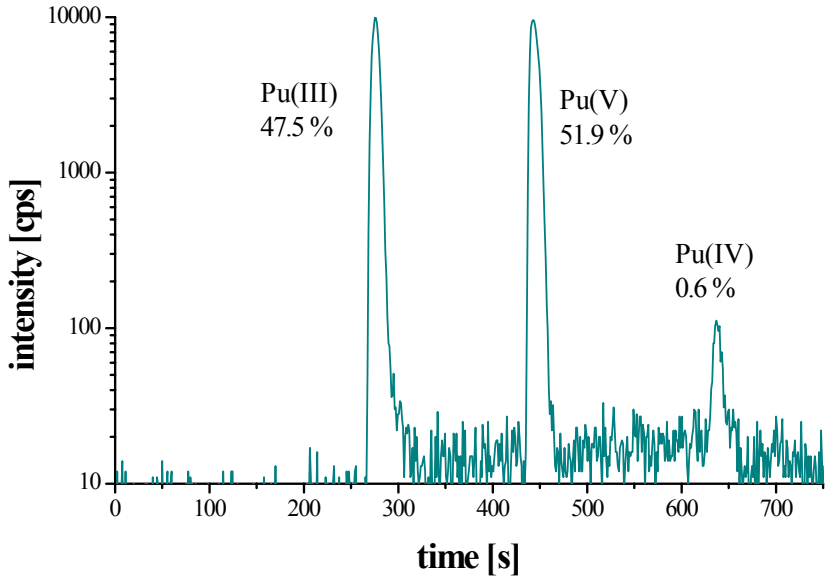

Fig. 7: Electropherogram of a sample containing plutonium in different oxidation states measured by CE-ICP-MS

A solution of 10 mg Aldrich humic acid to which a solution of Pu(VI) was added ($c_{Pu} = 5 \cdot 10^{-5}$ mol/l) was measured with CE-ICP-MS and absorption spectroscopy. While the absorption spectroscopy provided only the Pu(VI) content of the solution due to the high extinction coefficient of the Pu(VI), it was possible to determine also the other oxidation states of plutonium

by the CE-ICP-MS. The sample was measured at different times. *Figure 8* gives an overview about the Pu(VI) content as a function of time. A decrease of the Pu(VI) signal with time is observed with both methods, but the offset between the results of both methods cannot be explained so far.

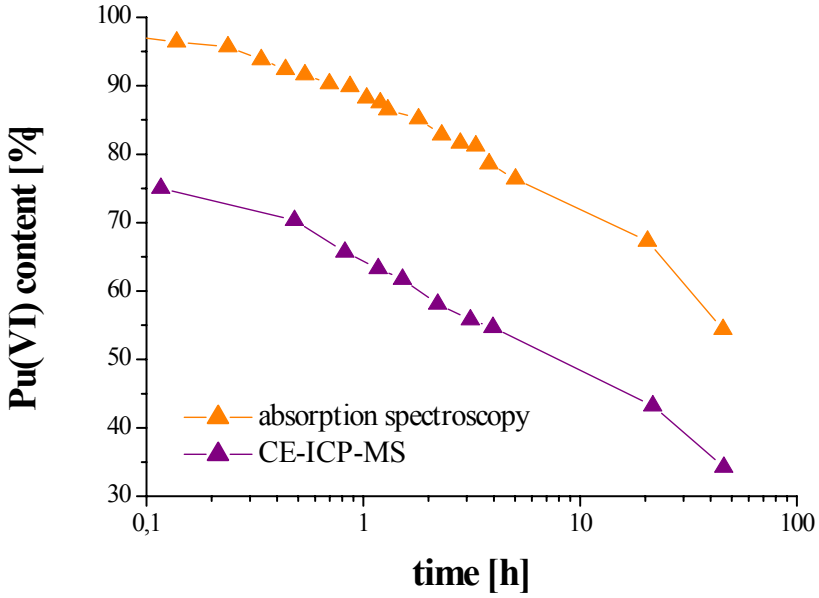

Fig. 8: Determination of the time dependence of Pu(VI) in a solution containing Aldrich humic acid measured by absorption spectroscopy and CE-ICP-MS

3.1.3 Application to Environmental Samples

The quality of an analytical method cannot be demonstrated through the mere application to synthetic samples but by the successful application to real environmental samples. Therefore, CE-ICP-MS was applied for plutonium in natural groundwater from the vicinity of Gorleben.

To the Gorleben groundwater, Pu(VI) was added and the pH value was adjusted to 1.7. A spectroscopic determination of the oxidation states was not possible because the solution was opaque and strongly coloured. With the CE-ICP-MS the oxidation states of plutonium occurring under natural conditions could be determined without any special sample treatment like ultrafiltration. An electropherogram of such a sample of groundwater 20 h after the addition of Pu(VI) at pH 1.7 is shown in *Figure 9*.
At a pH value higher than pH 5 adsorption of plutonium inside the capillary cannot be prevented.
The experiments with natural groundwater samples have demonstrated that the CE-ICP-MS is a reliable technique for the analysis of the oxidation states of plutonium and neptunium.

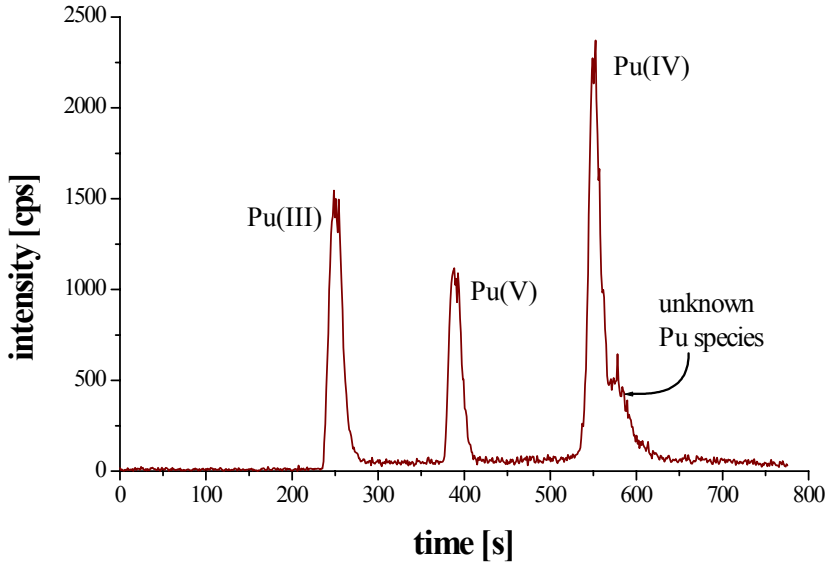

Fig. 9: Electropherogram of a groundwater sample from the vicinity of Gorleben at pH 1.7, 20 hours after addition of Pu(VI)

3.2 Complexation of Neptunium

3.2.1 Experimental Methods

In previous work, it could be shown that no significant difference is observed in the log β values for the Np(V) interaction with humic acid when direct or indirect speciation methods are used[6,10]. The speciation methods applied in these investigations were: electrophoretic ion focusing (EIF), anion exchange (AIX), ultrafiltration (UF), and as a direct method absorption spectroscopy in the NIR-region (940 - 1040 nm). However, most of these methods show limitations to a special metal concentration range. Only the UF method was applicable for the complete range of neptunium concentration (10^{-14} - 10^{-3} M) investigated throughout the project. The data are in agreement with the results from absorption spectroscopy at high metal concentration and for lowest metal concentration with the other indirect methods EIF and AIX.

The EIF- and AIX-method in these studies are limited to low metal concentrations. One explanation for the discrepancies between the log β_{LC}-values obtained by EIF and NIR absorption spectroscopy could be, that the electric field influences the equilibrium of the humate complexation reaction during separation at higher neptunium concentrations[6]. The AIX-experiments are limited to metal-ion concentrations lower than 10^{-6} mol/l (for HA concentrations below 100 mg/l and pH values between 6 and 8), because at higher metal-ion concentrations, the usually negatively charged complex becomes neutral due to charge neutralisation by the metal cation and hence is not completely sorbed on the exchange resin. In the metal-ion concentration range from 10^{-14} - 10^{-6} M the data for EIF, AIX and UF are in agreement.

NIR-Absorption spectroscopy requires 10^{-5} M neptunium or higher. Generally, the humate complexed Np(V) shows a new peak with a bathochromic shifted maximum near 990 nm. From the spectra the ratios [NpO_2^+] / [NpO_2HA] were calculated in a pragmatic way: based on the fact, that only the spectra for the free NpO_2^+-ion are well known[17-21]. For the curve fits, the peak parameters for the NpO_2^+-aquoion - peak maximum and full width at half maximum (FWHM) - were fixed at 980.4 $\pm$ 0.2 nm and 6.2 $\pm$ 0.2 nm, respectively. Both parameters were estimated from spectra of the pure NpO_2^+-aquoion in different buffer solutions in the wavelength range from 940 to 1040 nm. For the spectra of the humate complexed Np-fraction, some problems arise in the deconvolution of the peaks. Using only one peak with free parameters for the humate peak the deconvolution results in a blue shift and broadening of the deconvoluted peak especially in the data sets with increasing Np-concentration. Furthermore, with this procedure, no satisfying reproduction of the spectra is obtained.

Literature data for the complexation of neptunium with simple organic substances show also a bathochromic shift ($\Delta\lambda$) of the absorbance maximum of the NpO_2^+-ion, which follows roughly the complexation strength of the acids (*Figure 10*) [21-31]. Coordination of a second ligand leads to a further shift to a higher wavelength. A broadening (around one to two nanometers in the FWHM) of the spectral envelopes for ascorbate and citrate complexes compared to other Np(V) carboxylate species is reported, which is attributed to the existence of more than one conformation of the complexes in solution[24]. By plotting the red shift for the Neptunyl humate peak complexes against the complexation constants log β_{LC} in *Figure 10*, the values are very close to the diketone compounds and dicarboxylic ethers for a 1:1 coordination, and they are located between values of the 1:1 and 1:2 coordination of dicarboxylic-, α-hydroxo-carboxylic and α/β-amino-carboxylic acids. Both values, the red shift and the log β, for 1:1 complexation with simple monocarboxylic acids are too low for both, assuming that these simple molecules play no role in the complexation. The blue shift together with a broadening of the peaks of the absorption band of the humate peak with increasing neptunium concentration at constant humic acid concentrations however might be caused by changes in the coordination. For the deconvolution procedure it was decided to use only few peaks with only slightly variable parameters to get satisfactory fit curves for the spectra. The parameters are summarised in *Table 8* for the different humic acids. For the calculation of LC and log β_{LC} only the concentration of the free NpO_2^+ was calculated from the spectra and the others are neglected, because their relevance is not proven.
The complexed part of the total neptunium was calculated as:

$$[NpO_2HA] = [NpO_2^+]_{t,\ radiochem.} - [NpO_2^+]_{aq,\ spectr.}. \qquad \textbf{\textit{Equation 1}}$$

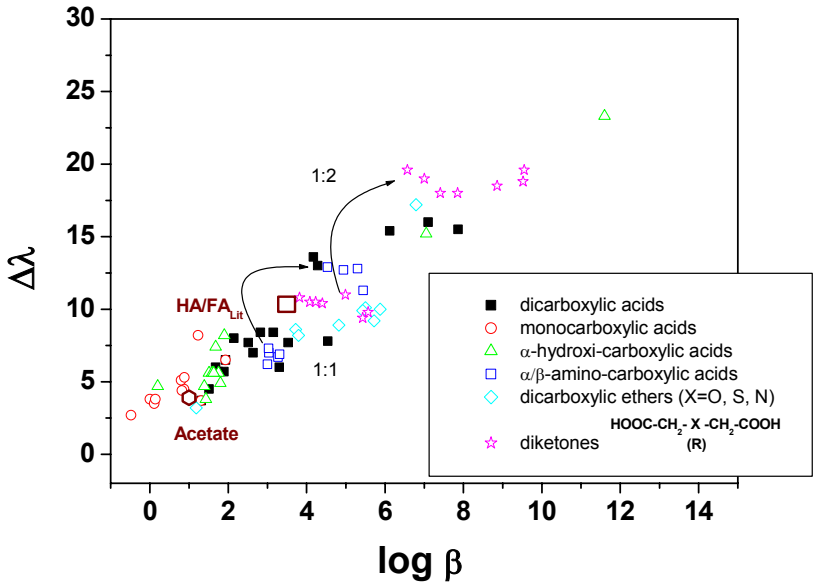

Fig. 10: Complexation of Np(V) with simple organic substances. Added are data from our own acetate complexation experiments and literature data for the HA/FA complexation of Np(V)[18-20]

Tab. 8: Fit parameters for different Np-humates

Species	λ_{max} [nm]	FWHM [nm]	pH	
NpO_2^+	980.2 - 980.4	6.0 - 6.4	7/8	different L, diff. concentration
NpO_2(AHA)-complex	987.0 - 987.5 991 - 992 999 - 1000	11 - 11.5 11 - 12 16 - 16.5	7/8	var. [L], var. [M]
NpO_2(M1)-complex	987.0 - 988.4 991 - 992 999 - 1000	11 - 12.7 11.5 - 12 10 - 12	7/8	var. [L], var. [M]
NpO_2(M42)-complex	985.1 - 985.4 989.5 - 990.2 998.2 - 998.7 1007.7 - 1008.2	6.2 - 6.5 9.8 - 10.2 11 - 11.2 6 - 7	7/8 7/8 7/8 8	var. [L], var. [M] high [M]

3.2.2 Different Humic Acids and Variation of Metal Ion Concentration

With the four speciation methods, different metal concentration regions were investigated using Aldrich humic acid and the synthetic humic acids M1 and M42.

Loading Capacity (LC)

The interaction of Np(V) with humic acids is described with the charge neutralisation model[3] that requires a correction of the actual humic acid concentration available for complexation at a given pH and ionic strength I. The obtained values for log β should be independent of the sort of humic acid, pH and I and therefore comparable for various conditions.
The neutralisation reaction that is considered for Np(V) is:

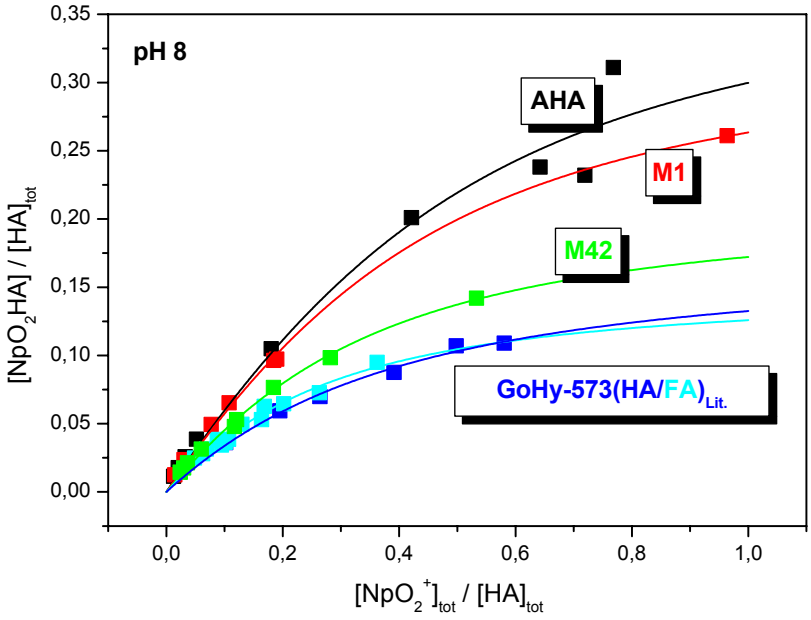

Fig. 11: Determination of the loading capacity at pH 8 for different humic acids. {HA} between 195 and 500 mg/l and variable total NpO_2^+-concentration.

$$\mathbf{NpO_2^+ + HA(l) \rightarrow NpO_2HA(l)}$$

From that LC results as:

$$[LC = [NpO_2HA(l)]_{max} / \{HA\} \cdot PEC \qquad \textit{Equation 2}$$

$[NpO_2HA(l)]_{max}$ is the maximal neptunium concentration permissible for complexation with functional sites of the humic acid, PEC is the proton exchange capacity and {HA} the humic acid concentration in g/l.

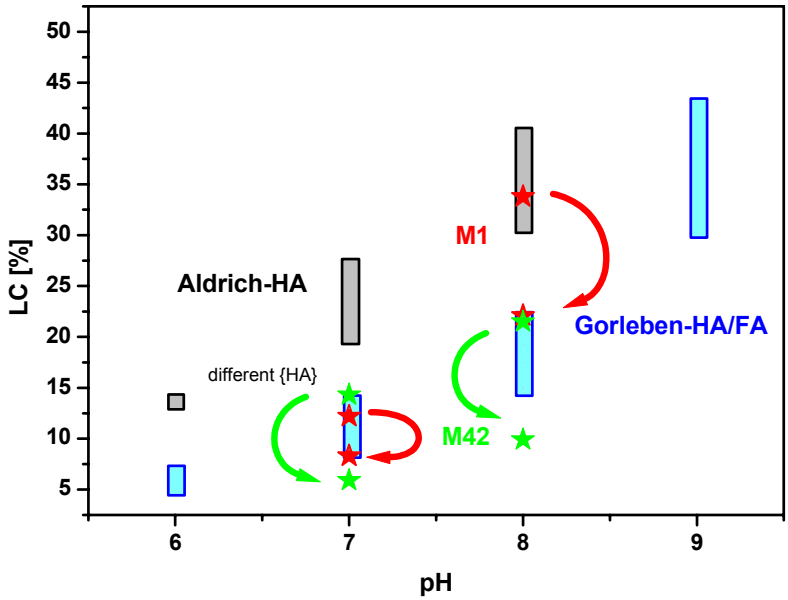

Fig. 12: Loading capacities at different pH values for several humic acids. $\{HA_{synth}\}$ between 30 and 500 mg/l and variable NpO_2^+-concentration. Arrows indicate a decrease of LC for decreasing humic acid concentration {HA}

The loading capacity (LC) of the humic acids decrease in the order (s. *Tab. 9*):
Aldrich HA > M1 > M42> GoHy-573.
Experimental data points are plotted in *Figure 11* together with literature data for GoHy humic and fulvic acid for pH 8[18-20]. A similar behaviour is found for pH 7.

A decrease in LC is indicated with decreasing humic acid concentration {HA}. This is shown in *Figure 12*. The two symbols for the M1 and M42 at the same pH value represent the LC values for different concentrations of the humic acid. As can be seen from *Figure 12* the LC values for M42 and M1 are close to the values of the purified Gorleben humic and fulvic acids. Only for M1 at pH 8 the values are similar to Aldrich-HA. The LC values obtained for the different humic acids are summarised in *Table 9* together with literature data.

Complexation constants (log β_{LC})

The complexation constant is obtained from the law of mass action according to the reaction postulated above

$$\beta_{LC} = [NpO_2HA(I)] / [NpO_2^+][HA(I)]_{free} \qquad \textbf{Equation 3}$$

with

$$[HA(I)]_{free} = LC * [HA(I)]_{total} - [NpO_2HA(I)] \qquad \textbf{Equation 4}$$

With the LC-values determined, the log β_{LC} were calculated for the different humic acids. In previous work[6-10], for Aldrich-HA, a decrease of the log β_{LC} values with increasing metal ion concentration was found. A similar effect can be seen in the experiments with the synthetic humic acids (values are summarised in *Table 10*). In *Figure 13,* these data were visualised

by plotting log β_{LC} vs. $[NpO_2^+]_{tot}$ together with values from the literature[6,18-20] (data regions are for Aldrich humic acid in grey and Gorleben humic and fulvic acid in blue).

Tab. 9: LC values for different humic acids with Np(V). Values in brackets are deduced from only view data points with a high variation and therefore are afflicted with large errors {HA}: concentration of HA in g/L; low {HA} ~ 30 mg/L; high {HA}~ 500 mg/L

Humic acid	pH	LC , [%]	Reference
Aldrich-HA	6	13.6	[6]
Aldrich-HA	7	27.1	[6]
Aldrich-HA	8	34	[6]
Aldrich-HA	7	10 ± 1.5	[32]
Aldrich-HA	8	35 ± 3.7	[32]
M42	7, low {HA}	(6)	This work
M42	7, high {HA}	14 ± 5	This work
M42	8, low {HA}	10 ± 1.4	This work
M42	8, high {HA}	21 ± 1.2	This work
M42	7	11 ± 1.1	[32]
M1	7, low {HA}	8 ± 2.1	This work
M1	7, high {HA}	12 ± 1.4	This work
M1	8, low {HA}	(22)	This work
M1	8, high {HA}	33 ± 1.2	This work

Tab 10: log β_{LC} at pH 7 and 8 for synthetic humic acids M1 and M42.

Humic acid	$[NpO_2^+]_{total}$	log β_{LC}
M1	$9 \cdot 10^{-14}$ - $2 \cdot 10^{-12}$ M	4.9 ± 0.1
M1	$3 \cdot 10^{-7}$ - $7 \cdot 10^{-4}$ M	4.1 ± 0.3
M42	$6 \cdot 10^{-12}$ - $2 \cdot 10^{-8}$ M	5.1 ± 0.1
M42	$5 \cdot 10^{-7}$ - $1 \cdot 10^{-3}$ M	3.9 ± 0.5
M42 from [32]	$5 \cdot 10^{-5}$ - $1.3 \cdot 10^{-3}$ M	3.50 ± 0.15

The M42 synthetic humic acid is very pure and contains very few inorganic impurities. As this substance also follows the increase in log β_{LC} with decreasing metal-ion concentration, it is concluded, that this is not an effect of mineralised inorganic impurities, that may be present even in the purified natural humic acids.

A similar decrease of the complexation constants with increasing metal ion concentration is also reported by other authors[33-34]. In Figure 14 these data from the literature[33-37] are added to our data for different humic acids. As can be seen, there is a good match between all the data.

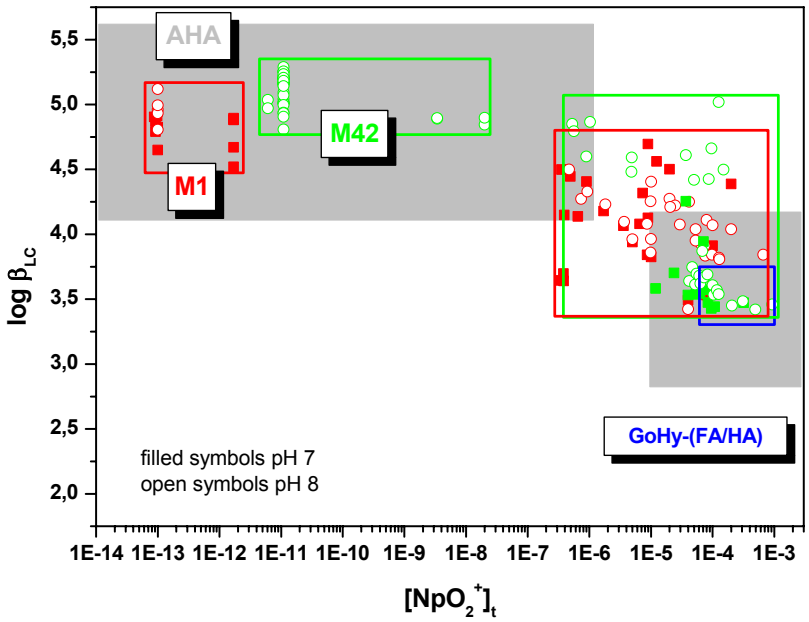

Fig. 13: log β_{LC} at pH values 6 - 8 for several humic acids. $\{HA_{synth}\}$ between 30 and 500 mg/l and variable NpO_2^+-concentration. Grey coloured areas represent the data region for Aldrich-HA[6 and data from this work], the blue box represent the GoHy-data from literature[18-20]. Green data points: M42; red data points: M1

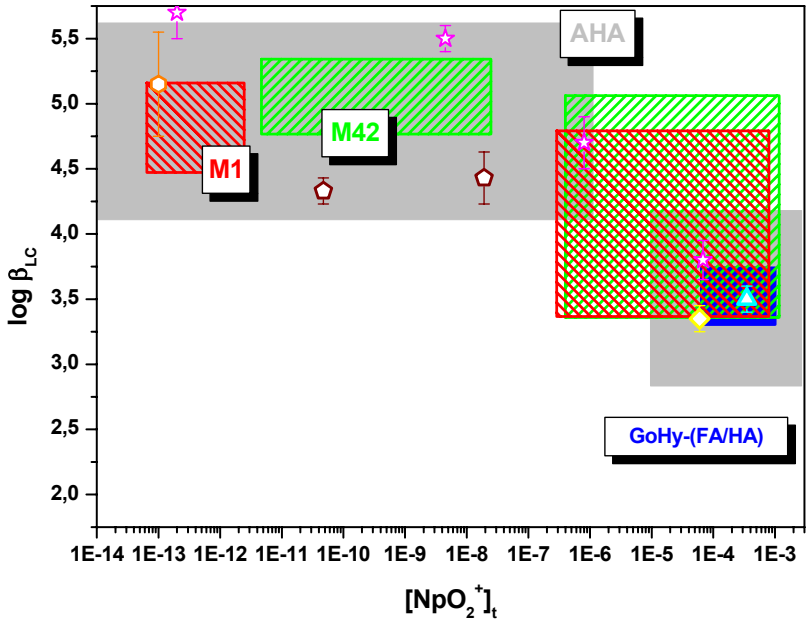

Fig. 14: log β_{LC} at different pH values for several humic acids from the literature and our work. Data regions correspond to Aldrich HA (grey), Gorleben HA (blue), M1 (red) and M42 (green). The symbols correspond to the following literature: stars [33], pentagons [34], triangle [35], diamond [36], hexagon [37] (where necessary the LC corrected log β values were recalculated from log K or log β_α values in some cases an estimation of LC was necessary)

Linear free energy relationships - expressed as logarithm of complexation constants relationships - can be useful for understanding the ionic bonding between hard Lewis acids and bases like f-element cations and carboxylic acids. From such relationships one might learn about the bonding in molecules like humic acid with actinides. *Figure 15* depicts the relationship between the logarithmic complexation constants of NpO_2^+ and UO_2^{2+} complexes with a variety of organic and inorganic ligands. The uranyl ion was selected for comparison because the hard Lewis character and the steric constraints imposed by the two axial oxygen atoms are similar for both cations. The line obtained by linear regression stands for very similar complexation behaviour of the neptunyl and uranyl ion. Deviations from this line may come from different structures of the NpO_2L^{1-n} and UO_2L^{2-n} complexes, e.g., a different number of donor atoms per ligand bound to the metal ions.

The complexation constants log β_{LC} for NpO_2HA and UO_2HA for Aldrich, M1, M42 and GoHy-573 HA obtained at higher metal concentrations fit very well into the linear relationship corresponding to very similar complexation of both. One should notice, that these complexation constants were deduced taking into account the loading capacities, that include the pH dependent deprotonation behaviour of the humic acid as well as the different complexation properties of humic acid towards both cations. This is expressed in different loading capacities for neptunyl and uranyl at various pH values.

Nevertheless, the influence of the neptunyl concentration on the complexation constants remains significant. By plotting the log β_{LC} for NpO_2HA and UO_2HA for total neptunium concen-

trations equal and lower than $2 \cdot 10^{-8}$ M into the free energy plot of *Figure 15*, it is obvious, that the complexes of NpO_2^+ becomes stronger with decreasing metal-ion concentration whereas the UO_2^+ complexes are more or less constant. Spectroscopic studies on curium at concentrations of ~ 10^{-8} M showed no effect on the complexation constant. It seems, that neptunium shows an extraordinary complexation behaviour. In the future, more attention should be devoted to the humic acid molecules to elucidate the complexation mechanism. A recent publication[40] mentioned that the general understanding of humic substances as large molecules might be wrong. New studies reveal more and more that humic substances are rather agglomerates of various smaller molecules with masses < 2000 Dalton and that the agglomeration process might be enhanced by metal ions. The impact of these findings on metal complexation reactions has to be considered in future studies.

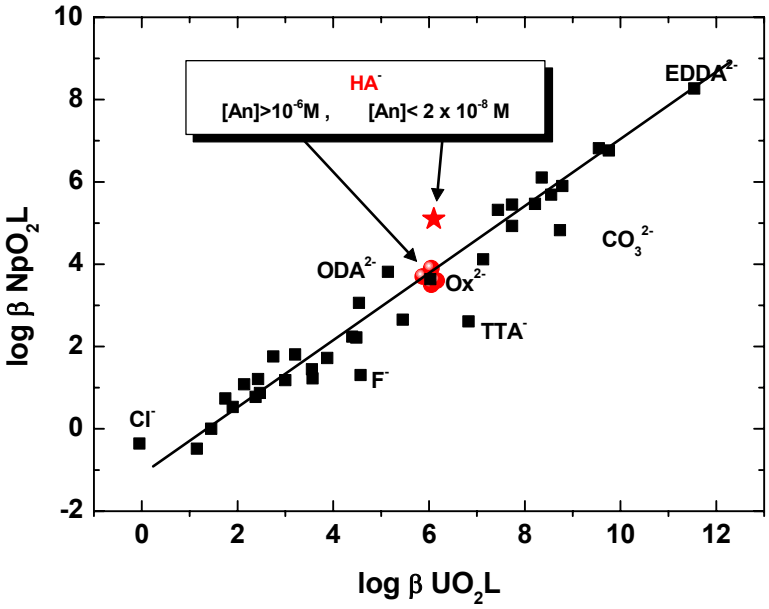

Fig. 15: Relationship of complexation constants for NpO_2^+ and UO_2^{2+} complexes with inorganic, carboxylate, aminocarboxylate, and β-diketone ligands. Data for the simple ligands are from [25] TTA^-: Thenoyltrifluoroacetate; Ox^{2-}: Oxalate; $EDDA^{2-}$: Ethylendiamine-N,N´-diacetate; ODA^{2-}: Oxydiacetic acid.

3.3 Redox Chemistry of Plutonium

3.3.1 Oxidation States

The stability of the plutonium solutions with the different oxidation states was determined. Stock solutions of Pu(VI) and Pu(IV) ($c \approx 10^{-4}$ mol/l) were measured in various time intervals by UV/VIS absorption spectroscopy. For Pu(VI) in 1 M $HClO_4$, a stability is given for at least 6 months. Solutions of Pu(IV) in 1 M $HClO_4$, show after 2 to 4 weeks first indications of disproportionation.

A chemical reduction of Pu(VI) to Pu(IV) by the use of sodium nitrite in diluted nitric acid solutions is possible. To exclude an influence of trace amounts of nitrite in the complexation with humic acids this procedure was not used for the preparation of Pu(IV) stock solution.

3.3.2 Plutonium and Aldrich Humic Acid

Prior to the investigations of the complex formation of plutonium with humic acids, it was necessary to find out which oxidation states are stable in the presence of humic acid. Only for oxidation states with sufficient stability, a reliable determination of the complex formation constants is possible.

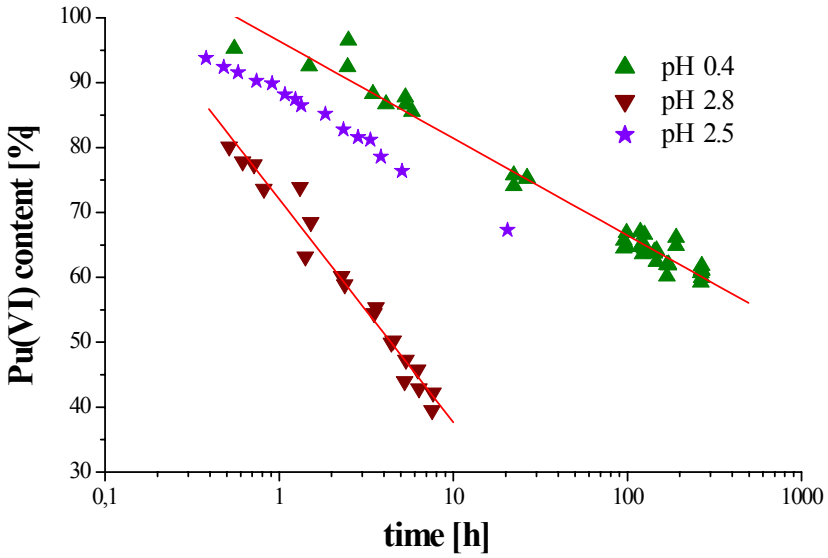

Fig. 16: Time depending Pu(VI) content after contact with Aldrich humic acid determined by absorption spectroscopy

It is known that Pu(VI) can be reduced by Aldrich humic acid and also by buffers like MES at a pH value 4[39]. Caused by this, the starting point for our investigations was chosen at pH values 0.4 and 2.8. The Pu(VI) stock solution was added to a solution containing humic acid and adjusted to the requested pH value. During the first experiments, the CE-ICP-MS coupling was not available, so the disappearance of the 831 nm signal of the Pu(VI) was determined by absorption spectroscopy. A third experiment was performed at a pH value of 2.5. There, the oxidation state content could be determined both by absorption spectroscopy and by CE-ICP-MS. The experimental conditions are summarised in *Table 11*. During the two first experiments, a reference sample with the same composition but without humic acid was measured. *Figure 16* shows the Pu(VI)-content as function of time of the samples determined by absorption spectroscopy. *Figure 17* shows the time dependent content of all occurring oxidation states of plutonium during the third experiment (pH 2.5) determined by CE-ICP-MS.

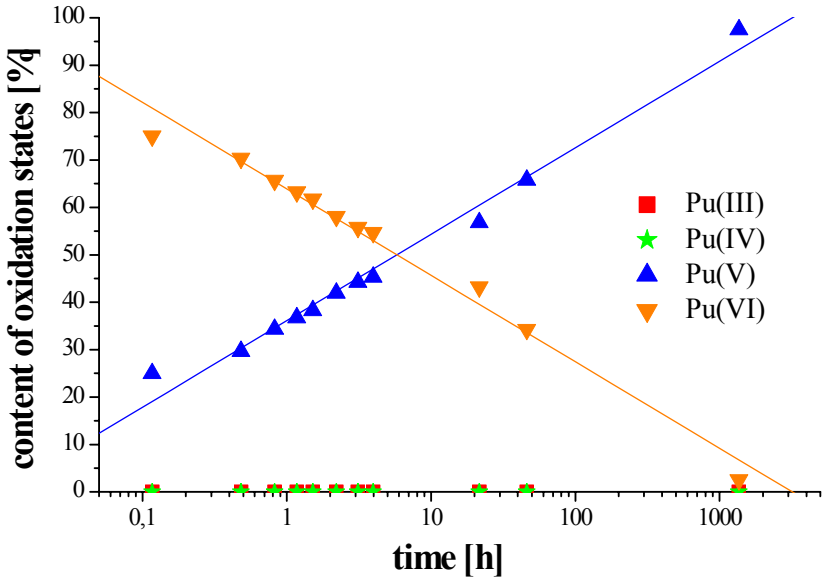

Fig. 17: Content of the different oxidation states of plutonium after addition of Pu(VI) to a solution containing Aldrich humic acid at pH 2.5 as a function of time

Tab. 11: Experimental conditions for investigating the stability of Pu(VI) in presence of Aldrich humic acid

Experiment	I	II	III
pH value	0.4	2.8	2.5
Electrolyte / buffer	1 M $HClO_4$	1 M $HClO_4$ 0.1 M MES	1 M $HClO_4$
C_{HA} [mg/l]	10	10	10
C_{Pu} [µmol/l]	30	30	50
Measurement by	UV (831 nm)	UV (831 nm)	UV (831 nm), CE-ICP-MS

It could be demonstrated that Pu(VI) is reduced to Pu(V). The reduction becomes faster with increasing pH value. A further reduction of Pu(V) could not be detected during the interaction time of more than 1000 hours. Under the pH conditions applied, the humic acid is precipitated. This precipitate was not agitated. By the use of ultrafiltration with a 1 kDalton membrane and LSC, it was possible to show 95 – 100 % of the plutonium is still in solution and not adsorbed on any walls, the filter membrane, or bound to the precipitated humic acid.

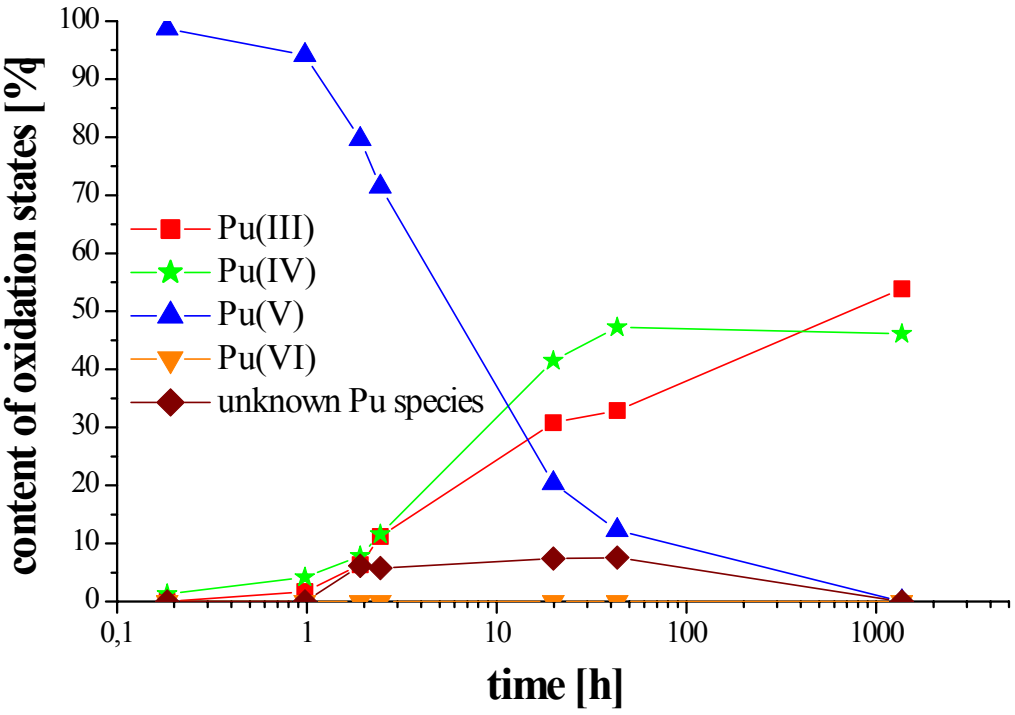

Fig. 18 : Content of different oxidation states of plutonium after addition of Pu(VI) to groundwater from the vicinity of Gorleben at pH 1.7 as a function of time

3.3.3 Plutonium in Gorleben Groundwater

In addition to Aldrich humic acid, the investigations were extended to groundwater from the vicinity of Gorleben. To suppress the hydrolysis, the experimental series started at a pH value of 1.7. The concentration of plutonium was 10 µmol/l. All the samples were produced in an inert gas box and kept there until the measurement.

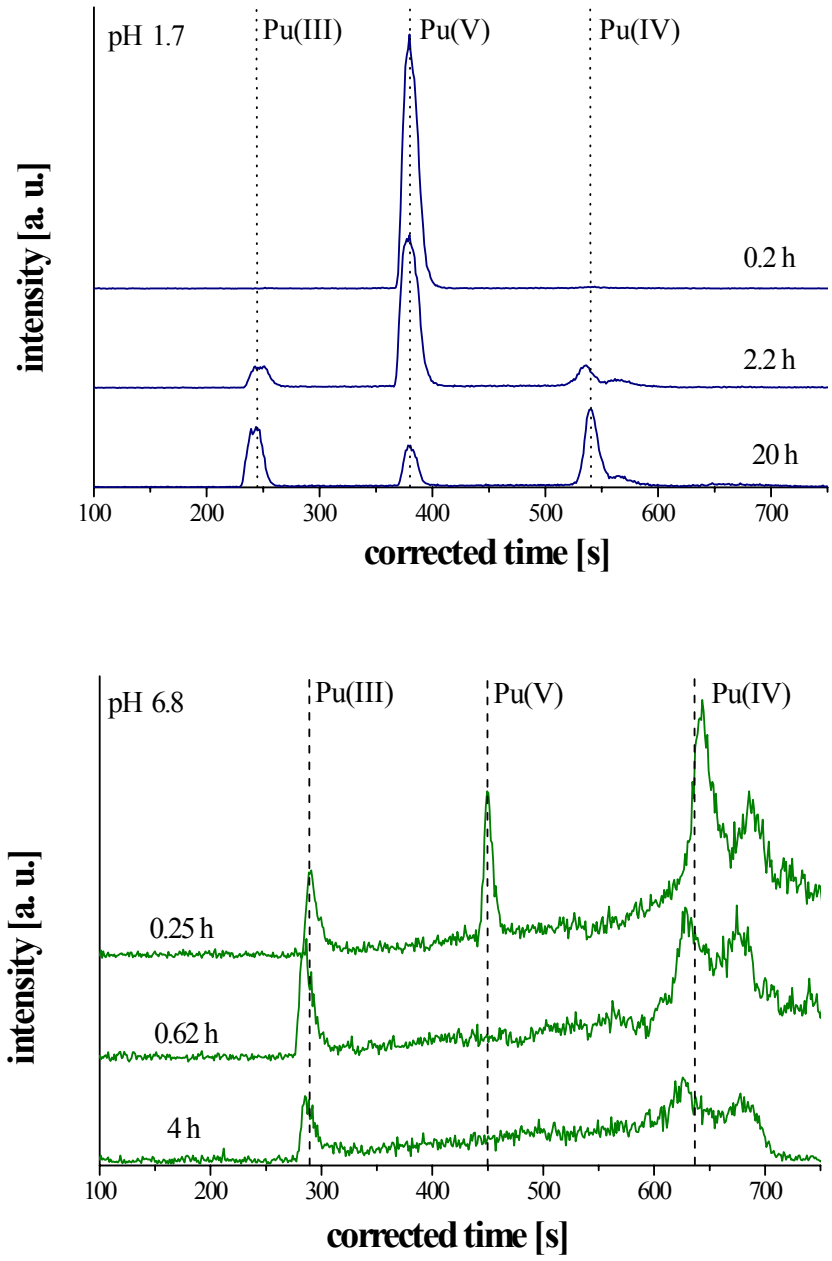

Fig: 19: Selected electropherograms of groundwater from the vicinity of Gorleben after addition of Pu(VI), measured after different times at pH 1.7 (top) and pH 6.8 (bottom)

The observed time dependent content of the different oxidation states is shown in *Figure 18*. It can be seen that Pu(VI) is reduced completely during five to ten minutes to Pu(V). Pu(V) is further reduced to Pu(IV), Pu(III), and an unknown plutonium species. The investigations were expanded to the pH values of 5 and 7 to reach real environmental conditions. *Figure 19* shows for pH 1.7 and 6.8 in each case three selected electropherograms. With these experiments, it could be shown unambiguously that the reduction rate increases with the pH

value. *Figure 20* illustrates this pH dependence for the Pu(V) content at pH 1.7, 5, and 7. With increasing pH, an increasing tendency of a reversible adsorption of probably hydrolysed plutonium was observed. At a pH value of 5 only 65 % and at pH 7 at least 35 % could be detected as free ions. The adsorbed plutonium could be removed from the surface of the capillary by rinsing with alkaline and acidic media. The hydrolysis species are known for their tendency to adsorb on all kinds of surfaces.

From these experiments, it could be concluded that, under environmental conditions, Pu(VI) and Pu(V) are not stable, but are reduced to Pu(IV) und Pu(III) depending on the pH value.

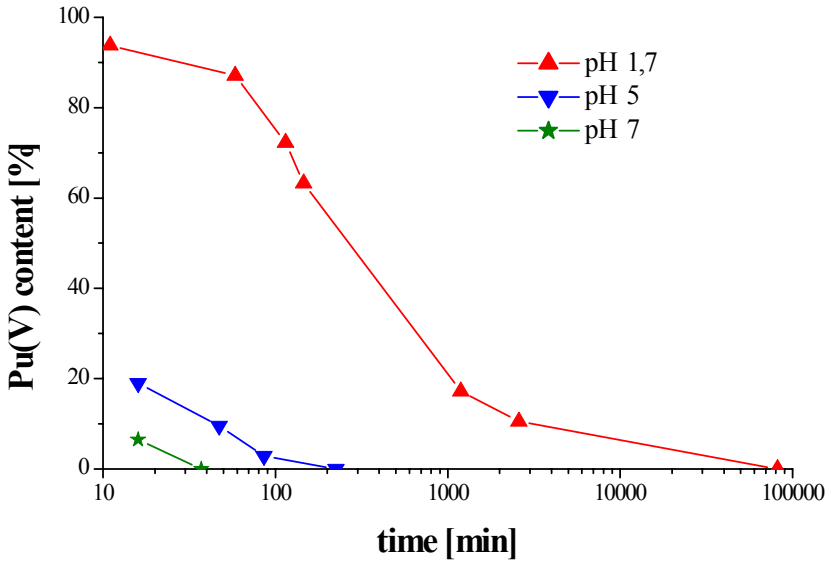

Fig. 20: Time depending Pu(V) content of groundwater sample from Gorleben after addition of Pu(VI) at different pH values

3.4 Complexation of Plutonium

From the investigations of the redox behaviour of plutonium in contact with humic acids one can conclude that not all oxidation states are relevant for the determination of complex formation constants with humic acids. Pu(VI) is reduced fast by Aldrich humic acid, and almost instantaneously by the Gorleben groundwater samples. Thus, Pu(VI) is not relevant for the safety assessment of a waste repository. For the Gorleben groundwater, it was also shown that Pu(V) is reduced rather quickly. So Pu(IV) and Pu(III) are the relevant oxidation states under the conditions of “Gorleben”. In a first step, Pu(IV) was selected for the investigations of the complexation behaviour with humic acid.

The kinetics of the complex formation is important for the determination of the complex formation constants. Therefore, the time dependence of the plutonium complexation was measured at three metal ion and two humic acid concentrations using ultrafiltration. These concentrations were chosen in order to offer similar concentrations of active complex centres

of the humic acid and metal ions. To minimise the tendency towards hydrolysis of the plutonium, the pH value was chosen to be 1.8. At this pH value it was shown by Bitea et al. that plutonium exists mostly as $[Pu(OH)_2]^{2+}$ [40].

Plutonium and the humic acid were mixed at pH 1.8 and shaken continuously in order to dispense the precipitating humic acid in the solution. After different times, small aliquots were removed and the recovery of the free plutonium ions was determined by ultrafiltration with subsequent LSC measurement. Plutonium solutions without humic acid were also investigated to obtain values for absorption effects due to hydrolysis. The experimental conditions are listed in *Table 12*, *Figure 21* shows the time dependent recovery of plutonium in these samples.

Tab. 12: Experimental conditions for investigations on complexation kinetics

pH value	1.8 (1.4 at higher Pu concentration)
Electrolyte / buffer	~ 0.1 M $HClO_4$; ~ 0.1 M NaOH, 0.01 M MES
C_{HA}	0 mg/l ; 1 mg/l ; 10 mg/l
C_{Pu}	$7.3 \cdot 10^{-8}$ mol/l ; $7.3 \cdot 10^{-7}$ mol/l ; $7.3 \cdot 10^{-6}$ mol/l
Conditions	room temperature , shaken continuously
Contact time	20 h ; 168 h ; 672 h
Sample preparation and measuring	ultrafiltration 1 k Dalton, LSC

With these experiments, it could be shown that in nearly all cases, the equilibrium was reached after one week. In two cases, a noticeable change between the recovery of plutonium was found between one day and one week ($c_{Pu} = 7.3 \cdot 10^{-8}$ mol/l, c_{HA} = 1 mg/l; $c_{Pu} = 7.3 \cdot 10^{-7}$ mol/l, c_{HA} = 10 mg/l respectively). Further experimental data with measurements at the same conditions ($c_{Pu} = 7.3 \cdot 10^{-8}$ mol/l; c_{HA} = 1 mg/l) after 1 day, 2 days, 4 days, and 7 days are shown in *Figure 22* illustrating that it takes up to almost one week for reaching the equilibrium.

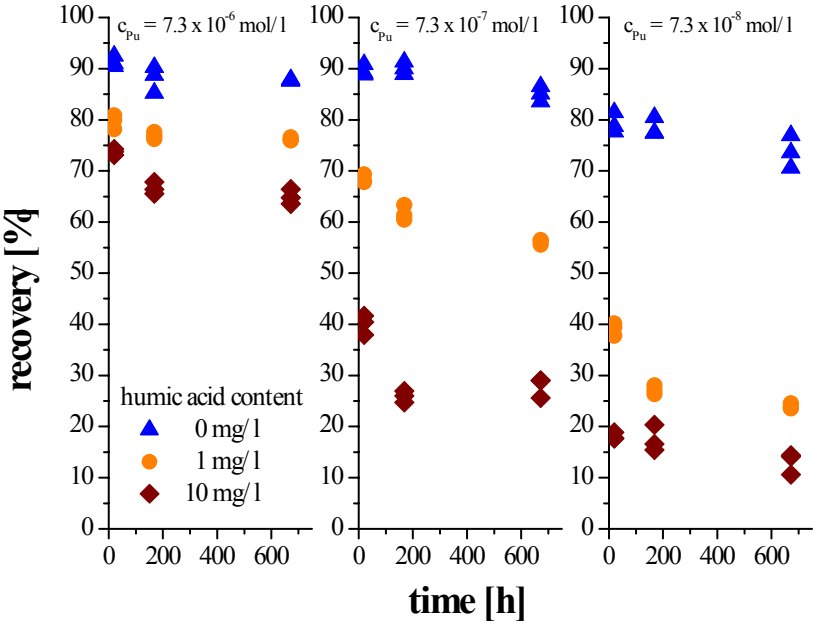

Fig. 21: Recovery of free plutonium after addition of Pu(IV) to a solution containing Aldrich humic acid as a function of time as determined by ultrafiltration and LSC at various metal ion- and humic acid concentrations; humic acid concentration: blue triangles: 0 mg/l; orange circles: 1 mg/l ; brown squares: 10 mg/l

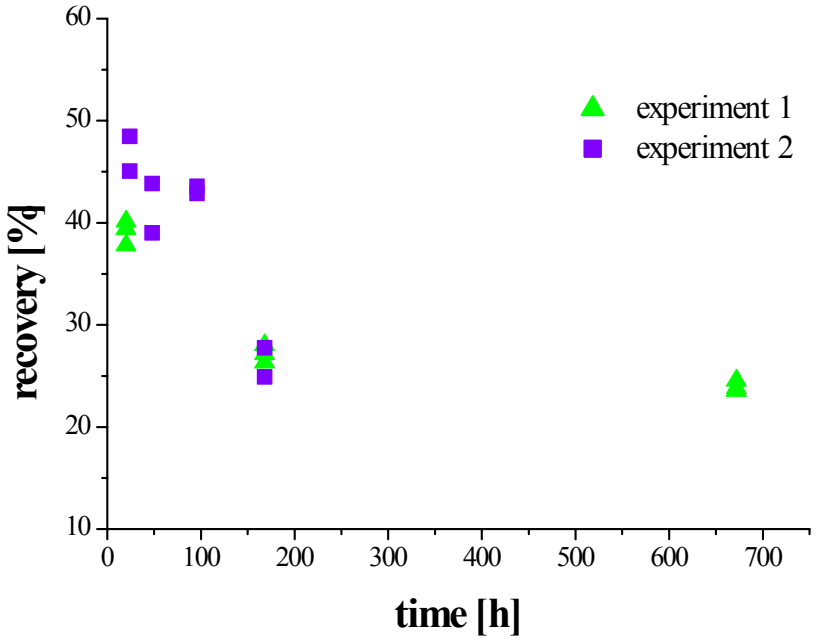

Fig. 22 : Time depending recovery of free plutonium at c_{Pu} = 7.3 · 10^{-8} mol/l and c_{HA} = 1 mg/l.

One possible explanation for this effect is the deprotonation degree α of the humic acid. It depends on the pH value and is small at a pH of 1.8. From the known deprotonation degree, a value for pH 1.8 was extrapolated by a Boltzmann fit. This fit is shown in *Figure 23*. The extrapolated deprotonation degree α is 2.7 %. *Table 13* gives an overview over the calculated correction of the number of effective complexing sites at the humic acid under these pH conditions.

Taking into account that under these conditions, two hydroxide ions are bound to the plutonium, it could be assumed that there are two free sites for each plutonium ion. At $c_{Pu} = 7.3 \cdot 10^{-8}$ mol/l and $c_{HA} = 1$ mg/l with an effective number of active humic acid binding sites of $c_{HA,eff} = 12.4 \cdot 10^{-8}$ eq/l, there is nearly the same number of free Pu and humic acid binding sites. This may explain why it takes so long to reach equilibrium.

Tab. 13: Results of the extrapolation of the effective PEC in solution corrected by the extrapolated deprotonation degree α.

	Tabulated value	In solution	In solution, α corrected
C_{Pu}		$7.3 \cdot 10^{-8}$ mol/l	$7.3 \cdot 10^{-8}$ mol/l
C_{HA}		$1 \cdot 10^{-3}$ g/l	$1 \cdot 10^{-3}$ g/l
PEC	$4.6 \cdot 10^{-3}$ eq/g	$4.6 \cdot 10^{-6}$ eq/l	$12.4 \cdot 10^{-8}$ eq/l

In a further experiment, the humic acid solution normally at pH 7 and the plutonium stock solution, normally at pH 0 were adjusted to pH 1.8 for three days and than mixed together. The obtained results scattered a lot and after one week a recovery yield of plutonium was measured similar to the blank sample without humic acid. One can assume, that during the three days at pH 1.8 Pu(IV) forms oligomeres and thus is not longer able to form complexes with humic acid. The precipitation of the humic acid at this pH value could also effect the reaction. For the determination of the complex formation constants, the solutions were mixed together, adjusted to the desired pH value, and shaken for one week before the recovery yield of plutonium was determined. These experiments are in progress and will be part of the new project.

It is also necessary to extend the experiments to higher pH values in order to be able to predict the migration behaviour of plutonium in natural groundwaters.

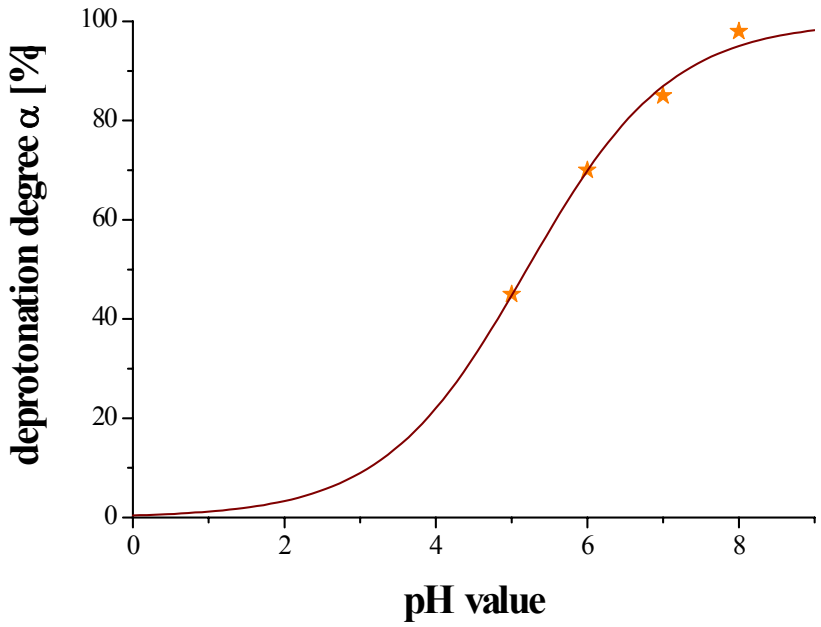

Fig. 23: Extrapolation (Boltzmann-fit) of the deprotonation degree α on dependence of the pH values.

3.5 RIMS

The RIMS technique has been used for isotope selective determination of plutonium in different samples such as sediments from the French nuclear weapons test site on the Mururoa-atoll, indicating a huge excess of plutonium-239 compared to plutonium 240, which is typical for nuclear weapons plutonium. Here, an overall plutonium-239 activity of 31 mBq/g (≈ $7 \cdot 10^9$ atoms(Pu-239)/g) was determined. In a water sample from the Irish Sea, the isotopes plutonium-238, 239, 240, 241, and 242 could be determined. Another example is the determination of plutonium in dust samples contaminated with plutonium from the reprocessing plant ("Wiederaufarbeitungsanlage Karlsruhe", WAK) at the "Forschungszentrum Karlsruhe". The isotope pattern is characteristic for "reactor plutonium". The isotopic composition of plutonium in a depleted uranium penetrator as used during the Balkan conflict was also measured with RIMS. That measurement indicates that the depleted uranium is contaminated with weapons plutonium.

RIMS measurements were also performed for other members of the collaboration in projects where particularly low concentrations of plutonium were determined.

3.6 Column Experiments with plutonium

In *Table 14*, the experimental conditions and in *Table 15*, the results from our column experiment are summarised together with experimental data from literature in the Gorleben system.

Tab. 14: Column experiments in the Gorleben system (anaerobic) with Pu-238,242 Cont.: Continuous feed of the column with Pu solution.

Experiment number	Injection mode	Contact time	Migration time	Rf	Recovery [%]	GoHy	DOC [mg C/l]	Reference
1	Cont.	12 h	19.5 h (+5.7 h)		3.2	532	30	This work
2	Cont.	5 d (+5 h)	1 – 109 h		34.5-3.2	532	30	[41]
3	Cont.	29 (+1.5) d	1 – 109 h		54.6-9.7	532	30	[41]
4	Pulse	≈ 28 d	9 h	0.96	52.5	2227	80	[42]
5	Pulse	≈ 28 d	9 h	0.97	63.7	2227	80	[42]
6	Cont.	4 a	9 h	1.01	40.2	2227	80	[42]
7	Pulse	4 a	28 h	1.24	0.24	1011	3.2	[42]

Tab. 15: Results of the column experiments in the Gorleben system

Experiment number	Concentration plutonium [mol/L]	Added plutonium oxidation state to GoHy	Plutonium oxidation state introduced onto column	Speciation method
1	$9.5 \cdot 10^{-6}$	IV/(III)	IV/(III)	CE
2	$1.2 \cdot 10^{-9}$	VI	IV/III	TTA, UF
3	$1.8 \cdot 10^{-9}$	VI	IV/III	TTA, UF
4	$8.4 \cdot 10^{-8}$	VI or III	IV (?)	UF
5	$8.4 \cdot 10^{-8}$	VI or III	IV (?)	UF
6	$1.3 \cdot 10^{-7}$	VI or III	IV (?)	UF
7	$5.5 \cdot 10^{-9}$	VI or III	IV (?)	UF

Pu(IV) was added directly in a relatively high concentration to the groundwater as recent experiments with EXAFS/XANES and XPS showed that, regardless of the oxidation state added in this concentration range, Pu colloids (eigencolloids as well as humic colloids) were the predominant species. In similar samples, EXAFS investigations showed both Pu-Pu interactions and a splitting into two oxygen shells as next neighbours that is interpreted as being due to interaction with the humic/fulvic substances[43].

The sample solution was also investigated by CE-ICP-MS prior to the introduction. These experiments showed that plutonium is in a very small part in the trivalent state and the rest in the tetravalent state. The latter occurs predominantly as polymeric species. The electropherograms of a cationic run with a stock solution of plutonium prior to its addition to the groundwater and the groundwater spiked with this solution after about 18 h reaction time are shown in *Figure 24*.

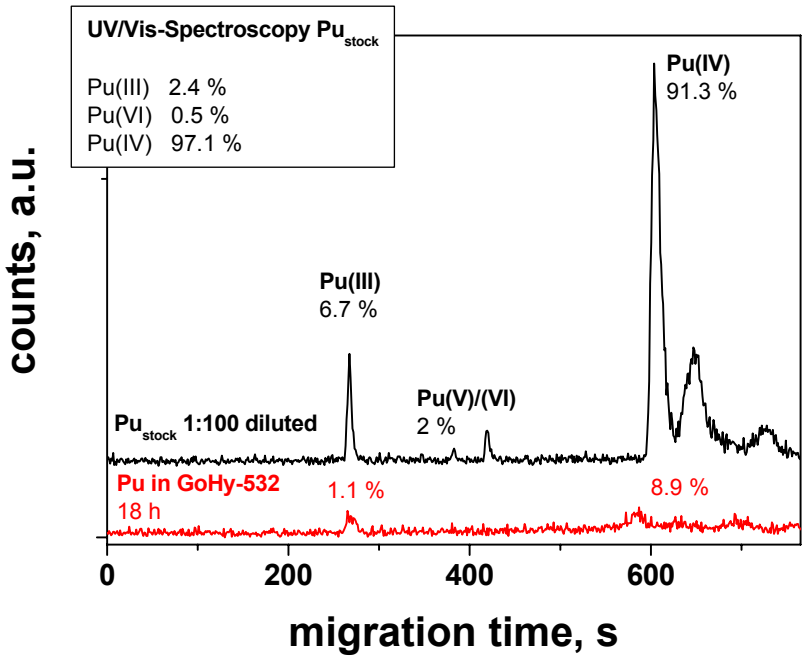

Fig. 24: Electropherograms of the stock solution of plutonium (black curve) that was added to the groundwater and the spiked groundwater after about 18 h (red curve). For comparison, the data from absorption spectroscopy of the undiluted plutonium stock solution are given

On the basis of washing steps after the separations on the capillary and a run with reversed electrodes to detect anionic species, the following fractions were found: about 10 % cationic species (Pu(III) and (IV)), 30 % anionic species (unidentified), neutral species in the range of 10 % and at least 50 % of the plutonium present as species that adsorb easily on the capillary wall (ascribed to polymeric species).

Figure 25 shows the elution curve of the column experiment. The eluted fraction of the total plutonium (Pu/Pu_0) is plotted vs. the number of pore volumes. The pore volume of the column was determined prior to the experiment with the tracer HTO. The elution of plutonium with the groundwater velocity or with a slightly enhanced velocity (that means within or slightly before one pore volume of the column) indicates its transport with the humic colloids. This was also corroborated by ultrafiltration experiments with different pore sizes were the plutonium activity in the filtrates followed the size pattern of the DOC of the groundwater.

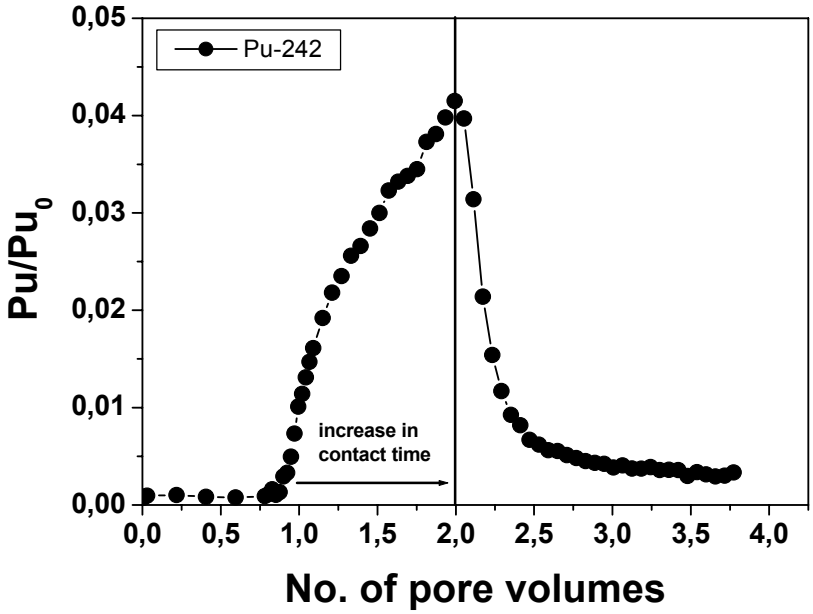

Fig. 25: Elution curve for the Pu-242 experiment

The recovery of plutonium is, compared to other experiments with tetravalent actinides in this concentration range, very low. Only 3.2 % of the total plutonium concentration were eluted in the first two pore volumes, whereas experiments with Np(IV) and Tc(IV) showed recoveries of about 80 %[44]. The very low recovery of our column experiment is ascribed to the relative short contact time of plutonium with the groundwater before the experiment. As was seen in batch experiments concerning the kinetics of the complexation reaction with humic acid in a synthetic solution with Aldrich humic acid at a lower pH, several days are required to reach a constant value. By plotting the recovery vs. the contact time, that was varied during the experiment due to the continuous introduction onto the column, it can be seen clearly that the recovery increases with increasing contact time (*Figure 26*).

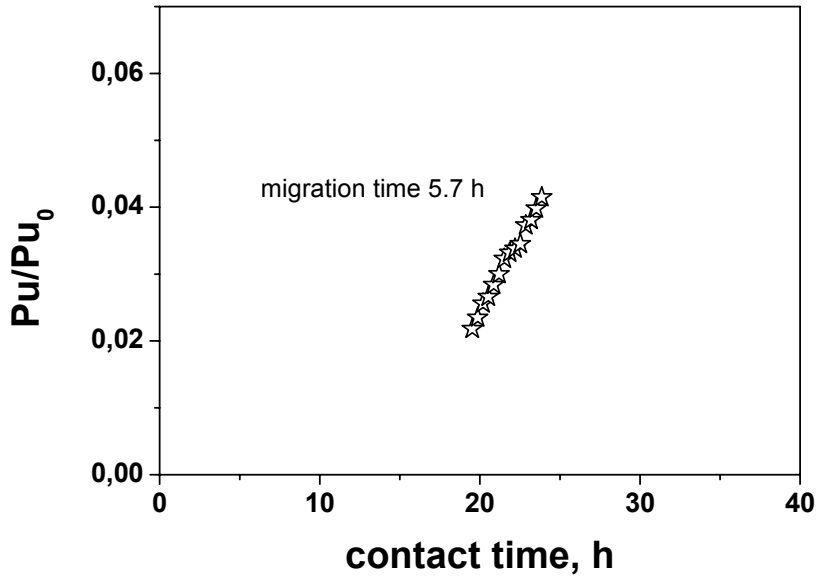

Fig. 26: Dependence of the recovery on the contact time during the column experiment.

4 Conclusions and Outlook

In the framework of this project, a method was developed based on coupling of CE to ICP-MS which enables the separation of the different oxidation states of plutonium and neptunium. It was possible to apply it for synthetic samples as well as for natural groundwater samples. With this technique, the redox behaviour of plutonium(VI) in contact with Aldrich humic acid and Gorleben groundwater could be investigated. Plutonium(VI) is reduced very fast under natural conditions (pH 7) and mainly Pu(IV) and Pu(III) are in the solution.

A future development should be the improvement of the detection limit by application of CE-RIMS (off-line coupling) and a shortening of the separation time by using CE-LIF (CE - laser induced fluorescence detection) and investigations of some species by CE-ESI-MS (CE - electron spray ionisation - mass spectrometry). In the field of colloidal and anionic species further investigations with CE-UV/VIS (DAD) and CE-ICP-MS are necessary.

For neptunium(V), complex formation for a large range of metal-ion concentrations (10^{-3} – 10^{-14} M) with Aldrich humic acid and synthetic humic acids by application of direct and indirect methods was investigated. A decrease of the log β_{LC} values with increasing metal-ion concentration was found for all humic acids. This seems to be extraordinary in comparison to uranium or curium. The impact of these findings on metal complexation reactions has to be considered in future studies.

Studies of the complex formation of plutonium(IV) and the associated kinetics must be continued taking into account also mixed humate and hydroxide complexes of plutonium. The determination of log β_{LC} values for Pu(IV) and Pu(III) with humic acids is a requirement to predict the migration behaviour of plutonium.

The migration behaviour of plutonium under “Gorleben” conditions was studied and shows, that in most cases, plutonium is reduced to Pu(IV) and Pu(III). Also neutral and anionic species were found with CE-ICP-MS in the effluent from the column, but most of the plutonium was adsorbed at the mineral phase. It is observed that the recovery of plutonium increases with increasing contact time before the injection.

5 Literature

1 Actinide and fission product partitioning and transmutation, OECD/NEA Report, Organisation for Economic Co-operation and Development-Nuclear Energy Agency: Paris, 1999. (PDF-file: http://www.nea.fr/html/trw/docs/neastatus99).

2 Schmeide, K.; Sachs, S.; Bubner, M.; Reich, T.; Heise, K. H.; Bernhard, G.; *Interaction of Uranium(VI) with Various Modified and Unmodified Natural and Synthetic Humic Substances Studied by EXAFS and FTIR Spectroscopy*, Inorganica Chimica Acta **2003**, 351, 133.

3 Kim, J. I.; Czerwinski, K. R.; *Complexation of Metal Ions with Humic Acid: Metal Ion Charge Neutralization Model,* Radiochimica Acta **1996**, 73, 5.

4 Torres, R. A.; Choppin, G. R.; *Europium(III) and Americium(III) Stability Constants with Humic Acid*, Radiochimica Acta **1984**, 35, 143.

5 Saito, A.; Choppin, G. R.; *Separation of Actinides in Different Oxidation States from Neutral Solutions by Solvent Extraction,* Analytical Chemistry **1983**, 55, 2454.

6 Seibert, A.; Mansel, A.; Marquardt, C. M.; Keller, H.; Kratz, J. V.; Trautmann, N.; *Complexation Behaviour of Neptunium with Humic Acid*, Radiochimica Acta **2001,** 89, 505.

7 Kuczewski, B.; Marquardt, C. M.; Seibert, A.; Geckeis, H.; Kratz, J. V.; Trautmann, N.; *Separation of Plutonium and Neptunium Species by Capillary Electrophoresis and Application to Natural Groundwater Samples,* Analytical Chemistry, **2003**, 75, 6769.

8 Kim, J. I.; Buckau, G.; *Characterization of Reference and Site Specific Humic Acids,* Report Radiochemie TU München, RCM 0218, 1988; Chapter 3.3..

9 Pompe, S.; Bubner, M.; Schmeide, K.; Heise, K. H.; Bernhard, G.; Nitsche, H.; *Synthesis, Radiometric Determination of Functional Groups, Complexation* In: Marquardt, C. M. (Ed.), *Influence of Humic Acids on the Migration Behaviour of Radioactive and Non-radioactive Substances under Conditions Close to Nature*, Final Report BMBF

Projects Nos. 02 E 8795 8 and 02 E 8815 0, Wissenschaftliche Berichte FZKA 6557, Karlsruhe (2000).

10 Mansel, A.; Montavon, G.; Seibert, A.; Artinger, R.; Keller, H.; Kim, J. I.; Kratz, J. V.; Marquardt, C. M.; Scherbaum, F.; Trautmann, N.; *Complexation Studies of Actinides with Humic Acids at Very Low Metal Concentrations.* In: Marquardt, C. M. (Ed.), *Influence of Humic Acids on the Migration Behaviour of Radioactive and Non-radioactive Substances under Conditions Close to Nature*, Final Report BMBF Projects Nos. 02 E 8795 8 and 02 E 8815 0, Wissenschaftliche Berichte FZKA 6557, Karlsruhe (2000).

11 Artinger, R.; Kienzler, B.; Schüßler, W.; Kim, J.I.; *Effects of Humic Substances on the 241Am Migration in a Sandy Aquifer: Column Experiments with Gorleben Groundwater / Sediment Systems,* Journal of Contaminant Hydrology **1998**, 35, 261.

12 Cohen, D.; *Electrochemical Studies of Plutonium Ions in Perchloric Acid Solutions,* Journal of Inorganic and Nuclear Chemistry **1961**, 18, 207.

13 Prange, A.; Schaumlöffel, D.; *A New Interface for Combining Capillary Electrophoresis with Inductively Coupled Plasma-Mass Spectrometry,* Fresenius Journal of Analytical Chemistry **1999**, 364, 452.

14 Li, J.; Umemura, T.; Odake, T.; Tsunoda, K.; A High-Efficiency Cross-Flow Micronebulizer Interface for Capillary Electrophoresis and Inductively Coupled Plasma Mass Spectrometry*,* Analytical Chemistry **2001**, 73, 5992.

15 Day, J. A.; Caruso, J. A.; Becker, S. J.; Dietze, H.-J.; *Application of Capillary Electrophoresis Interfaced to Double Focusing Sector Field ICP-MS for Nuclide Abundance Determination of Lanthanides Produced via Spallation Reactions in an Irradiated Tantalum Target,* Journal of Analytical Atomic Spectrometry **2000**, 15, 1343.

16 Kuczewski, B.; Diplomarbeit, TU Darmstadt 1999.

17 Sjoblom, R.; Hindman, J.C.; *Spectrophotometry of Neptunium in Perchloric Acid Solutions,* Journal of the American Chemical Society **1951**, 73, 1744.

18 Kim, J.I.; Sekine, T.; *Complexation of Neptunium(V) with Humic Acid*, Radiochimica Acta **1991,** 55, 187.

19 Marquardt, C.; Kim, J. I.; *Complexation of Np(V) with Humic Acid: Intercomparison of Results from Different Laboratories,* Radiochimica Acta **1998**, 80, 129.

20 Marquardt, C.; Kim, J. I.; *Complexation of Np(V) with Fulvic Acid*, Radiochimica Acta **1998**, 81, 143.

21 Jensen, M. P.; Nash, K. L.; *Thermodynamics of Dioxoneptunium(V) Complexation by Dicarboxylic Acids*, Radiochimica Acta **2001**, 89, 557.

22 Rizkalla, E.N.; Nectoux, F.; Dabos-Seignon, S.; Pages, M.; *Complexation of Neptunium(V) by Polyaminocarboxylate Ligands*, Radiochimica Acta **1990**, 51, 151.

23 Cilindro, L. G.; Keller, C.; *Complexation of some Transuranium Elements with Tropolone and β-Isopropyltropolon*, Radiochimica Acta **1974**, 21, 29.

24 Stout, B. E.; Caceci, M. S.; Nectoux, F.; Pages, M.; Choppin, G. R.; *Complexes of NpO2+ with Aliphatic Dicarboxylic Acids*, Radiochimica Acta **1989**, 46, 181.

25 Rizkalla, E.N.; Nectoux, F.; Dabos-Seignon, S.; Pages, M.; *Complexation of Neptunium(V) by Halo- and Hydroxycarboxylate Ligands*, Radiochimica Acta **1990**,51, 113.

26 Eberle, S. H.; Schaefer, J. B.; *Stabilitätskonstanten der Komplexe des Neptunyl(V)-Ions mit α-Hydroxykarbonsäuren,* Journal of Inorganic and Nuclear Chemistry **1968**, 31, 1523.

27 Eberle, S.H.; Wede, U.; *Actiniden(V)-Aminoessigsäurechelate*, Inorganic and Nuclear Chemistry Letters **1968**, 4, 661.

28 Eberle, S.H.; Wede, U.; *Konstitution und Stabilität der Chelate des fünfwertigen Neptuniums mit N-2-Hydroxyäthyliminodiessigsäure*, Inorganic and Nuclear Chemistry Letters **1969**, 5, 5.

29 Gross, J.; Wissenschaftliche Berichte KfK 1339, 1970.

30 Stöber, H.; Wissenschaftliche Berichte KfK 1657, 1972.

31 Brandau, E.; Wissenschaftliche Berichte KfK 1068, 1970.

32 Sachs, S.; Heise, K.H.; Bernhard, G.; *NIR Spectroscopic Study of the Neptunium(V) Complexation by Humic Acids with Different Functionalities*, FZR-343 Annual Report 2001, 14, Institut für Radiochemie, Forschungszentrum Rossendorf (PDF-file: http://www.fz-rossendorf.de/FWR/)

33 Tochiyama, O.; Yoshino, H.; Kubota, T.; Sato, M.; Tanaka, K.; Niibori, Y.; Mitsugashira, T.; *Complex Formation of Np(V) with Humic Acid and Polyacrylic Acid*, Radiochimica Acta **2000**, 88, 547.

34 Rao, L.; Choppin, G. R.; *Thermodynamic Study of the Complexation of Neptunium(V) with Humic Acids*, Radiochimica Acta **1995**, 69, 87.

35 Moulin, V.; Tits, J.; Decambox, P.; Moulin, C.; *Complexation of Lanthanides and Actinides with Humic Acids. In: Effects of Humic Substances on the Migration of Radionuclides: Complexation of Actinides with Humic Substances*, Third Progress Report CEC-contract FI2W-CT91-0083, Report Radiochemie TU München RCM 00593; 1993.

36 Hummel, W.; Glaus, M. A.; Van Loon, L. R.; *Complexation of Radionuclides with Humic Substance: The Metal Concentration Effect*, Radiochimica Acta **1999,** 84, 111.

37 Marquardt, C.; Herrmann, G.; Trautmann, N.; *Complexation of Neptunium(V) with Humic Acids at Very Low Metal Concentrations*, Radiochimica Acta **1996**, 73, 119.

38 Simpson, A.J.; Kingery, W.L.; Hayes, M.H.B.; Spraul, M.; Humpfer, E.; Dvortsak, P.; Kerssebaum, R.; Godejohann, M.; Hofmann, M.; *Molecular Structures and Associations of Humic Substances in the Terrestrial Environment*, Naturwissenschaften **2002**, 89, 84.

39 Mansel, A.; Dissertation, Universität Mainz 1999.

40 Bitea, C.; Kim, J.I.; Kratz, J.V.; Marquardt, Ch.; Neck, V.; Seibert, A.; Walther, C.; Yun J.I.; *A Study of Colloid Generation and Disproportionation of Pu(IV) in Aquatic Solutions by LIBD and LPAS,* Annual Report 2003, C4, Institut für Kernchemie, Universität Mainz, (PDF-file: http://www.kernchemie.uni-mainz.de/forschung/c4.pdf).

41 Artinger, R.; Fanghänel, Th.; Kuczewski, B.; Marquardt, C.; Schäfer, Th.; Seibert, A.; *Humic Colloid Mediated Transport of Plutonium Studied by Column Experiments.* In: Buckau, G. (Ed.), *Humic Substances in Performance Assessment of Nuclear Waste Disposal: Actinide and Iodine Migration in the Far-field*, Second Technical Progress Report EC Contract No. FIKW-CT-2001-00128, to be published.

42 Kim, J. I.; Zeh, P.; Runde, W.; Mauser, C.; Pashalidis, I.; Kornprobst, B.; Stöwer, Ch.; *Nuklidmigration (99Tc, 237Np, 238Pu, 241Am) im Deckgebirge und Salzstock des geplanten Endlagerortes Gorleben (Abschlußbericht)*. Report Technical University Munich RCM 01495, 1995.

43 Dardenne, K.; Denecke, M. A.; Seibert, A.; Marquardt, C. M.; *EXAFS Measurements of Pu(III,IV,V,VI) in Humic Rich Gorleben Ground Water*, to be published.

44 Artinger, R.; Buckau, G.; Zeh, P.; Geraedts, K.; Vancluysen, J.; Maes, A.; Kim, J. I.; *Humic Colloid Mediated Transport of Tetravalent Actinides and Technetium*, Radiochimica Acta **2003**, 91, 1.

Appendix C Institut für Anorganische Chemie und Radiochemie, Universität des Saarlandes

Investigations of the Behaviour of the Heavy Elements Cu, Zn, Cd, and Pb in the Ternary System Metal – Humic Acid – Sand

H.P. Beck, H. Wagner, T. Gottfreund, M. Zeitz

Final Report

Support Contract Number:
02 E 93095

Institut für Anorganische und Analytische Chemie
und Radiochemie FR. 8.14
Universität des Saarlandes, Saarbrücken

Anorganische und Analytische Chemie und Radiochemie
Universität des Saarlandes
P.O. Box 15 11 50
66041 Saarbruecken
Germany

www.uni-saarland.de/fak8/beck/

Content

List of symbols

A	Electrode surface
ASV	Anodic Stripping Voltammetry
β	Conditional Complexation constant
c	molar concentration
CE	Capillary Electrophoresis
CNM	Charge Neutralisation Model
D	Diffusion coefficient
DP	Differential-Pulse
Eq.	Equation
Fig.	Figure
HA	Humic Acid
HMDE	Hanging Mercury Drop Electrode
I	Ionic strength
K‘	Electrochemical constant
Kc	Equilibrium constant
L	Loading in % (compared to the maximum complexation)
LC	Loading Capacity
M	Molar
Me^{z+}	Metal ion
MES	2-(morpholino)-ethanesulfonic acid-monohydrate
MQ	MilliQ-Water
n	Number of electrons
PEC	Proton Exchange Capacity
PIPES	1,4-Piperazinediethane sulfonic acid
ppb	Parts per Billion
ppm	Parts per Million
rpm	rotations per minute
s	Rate of potential scan
SW	Square-Wave
Tab.	Table
UF	Ultrafiltration
V	Volt
V/V_P	Elution volume / pore volume
WDMT	Wageningen-Donnan-Membrane-Technique

Abstract

The project is mainly focused on the determination of the distribution of Cu, Zn, Cd and Pb in the ternary system consisting of these heavy metals, HA and sea sand. Two different humic acids were used in the investigations. The natural humic acid from Aldrich was characterized elsewhere by means of SEC, UF, CE, UV/Vis, IR. The synthetic humic acid M42 provided by the Forschungszentrum Rossendorf FZR was made according to the preparation of a „standard melanoidin“ by Enders and Theis Their characterisation is also described elsewhere. Both humic acids show a similar amount of carboxylic and phenolic groups together with a similar proton exchange capacity (around 5-6*10^{-3} mol protons per gram HA). Using three different analytical methods, stability constants for the humic acids with lead, zinc, copper and cadmium on the basis of the charge neutralisation model have been determined. Together with the direct measurement by stripping voltammetry the Donnan-membrane technique in combination with ICP-MS detection and the capillary electrophoresis with indirect UV/Vis-detection have been used for the aforementioned task. Therefore a wide concentration range from 1*10^{-8} M to over 1*10^{-4} M could be investigated. All obtained stability constants β of the different methods are in very good agreement with one another and with data from other sources. For lead we obtained a log β of 5.4 ± 0.2 (averaged over all pH-values and methods), Copper was found to have a log β of 5.2 ± 0.2, that of zinc and cadmium were an order of magnitude lower, log β around 4.0 ± 0.2. Furthermore batch- and column experiments were performed to examine the ternary system of heavy metals (Cu, Zn, Cd and Pb), Humic Acid and sea sand. Sea sand is a model component for a natural geomatrix, which is able to control the transport and availability of the metals in nature. A wide range of parameters were investigated to reveal the relations between the single influences. Beside the adsorption isotherms and pH-edges, the influence of Ca as a natural occurring competitor was investigated explicitly. Furthermore kinetical aspects like the preconditioning of the heavy metal with HA and the contact time of the solutions with sea sand were investigated as well as the reversibility of the adsorption. Column experiments were carried out by coupling a sand containing column online to the ICP-MS at two pH-values (near 6 and 7) and two HA concentrations (without HA; 25 ppm HA). The experiments give a close insight into the behaviour of the heavy metals in the ternary system.

1 Introduction

The project is mainly focused on the determination of stability constants for humic acids with the (toxic) heavy metals cadmium, lead and zinc. Copper is also used in the experiments as an example for a metal that forms strong complexes. The application of a synthetic humic acid as a model substance is investigated by determining its complexation constants with the metals. The influence of geochemical parameters like pH-value, ionic strength or different competing metal cations on the complexation is also investigated. As explained in the experimental section, a variety of methods for the determination of metal ions has been developed and applied to get a wide range of data necessary to compare the usefulness of the different methods and to prove the accuracy of complexation constants derived from either method.
A second main part of the project is to determine the influence of humic acid on the adsorption of heavy metals by solid phases. This was studied by batch and column experiments with humic acid, heavy metal and sea sand which are useful to get an insight in natural conditions.

2 Experimental

An important part of the project is the measurement of complexation constants of humic acids and heavy metals. There are several ways to do so:

- the uncomplexed metal is first separated from the complexed metal, for example with the *WDMT* or ultrafiltration, and in a second step measured externally.
- the uncomplexed metal is measured directly in the sample solution; this is possible by *Stripping Voltammetry* or UV/Vis-Spectroscopy ?;
- the uncomplexed metal is separated from the metal humate complex and measured in one step, for example with *Capillary Electrophoresis* or Electrophoretic Ion Focusing.

The given methods in italics as well as the batch- and column experiments will be explained in short in the following chapters.

2.1 Donnan Membrane Technique (WDMT)

The WDM-Technique was developed at the University of Wageningen (The Netherlands) to determine the bioavailability of toxic heavy metals in the environment [Tem00]. The “heart” of the method consists of the so called WDMT-cell. This cell is composed of a donor part and an acceptor part. Solutions are pumped permanently through both compartments by a peristaltic pump during the whole WDMT-run. The donor-cell contains the solution with the toxic heavy metal and the complexing ligand (e.g. EDTA, Salicylic Acid, Humic Acid). There is a 2 mM $Ca(NO_3)_2$-background solution In the donor as well as in the acceptor. Both compart-

ments are separated by a strong cation exchange membrane. Figure 1 shows the schematic build-up of the WDMT experiment. Calcium has a greater exchange tendency at the membrane than the heavy metals, because of its larger affinity to the membrane or its higher concentration. Therefore the Calcium initialises a kind of hopping mechanism. The free heavy metal is adsorbed at the cation exchange membrane and then remobilised by the Calcium. Therefore a flux of heavy metal from the donor solution to the acceptor solution arises. In such way only non-complexed metal can move to the acceptor solution, because of the retention capability of the negatively charged membrane and its Donnan potential. The complex itself or the negatively charged ligands are retained by the membrane. With the first advent of free metal in the donor solution a flux from acceptor to donor solution is established as well. When the system attains its equilibrium, the fluxes in both directions are about the same. Samples are then taken from both compartments and their heavy metal content is determined by ICP-MS. The metal content in the donor cell complies with the total amount of the heavy metal (free and bound), whereas the content of heavy metal in the acceptor cell is equal to the free metal concentration of the donor.

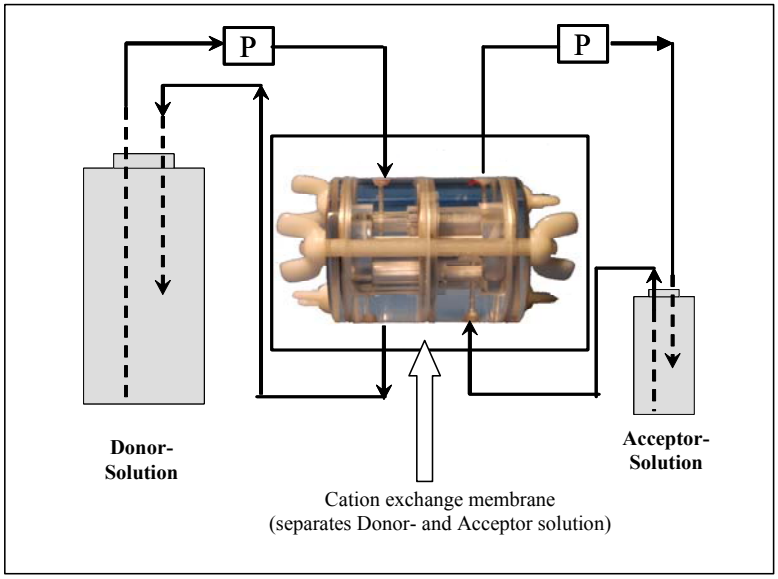

Fig. 1: Schematic built-up of the WDM-Technique

With this information, binding constants can be derived. An important fact is the ratio between the volume of the donor and the volume of the acceptor. The donor one has to be by far larger (≈ 1000 ml) than that of the acceptor (≈ 5 ml). In this case only a small amount of the total metal content has to migrate into the acceptor until the equilibrium is reached. The disturbances of the complex equilibrium can thereby be minimised. When using natural samples in the donor cell it is difficult to fit the composition of the background solution in the acceptor. Differences in the ionic strength of the background solution cause a concentration potential, which leads to an enrichment of the free metal in the compartment with higher ionic strength. In such cases an ionic strength correction has to be done [Tem00].

Before using the WDMT for the determination of binding constants between heavy metals and HA, we have verified the method by systems with defined ligands. In these cases the results can be modelled by speciation software. The WDMT showed excellent results in determining the free metal content in the system of Cu, Cd and EDTA. The experimental values match the calculated ones within deviation a few percent. Further detailed research was done with respect to ion strength correction. The correction used seems to work properly. The insights received by the verification were used to improve the WDM-technique and make it more applicable for the individual needs of humic acid analysis. By optimising the cell design, the equilibration time was shortened from 48 h to 16 h (for Cadmium). With the help of Donnan-Enrichment-procedures [Lam82] an improvement of the detection limit by one power unit was made.

All experiments show that the WDM-technique delivers extremely reproducible results and its application in humic acid analysis is rather promising.

2.2 Stripping Voltammetry

Stripping Voltammetry is a quantitative (and qualitative) electrochemical method where the signal proportional to the concentration is a current measured as function of the applied potential. It is a kind of the polarography with a hanging mercury drop (HMDE) as working electrode.

The build-up consists of a sample container with three electrodes (working electrode HMDE, reference electrode Ag/AgCl/KCl 3 M, and counter electrode Pt) inside, the so called three-electrode-array. The potential at the working electrode is controlled and kept constant with the help of a potentiostat (Fig. 2).

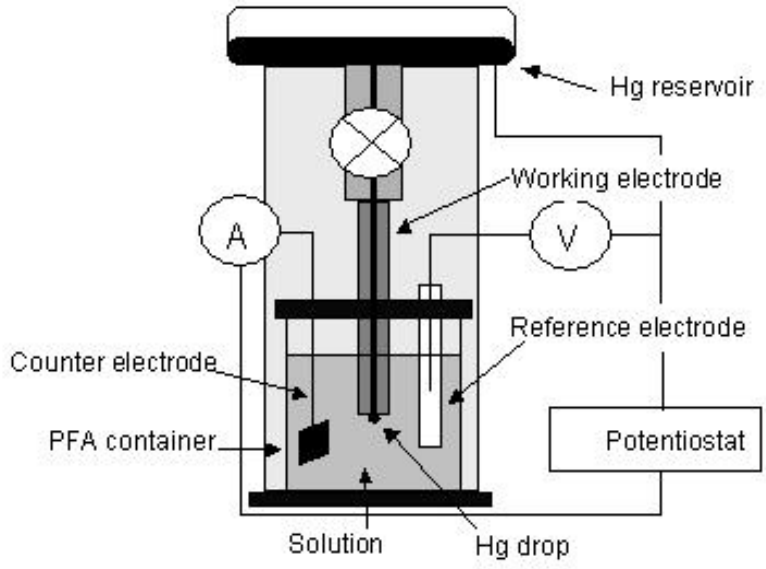

Fig. 2: Schematic build-up of the three-electrode circuit and potentiostat from EG&G

A measurement is quite simple: the analyte, in this case a metal ion, is deposited by reduction at a constant potential and constant stirring at the working electrode as amalgam. This is the deposition step. Then the stirring is stopped and there is no potential applied at the electrodes. The third step is the real measurement, the potential is changed linearly or pulsed from the starting value in positive direction (potential scan). Around the half-wave potential of the reaction:

$$Me(Hg) \rightarrow Me^{z+} + Hg \qquad \text{(Eq. 1)}$$

starts the re-oxidation of the amalgam (stripping step) to metal ion and mercury. The measured current ip (Eq. 2) during this re-oxidation is the measurement signal.

$$i_p = K' \cdot n^{3/2} \cdot A \cdot \sqrt{D} \cdot \sqrt{s} \cdot c \qquad \text{(Eq. 2)}$$

The use of deposition and stripping steps enhances the limit of detection by a factor of 1000 compared to classic polarography with a direct linear measurement.
Only the so called pulse methods, the Square-Wave Stripping Voltammetry and the Differential-Pulse Stripping Voltammetry were used for the determination. Small voltage pulses are overlaid on the potential change. For the SWASV it is a step like change with a positive and a negative potential pulse per step, the DPASV consists of a linear potential change overlaid with small positive pulses every 25-100 ms.

Their main advantage compared to spectroscopic methods like AAS or ICP-MS is the possibility to measure only the free and uncomplexed metal or metal bound in labile complexes. Metal ions bound in stable or inert complexes, for example chelate complexes, don't give an analytical signal. One can therefore distinguish with the help of a mass balance between free and bound metal.

2.3 Capillary Electrophoresis

Electrophoresis [Eng94] is the migration of charged molecules or atoms (ions) in a solution under the influence of an electric field. In case of Capillary Electrophoresis this migration takes place (most often) in thin fused-silica capillaries with inner diameters from 25 to 100 µm. The influence of the field on an ion causes a constant migration rate v for every ion within the solution: 25 to 100 µm (in the range of 25–110 µm/sec)
The interaction between frictional force (Stokes) and electrical ones is given by the relation:

$$v = \frac{z \cdot E \cdot F}{6 \cdot \pi \cdot \eta \cdot r \cdot N_A} \qquad \text{(Eq. 3)}$$

Cations with different electrophoretic mobility (different charge, radius, molar mass) are separated from other cations and from neutral or anionic molecules or atoms. The principal build-up of a CE its shown in Fig. 3: the capillary fits into two buffer vials and the high voltage

is applied through the capillary. A detector and the data acquisition are placed at one end of the capillary.

The idea of using Capillary Electrophoresis for the determination for complexation constants for metals isn't really new (especially in protein chemistry), but the direct separation of metal ions from their complexes is rarely used and - so far - even less in the case of humic acid complexes. A similar electrophoretic method that has been used with good success for the study of metal humate complexes is the Continuous Ion Focussing (Field Source Electrophoresis) which uses a similar separation mechanism as the CE.

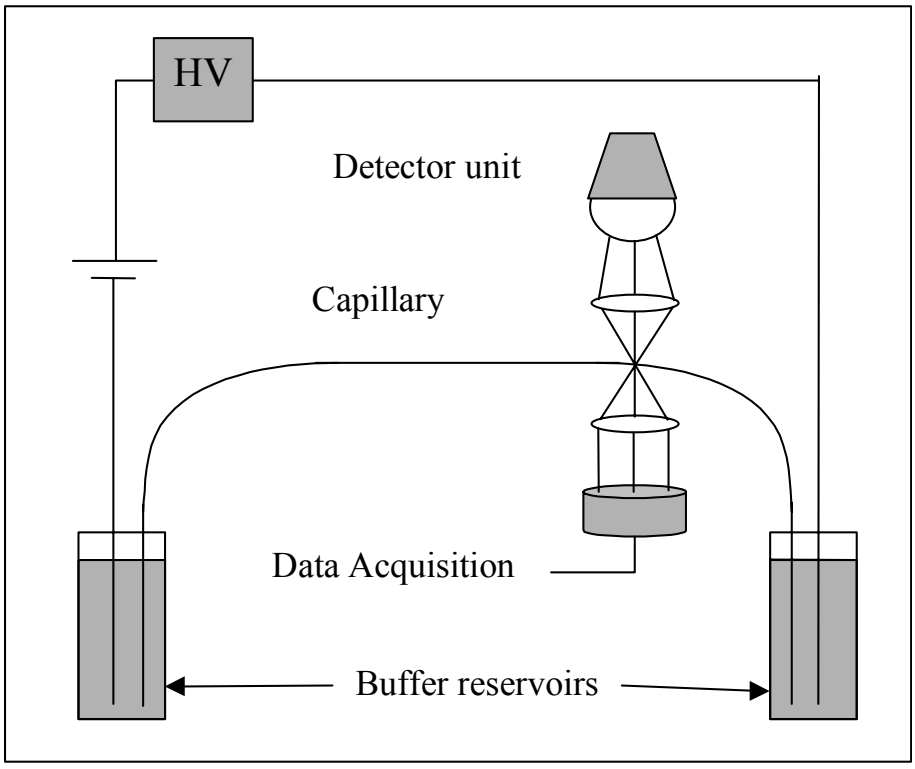

Fig. 3: Principal build-up of a capillary-electrophoresis system

2.4 Batch and Column experiments

Figure 4 shows the procedure of the batch experiments schematically. The experiments were performed in scintillation vessels, which have low adsorption properties. In the first step the vessels were cleaned by MQ-Water. Cleaning with acid is not recommended, because pH-errors often occur during the experiment. 2.5 g of purified sea sand (Merck) was weight into the cleaned vessels. The solution for each experiment was prepared separately. In these solutions all experimental conditions, like ion strength, pH, humic acid and the heavy metal concentration were adjusted. Experiments were performed with all metals together in one solution.

The only exceptions were sorption experiments, where each metal has to be applied separately due to the high concentration. The humic acid was allowed to equilibrate for 24 h which the heavy metals before contacting the solution with sea sand. If the pH-values has to be fixed during an experiment, buffer substances are required. In the case of pH 6 a 1 mM Mes buffer and at pH 7 a 1 mM PIPES buffer were added to the solutions. The background solution was modelled to a surface like water [Hub94]. All experiments were carried out twice. The mass ratio between solid phase (sea sand) and solution was fixed to 1:4. The solutions were contacted with sea sand and shaken for 2 days. During the shaking the temperature was kept at 21 ± 2°C. Afterwards the vessels were centrifuged at 3500 rpm. Samples were taken from the supernatant solutions. Diluted and acidified solutions were prepared to determine the remaining content of metal in the solution by ICP-MS. As the total concentration of the metal (before contacting it with the sand) is known and the unbound metal is measured it is possible to calculate the amount of bound metal. All experiments are performed in this way. The schematic build-up of the column experiments is shown in Figure 5.

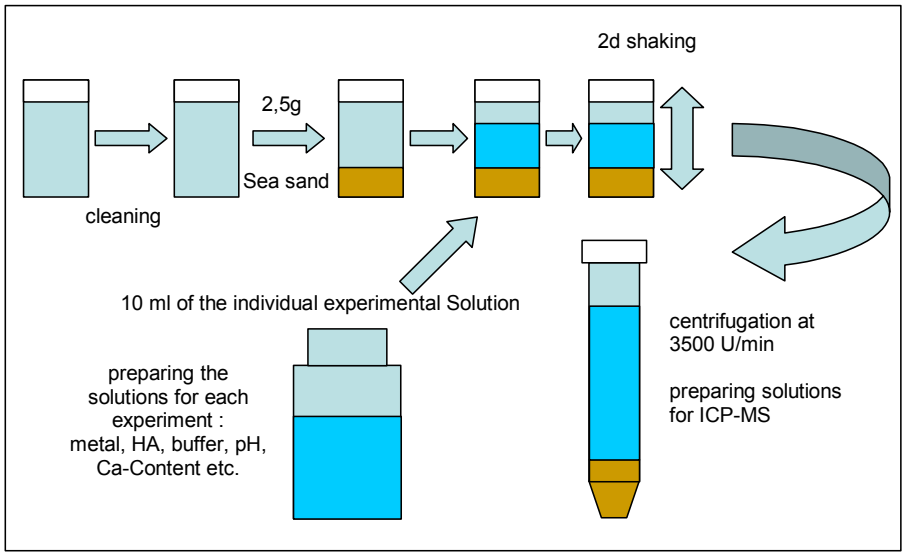

Fig. 4: Schematic procedure of the batch experiments

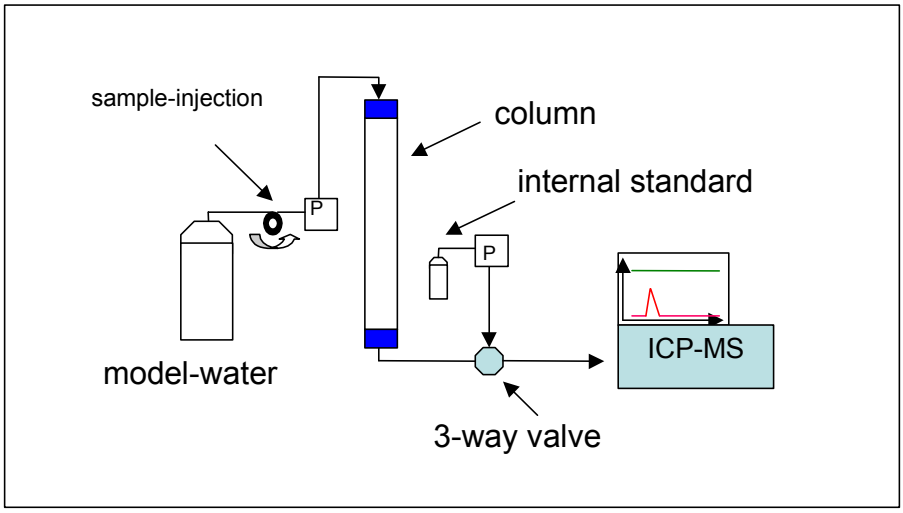

Fig. 5: Schematic build-up of the column experiments

An online coupling between the sand filled column and the ICP-MS was built up for the column experiments. A glass column (length: 25 cm, diameter: 1 cm) with Teflon fittings at both ends was filled with purified sea sand (approx. 26 g). The filling procedure can be described as follows: Water was given into the column and sand was added under stirring with a glass bar. A rubber hammer was beaten against the column to tighten the sand filling. A solution analogously prepared like the model water in the batch solutions was pumped through the column by a peristaltic pump. At least 1000 times the pore volume (V_P = 6.5 ml) were used to be sure that the column is well preconditioned. The background solution was of the same composition as in the batch experiments. But no buffer substances were added to adjust the pH value. The pore volume was determined experimentally by injection of an inert Br^--solution into the column. During the conditioning, the column output was connected to a waste bottle. The flow during the conditioning was set to 3 ml/min while it was fixed to 1 ml/min, while the column was connected to the ICP-MS. The output of the column is connected to a 3-way valve which itself is connected to the ICP-MS. The second channel of the valve is used to acidify the solution coming from the column and to provide the ICP-MS with three internal standards (Ga, In, Tl) for different mass regions. The internal standard was used to correct the instrumental drift during the experiment, which takes up to 12 h. At the beginning of each column experiment an external calibration with standard solutions was performed. The heavy metal solution was prepared in the same solution which was used to condition the column 24 h before the beginning of the experiment. After the calibration, the column was connected to the ICP-MS und the heavy metal containing solution was injected by a 500 ml loop of a 6-way valve.

2.5 Other Methods

Beside the methods mentioned above, a wide range of other methods was used for the measurement of humic acids and metal concentrations. UV/Vis-spectroscopy was used as detection method for both the humic acids and the metal ion concentrations (in the CE measurements). Metal concentrations from the Donnan measurements were determined by Inductively Coupled Plasma-Optical Emission Spectroscopy (ICP-OES), mostly for calcium, and by ICP-Mass Spectroscopy (ICP-MS) for the heavy metals. Furthermore IR-measurements CHN- Analyses, DOC-Determinations and potentiometric titration have been performed.

3 Results and Discussion

Stability constants for metal humate complexes were measured by the three mentioned methods in case of the Aldrich humic acid. Constants for the synthetically prepared HA M42 humic acid were measured only by Stripping Voltammetry.

3.1 Stability Constants of Humic Acids

3.1.1 Direct Methods

The determination of humic acid complexation constants requires knowledge of the amount of uncomplexed metal and the amount of metal bound to the humic acids in the equilibrium. With the help of Stripping Analysis and – in some cases – capillary electrophoresis, it is possible to measure the concentration ratio of free to complexed metal in the sample solution directly. The assumption is that the amount of total metal in the sample is known. The preparation of the sample solutions was always the same: a standard solution of humic acid and a standard solution for the ionic strength (KNO_3) were mixed and the appropriate pH was adjusted with HNO_3 or NaOH. After a short equilibrium time (around 30 min) the heavy metal was added from an aqueous standard solution. The pH was again adjusted if necessary. The solution was kept quiet for up to three days and then the free metal concentration was measured. This procedure was also applied to the CE measurements. The model humic acid M42 from the FZR is included in the study to show its similar behaviour in the complexation with metal ions. The synthesis of the M42 is described elsewhere. The M42 is similar to most natural humic acids with respect to their amount of carboxylic and other functional groups. With the use of the normal complexation constant K‘ (Eq. 4), derived from the law of mass action, one gets a dependence of the logK‘-values from the total ion concentration.

$$K' = \frac{[Me^{z+}] \cdot [HA]}{[MeHA]} \qquad \text{(Eq. 4)}$$

This K‘ depends also on the pH, ionic strength, humic acid concentration. The use of the Charge Neutralisation Model provides a conditional stability constant β independent of the aforementioned parameters. The Loading Capacity LC as a correction value is now a decisive parameter. β should now be constant and independent of the conditions. This is illustrated in Tab. 1 and Tab. 2 for the three cations lead, cadmium and zinc with the two humic acids and different pH-values.

Tab.1: Comparison of formation constants β of lead humate complexes at pH 4, 5 and 6, I = 0.01 mM with KNO_3, different methods (bottom line is M42 HA).

	pH 4.0	pH 4.0	pH 5.0	pH 5.0	pH 6.0	pH 6.0
	log β	LC	log β	LC	log β	LC
ASV	5.3 ± 0.3	20 ± 2%	5.3 ± 0.3	51 ± 5%	5.6 ± 0.2	64 ± 6%
CE[a]	-	-	5.1 ± 0.6	45 ± 14%	-	-
CE[b]	-	-	5.3 ± 0.1	32 ± 2%	-	-
UF/AAS	5.0 ± 0.2	37 ± 2%	-	-	-	-
ASV	-	-	5.1 ± 0.2	49 ± 5%	5.4 ± 0.2	62 ± 5%

a: without b: with 2 mM $Ca(NO_3)_2$ as buffer addition

Tab. 2: Comparison of stability constants β for zinc and cadmium humate complexes at pH 5 and 6, I = 0.01 mM with KNO_3, for Aldrich (top) and M42 HA (bottom), measured with ASV

	pH 5.0	**pH 5.0**	**pH 6.0**	**pH 6.0**
	log β	**LC**	**log β**	**LC**
Zinc	4.0 ± 0.1	43 ± 2%	4.1 ± 0.1	51 ± 2%
Cadmium	4.0 ± 0.1	41 ± 2%	4.1 ± 0.1	48 ± 2%
Zinc	4.0 ± 0.3	48 ± 2%	4.1 ± 0.2	55 ± 2%
Cadmium	4.2 ± 0.2	47 ± 2%	4.4 ± 0.3	54 ± 4%

Both humic acids show similar complexing behaviour, the log β-values are very similar and equal within the limit of error for all three metals.
Depending on the method, there are minor differences in log β-values and changes in the LC (Tab.1 for lead). However, all stability constants are equal within the limit of error, changes in LC are due to the influence of the method or minor differences in the buffer (CE with Ca).

3.1.2 Wageningen-Donnan-Membrane-Technique (WDMT)

The WDM-technique was verified thoroughly before applying it for the determination of binding constants [Zei03] between humic acid and heavy metal. To calculate the log β values for Cu, Zn, Cd and Pb it is necessary to determine the LC first. These experiments were performed in the so called titration-mode and because of the high concentration necessary for these experiments. They were performed for each metal separately. The titration mode is explained in the following paragraph: a 2 mM $Ca(NO_3)_2$ background solution was given in the Donor cell (V = 1000 ml) and in the Acceptor cell (V = 5 ml). In addition HA was added to the Donor cell to a HA concentration of 25 ppm. The pH value was adjusted to 5.0 ± 0.2 by adding KOH or HNO_3.
The lowest metal concentration was given to the Donor cell and the solutions were allowed to equilibrate 24 h before the WDMT-run was started. Preceding experiments [Zei03] show that at the given ratio between Donor and Acceptor volume the equilibrium is reached within 24 h. Therefore the run was stopped after 24 h and samples were taken from the Donor and the Acceptor was exchanged by a new one (only containing background solution with the same pH).

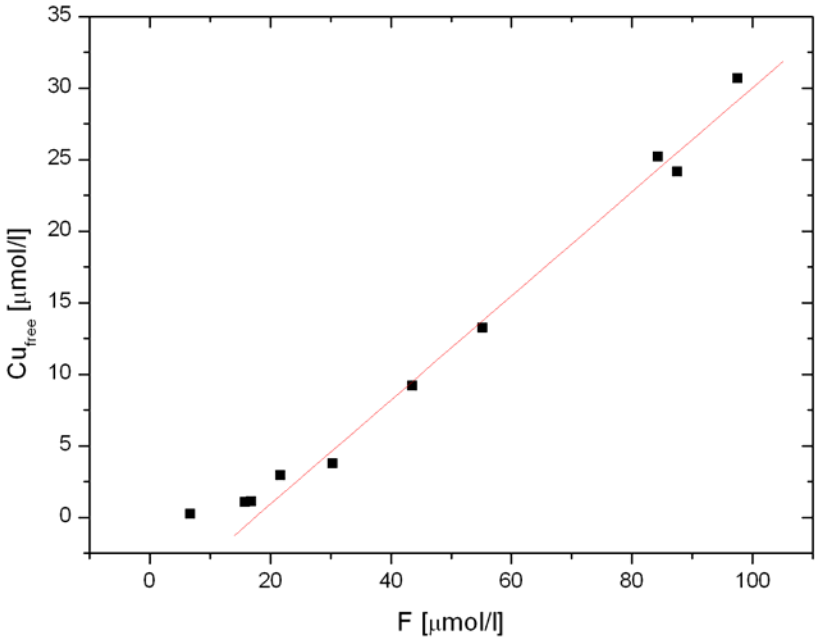

Fig. 6: Determination of the loading capacity of Cu; c(HA) = 25 ppm, pH = 5.0, 2 mM $Ca(NO_3)_2$-background solution. (F was taken from the definitions in the CNM)

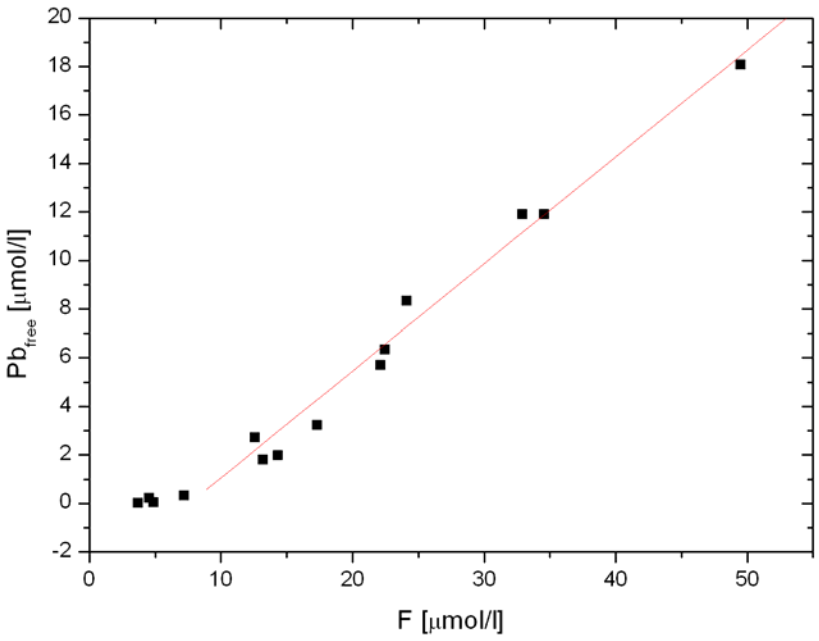

Fig. 7: Determination of the loading capacity of Pb; c(HA)=25 ppm, pH = 5.0, 2 mM $Ca(NO_3)_2$-background solution. (F was taken from the definitions in the CNM)

An additional amount of heavy metal was given to the Donor and after equilibration the WDMT-run was started again. Samples of the Donor and the Acceptor from each run were measured by ICP-MS and evaluated by the Charge Neutralisation Model. Figure 6 and 7 show the results for the strong complexing metals Cu and Pb. At the given conditions of 2 mM $Ca(NO_3)_2$ background solution at pH 5.0 the log β for Cu is 5.3 ± 0.1 and the corresponding LC is 35 %. Pb gives a log β-value of 5.6 ± 0.1 and a LC of 47 % under the same conditions. Both values fit well with the results determined by other methods (see Fig. 8). Unfortunately it was not possible to calculate LC values from the WDMT-runs of Cd and Zn. Small deviations (in percent range) of the measured amounts lead to a great error in the derivation of the LC. But it could be shown [Zei03] that this is not a problem of the WDMT, but instead of the CNM at low loadings of humic acid with metals. The measured values of all metals fit well to data derived from the NICCA-Donnan-Model. Therefore LC values were calculated from the NICCA-Donnan-Model and applied to the WDMT-data of Cd and Zn. This results in log β_{Cd} = 4.1 (LC = 19) and log β_{Zn} = 4.15 (LC = 17). These values agree very well again with experiments performed with other methods (see Fig. 8).

It can be summarised that the WDM-technique is a reliable and highly reproducible method to determine binding constants for heavy metal humic acid systems.

3.1.3 Comparison and Review

There are many stability constants from different sources and different methods. Some of these are shown in Fig. 8 to give an overview and the possibility to classify the data.

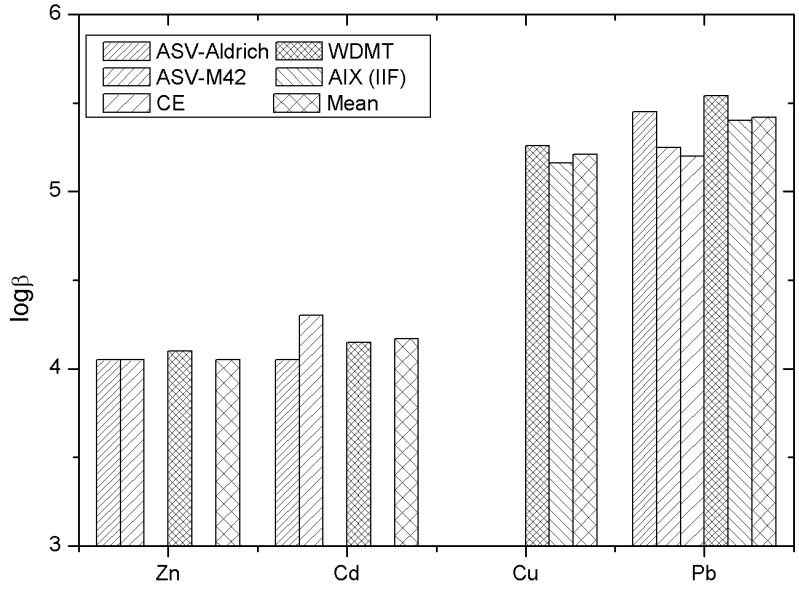

Fig. 8: Overview on the stability constants β derived from this and other publications [BER00, IIF01], pH = 5.0, different ionic strengths

All log β-values, either obtained in this or in former works, are equal within the limit of error, except for those measured by Ultrafiltration. It is obvious that stability constants from Ultrafiltration measurements are on an average higher than the rest. This could be due to adsorption of metal ions at membrane and filter materials. One drawback of the Charge Neutralisation Model should be mentioned here. If one tries to get LC or β-values at trace metal concentrations, the CNM doesn't work anymore. This is illustrated in Fig. 9, where the use of the CNM at a concentration ratio metal to humic acid of around 1:10 is compared with a ratio around 1:100.

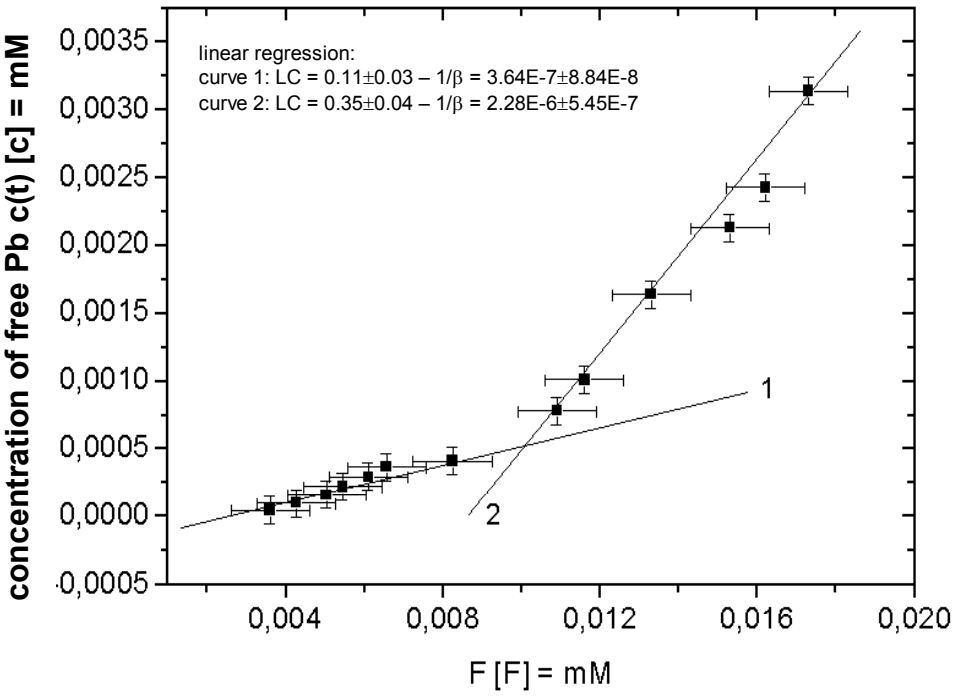

Fig. 9: Determination of LC and β in the system Aldrich HA/lead, c(HA) = 5 mg/l, pH = 4.5, I (MES/KNO_3) = 5 mM, curve1: c(Pb) = 0.1 - 0.7 µM, curve2: c(Pb) = 1.2 - 6.4 µM

One gets two different values for the LC depending on the concentration ratio of humic acid to metal ions. The reason for this is obviously the fact, that the assumption for the use of the Charge Neutralisation Model is no longer valid at low concentrations. There is no more 1:1-complexation, that is one metal ion with one positive charge per one ligand functional group with one negative charge, but there are too many functional groups and the equations do not fit anymore.

To a certain degree, the application of the CNM is limited to the concentration ratio that is given in the assumptions, that is around 1:1 metal to humic acid.

3.2 Influence of Geochemical Parameters

Some (geo)chemical parameters have a significant influence on the complexation behaviour of humic acids with heavy metals, be it due to changes in the humic acid itself or an influence on the heavy metal. These parameters include the pH-value, ionic strength, competing cations or anions and some others, that weren't observed.

3.2.1 pH-Value and Ionic Strength

The significant influence of the pH-value on the complexation of lead, zinc, cadmium and copper is already shown in the previous chapter (3.1.1). An increase of the pH from 4 to 6 results in an increase of the Loading Capacity due to more available functional groups for complexation. In the same direction and due to the same reason the complexation constants K' derived from Eq. 4 (Fig. 10) increase.

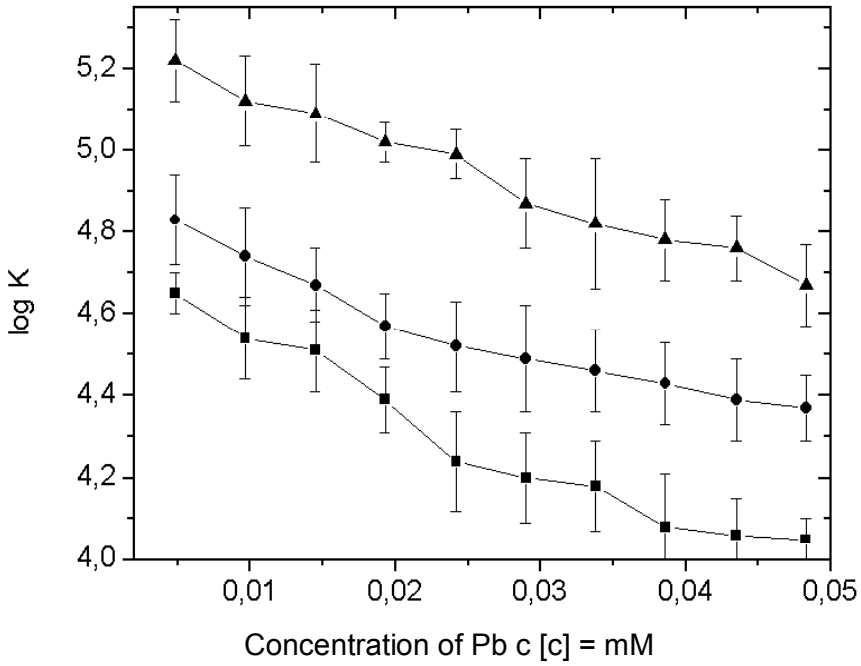

Fig. 10: Dependence of the log K'-value on the lead concentration, c(HA) = 5 mg/l, I = 5 mM, pH (top down) = 6.0 / 5.0 / 4.3, Aldrich HA

The ionic strength shows a comparable influence, with increasing ionic strength one gets a decrease in the log K'. This is because of competition of the metal ions making the ionic strength (mostly very weak complexants like sodium or potassium) and the heavy metal ions for the functional groups (shielding effect). Another reason can be changes (smaller cage-like molecules) in the humic acid structure.
However, log β-values are more or less independent of pH or ionic strength and so far better comparable than log K'-values.

3.2.2 Competing Complexation

Another aspect of geochemical parameters is the influence of natural by occurring cations or metals on the complexation of humic acid with the pollutant heavy metals.
There are a lot of possibilities here, i.e. alkaline and alkaline-earth metals, aluminium, iron or manganese. Magnesium, calcium and aluminium are chosen here due to the amount they are found in the environment and the absence of further chemical reactions but hydrolysis. Of these, aluminium as trivalent cation shows the strongest influence followed by calcium and magnesium. This is shown with zinc as an example in Figure 11.

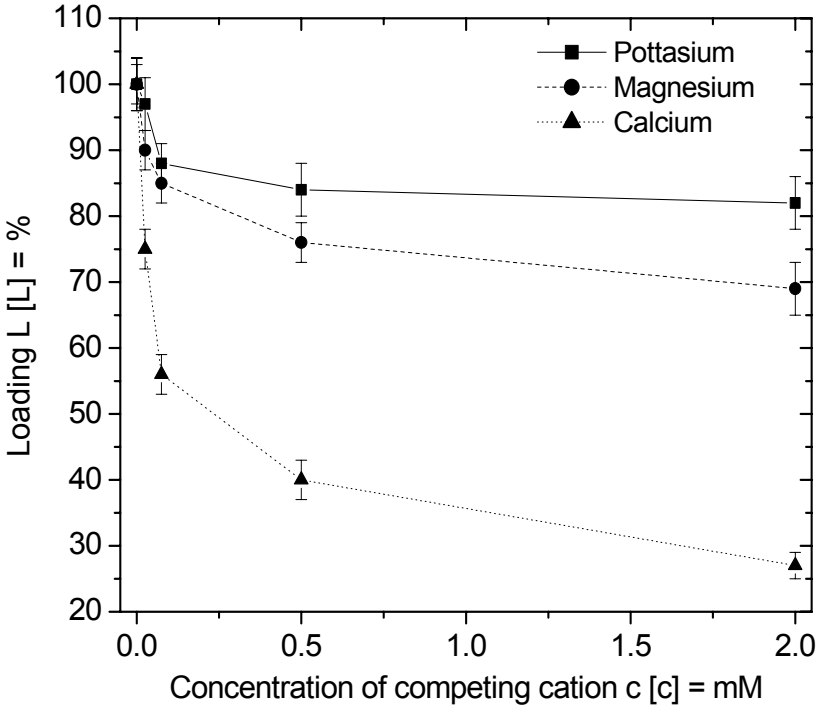

Fig. 11: Influence of K(I), Mg(II) and Ca(II) on the loading of Aldrich HA with Zn, c(Zn) = 1.6 µM, pH = 5.0, I(MES/KNO_3) = 5 mM (basic solution), c(HA) = 20 mg/l

One can see that potassium also has a minor influence on the complexation behaviour of zinc but a 1000 times excess of potassium results only in a decrease of complexation by 20 % compared to a solution without potassium. Magnesium and calcium show larger effects up to 75 % decrease in complexation and with aluminium, not shown here, there was no complexed zinc measurable.
Lead as a stronger complexing metal shows a slightly different but overall similar behaviour with potassium and magnesium and especially with calcium and aluminium as antagonists (Fig.12). Potassium and magnesium didn't show a measurable influence on the complexation of humic acid with lead, only a 1000 fold excess of potassium and magnesium resulted in minor changes in the complexation constants, but this was only due to an influence of the ionic strength. Both metals are weak complexing metal ions to prevent the lead from forming humate complexes.

However, calcium and aluminium do. Calcium is capable of decreasing the complexation up to 60 % at an 1000 fold excess and aluminium even up to 95 % (though aluminium doesn't occur as trivalent cation Al^{3+} at a pH 4.5 but as mono or divalent hydroxo complexes $Al(OH)^{2+}$ or $Al(OH)_2^{+}$).
In a natural system humic acid would be loaded with a high amount of these metal ions and would consequently form much less stable complexes (stable in the sense of log K') with the heavy metals.

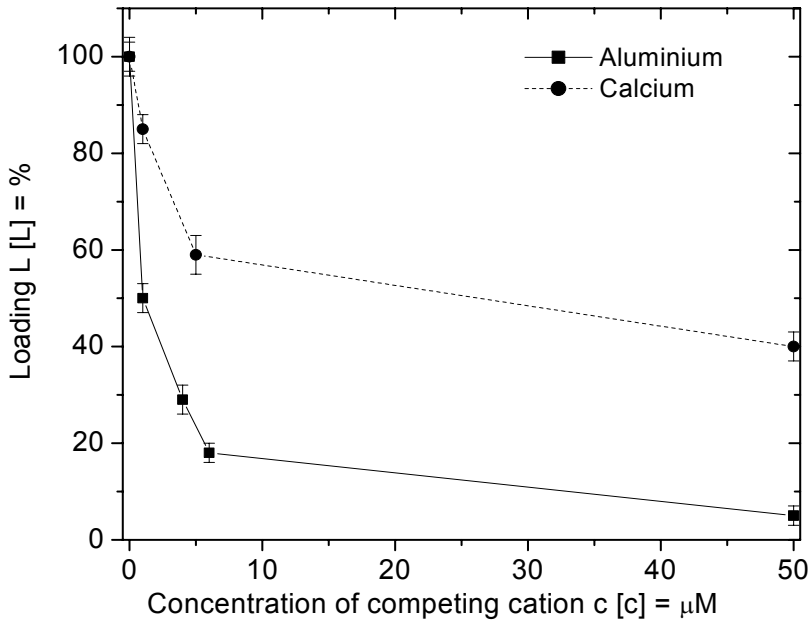

Fig. 12: Influence of Ca(II) and Al(III) on the loading of Aldrich HA with Pb, c(Pb) = 0.48 μM, pH = 4.5, I(MES/KNO_3) = 10 mM (basic solution), c(HA) = 20 mg/l

3.3 The System Humic Acid – Metal – Sand

3.3.1 Batch experiments

Batch experiments are helpful tools to decide whether a geomatrix is suitable for being a barrier for cation transport or not. With the help of batch experiments the influence of each parameter like pH-value, ion strength or water hardness can be examined. In this way it is possible to find capable geo barriers for toxic heavy metals or radioactive metals. In this work sea sand was used as a reference matrix.

3.3.1.1 General aspects

The system of heavy metals, humic acid and sea sand seems to be quite simple at a first view. But at a closer look one will see a lot of interdependencies which are summarised in Fig. 13. There are interactions between the humic acid and the sea sand as well as with the heavy metals. Furthermore the Ca in the background solution (which simulates natural sur-

face water) influences the system (concentration of the ions in the background solution after conditioning in mmol/l: Na: 1.46; K: 0.072; Ca: 0.6; Mg: 0.35 measured by AAS and HCO_3^-: 0.873 determined by acid-base titration). To determine the different interactions and the amount of heavy metal sorbed under various conditions, a lot of experiments were performed. A survey of these experiments in summarisation is given in Fig. 14.

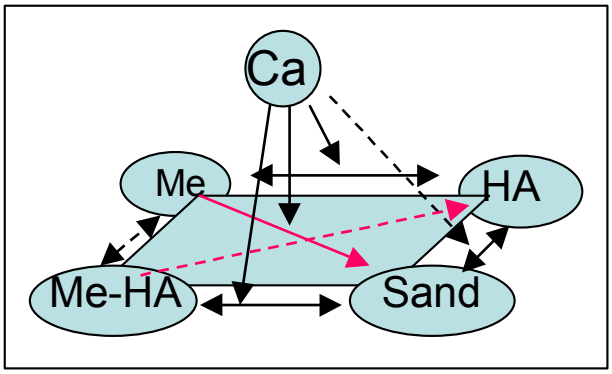

Fig.13: Interdependencies in the ternary System

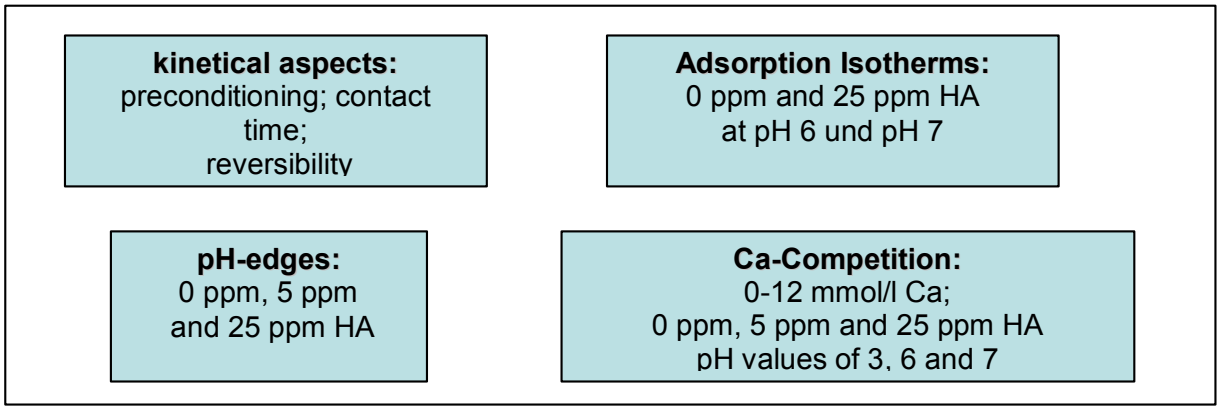

Fig.14: Overview of the performed batch experiments

3.3.1.2 Determination of kinetical aspects

Kinetic aspects are of great importance for all experiments with humic acids. The following experiments were performed to examine the influence of the preconditioning time on the sorption behaviour of Cu, Zn, Cd and Pb. All experiments were carried out as described in chapter 2.4 whereas one kinetical parameter was varied. The influence of the preconditioning of humic acid and heavy metals was examined first. In this case the contact time was varied from 2.5 h to 225 h. The sorption was to be found nearly independent form the preconditioning. In the case of the strongly sorbing metals the sorption shows a slight decrease with increasing time of preconditioning [Zei03]. For all following experiments a preconditioning time of 24 hours was selected.

In a further experiment the contact time of the already preconditioned solution with sea sand was examined. The contact time was changed from 6 h up to 350 h. The results at pH 7.35 without HA and at 6.35 with 25 ppm HA are shown in figure 15 and 16. The experiments

without HA shows an increase in the sorption with increasing conditioning time for Zn and Cd, while the heavy sorbing metals Cu and Pb show no dependence during the examined time scale.

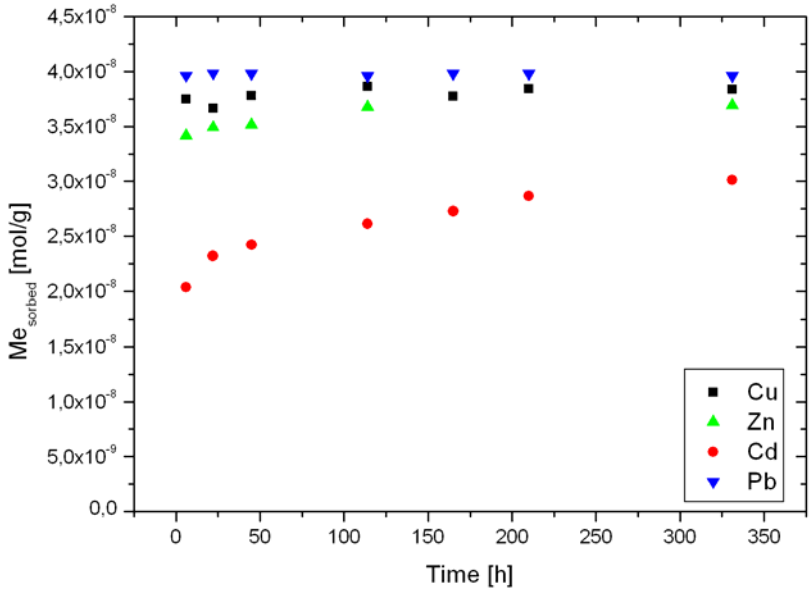

Fig. 15: Dependence of the heavy metal sorption on the contact time of the solution with sea sand, pH 7.35

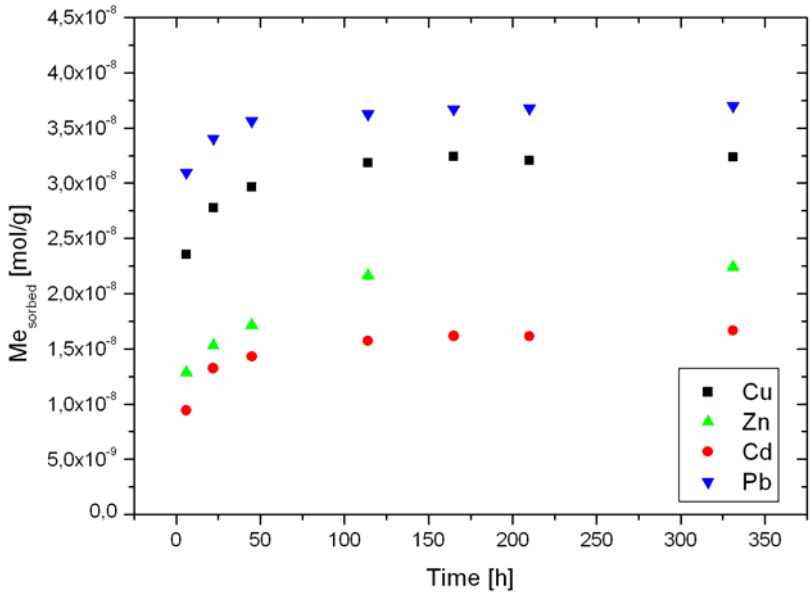

Fig. 16: Dependence of the heavy metal sorption from the contact time of the solution with sea sand: 25 ppm HA pH 6.35

In the experiment with 25 ppm HA all metals show a kinetic behaviour during the first 48 h. After 48 h there is no further increase unlike in the experiment without HA, were the sorption gradually increases over the total examined time scale. The HA seems to have the function of a mediator, which stabilises the whole ternary system. The contact time was fixed to 48 h for all further experiments. The reversibility of the sorption is an important aspect for the interpretation of sorption experiments. Fast desorption kinetic is an indication for surface sorption or ion exchange. Irreversibility, in contrast, is an indication for a surface precipitation or an incorporation of the heavy metal into the crystal lattice of the matrix. To examine desorption kinetics two experiments at pH 6.3 and 7.4 were performed as described in chapter 2.4. After the centrifugation 9 ml of the solution were removed and the same amount of a fresh background solution (with the same pH value) was added. The heavy metal content of the solution was observed in a time interval from 0 h to 360 h. Figure 17 (results for pH 6.3) shows that the heavy metal equilibrium is reached fast and the values agree well with the sorption results taken from the pH-edge without HA at pH 6.3 (see Fig. 19). At pH 7.4 the results are similar and can be found elsewhere [Zei03].

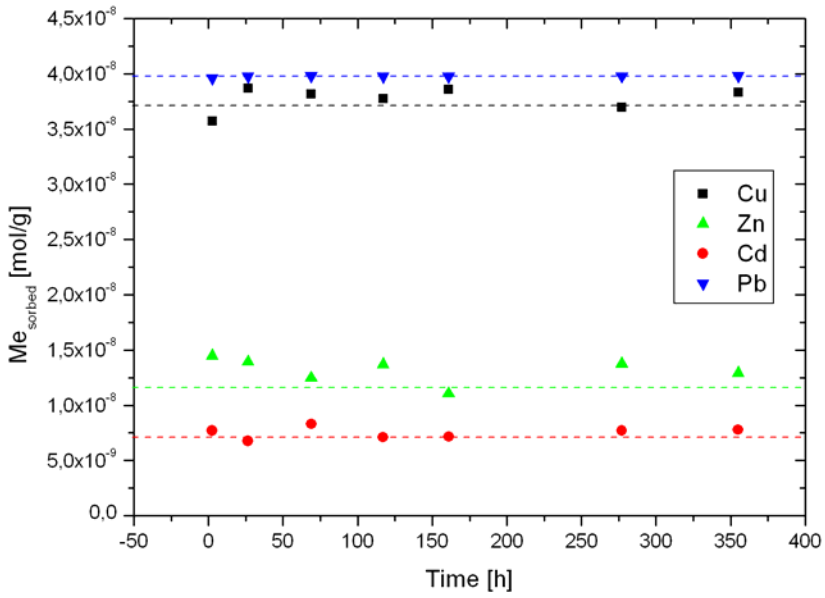

Fig. 17: Reversibility of the heavy metal sorption; (dashed lines: reference sorption taken from the pH-edges (see Fig.18)

3.3.1.3 Interaction of Humic Acid and Sea Sand

Humic acid has two ways to influence the metal transport in ternary systems consisting of heavy metal, humic acid and sea sand. On the one hand HA binds metals and stabilises them in the solution. On the other hand, HA can bind itself to the sand. The bound HA can adsorb heavy metals too and in that way the metal concentration in the solution is decreased. HA is able to enhance the mobilisation of heavy metals as well as to diminish it, depending on its allocation. Information about the allocation of the HA in the ternary system

are therefore essential to interpret sorption experiments and to estimate the mobility of heavy metals in the environment.
To reveal the influence of the pH-value on the sorption of humic acid on sea sand, batch experiments were performed. A 25 ppm solution of HA was used and the experiments were performed as described in chapter 2.4 (instead of plastic vessels glass vessels were used, to minimise the underground pollution with Carbon). Figure 18 shows the results of this examination:

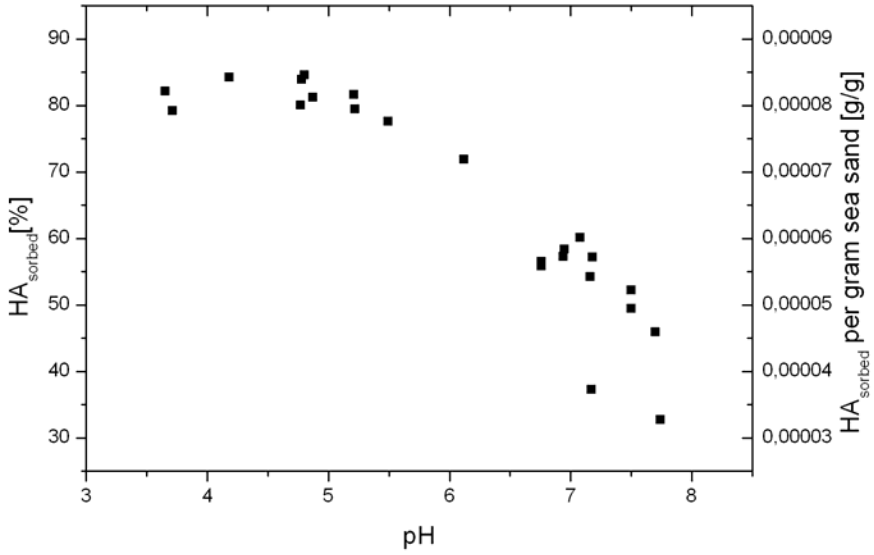

Fig. 18: Interaction of humic acid and sea sand depending on pH

The humic acid sorption on sea sand reaches its maximum for pH-values lower than 5. In this case, 80 - 85% of the HA are bound. This corresponds to a bound humic acid mass of 80 – 90 µg/g sea sand. At pH values over 5 the sorption decreases in a linear manner. The sorption decreases on only 45% of the used HA at pH 7.5 which corresponds to a sorption of 40 – 50 µg/g sea sand. In the pH-range between 6 and 8 the dependence of the sorption on pH is strong. This behaviour can be explained by the deprotonation of both, the humic acid and the sand with increasing pH.
With increasing surface charge, humic acid and sea sand repel each other and the sorption decreases. The experiment demonstrates that the role of humic acid as a geocoating agent has well to be taken into consideration.

3.3.1.4 pH-Edges

So-called pH-edges show the pH-dependence of the adsorption of heavy metals on sea sand. The influence of HA was investigated as well, by repeating the experiments with 5 ppm and 25 ppm HA. Experiments were performed as described in chapter 2.4 and the pH was varied between 3 and 9 by adding HNO_3 or KOH.
Figure 19 and 20 show the result of the experiments without HA and with 25 ppm HA. The sorption increases in the following order: Cd < Zn < Cu < Pb. The graphs show the typical s-curved behaviour of pH-edges. Cd and Zn possess a slightly increasing adsorption in the pH-

range from 3 to 6. Zn has its leap between pH 6 and 7, while Cd has the leap at higher pH-values between 6 and 9. The sorption of copper increases from pH 3 and between 5 and 6.5 the sorption increases strongly. At pH 6.5 nearly all copper is bound. The sorption of Pb is even stronger than that of Cu. Nearly 100% of the used lead is already bound at pH 6.

The results of the experiments with 25 ppm HA are shown in figure 19. They can be interpreted best by regarding the low adsorbed metals Zn and Cd separately. HA seems to have only little influence on the sorption of Cd and Zn. It is only the maximum amount of metal is reduced due to the complexation with humic acid. The maximum amount of Cu and Pb is reduced in the same way. Furthermore HA reduces the Cu and Pb sorption at low pH-values significantly.

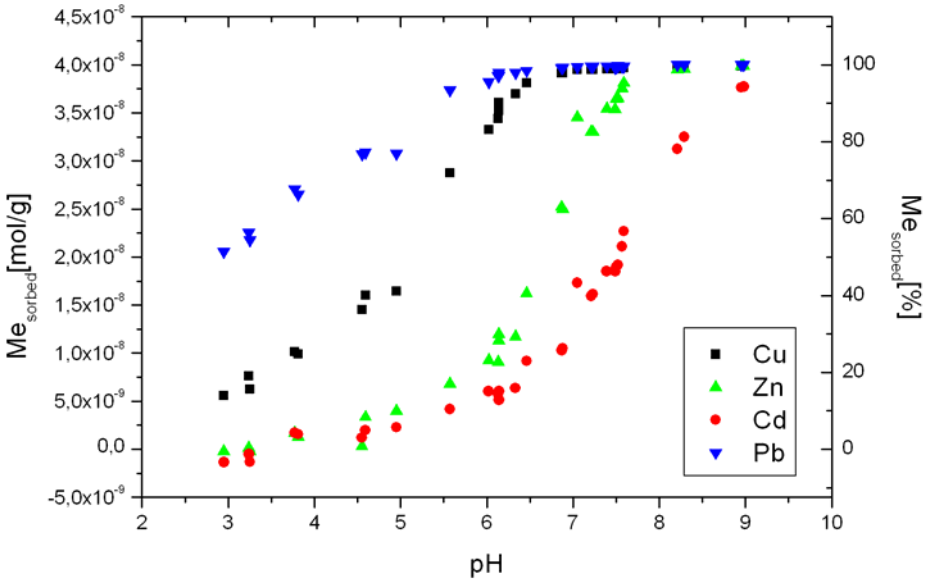

Fig. 19: pH-edges for Cu, Zn, Cd and Pb without humic acid

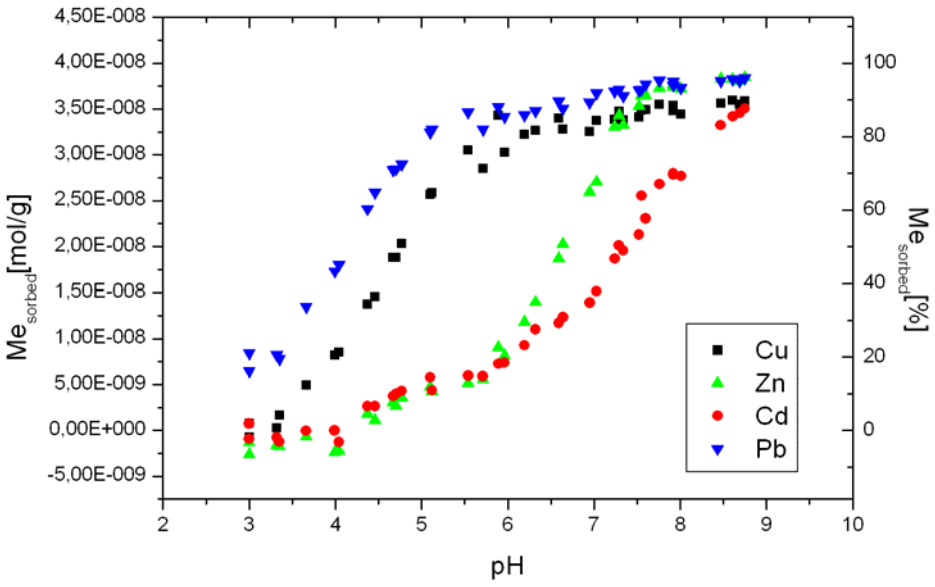

Fig. 20: pH-edges for Cu, Zn, Cd and Pb with 25 ppm humic acid

3.3.1.5 Adsorption Isotherms

Adsorption isotherms were determined for Cu, Zn, Cd and Pb without HA and with 25 ppm HA at two pH values (one near pH 6 and one near pH 7). The experiments were performed as described in Chapter 2.4. Humic acid and the metal were allowed to precondition for 24 h and the contact time with sea sand was 48 h. Concentrations were varied from $5*10^{-8}$ M up to 10^{-3} M. Figure 21 shows the adsorption isotherms of Cd (the rest of the results is shown elsewhere [Zei03]).

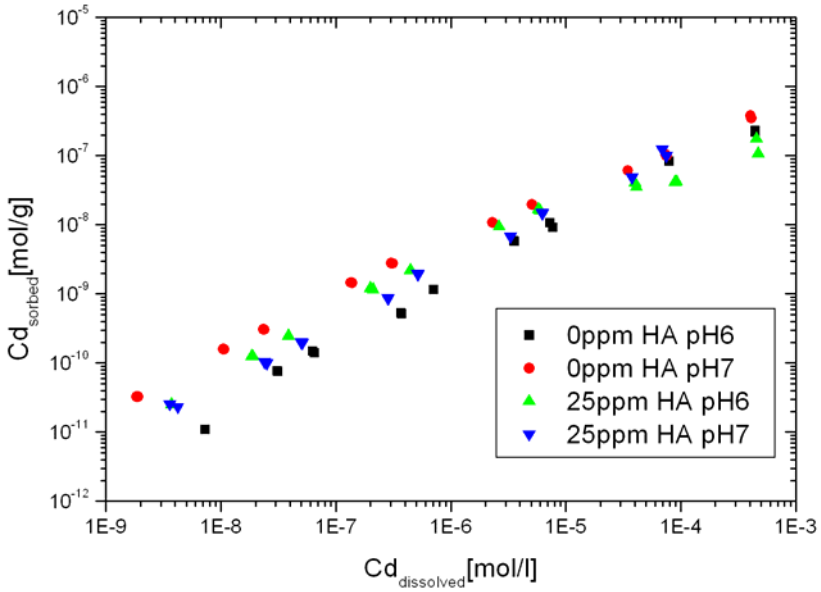

Fig. 21: Adsorption isotherms for Cadmium at different HA concentrations and pH values ($Cd_{sorb} + Cd_{diss} = Cd_{tot}$)

All isotherms have a rather linear behaviour with a small deviation to lower adsorption at small concentrations of dissolved Cd. This is typical for isotherms with Nernst behaviour at small concentrations and Freundlich behaviour at medium to high concentrations [Rab98]. Figure 21 shows the higher sorption at pH 7 compared with the sorption at pH 6. These results are in a good agreement to those from the pH-edges (Fig. 19). Zn has similar isotherms, but because of the high natural occurrence of Zn, the quality of Zn isotherms is limited at low concentrations. Cu and Pb are highly sorbed. It was impossible to get Pb isotherms at pH 7, because the remaining Pb concentration in the batch experiments (after contacting it with sand) were lower than the concentration of the blank solutions.

An interesting aspect is the influence of humic acid on the sorption isotherms. At pH 6 the addition of HA leads to an increase in the heavy metal sorption. In contrary at pH 7 the same amount of HA causes a decrease of sorption, compared to the same experiment done without HA. An explanation can be found by taking the sorption of HA to sea sand into account. At pH 6 more HA is bound to the sand than at pH 7 due to the higher protonation of both of them. At pH 7 more HA is available in the solution. Therefore more heavy metal can be stabilised in the solution and the sorption is decreased compared to the analogous experiment

without HA. If there is more HA sorbed at the sand (like at pH 6) then additional metal can be bound to the solid phase as a ternary complex. As a result the sorption is smaller than that in the experiment without HA.

3.3.1.6 Influence of the Water Hardness

In nature there are a lot of cations, competing with heavy metals for binding sites on the geomatrix. Among them Ca and Mg are the most important competitors. Ca and Mg (together with hydrogen carbonate) are responsible for the water hardness of all natural waters. Strictly the water hardness is defined as the content of Mg, Ca, Sr and Ba, but the last two can practically be neglected for surface waters. In this experiment the influence of the sum concentration of Ca and Mg was varied between 0 - 12 mmol/l (in all other batch and column experiments of this work the sum concentration of Ca and Mg in the background solution was adjusted to 1,33 mmol/l). The experiments were performed as described in chapter 2.4. At pH 3.25 no additional buffer was needed, at pH 6 a 1 mM Mes and at pH 7 a 1 mM PIPES buffer was used to keep the pH value constant. These results can be interpreted best, by regarding the weak adsorbing metals (Zn, Cd) separately from the strong sorbing ones (Cu, Pb).
Cd (Fig. 22) and Zn (Fig. 23) show the expected results. With increasing Ca and Mg content, the sorption of each heavy metal is decreased gradually. The pH dependence can be seen as well and it is in a good agreement with the dependence observed for the pH-edges.

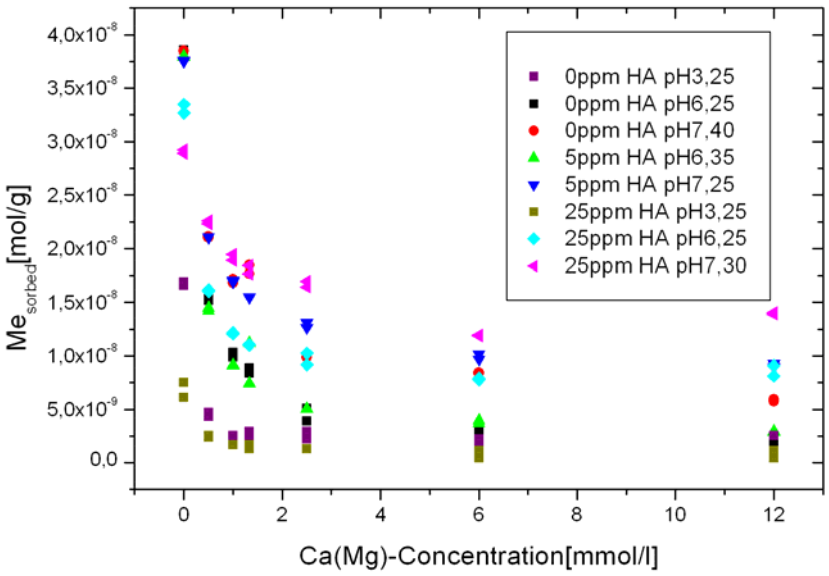

Fig. 22: The sorption of Cd depending on pH, HA concentration and water hardness

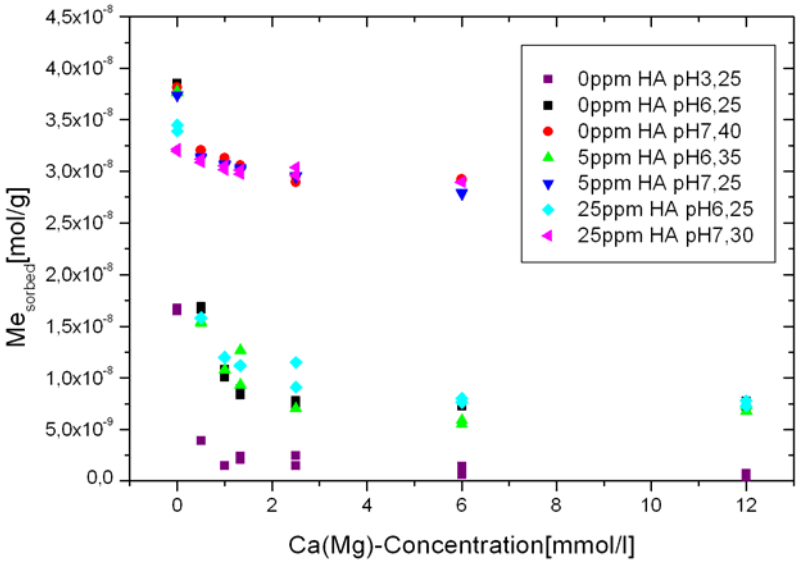

Fig. 23: The sorption of Zn depending on pH, HA concentration and water hardness

From pH 6 to 7 the adsorption of Zn increases significantly, while the pH-dependence of Cd is quite low. With increasing pH the base sorption of the heavy metals increases, while the curvature remains constant. The influence of HA on the sorption is quite limited in the case of the weak complexing metals. A concentration of 5 ppm HA causes nearly no change in the heavy metal sorption, probably due to the fact that nearly all the humic acid is bound to the sea sand under these conditions. A concentration of 25 ppm HA enhances the sorption of Cd at pH 6 and 7 and of Zn at pH 6. If the heavy metal is strongly bound to the sand, like Zn at pH 7.3 even 25 ppm HA shows no influence on the sorption behaviour.

The bound heavy metals Cu (Fig. 24) and Pb (Fig. 25) show a distinctive sorption behaviour depending on the water hardness and the HA concentration. At pH 3.25 the behaviour of Cu and Pb is like that of Zn and Cd. The sorption decreases with increasing water hardness. HA enhances the sorption in addition, due to the great amount of HA which is bound to the sand under these conditions (see Fig. 18). At the low pH value of 3.25 the sorption of Pb is higher than that of Cu, as expected from the pH-edges.

At the highest pH values at 6.25 and 7.4 the sorption of Cu and Pb is nearly independent of the water hardness. Nearly 100% of the used metal is bound to the sea sand. The competing ability of Ca and Mg is not strong enough to remobilise the metal again. HA at a concentration of 5 ppm is able to keep a small amount of Cu and Pb in the solution at pH 6.25. At pH 7.4 the sorption ability of the sand surpasses the complexing ability of the HA and all the metal is bound to the sand. An interesting case is the sorption of Cu and Pb with 25 ppm HA in the solution. Here the sorption seems to be enhanced with increasing water hardness. This result is far from expected, but simple to explain. 25 ppm HA stabilises a certain amount of heavy metal in the solution. By increasing the water hardness the metal bound by HA is released and can be sorbed by the sea sand again.

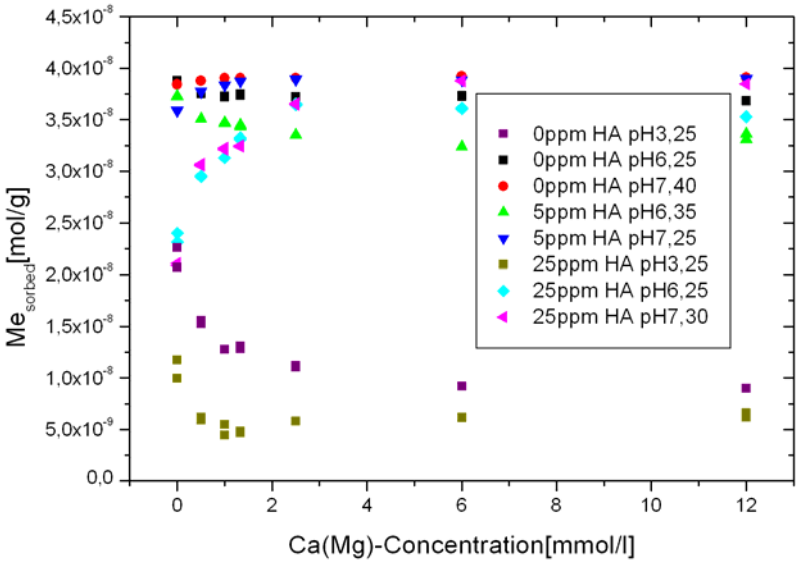

Fig. 24: The sorption of Cu depending on pH, HA concentration and water hardness

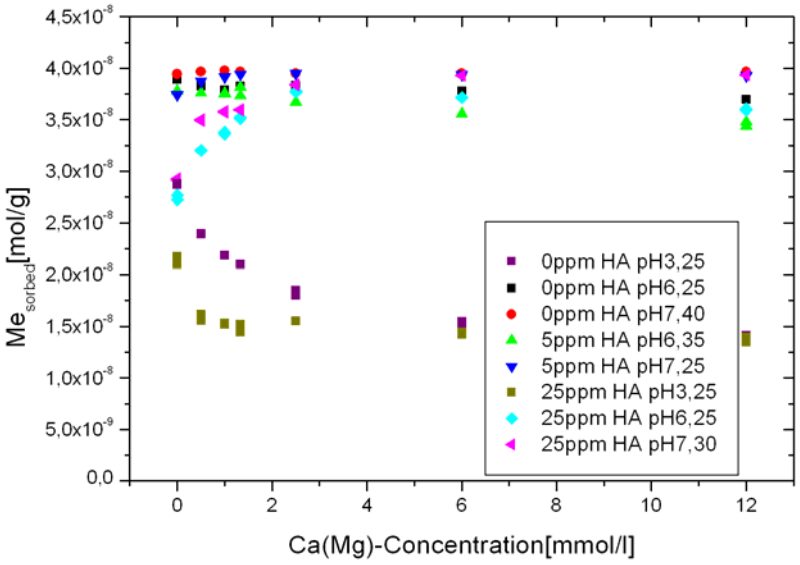

Fig. 25: The sorption of Pb depending on pH, HA concentration and water hardness

3.3.2 Column Experiments

To transfer experiments under laboratory conditions to natural systems several aspects have to be considered. In natural systems the contact between the solid phase where the sorption takes place and the heavy metal containing solution may not be permanent. Therefore the equilibrium may not be like it is in batch experiments Column experiments describe the natural situation of non equilibrium in a much better way. The experiments were performed as summarised in chapter 2.4. Four column experiments were done: two experiments without HA at pH 6.15 and pH 7.4 and another two with 25 ppm HA at pH 6.4 and pH 7.4. Before each experiment the column was conditioned with at least 1000 pore volumes of the background solution (without humic acid). At the beginning of the experiment 500 µl of a mix of Cu, Zn, Cd and Pb (10^{-5} M each) was injected by a 6-way valve. The concentration of Cu and Pb were the highest possible concentrations without the risk of precipitation at the selected pH-values and without causing the precipitation of the humic acid. Unfortunately the detection limit of the ICP-MS was only sufficient to detect the chromatograms of Cd (Fig. 26) due to its low underground.

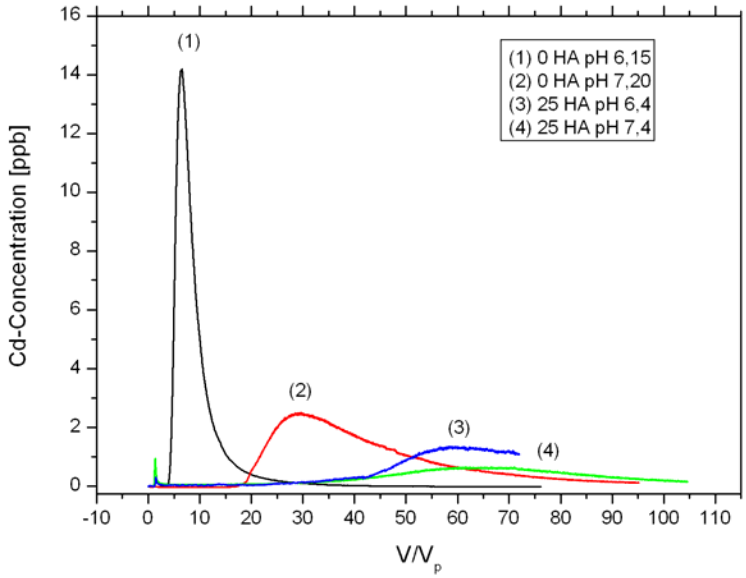

Fig. 26: Chromatograms of Cd; Conditions: 500 µl Cd (10 µM), 0 ppm HA and 25 ppm HA at pH 6.4 and 7.4 respectively; V/V_p: elution volume/pore volume

Zn could not be detected because of its high underground. Cu as well as Pb is highly sorbed and the resulting concentrations of the chromatograms are too low to be detected even with ICP-MS. The Cd chromatogram without HA at pH 6.15 has its peak maximum at $V/V_P = 7$. The peak broadens with increasing pH (7.4) due to the higher sorption and the peak maximum moves towards $V/V_P = 28$. In the experiments with 25 ppm HA it is difficult to determine the peak maxima exactly, because the chromatograms are rather flat. The peaks lie around $V/V_P = 60$. But more interesting is the fact that the peak does not have such a strong shift it does in the experiments without HA. As described in chapter 3.3.1.2 the HA seems to play a role as a mediator in the ternary system which makes the system more stable.

In the experiments with 25 ppm HA another small peak can be found for all metals at the beginning (V/VP ≈ 1) of all chromatograms (Fig. 27). This peak results from metal which is bound to a colloidal fraction of the HA. As this colloidal HA does not interchange with the sand because of its size the bound metal is transported inertly through the column. The amount of inertly transported metal increases from pH 6.4 to pH 7.4 and the found percentages lie between 2 - 4 % of the total metal concentration. The recovery rate for the analysed metals of all column experiments lies between 80 and 90 %.

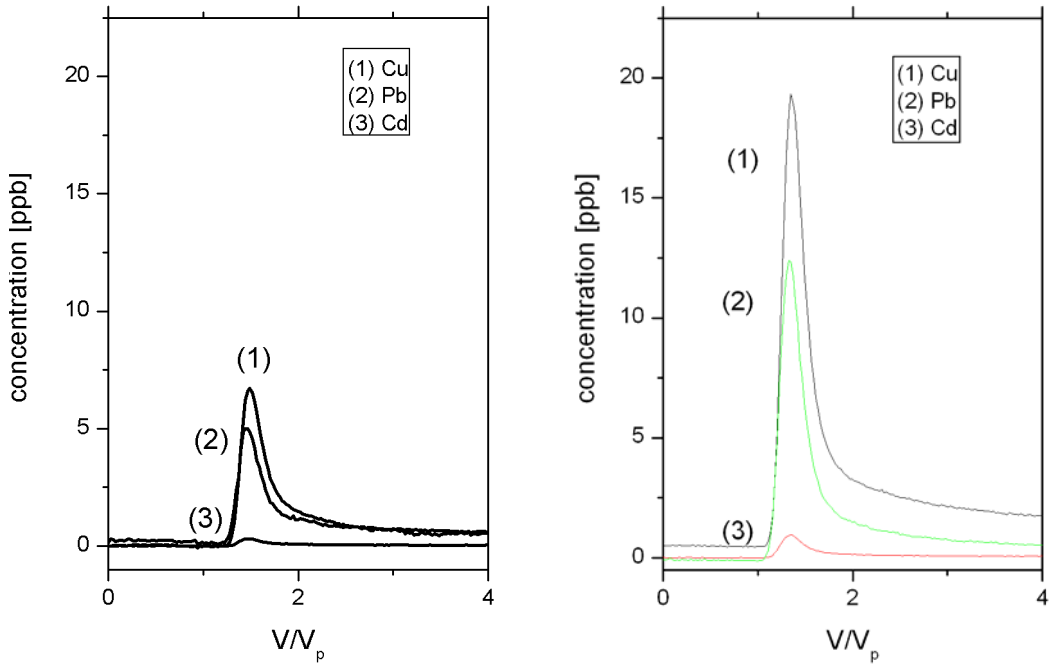

Fig. 27: Peaks at $V/V_P \approx 1$ for all metals; Conditions: 500 µl of each metal (10 µM); 25 ppm HA, pH 6.4 (left) pH 7.4 (right)

4 Conclusion and Outlook

The ternary system consisting of heavy metals (Cu, Zn, Cd and Pb), humic acids (Aldrich HA and artificial HA synthesized by the FZR) and sea sand has been examined. Furthermore natural conditions have been applied to simulate environmental parameters. The complex ternary system was divided into 3 binary subsystems: heavy metal - humic acid, humic acid - sea sand and heavy metal - sea sand. As there are interdependencies between the subsystems, experiments with the ternary system were applied as well.

One of the main topics was the determination of binding constants for the heavy metal - humic acid system. Therefore several determination methods like Stripping Voltammetry, Wageningen-Donnan-Membrane-Technique, and Capillary Electrophoresis were developed or improved for this purpose. The binding constants were derived with the help of the CNM and are in good agreement with other values taken from literature (see Fig. 8).

For lead we obtained a log β of 5.4 ± 0.2 (averaged over all pH-values and methods), copper was found to have a log β of 5.2 ± 0.2, that for zinc and cadmium was an order of magnitude lower, log β was around 4.0 ± 0.2. The Stripping Voltammetry was further used to examine the influence of naturally occurring competing cations on the binding of heavy metals. In this way it could be shown that Ca, Mg and Al ions inhibit the binding of heavy metals to the humic acid significantly.
A large amount of batch experiments were performed to examine the remaining subsystems. To be close to natural conditions a background solution was used in all batch experiments which simulates a surface water. In this way kinetical aspects of the sorption were examined. The influence of preconditioning could be shown as well as the reversibility of the adsorption. Adsorption isotherms, pH-edges and the influence of the water hardness were examined in quite a detailed way.
Column experiments were performed to simulate a natural system where equilibrium between the single components is not reached. The column experiments could only be interpreted for Cd because of the high underground of Zn in the used waters and the low concentration of Cu and Pb (caused by the high adsorption of these metals). However, the experiment with Cd shows an interesting aspect. The HA seems to play the role of a mediator which makes the ternary system more stable against influences like the pH-value. Furthermore the HA slows down the transportation of the metals while a small amount is accelerated and transported inertly through the column bound by colloidal HA.

Appendix

Chemicals

The humic acids were provided by Aldrich (natural HA) and the Forschungszentrum Rossendorf FZR (synthetic humic acid M42). The nitrates of lead, zinc, copper, cadmium, calcium, magnesium, aluminium and potassium from Merck were used in p.a. or suprapur quality according to the measured concentration range.
Imidazole and glycolic acid from Merck were used in p.a. quality, also morpholino-ethane sulfonic acid. Water was used in double deionised form produced with a pure water system from Millipore (electrical resistance R = 18.2 MΩ). The cation exchange membrane for the WDMT was purchased by BDH (No 55165 2U)

Instruments

pH-Measurements
The pH-measurements were carried out with pH-electrodes from Metrohm (CH) and pH-meters from WTW, WTW pH 521 and WTW pH 91.

UV/Vis-Spectroscopy
Spectra and concentration measurements of humic acids were carried out with a UV/Vis-Spectrometer Lambda 25, Perkin Elmer with software for Windows 95. Detection for the CE was carried out with the built-in Diode Array Detector or the UV/Vis-Detector with four fixed wavelengths (210, 214, 254 and 280 nm).

ICP-OES
The Atomic Emission Spectrometer Plasma 2000 from Perkin Elmer with the software was used for the metal quantification with ICP-OES.

Stripping Voltammetry
The EG&G Princeton Applied Research SMDE Model 303A with a potentiostat/galvanostat M263A and the software M270/M250 research electrochemistry software version 4.30 were used for the stripping voltammetry measurements. A self-made cooling unit for the PFA-sample container were used for temperature control.

Capillary Electrophoresis
All CE-measurements were carried out on a CE MDQ from Beckman Coulter with the software P/ACE MDQ version 2.30, fitted with two detectors, a DAD and a UV/Vis fixed wavelength. The quartz capillaries were fused-silica ones from Polymicro Technologies with inner diameters of 75µm.

ICP-MS

All ICP-MS measurements were carried out on a Plasma Quad 3 instrument from VG Elemental.

5 References

[Ber00] Wissenschaftliche Berichte, FZKA 6557, C.M. Marquardt (Ed.)
[Eng94] Engelhardt H., Beck W., Schmitt Th., Kapillarelektrophorese, Vieweg-Verlag, 1994
[Hub94] Huber L., Frimmel F. H., Vom Wasser, 83, 9-22 (1994)
[IIF01] oral note
[Lam82] Lampert J. K.; Dissertation, Wisconsin-Madison (USA), 1982
[Rab98] Rabung T.; Dissertation, Saarbrücken, 1998
[Tem00] Temminghoff, E. J. M., Plette, C. C., Riemsdijk W. H. Van, Anal. Chem, 2000, 417, 149
[Zei03] Zeitz M., Dissertation, Saarbrücken, 2003

Appendix D Institut für Interdisziplinäre Isotopenforschung e. V., Leipzig

Investigations on the Influence of Trivalent Electrolytes on Complexation and Adsorption of Heavy Metals with Humic Substances by Means of Radioactive Tracers

H. Lippold, D. Rößler, H. Kupsch

Final Report

Support contract number
02 E 9329

Institut für Interdisziplinäre Isotopenforschung e. V. (IIF)
Permoserstr. 15
04318 Leipzig
Germany

www.iif-leipzig.de

Table of contents Table of contents

Abstract

The research project under report was concerned with the complexation and adsorption of actinides in interaction with aquatic humic colloids with special regard to the influence of geochemical conditions. The constituent processes of solid-liquid distribution of metal species in systems containing humic substances were investigated in batch and column experiments. Main focus was placed on aspects of colloid charge compensation induced by protons and trivalent metals. In order to gain analytical access to measurements at adequate concentration levels, techniques for radiolabelling of humic substances were developed. Radioactive isotopes of rare earth elements were employed as analogue tracers of actinides.
The pH dependence of the influence of humic substances on metal adsorption was investigated for several representative geogenic solids with different acid-base properties. The findings could be reproduced on the basis of the respective pH dependencies of metal-humate complexation and humic acid adsorption. It was shown that a transition from mobilisation to demobilisation can be effected by just a minor decrease in pH. Adsorption of different humic substances is related to their specific properties and is primarily determined by their pH-dependent charge density. By radioanalytical measurements of octanol-water partitioning, it was demonstrated that the hydrophilic properties of the colloids are controlled by the solution parameters. Column experiments with radiolabelled humic materials provided evidence of irreversible adsorption processes as well as of a weighted distribution of the reactive components within the total system in terms of mobility.
A major task of the project was to evaluate the influence of competitive reactions of higher-valent geogenic electrolyte constituents on actinide-humate complexation. Investigations with various humic substances showed that displacement effects are not significant unless the metal-loading capacity is nearly exhausted. Thus, the role of multivalent metals is mainly characterised by the concomitantly induced flocculation process which leads to complete immobilisation of the colloids. The exchange reaction is subject to kinetic effects. Essential principles of the flocculation process were elucidated by systematic studies depending on concentration, pH value and ionic strength. Complex stability and flocculation efficiency of trivalent metals were found to be interrelated.

List of acronyms

BET Brunauer-Emmett-Teller
DOC Dissolved Organic Carbon
FA Fulvic Acid
GPC Gel Permeation Chromatography
HA Humic Acid
HS Humic Substance
ICP Inductively Coupled Plasma
MS Mass Spectrometry
OES Optical Emission Spectroscopy
PE Polyethylene
PET Positron Emission Tomography
PP Polypropylene
TRIGA Training, Research, Isotopes, General Atomics
UV Ultra-Violet
XRF X-Ray Fluorescence

List of symbols

A Peak area
A_{sp} Specific surface area
c Concentration
I Ionic strength
K_d Partition coefficient (solid-liquid distribution)
$P_{O/W}$ Partition ratio (octanol-water distribution)
$T_{1/2}$ Half-life
Γ Adsorbed amount

Square brackets in axis titles denote concentrations.

1 Introduction

In case of a release from subterranean radioactive waste repositories, migration of actinides can be facilitated considerably by aquatic colloids, which are ubiquitous in natural systems [1-4]. In particular, the outstanding complexing ability of humic and fulvic acids (HA, FA), main constituents of the dissolved organic carbon (DOC), can dominate the speciation of multivalent metal ions [5, 6]. In this way, adsorption onto the solid phase is largely impeded under appropriate conditions [7-9]. Aiming at the development of predictive transport models that account for the impact of colloid-borne migration, systematic studies on humate complexation of actinides and chemical analogues have been put into progress.

The fate of the contaminant metals is, however, not sufficiently described by complex stability since the mobilising effect is also determined by the solid-liquid partitioning of the carrier colloids, being subject to the geochemical circumstances, which will not be invariant in the course of migration over long distances. For the purpose of a comprehensive modelling, it is therefore necessary to specify the respective conditions leading to an enhancement or confinement of migration. Within the scope of the project, systematic investigations on the fundamental partitioning processes (complexation, adsorption, precipitation) were performed by static and dynamic experiments employing various humic materials and geogenic solids.
Altogether, the investigations are focused on the implications of colloid charge compensation induced by protons (influence of pH) and trivalent metal ions. Due to their high binding affinity, multivalent metals are expected to exhibit an especially high competitive potential in respect of actinide-humate complexation. Additionally, these metals are known to be most effective as coagulants. In view of the humic colloid-borne transport, the coagulation-flocculation process may be more important than the competitive effect in that it results in complete immobilisation. For this reason, both aspects were considered jointly in the present study. Most experiments were conducted with aluminium according to its abundance. Comparative measurements with gallium, indium, scandium, yttrium and lanthanum were performed in order to determine the scope of specific properties at equal ion charge.

Major emphasis was placed on the analytical access to very dilute systems as considered in pertinent scenarios. This need arises from the fact that the partitioning of metal ions to DOC has been found to depend on concentration [10, 11]. In general, conventional analytical methods are too insensitive for measurements at adequate concentration levels. To overcome this limitation, radioisotopes of rare earth elements (^{140}La, ^{160}Tb) were utilised as short-lived analogue tracers of trivalent actinides, allowing experiments in the sub-nanomolar range to simulate realistic settings. Furthermore, radiolabelling techniques for humic substances were developed and applied to enable studies on systems with low DOC content. Due to the chemical heterogeneity of natural carbon compounds, labelling turns out to be especially difficult in terms of stability and selectivity. In order to represent the humic substance as a whole, e. g. for partitioning measurements, a non-selective labelling reaction is required. For studies on the transport behaviour of heavy metals, however, it is necessary to consider just those components which are actually involved in the interaction process. To characterise these reactive constituents, specific labelling procedures are needed as well.

2 Experimental

2.1 Materials

2.1.1 Humic substances

Five different humic substances (HS) were chosen for comparative investigations. Natural aquatic and soil HS were sampled from the raised bog “Kleiner Kranichsee” (near Carlsfeld, Saxony, Germany). Humic and fulvic acids (5 - 10 g) were isolated in accordance with the procedures adopted by the International Humic Substances Society [12, 13]. A commercially available humic acid was obtained as sodium salt from Sigma-Aldrich (Germany). Purification was accomplished following the instructions given by Kim and Buckau [14]. The protonated product is herein referred to as Aldrich HA. Synthetic humic acid M42 [15] was supplied from Forschungszentrum Rossendorf, Institute of Radiochemistry. The substances were stored in a desiccator.

2.1.2 Geogenic solids

Granite, phyllite and diabase were sampled in the “Mansfelder Land” (Saxony-Anhalt, Germany). After crushing and grinding in an agate mortar, the materials were sieved to a 2 - 3 mm grain size fraction and were washed with water to remove soluble impurities and abraded powder. Sea sand was purchased from Merck and was likewise washed after sieving to 2 - 3 mm.

2.1.3 Radionuclides

Production of lanthanum-140. No-carrier-added ^{140}La ($T_{1/2}$ = 40.3 h) was obtained from a ^{140}Ba/^{140}La generator. ^{140}Ba ($T_{1/2}$ = 12.8 d) was isolated from the fission products of ^{235}U. Neutron irradiation of $UO_2(NO_3)_2$ (~ 1 mg mL^{-1}, 90% ^{235}U) was performed at the TRIGA Mark II reactor of the University of Mainz. After separation of non-fissioned material by anion exchange (Bio-Rad AG 1-X8) in 8 M HCl, barium was isolated by precipitation with concentrated HCl and Ba/Sr carrier at 0°C (resulting activity: ~ 3 MBq). The decay product ^{140}La was extracted from aqueous solution with 0.1 M 8-hydroxyquinoline in $CHCl_3$ at pH 8. To yield the ionic species in a radiochemically pure form, the organo-complex was decomposed by wet combustion with $HClO_4$. The residue was finally taken up in 0.1 M $NaClO_4$, followed by pH adjustment. Radionuclidic purity was verified by gamma spectrometry using a Ge detector (Ortec, GEM-40190-P). Experimental concentrations were adjusted by carrier addition.

Other radionuclides. [^{160}Tb]Tb ($T_{1/2}$ = 72.3 d) was produced by neutron activation of ^{159}Tb (1 mg mL^{-1}, as nitrate) at the TRIGA Mark II reactor. 50 h of irradiation at a neutron flux of 7×10^{-11} n cm^{-2} s^{-1} yielded a specific activity of 1.2 MBq mg^{-1}. After transformation into the perchlorate system, a stock solution of 10^{-5} M [^{160}Tb]Tb in 0.1 M $NaClO_4$ was prepared.
[^{111}In]$InCl_3$ ($T_{1/2}$ = 2.8 d) and [^{131}I]NaI ($T_{1/2}$ = 8.0 d) were provided by Amersham (Germany) and were used as received.

2.2 Methods

2.2.1 General remarks

All experiments were conducted at room temperature under aerobic conditions. Water was purified with a Barnstead Nanopure system. The pH was adjusted by adding diluted $HClO_4$ or NaOH, using a Sentix 41 electrode (WTW, Weilheim, Germany) for measurement. Unless otherwise noted, usage of buffer systems was avoided. Stock solutions of HA or FA were discarded 2 weeks after preparation.
ICP-spectrometric analyses are based on matrix-matched calibrations with Merck standards. ICP-OES was performed with a Spectroflame P/M instrument (Spectro, Germany), ICP-MS was conducted by means of a Plasmaquad Excell spectrometer (VG Elemental, UK). Samples were acidified with 20 µL of 65% HNO_3, which was carried out immediately before analysis to avoid precipitation of HA. Filtering was performed if necessary.
A gamma counter 1480 Wizard (Wallac, Finland) was used for activity measurements. All samples of a test series were brought up to equal volumes to ensure a uniform measuring geometry.

2.2.2 Sequential chromatographic analysis

The method was introduced as a specific application of gel permeation chromatography (GPC) to evaluate radiolabelling techniques for HS with respect to stability and selectivity [16]. In addition to the separation by molecular weight, the humic materials are further discriminated into mobile and immobile components. Depending on the pH value, HS samples are partly retained on the gel matrix. Subsequent to the size fractionation of the mobile part under selected solution conditions (1st sequence), the immobilised components are eluted in two rinsing steps with 0.1 M NaOH (2nd sequence) and 0.1 M HCl (3rd sequence), respectively.
A Knauer GPC system with UV detector (254 nm) was additionally equipped with a NaI(Tl) scintillation detector, a conductometer and a pH meter. Data were acquired every 10 s. Separations were carried out with Fractogel TSK-HW 50 (F) from Supelco in a 40 × 1.6 cm glass column at a flow rate of ~ 80 mL h^{-1}. For analysis, 1 mL of a 0.1 g L^{-1} solution of labelled HS (~ 1 MBq) was injected by means of a Rheodyne valve. Peak positions were corrected for the dead volume between the detectors.

2.2.3 Adsorption experiments

Batch experiments. 15 g of 0.1 M $NaClO_4$ were contacted with an appropriate amount of solid (sand, granite: 1 g; phyllite, diabase: 0.1 g) in 20 mL PE vials. After weighing these samples, pH adjustment was accomplished by addition of acidic or alkaline 0.1 M $NaClO_4$ until the buffering capacity of the rock materials was exhausted. Up to 20 readjustments over a period of several weeks were necessary for conditioning. The systems were then made up to a fixed volume by removing a calculated amount of solvent gravimetrically, accounting for the vol-

umes of metal and / or HS stock solutions to be added thereafter. For equilibration, the samples were rotated end-over-end at 20 rpm for 48 h. After sedimentation, aliquots were taken for analysis. Depletion was determined radioanalytically in relation to reference solutions with the same starting concentrations. The final pH was measured after analysis. In the case of sand, conditioning could be performed within the course of the adsorption experiment by adding a proper amount of acid together with the adsorptives. This simplified procedure was, however, not applied in the pH-dependent investigations with [^{160}Tb]Tb (chapter 3.3.2.).

Column experiments. The GPC equipment described in chapter 2.2.2. was used to examine the permanent retention of differently labelled HS at geogenic matrices under flow conditions. For that purpose, the glass column was filled with 5 g of adsorbent material. A near-neutral solution of 0.1 M $NaClO_4$ (no pH adjustment) was pumped through the column at a flow rate of ~ 12 mL h^{-1} in an upward direction. Pre-conditioning in a closed-loop mode was not performed since an accurate simulation of geogenic conditions was not intended within the scope of these experiments. Rinsing steps were omitted; recoveries were related to a bypass run without retention, based on the respective peak areas.

2.2.4 Measurement of metal-humate complexation

8 mL systems were prepared by adding pH-adjusted stock solutions of metal and HS (in 0.1 M $NaClO_4$ each) to the solvent (0.1 M $NaClO_4$, likewise pH-adjusted). These samples were allowed to equilibrate for 48 h in PE vials. The anion exchange method was applied for metal speciation [17, 18], using Sephadex DEAE A-25 (Sigma-Aldrich) as a separating agent. Prior to use, the exchange resin was washed with methanol, rinsed with 0.1 M $NaClO_4$ and kept therein after equilibration to the desired pH. For measurements, it was introduced as a slurry of approx. 200 mg to 4 mL aliquots of the equilibrated solutions, which was ensured to be sufficient to adsorb the organically bound metal fraction quantitatively. After shaking for 1 min and sedimentation, 3 mL were taken for analysis. The decrease in metal concentration was determined by ICP-OES (Al, Sc), ICP-MS (Ga, Y) or radiotracer analysis ([^{111}In]In, [^{140}La]La, [^{160}Tb]Tb). Generally, concentrations in the processed aliquots were corrected for the water content of the slurry. The final pH was verified to be unchanged.

2.2.5 Flocculation experiments

Flocculation of metal / HA systems was investigated by jar tests in clear glass vials. 10 mL HA solutions with varying metal contents were prepared by using pH-adjusted stock solutions and solvents. The samples were left to stand undisturbed over a period of 2 weeks. Sedimentation of flocculated HA was then examined by visual inspection or by measuring the UV absorbance (254 nm) of the supernatant with a spectrophotometer Cadas 100 (Lange, Germany). Metal concentrations were determined by ICP-OES.

2.2.6 Measurement of octanol-water partitioning

Both solvents were mutually saturated by rotating end-over-end in 2 L bottles. Partitioning experiments with radiolabelled HS were carried out in 5 mL PP screw-cap test tubes. 2 mL portions of aqueous HS solutions were overlaid with 2 mL of octanol. For equilibration, the tubes were shaken horizontally along their longitudinal axes at 50 motions per minute, preventing emulsification. After 1 h, both phases were sampled with an Eppendorf pipette (organic phase: 1000 µL, aqueous phase: 50 µL) and were analysed by gamma counting.

3 Results and discussion

3.1 Characterisation of humic substances and geogenic solids

3.1.1 Humic substances

Table 1 shows the elemental compositions of the purified humic materials used in the project. The contents of moisture and ash were determined gravimetrically after heating at 80°C for 24 h and at 800°C for 6 h, respectively. Carbon, hydrogen and nitrogen analyses were conducted with a CHN-O Rapid elemental analyser (Foss-Heraeus, Germany). The H value was corrected for the moisture content. Sulphur was determined by ICP-OES. The oxygen content was taken as the remaining difference to 100% on an ash and moisture free basis. Molar ratios have been specified in the table since the H / C ratio is indicative of the overall aliphatic or aromatic character of HS, whereas the O / C ratio can be related to the content of phenolic and carbohydrate structures. O / C ratios of the three bog HS are significantly higher than those of Aldrich HA and HA M42. In addition, the N content of HA M42 and the S content of Aldrich HA may be noticed as outstanding values. Residual metal contents were determined with 50 mg L^{-1} solutions by ICP-OES without prior digestion. Generally, silicon and iron constitute the largest fraction of inorganic impurities.

3.1.2 Geogenic solids

Some characteristics of the rock materials are given in Table 2, data of sea sand included. Specific surface areas A_{sp} were obtained by the BET method using krypton as adsorptive gas, XRF data were adopted from Ref. [20]. The pH_{eq} value was measured after equilibration of 1 g solid with 15 mL 0.1 M $NaClO_4$ for a period of 2 weeks.
In adsorption experiments, generation of fine-powdered abrasions from the rock materials could not be prevented entirely. It was, however, ascertained that the sorption capability of this fraction does not differ essentially from that of the mm-sized particles. The pH-dependent leaching of metal ions in solid-liquid systems is described in chapter 3.3.2.

Table 1. Elemental compositions of HA and FA. Contents of C, H, N, S, O are normalised to an ash and moisture free basis, metal contents are based on dry weight.

		Aldrich HA	Bog soil HA	Bog water HA	Bog water FA	HA M42	HA M42 *from Ref. [19]*
Ash	(w%)	< 0.3	3.1	2.7	2.0	< 0.3	0.3
H_2O	(w%)	1.6	5.8	5.0	4.5	6.0	5.2
C	(w%)	57.0	53.1	53.5	53.0	59.1	61.8
H	(w%)	4.4	4.5	4.1	4.3	4.8	4.6
N	(w%)	1.3	2.7	2.7	0.6	4.7	4.8
S	(w%)	3.5	0.4	0.7	0.6	0.2	-
O	(w%)	33.8	39.3	39.0	41.5	31.2	28.8
H / C	(n/n)	0.92	1.02	0.92	0.97	0.97	0.88
O / C	(n/n)	0.45	0.60	0.59	0.62	0.40	0.35
Al	(mg g^{-1})	< 0.5	1.2	1.7	0.9	1.0	0.04
Ca	(mg g^{-1})	0.6	< 0.5	1.1	1.8	1.9	0.82
Cu	(mg g^{-1})	< 0.2	< 0.2	0.6	0.2	0.6	
Fe	(mg g^{-1})	3.3	6.0	22.4	0.4	0.3	< 0.02
K	(mg g^{-1})	< 2.0	< 2.0	5.2	< 2.0	3.6	
Mg	(mg g^{-1})	< 0.1	< 0.1	0.2	< 0.1	0.2	0.02
Si	(mg g^{-1})	3.2	10.7	5.1	5.5	14.2	0.09
Zn	(mg g^{-1})	< 0.2	< 0.2	0.8	< 0.2	0.6	

Table 2. Characterisation of the solid materials used in adsorption experiments (n.m. = not measured).

		Phyllite	Diabase	Granite	Sand
A_{sp}	(m^2 g^{-1})	6.5	0.3	2.1	0.2
pH_{eq}		7.0	9.0	5.4	5.9
XRF data	(mg g^{-1})				
Si		119.0	109.6	158.5	181.5
Al		76.0	42.7	n.m.	n.m.
Fe		55.4	81.3	16.4	2.3
K		28.7	n.m.	31.3	2.2
Ca		1.6	29.9	1.7	0.8
Ti		7.1	10.8	0.9	0.2
Mn		0.6	1.5	0.4	-

3.2 Radiolabelling of humic substances

3.2.1 Labelling reactions

Introducing a radioactive label to HS can be accomplished in different ways. Indirect methods, i. e. coupling with pre-labelled organic compounds, seem to be favourable because of the manifold possibilities to form stable linkages. On the other hand, the inherent properties of the humic material will be more or less affected by the carrier groups. Chemical reactions for direct labelling of HS are rather limited. Within the framework of this project, two general approaches were employed: radiohalogenation of the aromatic backbone and complexation of the acidic functionalities with metallic radionuclides (Figure 1). Halogenation with ^{131}I was chosen as a non-selective labelling method since this reaction was not expected to exhibit a pronounced selectivity toward particular constituents of the HS system. In contrast, complex formation with ^{111}In was used as a specific labelling reaction to represent the reactive entities with regard to actinide-humate interaction.

Several techniques for radiohalogenation of HS have been described in literature, which are adopted from radiochemical procedures used in protein research. Radioiodination is achieved by electrophilic substitution at activated positions after oxidation of [$^{125/131}$I]I$^-$. Chloramine-T or hydrogen peroxide in the presence of peroxidase enzymes were used as oxidising agents [21-23]. A problem of this procedure consists in the necessary removal of the auxiliary reagents, which are likely to be entangled in the cross-linked network of HS molecules. For our investigations, we utilised the iodogen method, which was specially developed for radioiodination of proteins under mild oxidising conditions in order to prevent degradation of the substrate [24]. Since iodogen (1,3,4,6-tetrachloro-3a,6a-diphenylglycouril) is insoluble in water, the reaction is performed in a heterogeneous system, i. e. there is no need to separate the oxidising agent from the labelled material.

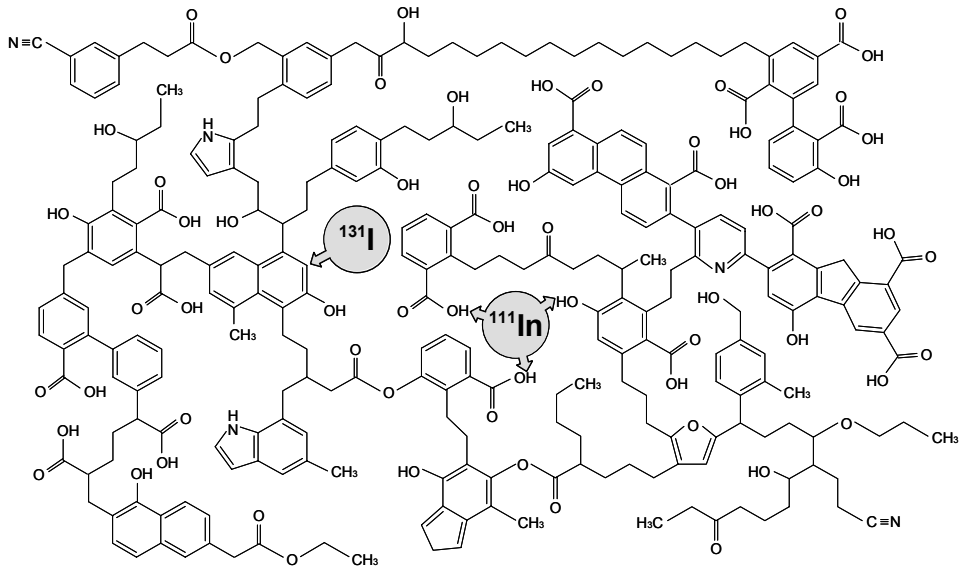

Figure 1. Two ways of introducing a radiolabel to humic substances (structural formula adapted from Ref. [25]).

Radioiodination was performed in 500 µL glass vials with 150 µg iodogen, which was added in 200 µL chloroform to produce a coating on the surface after evaporation of the solvent. Reaction with [^{131}I]NaI and HS was conducted at pH 8 (borate buffer), shaking permanently for 10 min. Input activities were suited to yield specific activities of about 10 MBq per mg HS after purification.

The performance of this technique was evaluated by sequential chromatographic analysis (Figure 2). Comparing the signal traces obtained by UV and gamma detection, there is no indication of selectivity. However, the radiochromatogram contains a small additional peak which can be assigned to free $^{131}I^-$, as is evident from the comparison with the chromatogram of [^{131}I]NaI (not shown). The peak area increases considerably if the labelled sample is exposed to daylight over a longer period of time. Consequently, the loss of radiolabel may be attributed to the photosensitivity of C-I bonds and is thus avoidable if experiments are performed in the dark.

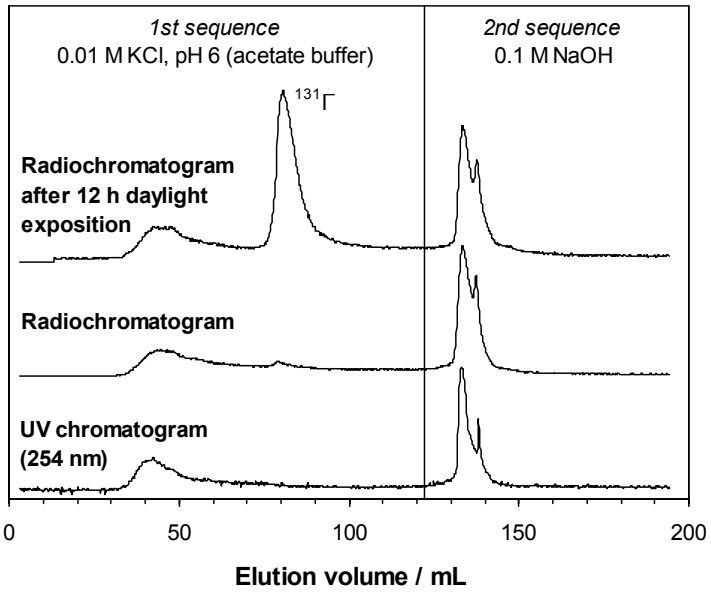

Figure 2. Sequential chromatographic analysis of ^{131}I-labelled Aldrich HA.

For complexation, [^{111}In]$InCl_3$ was added to the HA solution and was allowed to react for 30 min, followed by purification as described in chapter 3.2.2. A sequential chromatographic analysis is depicted in Figure 3. Contrary to the ^{131}I labelling, there is no additional radiopeak within the 1st sequence. Instead, the immobilised In-humate fraction is attacked by the treatment with NaOH in the 2nd sequence. A certain amount of ^{111}In is deposited as hydroxide and re-solubilised with HCl in the 3rd sequence.

At moderate pH values, the label appears to be persistent, even though the stability of metal-humate complexes is considered to be rather low compared to covalent bonds. As discussed later in this report, the persistence is probably due to a partial irreversibility of humate complexation in the special case of higher-valent metal ions. Provided that the labelled material is purified thoroughly, complexation is thus comparable to covalent labelling in terms of stability.

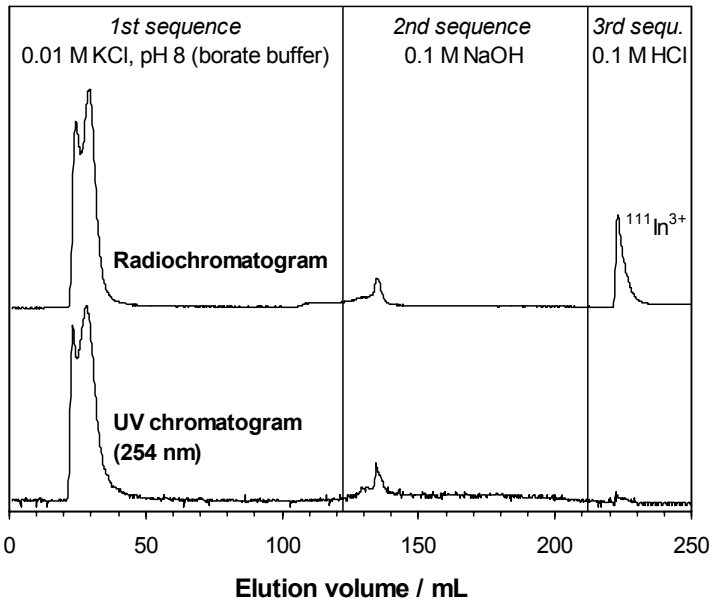

Figure 3. Sequential chromatographic analysis of ^{111}In-labelled bog soil HA.

3.2.2 Purification of radiolabelled humic material

Separation of radionuclides which are not bound or loosely bound to the humic molecules is essential for any kind of partitioning measurements since major amounts of free labelling material would lead to erroneous results. Three different methods have been worked out for this purpose:

Ultrafiltration. Solutions of labelled HS were passed through 3 kD centrifugal filters (Amicon). The filters were then reversed and backflushed with the appropriate solvent. In principle, the method is applicable to HA and FA as well. In the latter case, however, material losses may be more notable because of the lower molecular weight of FA. This kind of purification is most suitable for ^{111}In labelling.

Precipitation. Labelled HA was precipitated by acidification to pH < 1 with concentrated HCl or $HClO_4$. After centrifugation, the supernatant was discarded, and the precipitate was redissoluted with 10^{-3} M NaOH. This procedure was repeated three times, which is sufficient to remove unbound labelling material almost completely as demonstrated in Figure 4. The method is more rapid than ultrafiltration, but not applicable to fulvic acids. Furthermore, it is not suitable for purification of ^{111}In-labelled material since protonation is a competitive reaction to metal complexation, occurring at the same binding sites.

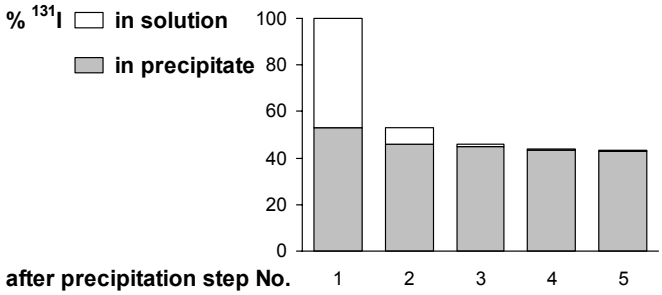

Figure 4. Purification of ^{131}I-labelled HA by repeated precipitation / redissolution (activity in precipitate and supernatant).

Adsorption. The DAX-8 method for preparative isolation of HS from water samples was adopted for the purification of labelled HS. A 5 mL disposable syringe was employed as a miniaturised separation column. A bed volume of ~ 1 mL DAX-8 granules (Supelite™, Sigma-Aldrich), supported by a fitted paper filter, proved to be sufficient for the treatment of 1 mg of HS.

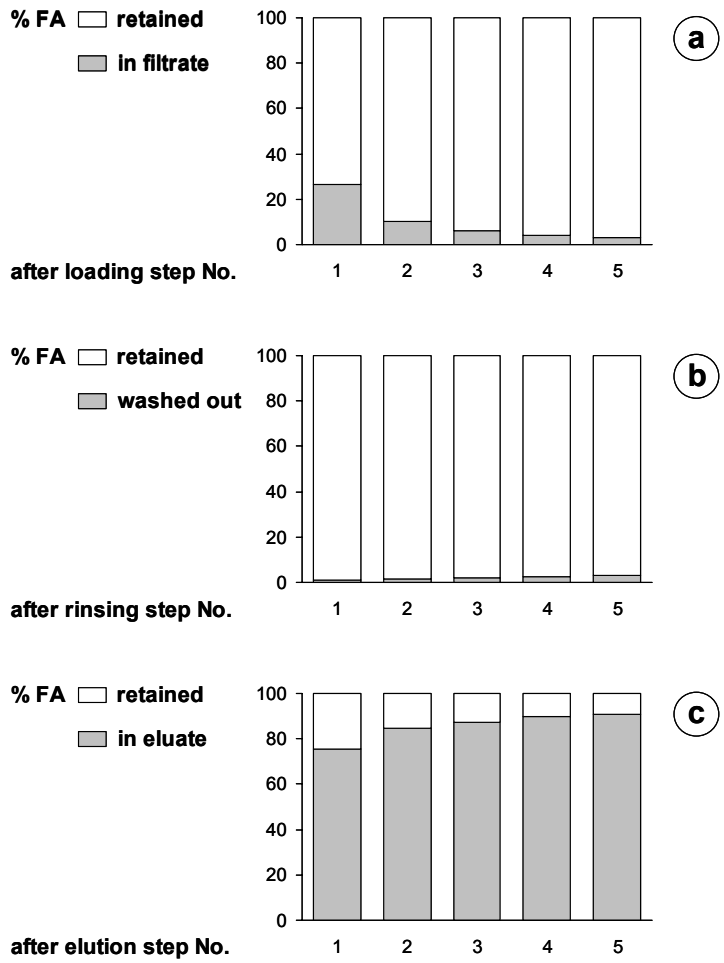

Figure 5. Behaviour of a fulvic acid during the purification process at DAX-8.

The adsorbent was conditioned by passing several bed volumes of 0.01 M $HClO_4$ through the syringe. The solution of labelled HS was likewise acidified to pH 2 and recycled through the column five times. The fixed HS was then washed with 8 column volumes of 0.01 M $HClO_4$ and finally eluted with two column volumes of 0.01 M NaOH. As can be seen from Figure 5, there are only minor losses of FA in all steps. This rapid and convenient method is applicable to HA and FA and is suitable for both labelling techniques.

3.3 Effect of humic substances on metal adsorption depending on the pH value

3.3.1 Investigations on the system La(III) / Aldrich HA / sand

In all experiments on ternary systems (metal / HS / solid) as well as in studies on binary subsystems, equilibration times were fixed on the basis of time-dependent measurements of HA adsorption shown in Figure 6. Adsorption increases rapidly within the first hours of end-over-end rotation and exhibits an asymptotic trend on a time scale of about 2 days. An equilibration time of 48 h was adopted since further changes in adsorption are within the limits of accuracy.

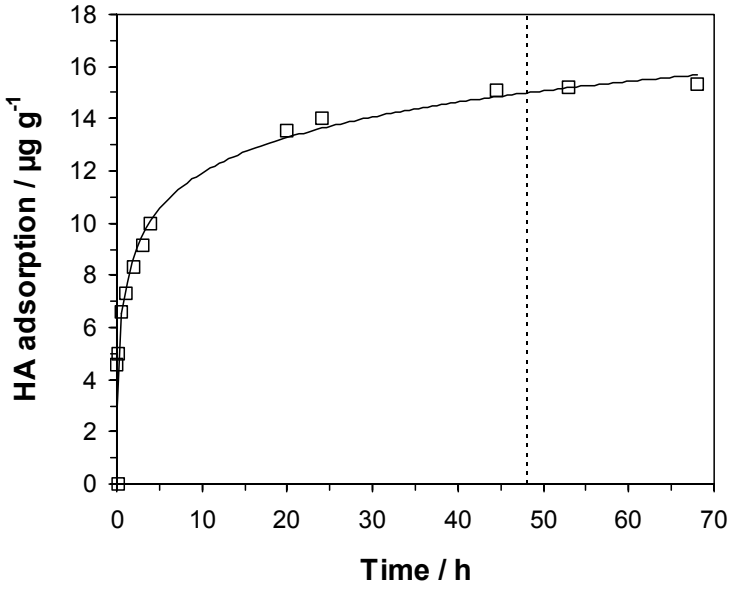

Figure 6. Kinetics of adsorption of Aldrich HA (5 mg L^{-1}) on sand at pH 5 in 0.1 M $NaClO_4$ (radiotracer experiments with ^{131}I-labelled HA).

Adsorption of metal ions in the presence of HA is determined by two processes in addition to the direct interaction of metal and solid: Humate complexation and HA adsorption. Either process is strongly dependent on pH as can be seen from the following figures. By using the ^{131}I labelling technique, it became possible to determine adsorption isotherms of humic materials down to concentrations lower than 1 mg L^{-1}, which is well below the detection limit of DOC analysers. A further advantage consists in the even distribution of signal sources over

the multicomponent system. If UV absorption is used for analysis, measurements are distorted owing to the weighted distribution of chromophoric groups within the total system, i. e. species with a higher density of chromophores are overrepresented in the UV signal.

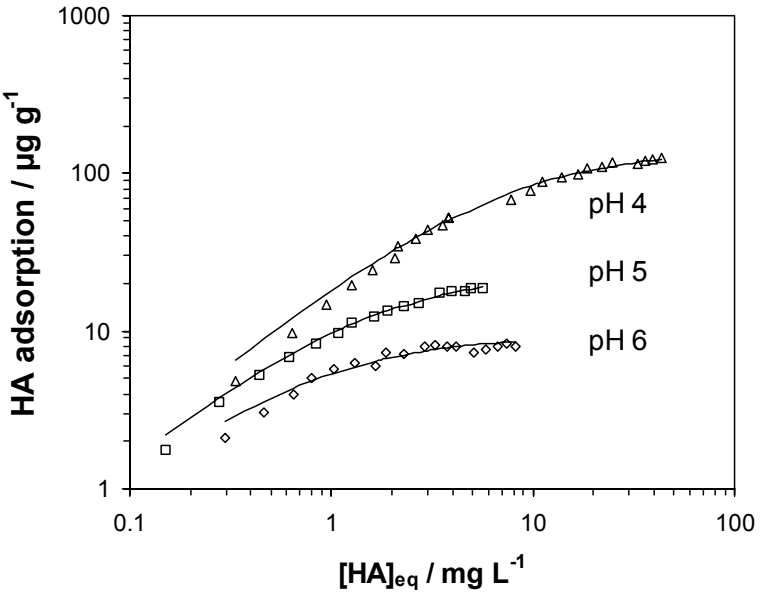

Figure 7. Adsorption isotherms of Aldrich HA on sand in 0.1 M $NaClO_4$ at different pH values (radiotracer experiments with ^{131}I-labelled HA).

Figure 7 represents adsorption isotherms of Aldrich HA on sand at different pH values. The isotherm shapes can be assigned to the Langmuir type (see curve fits). Adsorption increases considerably on acidification, the difference between pH 4 and pH 5 being much larger than that between pH 5 and pH 6. Moreover, higher concentrations are necessary to reach the plateau region of adsorption at pH 4 (note logarithmic scale). The pH dependence is explained by the protonation / deprotonation of acidic centres both at the humic colloids and at the sand surface. At high pH, the release of protons leaves a negative surface charge on both sides, and adsorption is counteracted by electrostatic repulsion.

On the other hand, the increased dissociation provides more sites for metal complexation. As shown in Figure 8, humate complexation of lanthanum is substantially higher at pH 6 than at pH 4. The application of ^{140}La as a radiotracer allows measurements down to picomolarconcentrations. Obviously, the ratio of aqueous and organo-complexed metal species remains unchanged within the range investigated.

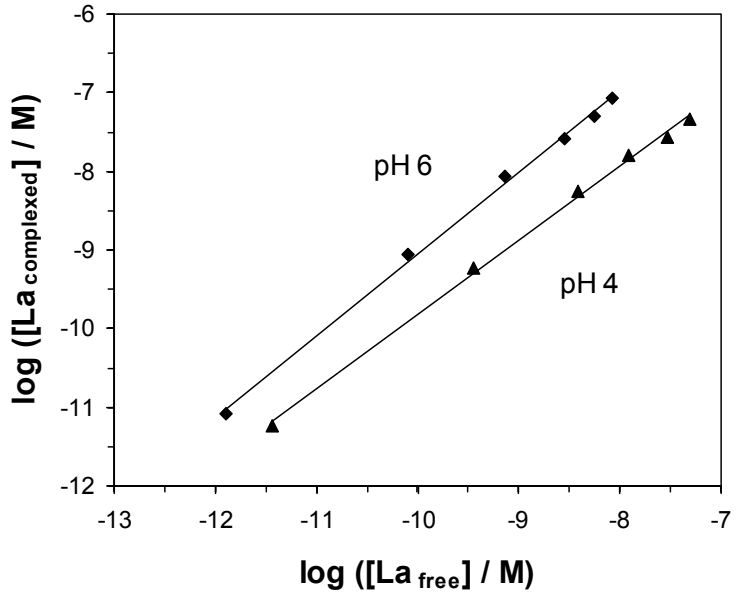

Figure 8. Humate complexation of La(III) with Aldrich HA in 0.1 M $NaClO_4$ at pH 6 and pH 4 depending on metal concentration (radiotracer experiments with [^{140}La]La).

The combined effects of these processes on the pH-dependent adsorption behaviour of La(III) are visualised in Figure 9 where the influence of HA presence is demonstrated for pH 4 and pH 6. Already at a relatively low HA concentration of 5 mg L^{-1}, adsorption isotherms are shifted markedly in both cases. However, the changes tend toward opposite directions.

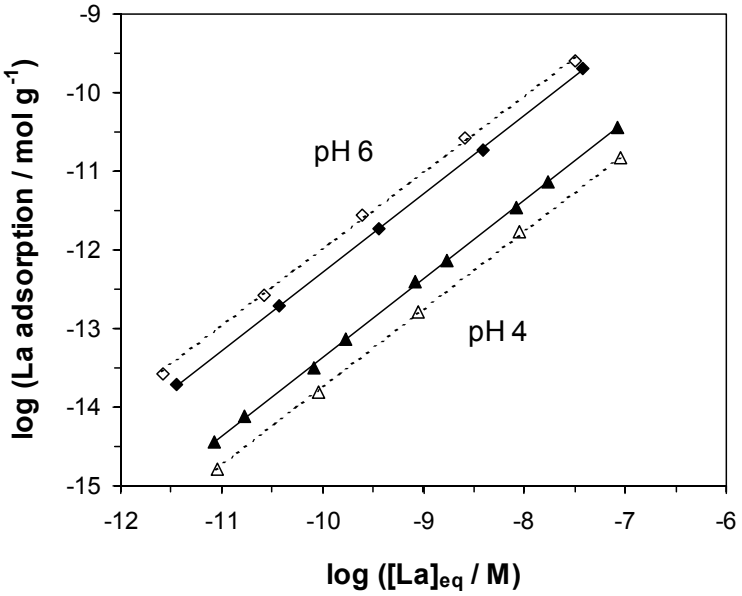

Figure 9. Adsorption of La(III) on sand in 0.1 M $NaClO_4$ at pH 6 and pH 4 in the absence (open symbols) and in the presence (full symbols) of 5 mg L^{-1} Aldrich HA (radiotracer experiments with [^{140}La]La).

At pH 6, metal adsorption is decreased in the presence of HA. Humate complexation and adsorption of La stand in competition to each other since HA adsorption is of minor importance at this pH. Consequently, migration of actinides would be facilitated in this case. In contrast, metal adsorption is actually mediated by the HA at pH 4 in that additional La is co-adsorbed as a humate complex. In this way, the presence of DOC turns from a source to a sink in terms of actinide migration. Remarkably, the reversal of the influence occurs within the geochemically relevant pH range. By these findings, the problematic role of humic colloids is relativised.

Figure 10 shows analogue investigations at an elevated concentration level (50 mg L^{-1} HA, La concentrations in the micro molar range). In these experiments, the temporal succession of introducing La and HA was varied. After pre-equilibration of two components for 3 days, the third component was added, and the system was equilibrated for further 3 days.

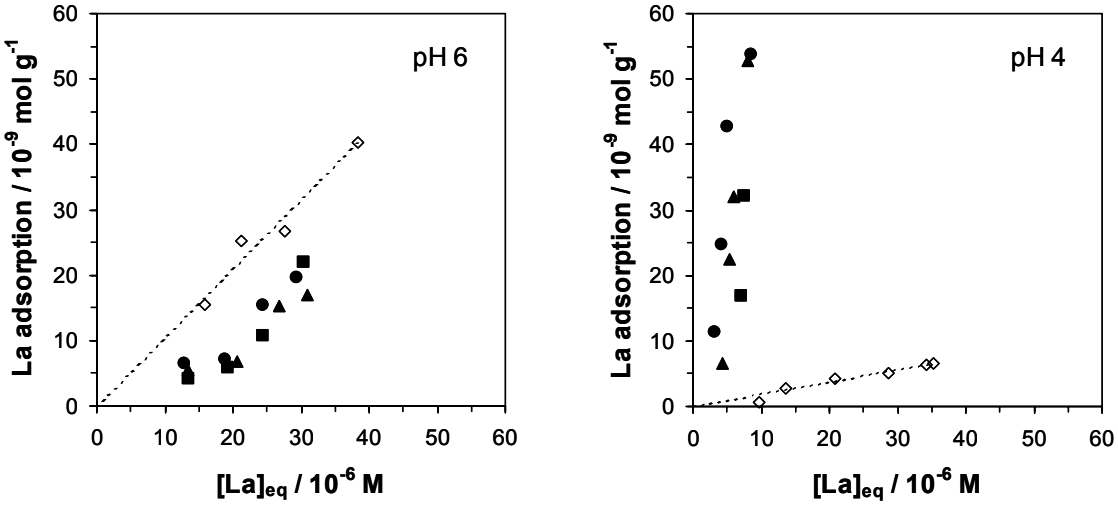

Figure 10. Adsorption of La(III) on sand in 0.1 M $NaClO_4$ at pH 6 and pH 4 in the absence (open symbols) and in the presence (full symbols) of 50 mg L^{-1} Aldrich HA, conducting different modes of equilibration: ▲ La + HA to sand, ■ La to HA + sand, ● HA to La + sand (pre-equilibration and main equilibration 3 days each, analysis by ICP-OES).

Within the limits of accuracy, it turned out to be irrelevant whether the components are contacted simultaneously or in two steps. Hence, the one-step mode was maintained in the following. To discuss the results in terms of reversibility, it must be taken into account that humate complexation and HA adsorption cannot be considered as equilibrium processes, as is demonstrated in later chapters. Thus, the coincidence at pH 6 merely indicates that the direct interaction of metal and solid is reversible, whereas the coincidence at pH 4 suggests that the complexing ability of HA is not changed significantly in the adsorbed state.

3.3.2 Investigations on the system Tb(III) / Aldrich HA / geogenic solids

With the objective to ascertain to what extent the above findings may be generalised, the transition from mobilisation to demobilisation was investigated for other geogenic matrices with different acid-base properties: granite, phyllite and diabase (for characteristics, see chapter 3.1.2.). In these experiments, the longer-lived ^{160}Tb was used instead of ^{140}Ba/^{140}La because pH adjustment of solid-liquid systems proved to be a time-consuming process for the materials under study. Deviating from the studies with La, pH-dependent measurements were performed for fixed initial concentrations of Tb and HA in order to determine the pH of changeover exactly. Adsorption data are represented as partition coefficients K_d, which are defined by Eq. (1) where Γ is the adsorbed amount per unit mass of solid, and c is the equilibrium concentration of a component.

$$K_d = \frac{\Gamma}{c} \tag{1}$$

The pH-dependent influence of humic acid on Tb adsorption onto phyllite, diabase, granite and sand is shown in Figure 11. The accessible pH range is limited to values up to 6.4 due to the onset of Tb hydroxide precipitation. Obviously, the changeover from a competitive situation to an aided adsorption on acidification is not confined to the sand matrix but seems to be a general phenomenon. In all cases, there is a crossing of the pH-dependent adsorption functions (“pH edges”) in the absence and in the presence of HA. At pH values above the crossing point, the humic acid effects a mobilisation, yet below, a demobilisation of the metal compared to the corresponding solid-liquid distribution in the absence of DOC. For diabase, granite and sand, the reversal already occurs at slightly acidic pH values (pH ~ 5) and is thus relevant in view of geochemical systems. Only for phyllite, the pH required for demobilisation is out of range (pH ~ 3), i. e. the presence of humic colloids would be unfavourable in any case.

The pH edges of Tb adsorption in the absence of HA exhibit different profiles. A steady increase is observed for diabase and sand, while the curves for phyllite and granite show a maximum. This is explained by an overlap of two contrary pH-dependent effects. On the one hand, the solid surfaces are deprotonated with increasing pH, thereby promoting adsorption of positively charged ions. On the other hand, hydrolysis becomes important, leading to formation of coordinated metal species with a reduced net charge. Since the individual solids vary in acidity and proton exchange capacity, the two processes are balanced differently.

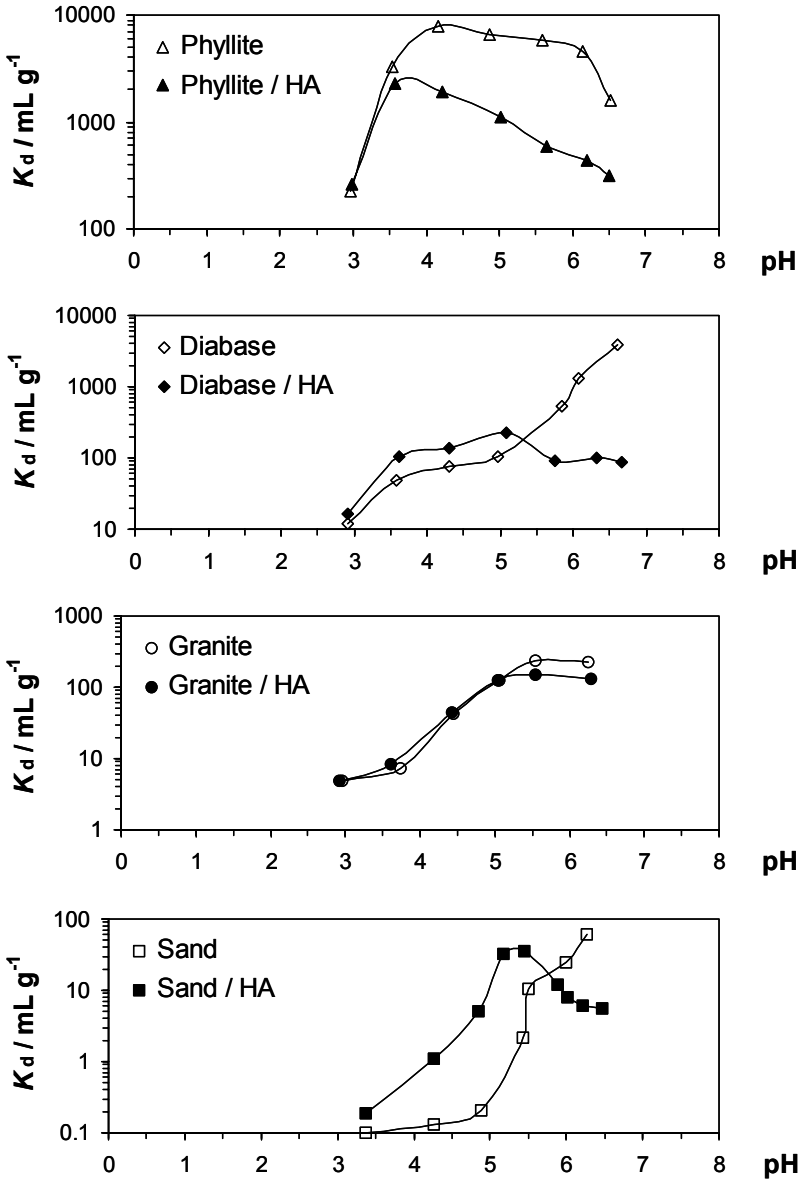

Figure 11. Adsorption of Tb(III) (10^{-7} M) on geogenic solids in 0.1 M $NaClO_4$ depending on the pH value in the absence (open symbols) and in the presence (full symbols) of 5 mg L^{-1} Aldrich HA (radiotracer experiments with [^{160}Tb]Tb).

To understand the underlying principles of the pH edges in the presence of HA, humate complexation of Tb and adsorption of HA were likewise investigated in pH-dependent experiments. As can be seen from Figure 12, the extent of Tb-humate complexation decreases considerably on acidification since the binding sites are blocked by protonation. Whereas the metal is complexed almost completely at pH > 6, the organically bound fraction is reduced to nearly 10% at pH 3.

In Figure 13, the pH edges of the humic acid are shown for the four adsorbents. Generally, adsorption is increased on acidification because the negative charges of adsorptive and adsorbent are diminished. In contrast to humate complexation where the pH dependence is most pronounced in the acidic range, the gradient of HA adsorption vanishes at pH < 4,

which indicates that protonation of the acidic surface centres is completed already under weakly acidic conditions.

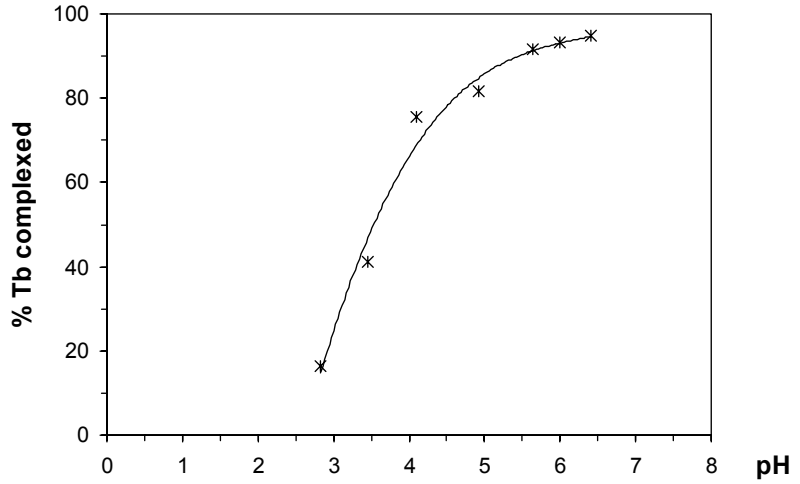

Figure 12. Humate complexation of Tb(III) (10^{-7} M) with Aldrich HA (5 mg L^{-1}) in 0.1 M $NaClO_4$ depending on the pH value (radiotracer experiments with [^{160}Tb]Tb).

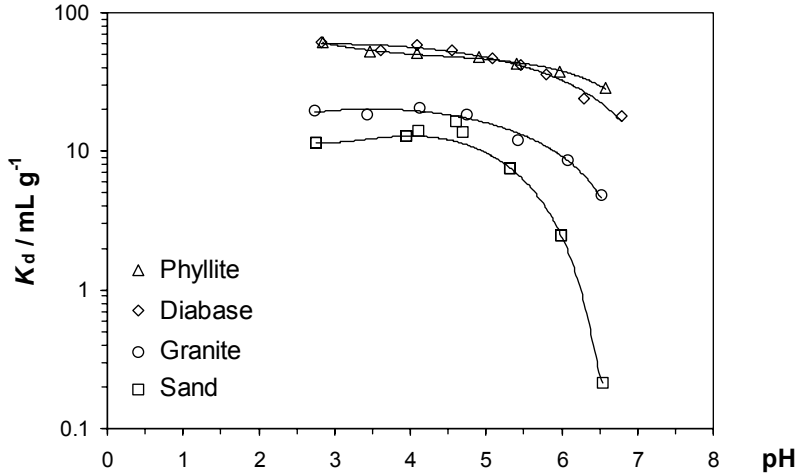

Figure 13. Adsorption of Aldrich HA (5 mg L^{-1}) on geogenic solids in 0.1 M $NaClO_4$ depending on the pH value (radiotracer experiments with ^{131}I-labelled HA).

Equipped with the knowledge of the pH dependencies of humate complexation and HA adsorption, it is possible to explain the relation between the pH edges of Tb adsorption in the absence and in the presence of HA (Figure 11). With increasing pH, dissociation of acidic groups leads to a corresponding gain in binding sites at the colloids (Figure 12) and also to a hindrance of colloid-matrix interaction due to the build-up of an electrostatic barrier (Figure 13). Consequently, a competitive situation arises between metal adsorption and humate complexation. On lowering the pH, humic acid is adsorbed increasingly, thereby adopting a

mediating function. Since, however, humate complexation declines concurrently, the curves converge again at more acidic pH.
The situation may be described by a multi-partitioning model where the single processes are considered as a system of interdependent equilibria as depicted in Figure 14. On the basis of this scheme, an attempt was made to reproduce the pH-dependent influence of HA on Tb adsorption quantitatively.

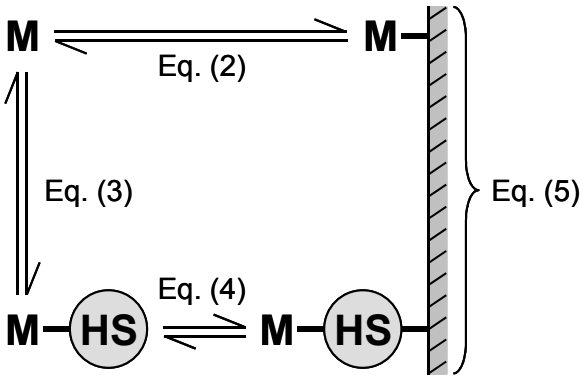

Figure 14. Multi-partitioning approach for metal adsorption in the presence of humic substances.

A partitioning equilibrium was assumed for direct metal adsorption, metal-humate complexation and HS adsorption, represented by Eqs. (2) - (4) where the indices M, S and HS mean “metal”, “solid” and “humic substance”, respectively, and $c_{\mathrm{M}}^{\mathrm{HS}}$ denotes the concentration of organo-complexed metal.

$$K_{\mathrm{d}}^{\mathrm{M/S}} = \frac{\Gamma_{\mathrm{M}}}{c_{\mathrm{M}}} \tag{2}$$

$$K_{\mathrm{d}}^{\mathrm{M/HS}} = \frac{\Gamma_{\mathrm{M}}^{\mathrm{HS}}}{c_{\mathrm{M}}} = \frac{c_{\mathrm{M}}^{\mathrm{HS}}}{c_{\mathrm{M}}\, c_{\mathrm{HS}}} \tag{3}$$

$$K_{\mathrm{d}}^{\mathrm{HS/S}} = \frac{\Gamma_{\mathrm{HS}}}{c_{\mathrm{HS}}} \approx \frac{\Gamma_{\mathrm{M\text{-}HS}}}{c_{\mathrm{M\text{-}HS}}} \tag{4}$$

By combining these equations, one obtains Eq. 5 for co-adsorption of M and M-HS:

$$K_{\mathrm{d}}^{(\mathrm{M+M\text{-}HS})/\mathrm{S}} = \frac{K_{\mathrm{d}}^{\mathrm{M/S}} + K_{\mathrm{d}}^{\mathrm{HS/S}}\, K_{\mathrm{d}}^{\mathrm{M/HS}}\, c_{\mathrm{HS}}}{1 + K_{\mathrm{d}}^{\mathrm{M/HS}}\, c_{\mathrm{HS}}} \tag{5}$$

To reconstruct the pH edge of Tb adsorption in the presence of HA, the experimental values of $K_d^{M/HS}$, $K_d^{HS/S}$ and c_{HS} as a function of pH were fitted by polynomials, and $K_d^{(M+M\text{-}HS)/S}$ was calculated for the experimental $K_d^{M/S}$ / pH data. Figure 15 shows the results of such a calculation for granite as an example.

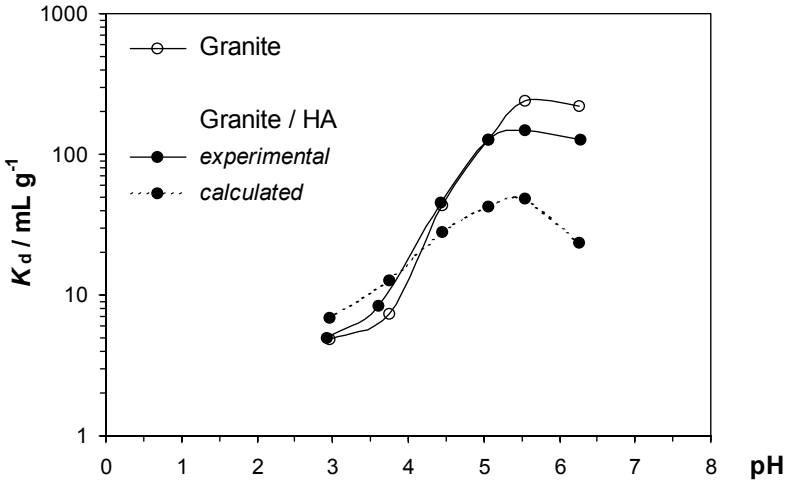

Figure 15. Reconstruction of the influence of HA on the pH-dependent adsorption of Tb onto granite on the basis of the separately measured pH dependencies of the constituent processes by means of a multi-partitioning approach (Eq. 5).

Although there is a significant discrepancy between experimental and calculated values, the changeover from mobilisation to demobilisation is reproduced properly. Note that this modelling was performed without any parameter adjustment. The deviations indicate that humate complexation is overrated in the calculation, which may be due to the fact that mineral leaching was not taken into account. As can be seen from Table 3, release of metal ions from the geogenic solids is substantial, especially in acidic solution. Accordingly, competitive complexation of these metals may be important (see chapter 3.6.1.). Data for $K_d^{M/HS}$ were, however, acquired in the absence of competing ions. Furthermore, equating the measured adsorption of HS with the behaviour of the organo-complex M-HS (Eq. 4) represents a simplification. As demonstrated in later chapters, HS constituents are not equally involved in humate complexation. Finally, the adsorbed species M and M-HS were considered independently of each other, neglecting that metal adsorption can be impeded by blockade effects of M-HS and, on the other hand, adsorption of M-HS is promoted by metal adsorption since the negative surface charge is compensated.

Table 3. Leaching of metal ions from the geogenic solids during equilibration, depending on the pH value. (Measurements were performed in conjunction with the pH edge experiments for HA, using ICP-OES.)

	pH	Ca (µM)	Mg (µM)	Al (µM)	Fe (µM)	Si (µM)
Phyllite	2.8	1008	768	476	14	725
	3.5	939	618	49	1	348
	4.1	853	569	11	< 1	210
	4.9	762	504	2	< 1	156
	6.0	718	475	1	< 1	111
Diabase	2.8	1821	1038	787	652	1002
	3.6	1619	513	289	316	479
	4.1	1528	343	153	144	329
	4.6	1386	242	43	45	226
	5.1	1298	210	8	5	193
Granite	2.7	397	122	637	315	927
	3.4	266	73	210	130	264
	4.1	161	47	61	21	84
	4.7	128	42	12	1	54
	5.4	121	40	< 1	< 1	48
Sand	2.7	8	10	108	6	85
	3.3	6	7	84	3	85
	3.9	3	4	59	1	75
	4.6	3	3	16	< 1	55
	5.3	4	3	3	< 1	42

3.4 Adsorption behaviour of different humic substances

3.4.1 Batch experiments

Figure 16 shows adsorption isotherms of different humic substances on sand. Generally, adsorption is significant already at pH 6, i. e. the capability of a demobilisation of metal ions on acidification is not confined to the Aldrich material. Langmuirian behaviour is observed in all cases (see curve fits). As is evident from the pH dependence described in chapter 3.3., adsorption of HS is essentially determined by the charge density of the colloids. Accordingly, the fulvic acid is least adsorbed due to the increased content of acidic groups. The highest adsorption is found for the bog soil HA. Adsorption isotherms of Aldrich HA and HA M42 are nearly superimposed and are placed between the natural aquatic HA and FA. Thus, both materials are qualified as reference substances for natural aquatic HS.

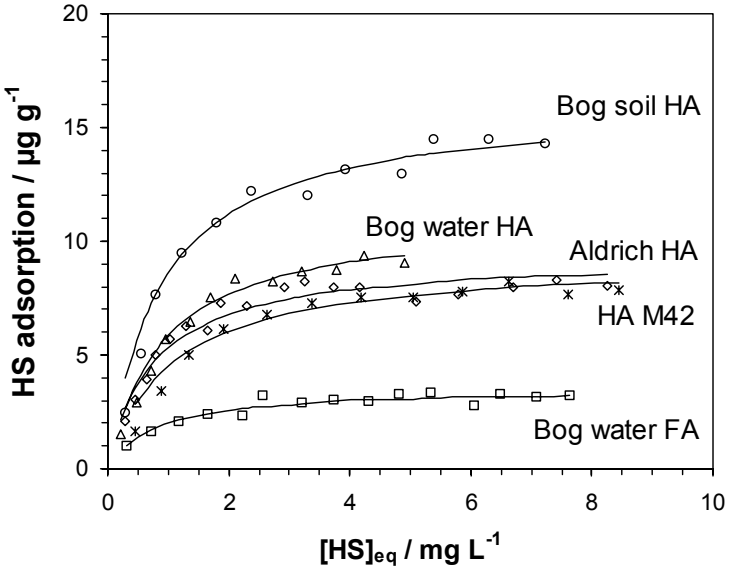

Figure 16. Adsorption isotherms of different HS on sand in 0.1 M $NaClO_4$ at pH 6 (radiotracer experiments with ^{131}I-labelled HS).

3.4.2 Column experiments

The static measurements described in the previous chapter refer to the marginal case of equilibrium adsorption, which is not attained under flow conditions. Nonetheless, equilibrium constants are needed as input data for transport models, and batch experiments are most suitable for the study of fundamentals such as the influence of substantial factors and physico-chemical conditions. However, for instance, reversible and irreversible adsorption cannot be distinguished. The following column experiments were undertaken to characterise HS adsorption in terms of reversibility and selectivity. For this purpose, differently labelled HS were introduced by pulse injection into a continuous open-loop flow of 0.1 M $NaClO_4$ solution (for details see chapter 2.2.3.).
As can be seen from the charts in Figure 17, recovery is significantly lower than 100% for all HS and geogenic solids under study. In spite of the permanent rinsing flow, a certain fraction is retained at the solid matrix. Interestingly, recoveries based on ^{131}I labelling (upper bars) are quite different from those based on ^{111}In labelling (lower bars). As a rule, recoveries are lower in the latter case. Obviously, the ^{111}In labelling process, standing for actinide-humate interaction, is selective towards HS molecules with a lower mobility compared to the bulk of the multi-component system which is represented by ^{131}I labelling. Alternatively, molecules affected by complexation may be rendered more immobile. In general, the difference is most pronounced for the fulvic acid. These findings point out that the behaviour of actinide-humate complexes is not necessarily identical with the behaviour of humic or fulvic acids as a whole.

Similar experiments were performed with the gel matrix used for sequential chromatographic analysis (chapter 2.2.2.). In this case, GPC was run at different pH values (1st sequence), and the immobilised fraction was eluted with 0.1 M NaOH (2nd sequence). In Figure 18, the ratios of the respective peak areas *A* (UV chromatograms) are shown for the different humic substances.

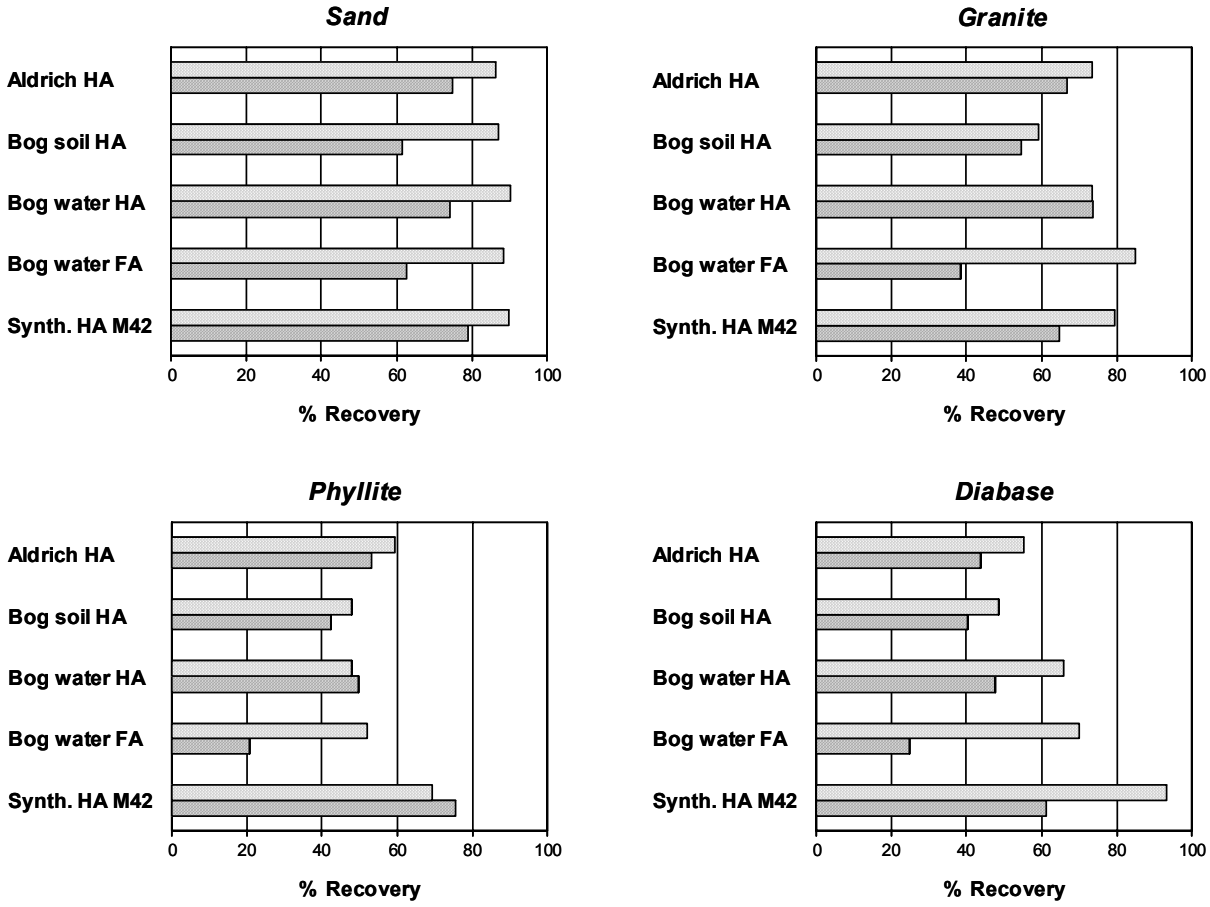

Figure 17. Column experiments on permanent retention of HS at geogenic matrices, applying ^{131}I labelling (upper bars) and ^{111}In labelling (lower bars). For exp. details see chapter 2.2.3.

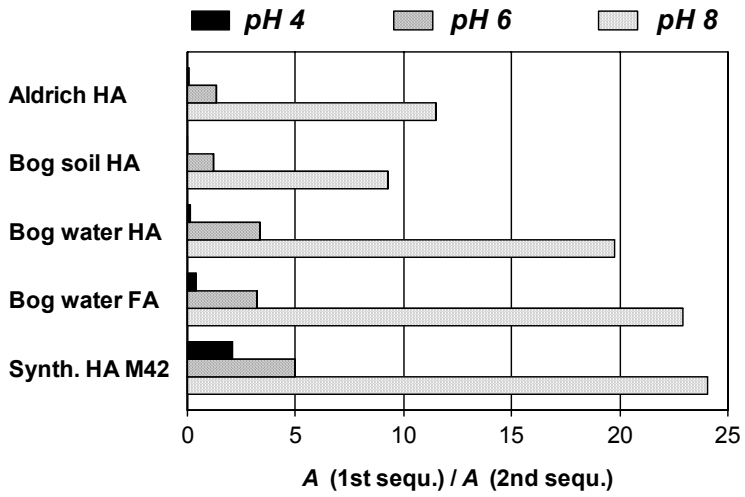

Figure 18. Ratios of the peak areas of 1st and 2nd sequence in sequential chromatograms (UV detection) of HS for different pH (0.01 M KCl, pH 6: acetate buffer, pH 8: borate buffer).

Evidently, immobilisation within the column is essentially controlled by the pH value, the dependence being the same as found in batch adsorption experiments with geogenic solids. Consequently, it may be assumed that the permanent retention is due to irreversible adsorption processes rather than filtration by clogging effects, which would not exhibit this pH dependence.

3.5 Octanol-water partitioning of humic substances

Owing to the complex nature of HS, the influence of external parameters on solid-liquid partitioning is not only explained by the variable charges of adsorptive and adsorbent but also by intrinsic changes within the colloids. Octanol-water partitioning was chosen as a criterion to reflect these alterations under varying solution conditions, thereby excluding the effect of the solid phase. Detailed investigations on liquid-liquid partitioning of HS were hitherto missing in literature, which is also due to experimental reasons. Since HS are prone to be adsorbed at the walls of the containing vessel, both phases have to be analysed directly. In the case of strongly asymmetric partition equilibria, the sensitivity of usual detection methods (DOC analysis, UV photometry) is not sufficient. This analytical problem was overcome by radiolabelling of HS, providing a signal intensity that allows reliable measurements even at low solute concentrations as encountered in nature.

As depicted in Figure 19, partitioning of HS represents the sum of numberless interdependent equilibria, superimposed by aggregation processes which are determined by the respective solvent. The Nernst partition law strictly applies to the distribution of identical species and is thus restricted to pure non-ionic substances which do not associate or dissociate. For that reason, a thermodynamic treatment of HS partitioning would be unfounded. Partition ratios were solely employed as a measure to characterise HS with respect to their overall hydrophilicity.

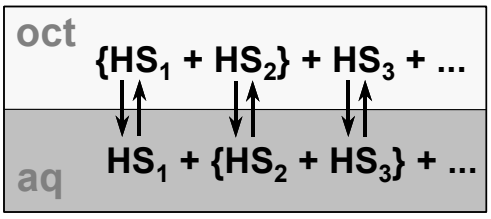

Figure 19. Schematic representation of HS partitioning in the octanol-water system.

Experiments were performed depending on pH, ionic strength *I* and HS concentration *c*. Furthermore, results obtained by different labelling techniques were compared. In Figure 20, partition ratios $P_{O/W} = c_O / c_W$ of different HS are represented as negative logarithms indicating the degree of hydrophilicity. To demonstrate the effects of the respective parameter variations, data are depicted in relation to a fixed set of variables in each diagram.
According to their nature as polyelectrolytes, HS exhibit a strong preference for the aqueous phase, aquatic HS being more hydrophilic than HS extracted from solid material (Aldrich HA, bog soil HA). The affinity for the aqueous environment is enhanced on raising the pH value

from 4 to 6 (chart a) since deprotonation of the acidic groups is accompanied with a gain in polarity. An increase in ionic strength has a similar effect (chart b), which may be attributed to structural changes induced by the background electrolyte, leading to an augmented exposure of hydrophilic units within the colloids. As well, partition ratios of HS proved to be dependent on concentration (chart c), emphasising the inapplicability of Nernst's law.
If ^{131}I labelling is employed instead of ^{111}In labelling, partition ratios indicate a more hydrophobic behaviour (chart d), providing further evidence that the target structures of metal-humate complexation are not evenly distributed over the total ensemble of HS entities. As can be concluded from structural comparisons between humic and fulvic acids, the functional groups susceptible to complexation are concentrated in smaller colloids, rendering them more hydrophilic than the average of the polydispersive system. By using ^{111}In as a radiolabel, these entities are over-represented.

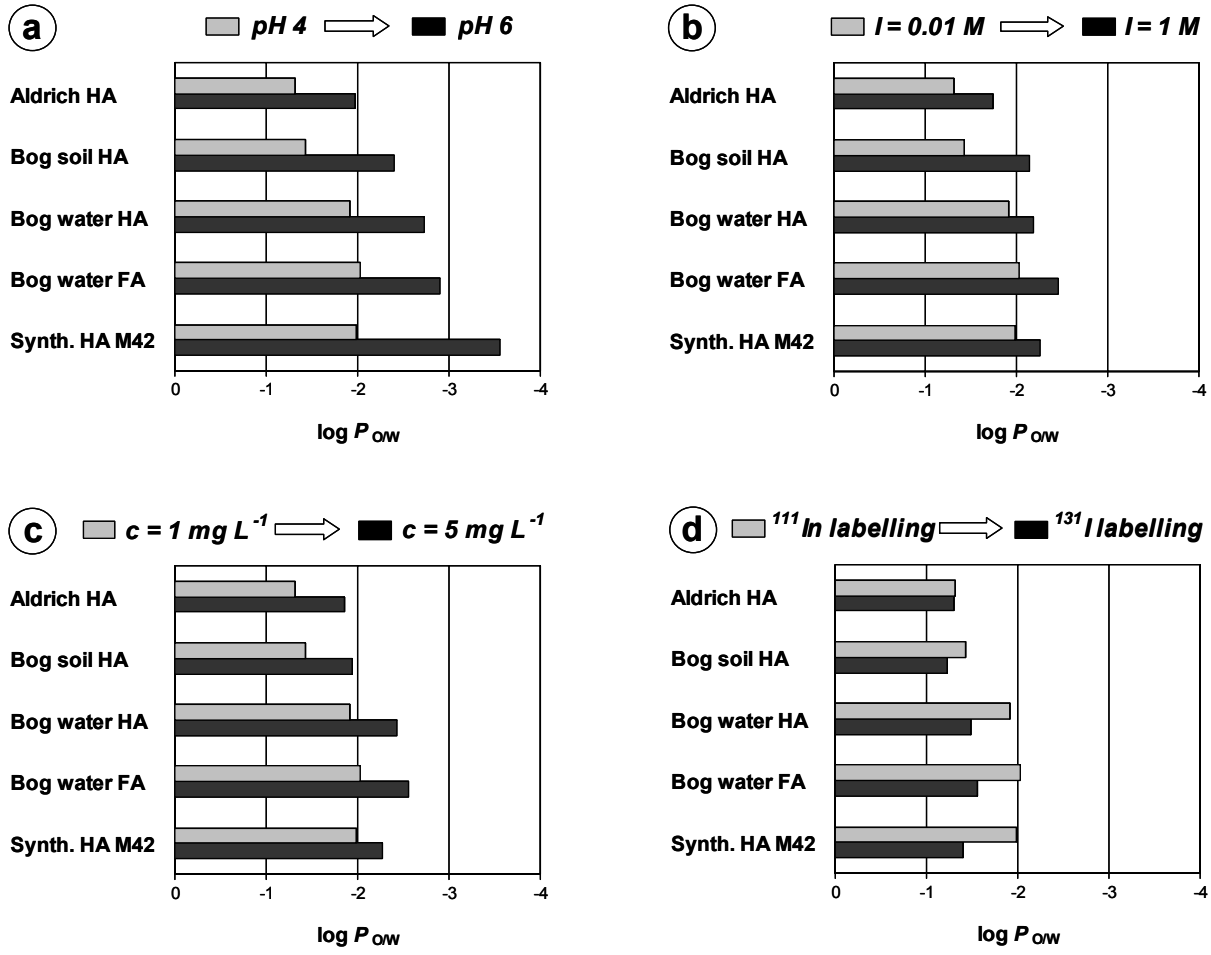

Figure 20. Octanol-water partition ratios of radiolabelled HS depending on pH value (a), ionic strength (b), HS concentration (c) and labelling technique (d). The upper parts of the bar pairs refer to 1 mg L^{-1} ^{111}In-HS in 0.01 M $NaClO_4$ (pH 4) in each diagram, the lower parts represent the effect of the parameter variation indicated on top of the respective chart.

To conclude, radioanalytical partitioning measurements proved to be a useful tool to reflect changes in HS characteristics induced by internal and external alterations.

3.6 Competitive effects of Al(III) on complexation and adsorption of La(III) with humic substances

3.6.1 Effects on complexation

The following radiotracer studies were undertaken with the objective to specify a threshold concentration of aluminium above which displacement of actinide ions from humic colloids becomes important. To enable general conclusions to be drawn, various humic substances were involved. An HS concentration of 5 mg L^{-1} was chosen to represent an average content of DOC.

Competitive complexation of La and Al with four different HS was first studied at a La concentration of 10^{-11} M (Figure 21a), i. e. as close as possible to actinide concentrations as they are expected in migration processes. The concentration of organically bound La is shown depending on the total concentration of Al. Within the limits of accuracy, the complexed La fraction remains constant throughout the sub-micromolar range, in spite of an Al excess of up to 10^5. Only above an Al concentration of 10^{-6} M, there is a clear decreasing trend, which applies to all HS under investigation.

No attempt was made to account for residual metal contents within the humic material. As is evident from the resistance toward the purification process (see chapter 3.1.1.), this fraction is not equivalent to introduced metals in that it does not participate in exchange processes. A summary treatment would thus be inappropriate.

The experiments were repeated at a La concentration of 10^{-8} M (Figure 21b). Again, displacement is not detectable at Al concentrations below 10^{-6} M. Obviously, the occurrence of competitive effects is confined to high metal loads, irrespective of the excess of Al over La. Unless the capacity of the colloids is nearly exhausted, the presence of competing metal ions appears to be irrelevant in respect of humate complexation.

In the above experiments, both metals were contacted simultaneously with the humic substances, which does not actually correspond to real situations to be considered since the contact with the competing ion will occur prior or subsequent to actinide-humate complexation. For that reason, displacement was examined under different equilibration conditions (Figure 22). It is obvious that the distribution of free and complexed La changes significantly if the metals are introduced in two steps. Compared to the simultaneous complexation of La and Al, the competitive effect is more pronounced if aluminium is pre-equilibrated with humic acid prior to the addition of lanthanum and is less pronounced in the reverse case.

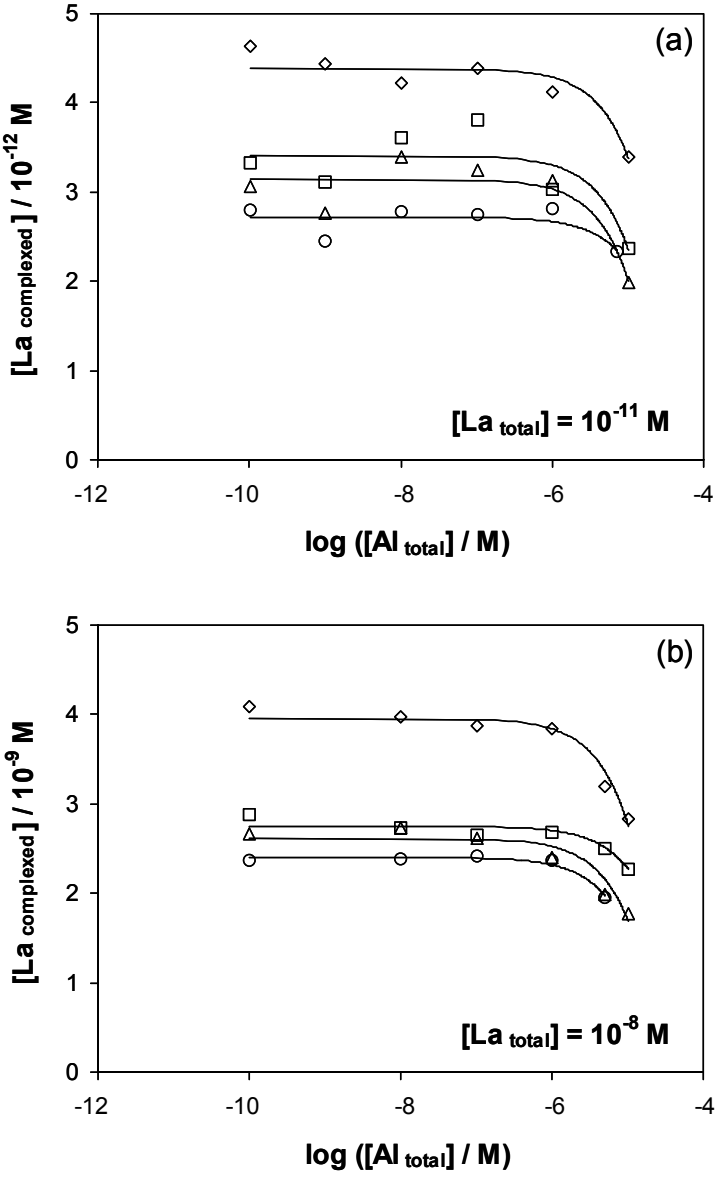

Figure 21. Influence of Al(III) on humate complexation of La(III) with various HS (5 mg L^{-1}) in 0.1 M $NaClO_4$ at pH 4 (radiotracer experiments with [^{140}La]La). Humic substances: ◇ Aldrich HA, □ Bog Water FA, △ Bog Water HA, ○ Bog Soil HA.

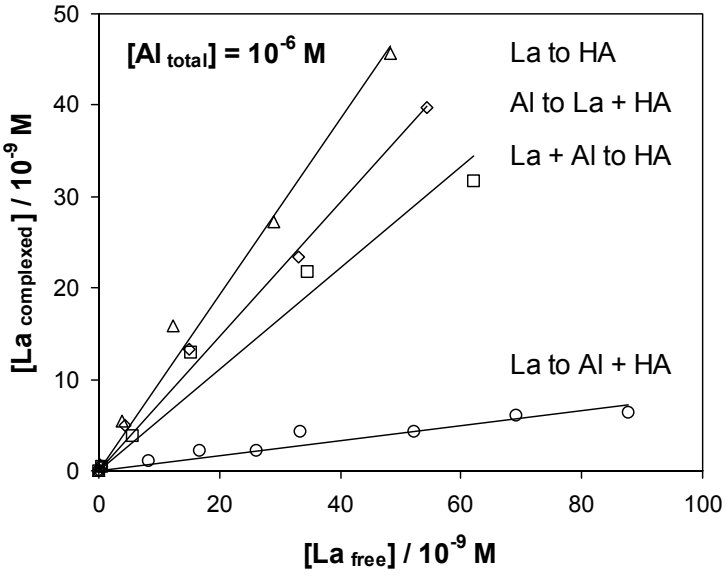

Figure 22. Humate complexation of La(III) and Al(III) with Aldrich HA (5 mg L^{-1}) in 0.1 M $NaClO_4$ at pH 4 depending on the mode of introducing the metal ions (equilibration time: 48 h or 2 × 24 h in case of two-step addition, radiotracer experiments with [^{140}La]La).

The metal exchange is thus kinetically hindered, suggesting that the binding process is accompanied by structural changes within the colloidal network, leading to a partial irreversibility. These findings are in accordance with batch and column experiments on actinide-humate complexation which yielded evidence that complex dissociation is, in part, subject to kinetic hindrance [26, 27].

3.6.2 Effects on adsorption

The influence of competitive humate complexation on the mobility of actinide ions depends on the solid-liquid partitioning of the humic colloids under the present geochemical conditions. In circum-neutral solutions, the facilitated transport of metal ions is counteracted by competitive complexation. Contrary, at low pH where metal adsorption is enhanced by humate adsorption (see chapter 3.3.), a mobilising effect is expected. Figures 23 and 24 show La adsorption onto sand under the same competitive conditions as in the above studies on complexation.

No influence was observed in systems without of HA. In the presence of HA, adsorption tends to decrease above the threshold concentration of 10^{-6} M Al where competition becomes significant (Figure 23). Nonetheless, the effect turns out to be of minor importance in this respect. Accordingly, a possible dependence on the temporal succession of equilibration steps was not detectable within the limits of error (Figure 24).

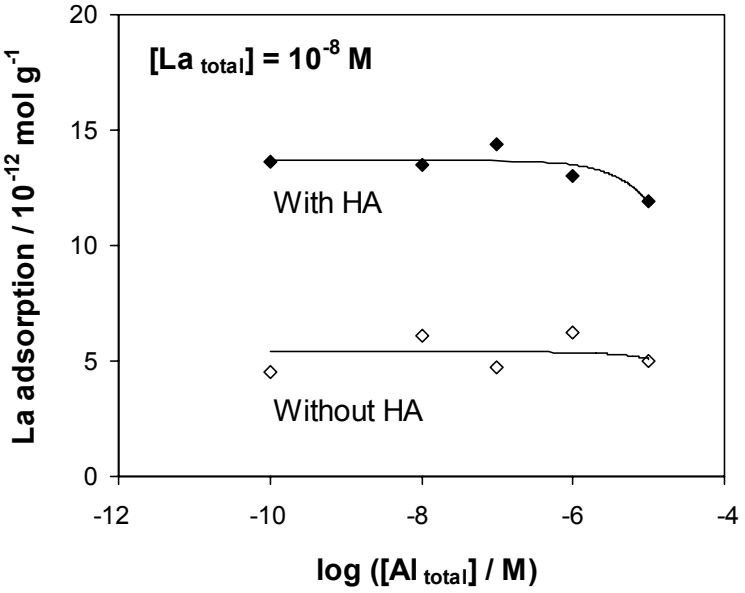

Figure 23. Influence of Al(III) on adsorption of La(III) onto sand in the absence and in the presence of Aldrich HA (5 mg L^{-1}) in 0.1 M $NaClO_4$ at pH 4 (radiotracer experiments with [^{140}La]La).

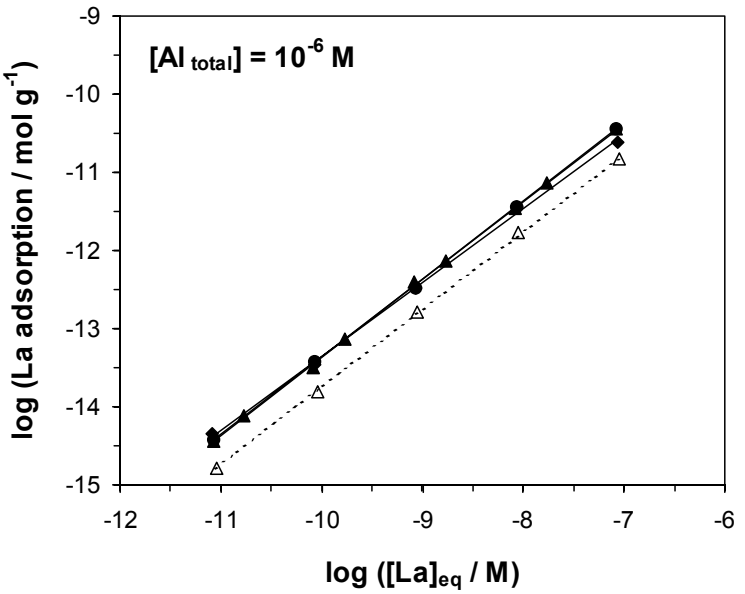

Figure 24. Adsorption of La(III) onto sand in the absence and in the presence of Al(III) and Aldrich HA (5 mg L^{-1}) in 0.1 M $NaClO_4$ at pH 4 depending on the mode of introducing the metal ions (equilibration time: 48 h or 2 × 24 h in La / Al systems). Modes of equilibration: △ La to sand, ▲ La + HA to sand, ◆ Al to La + HA + sand, ● La to Al + HA + sand (radiotracer experiments with [^{140}La]La).

3.7 Immobilisation of humic colloids by flocculation on loading with trivalent metals

3.7.1 Investigations on the system Al(III) / Aldrich HA

The investigations on Al competition are limited to concentrations not higher than 10^{-5} M. If this value is exceeded, coagulation of the humic colloids is induced as a consequence of the high metal loads. Depending on the dosage of Al, precipitation takes place within a period of few minutes up to several days. To characterise the impact of higher-valent electrolytes on the colloid-borne migration, it is essential to include flocculation as an immobilising process.
In Figure 25, flocculation of Aldrich HA induced by Al is demonstrated for different HA concentrations by means of the UV absorption of the supernatant, measured 2 weeks after addition. Due to the polydispersity of the colloidal system, coagulation proceeds gradually with increasing metal concentration (see also Figure 27). Up to a certain metal content, HA solutions remain stable. On further addition, an increasing proportion of HA is precipitated until a maximum flocculation is attained. The higher the concentration of HA, the more Al is required. Consequently, the process is clearly attributable to charge compensation, the necessary metal concentration being determined by the total capacity of the colloids.

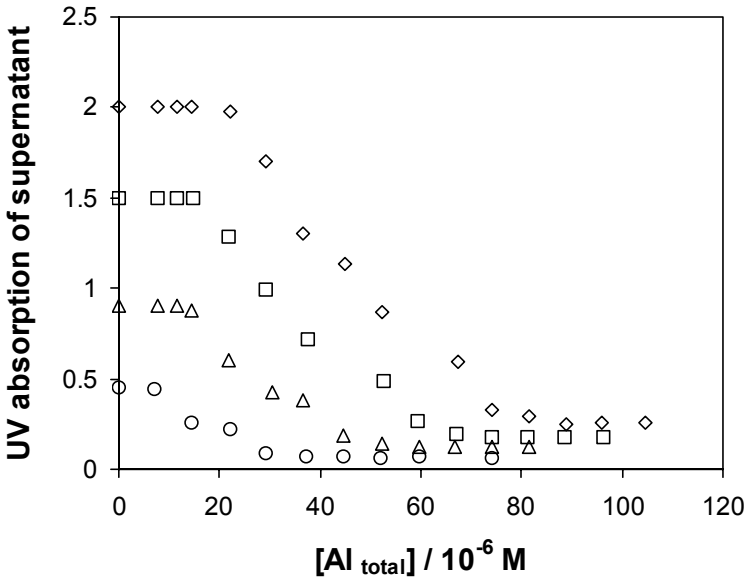

Figure 25. Flocculation of Aldrich HA on addition of Al(III) at pH 4. Data series represent the decrease in the UV absorption (254 nm) of the supernatant for different starting concentrations of HA: ◇ 50 mg L^{-1}, □ 37.5 mg L^{-1}, △ 25 mg L^{-1}, ○ 12.5 mg L^{-1}.

Figure 26a shows that the metal concentration required for maximum precipitation is influenced by pH and ionic strength. If the pH value is raised from 4 to 6, deprotonation of acidic groups results in a higher colloid charge to be compensated. Furthermore, the effective charge of the aluminium species is reduced due to hydrolysis. An increase in ionic strength promotes the coagulation process, which is ascribed to the charge screening effect of the supporting electrolyte.

HA solutions are not depleted entirely by flocculation. As can be seen from Figures 25 and 27, there is a certain fraction which is resistant to precipitation even at metal concentrations far beyond the flocculation interval. The residual UV absorption depends linearly on the total HA concentration as shown for Al in Figure 26b. Interestingly, the resistant HA proportion is also found to be dependent on pH and ionic strength. Most likely, the extent of depletion is related to the amount of Al which is involved in the flocculation process (cf. Figure 26a). Owing to its cross-linking ability, Al is more effective than protons in that it effects a co-precipitation of HA entities which would otherwise be excluded from coagulation under the respective conditions. This supports the notion that the confined reversibility of humate complexation of higher-valent metals is due to permanent structural alterations induced by intra and intermolecular bridging effects.

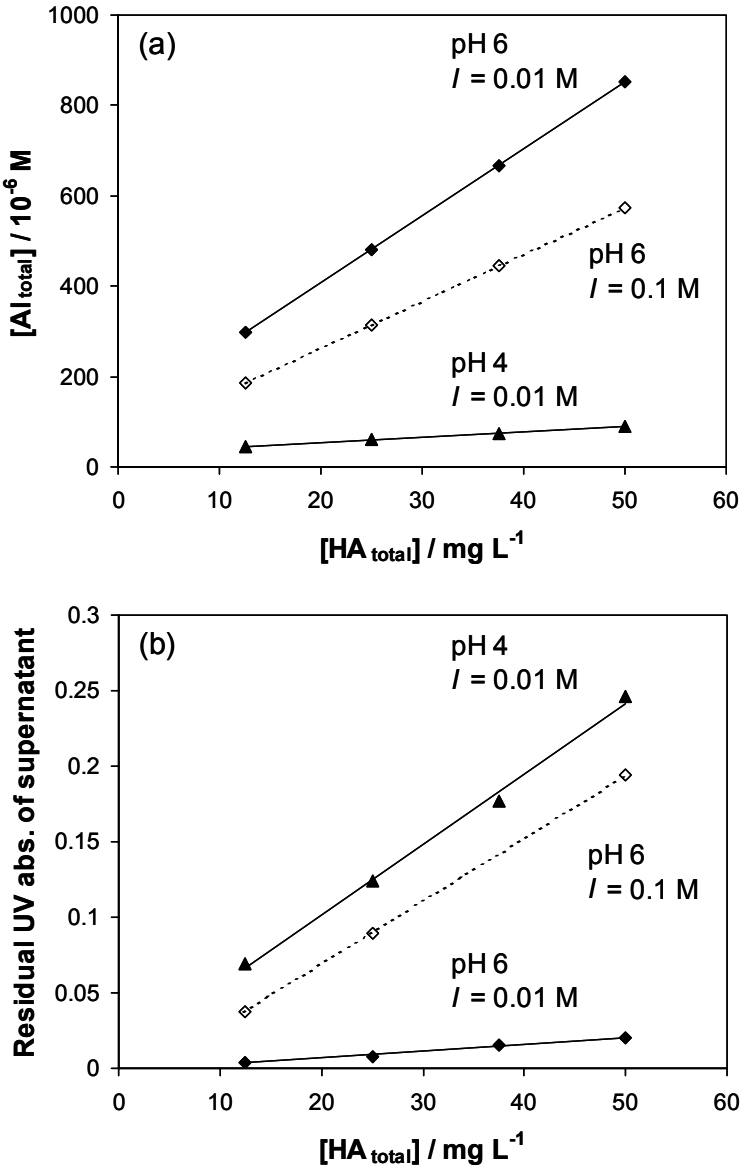

Figure 26. Effect of pH and ionic strength on the Al concentration required for maximum flocculation (a) and on the corresponding residual UV absorption (254 nm) of the supernatant (b).

3.7.2 Comparison of flocculation efficiencies and complex stabilities for trivalent metals

Flocculation of Aldrich HA was also investigated for other trivalent metals. In Figure 27, flocculation by Al is shown in comparison with Ga, In, Sc, Y and La. In spite of the equal ion charge, the individual metals differ in efficiency. For example, the concentration of Sc at maximum precipitation amounts to about a tenth of the required Al concentration.

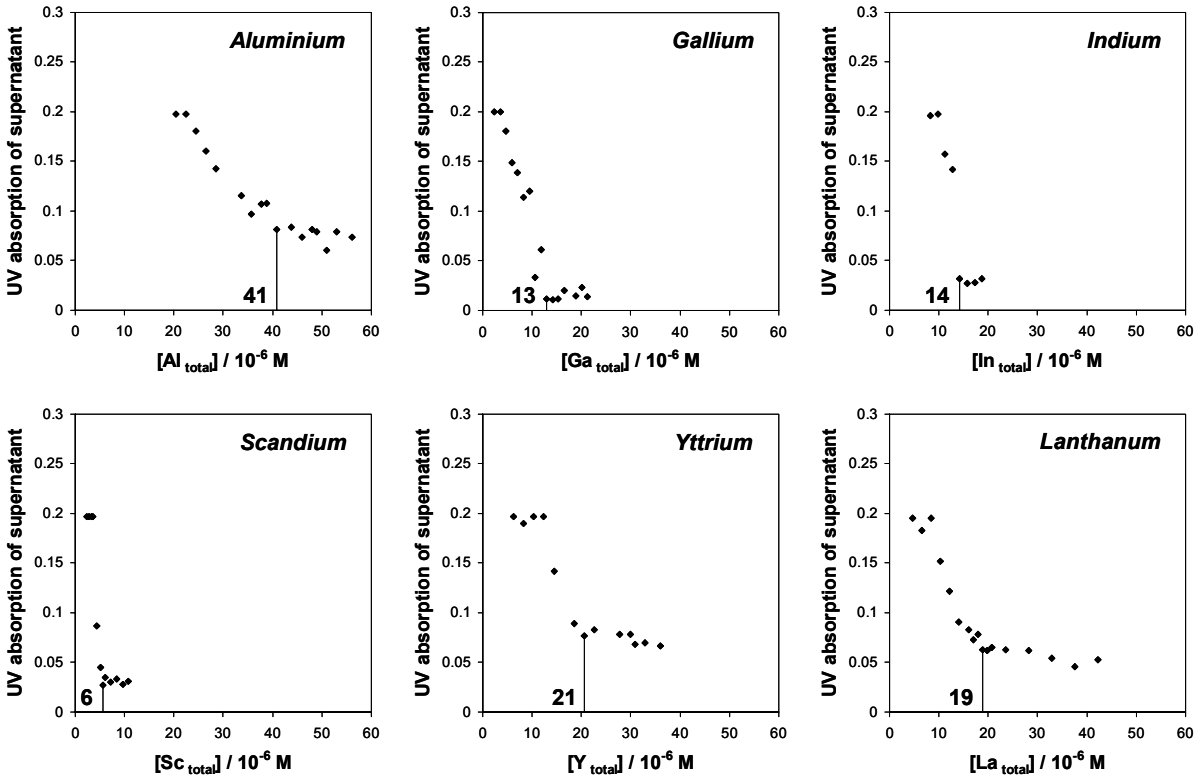

Figure 27. Flocculation of Aldrich HA (5 mg L^{-1}) induced by trivalent metals in 0.1 M $NaClO_4$ at pH 4, demonstrated by means of the UV absorption (254 nm) of the supernatant.

It seemed likely that the variations are due to differences in the degree of metal-humate interaction. In order to verify this assumption, speciation measurements were conducted under the same experimental conditions as employed in the flocculation studies. The results are depicted in Figure 28, where the concentrations of organically bound metals are plotted against the respective total concentrations. Again, considerable differences are observed among the trivalent elements. Because of the absence of any curvature, the data cannot be evaluated on the basis of loading capacities according to the charge neutralisation model [28], although metal loads are close to saturation in these experiments.

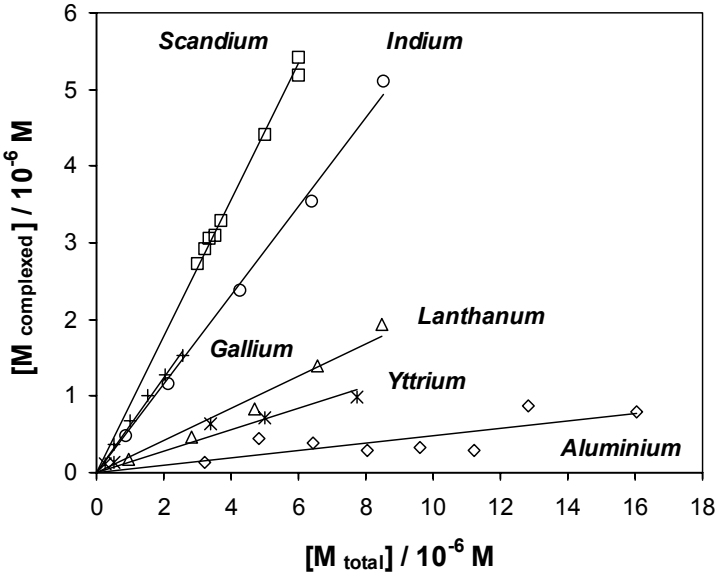

Figure 28. Complexation of trivalent metals with Aldrich HA (5 mg L^{-1}) in 0.1 M $NaClO_4$ at pH 4.

In Table 4, the complexed proportions (slopes of the regression lines in Figure 28) are listed together with the respective flocculation limits indicated in the diagrams of Figure 27. Obviously, both quantities are inversely related, supporting the proposition that the mechanism of flocculation is based on homocoagulation of humic material induced by charge compensation. There is no indication of a heterocoagulation with metal hydroxides.

Table 4. Compilation of flocculation efficiencies and respective complexed proportions.

	[M_{total}] required for max. pptn. (µM)	**Complexed proportion**	**[$M_{complexed}$] at max. pptn. (µM)**
Sc	6	89%	5.3
Ga	13	62%	8.1
In	14	58%	8.1
La	19	21%	4.0
Y	21	14%	2.9
Al	41	5%	2.1

By combining the results from speciation and flocculation experiments, one can calculate the concentrations of those metal ions which are adherent to the colloids when flocculation is completed. These values (also shown in Table 4) differ to some extent, which may be indicative of different degrees of hydrolysis, although this process does not play a major role at pH 4 in dilute systems.

Altogether, the binding affinities vary within a range that is by far not comparable to the discrepancy in the natural abundances of Al and the other trivalent metals under study. In conclusion, since it has been ascertained that the occurrence of both competitive complexation and flocculation is confined to high metal loads, it can be stated that polyvalent trace metals are not a decisive factor in terms of the humic colloid-borne transport, even though they can still be present in large excess over released actinides. The relevance of these effects is in fact limited to major elements like aluminium and iron.

4 Conclusions and outlook

Already a minor DOC presence was found to affect the mobility of heavy metals in geochemical systems considerably. Due to the strong interaction, metal partitioning is essentially determined by the solid-liquid distribution of the humic carrier colloids in the form of adsorption and flocculation processes. Both mechanisms were shown to be highly sensitive towards alterations in solution parameters such as pH value and electrolyte content. As a consequence, both mobilisation and demobilisation of contaminant metals are possible to occur depending on the particular circumstances.
The environmental conditions of the colloid-borne transport are specific to each geochemical system and must be examined individually in order to describe their influence. Besides geogenic factors, implications of anthropogenic inputs have to be considered as well. To establish a database for the development of site-specific transport models, the elementary partitioning processes (complexation, adsorption, flocculation) must be studied under milieu conditions which are determined by potential host formations. Whereas many data are already available for saline systems, extensive investigations are still required for clay and granite as alternative formations. The findings on the influence of aluminium raise questions with regard to the role of iron as the most abundant higher-valent metal in natural waters. Owing to their analytical potential, radiotracer techniques are assigned a key position in these investigations. The understanding of the complex distribution processes represents a basis for dynamic studies accounting for the influence of kinetic and hydrodynamic effects under flow conditions. Further developments of selective and non-selective labelling procedures, also for PET investigations with geogenic matrices, are intended for this purpose.

5 References

[1] Lieser, K. H., Ament, A., Hill, R., Singh, R. N., Stingl, U., Thybusch, B., *Radiochim. Acta* **49** (1990) 83-100.

[2] Choppin, G. R., *Radiochim. Acta* **58/59** (1992) 113-120.

[3] Kim, J. I., Delakowitz, B., Zeh, P., Klotz, D., Lazik, D., *Radiochim. Acta* **66/67** (1994) 165-171.

[4] MacCarthy, J. F., Sanford, W. E., Stafford, P. L., *Environ. Sci. Technol.* **32** (1998) 3901-3906.

[5] Dearlove, J. P. L., Longworth, G., Ivanovich, M., Kim, J. I., Delakowitz, B., Zeh, P., *Radiochim. Acta* **52/53** (1991) 83-89.

[6] Kim, J. I., Zeh, P., Delakowitz, B., *Radiochim. Acta* **58/59** (1992) 147-154.

[7] Marley, N. A., Gaffney, J. S., Orlandini, K. A., Cunningham, M. M., *Environ. Sci. Technol.* **27** (1993) 2456-2461.

[8] Artinger, R., Kienzler, B., Schüßler, W., Kim, J. I., *J. Contam. Hydrology* **35** (1998) 261-275.

[9] Buckau, G., Artinger, R., Fritz, P., Geyer, S., Kim, J. I., Wolf, M., *Appl. Geochem*. **15** (2000) 171-179.

[10] Bidoglio, G., Grenthe, I., Qi., P., Robouch, P., Omenetto, N., *Talanta* **38** (1991) 999-1008.

[11] Seibert, A., Mansel, A., Marquardt, C. M., Keller, H., Kratz, J. V., Trautmann, N., *Radiochim. Acta* **89** (2001) 505-510.

[12] Aiken, G. R., in: “Humic substances in soil, sediment and water: Geochemistry and isolation”, Aiken, G. R., MacKnight, D. M., Wershaw, R. L., MacCarthy, P. (Eds.), Wiley-Interscience, New York, 1985, pp. 363-385.

[13] Swift, R. S., in: “Methods of soil analysis. Part 3: Chemical methods”, Sparks, D. L. (Ed.), Soil Sci. Soc. Am., Madison, 1996, pp. 1018-1020.

[14] Kim, J. I., Buckau, G., “Characterization of reference and site specific humic acids”, RCM report 02188, Technische Universität München, 1988.

[15] Pompe, S., Brachmann, A., Bubner, M., Geipel, G., Heise, K. H., Bernhard, G., Nitsche, H., *Radiochim. Acta* **82** (1998) 89-95.

[16] Rößler, D., Franke, K., Süß, R., Becker, E., Kupsch, H., *Radiochim. Acta* **88** (2000) 95-100.

[17] Hiraide, M., Tillekeratne, S. P., Otsuka, K., Mizuike, A., *Anal. Chim. Acta* **172** (1985) 215-221.

[18] Montavon, G., Mansel, A., Seibert, A., Keller, H., Kratz, J. V., Trautmann, N., *Radiochim. Acta* **88** (2000) 17-24.

[19] Pompe, S., Bubner, M., Schmeide, K., Heise, K. H., Bernhard, G., Nitsche, H., in: "Influence of humic acids on the migration behaviour of radioactive and non-radioactive substances under conditions close to nature", Marquardt, C. M. (Ed.), Wiss. Berichte FZKA 6557, Forschungszentrum Karlsruhe, 2000, pp. 125-235.

[20] Kupsch, H., Mansel, A., "Geochemische Untersuchungen zur Retention von reaktiven Kohlenstoffverbindungen für toxische Schwermetalle", Abschlussbericht zum BMBF-Projekt 02 C 0709, Institut für Interdisziplinäre Isotopenforschung Leipzig, 2003.

[21] Carlsen, L., Lassen, P., Christiansen, J. V., Warwick, P., Hall, A., Randall, A., *Radiochim. Acta* **58/59** (1992) 371-376.

[22] Warwick, P., Carlsen, L., Randall, A., Zhao, R., Lassen, P., *Chemistry and Ecology* **8** (1993) 65-80.

[23] Christiansen, J. V., Carlsen, L., *Radiochim. Acta* **52/53** (1991) 327-333.

[24] Fraker, P. J., Speck, J. C., *Biochem. Biophys. Res. Commun.* **80** (1978) 849-857.

[25] Schulten, H.-R., Schnitzer, M., *Naturwiss.* **80** (1993) 29-30.

[26] Schüßler, W., Artinger, R., Kienzler, B., Kim, J. I., *Environ. Sci. Technol*. **34** 2000 2608-2611.

[27] Geckeis, H., Rabung, T., Ngo Manh, T., Kim, J. I., Beck, H. P., *Environ. Sci. Technol*. **36** (2002) 2946-2952.

[28] Kim, J. I., Czerwinski, K. R., *Radiochim. Acta* **73** (1996) 5-10.